Universidad
Carlos III de Madrid

DOCTORAL THESIS

BLIND INTERFERENCE ALIGNMENT FOR CELLULAR NETWORKS

Author: MÁXIMO MORALES CÉSPEDES

Advisor: ANA GARCÍA ARMADA

Departamento de Teoría de la Señal y Comunicaciones

Leganés, November 2015

Tesis Doctoral: BLIND INTERFERENCE ALIGNMENT
FOR CELLULAR NETWORKS:

Autor: Máximo Morales Céspedes

Directora: Dra. Ana García Armada

El tribunal nombrado para juzgar la tesis doctoral arriba citada, compuesto por los doctores

Presidente:

Vocal:

Secretario:

acuerda otorgarle la calificación de

Leganés, a

Dedicado a mi familia.

Abstract

Managing the interference is the main challenge in cellular networks. Multiple-Input Multiple-Output (MIMO) schemes have emerged as a means of achieving high-capacity in wireless communications. The most efficient MIMO techniques are based on managing the interference instead of avoiding it by employing orthogonal resource allocation schemes. These transmission schemes require the knowledge of the Channel State Information at the Transmitter (CSIT) to achieve the optimal Degrees of Freedom (DoF), also known as multiplexing gain. Providing an accurate CSIT in cellular environments involves high-capacity backhaul links and accurate synchronization, which imply the use of a large amount of network resources. Recently, a Blind Interference Alignment (BIA) scheme was devised as a means of achieving a growth in DoF regarding the amount of users served without the need for CSIT in the Multiple-Input Single-Output (MISO) Broadcast Channel (BC). It is demonstrated that BIA achieves the optimal DoF in the BC without CSIT. However, the implementation of BIA in cellular networks is not straightforward. This dissertation investigates the DoF and the corresponding sum-rate of cellular networks in absence of CSIT and their achievability by using BIA schemes.

First, this dissertation derives the DoF-region of homogenous cellular networks with partial connectivity. Assuming that all the Base Stations (BSs) cooperate in order to transmit to all users in the network, we proposed an extension of the BIA scheme for the MISO BC where the set of BSs transmits as in a network MIMO. It is shown that the cooperation between BSs results futile because of the lack of full connectivity in cellular networks. After that, this dissertation presents several transmission schemes based on the network topology. By differentiating between users that can treat this interference optimally as noise and those who need to manage the interference from neighbouring BSs, a network BIA scheme is devised to achieve the optimal DoF in homogeneous cellular networks.

Second, the use of BIA schemes is analyzed for heterogeneous cellular networks. It is demonstrated that the previous BIA schemes based on the network topology result non-optimal in DoF because of the particular features of the heterogenous cellular networks. More specifically, assuming a macro-femto network, cooperation between both tiers leads to a penalty for macro users while femto users do not exploit the particular topology of this kind of network. In this dissertation, the optimal linear DoF (lDoF) in a two-tier network are derived subject to optimality in DoF for the upper tier. It is demonstrated that, without CSIT or any cooperation between tiers, the lower tier can achieve non-zero DoF while the upper tier attains the optimal DoF by transmitting independently of the lower tier deployment. After that, a cognitive BIA scheme that achieves this outer bound is devised for macro-femto cellular networks.

The third part of this dissertation is focused on the implementation of BIA in practical scenarios. It is shown that transmission at limited SNR and coherence time are the main hurdles to overcome for practical implementations of BIA. With aim of managing both constraints, the use of BIA together with orthogonal approaches is proposed in this work. An improvement on the inherent noise increase of BIA and the required coherence time is achieved at expenses of losing DoF. Therefore, there exists a trade-off between multiplexing gain, sum-rate at finite SNR and coherence time in practical scenarios. The optimal resource allocation for orthogonal transmission is obtained after solving a very specific optimization problem. To complete the characterization of the performance of BIA in realistic scenarios a experimental evaluation based on a hardware implementation is presented at the end of this work. It is shown that BIA outperforms the sum-rate of schemes based on CSIT such as LZFB because of the hardware impairments and the costs of providing CSIT in a realist implementation.

Agradecimientos

Mi primer y más importante agradecimiento va dirigido a mis padres que siempre me han apoyado en todas mis decisiones y a mis dos hermanos con los que he tenido la suerte de convivir durante los últimos años, y que además me aguantan.

A mis compañeros de trabajo con los que tantos buenos ratos he pasado Ana S., Ozge, Omar, Javier, Cecilia, Alex, Alejandro, Borja... Tampoco me puedo olvidar de los compañeros con los que no trabajaba codo con codo pero que han formado parte de cada día en la Universidad, Jesús, Víctor, Pablo, Wilton, Fran, Isa, Luca... como echamos de menos a Luca. De todos los compañeros tengo que hacer un hueco especial a Juanjo, creo que los dos hemos pasado por momentos difíciles durante estos cuatro años de los que hemos sabido huir cuando hablábamos entre nosotros (dicho así hasta parece serio).

Por suerte he podido descubrir un país en el que me encuentro como en mi propia casa durante el desarrollo de este trabajo. En Grecia he aprendido a vivir con más tranquilidad, saber que bueno, todo tiene solución. Durante esta etapa he conocido a grandes amigos como Nikola o Giannis. Pero sobre todo a Ángela, que a pesar de que últimamente estamos un poco desconectados, todo vuelve a ser como siempre cada vez que nos vemos. Durante mi estancia en Grecia también he conocido a Jorge y Dimitris, que además de ser grandes amigos, me han influenciado profesionalmente en gran manera. Se puede encontrar su huella en este trabajo.

During the time I spent in the USA, I met very special people. First, I want to thank to the Campbell family, Charlotte, Josh, Kristen, Mr Bear... they make every day special. I would specially like to thank Professor Syed Jafar for his invaluable comments and suggestions.

Sé que me olvido de mencionar a mucha gente, Diego, Ro, Agustín, Gabi... amigos de distintos lugares que siempre han estado ahi y que de alguna manera, también han influenciado este trabajo.

Finalmente, a mi tutora, Ana, tengo que agradecerle su optimismo infatigable y su capacidad de motivación. Hace 5 anõs quería terminar un Proyecto Fin de Carrera lo antes posible y gracias a ella estoy presentando este trabajo, el cual espero que solo sea una parte de futuras colaboraciones.

Contents

List of Figures

List of Tables

Abbreviations

AMPS	**A**dvance **M**obile **P**hone **S**ystems
AWGN	**A**dditive **W**hite **G**aussian **N**oise
BC	**B**roadcast **C**hannel
BD	**B**lock **D**iagonalization
BIA	**B**lind **I**nterference **A**lignment
cBIA	**c**ooperative **B**lind **I**nterference **A**lignment
nBIA	**n**etwork **B**lind **I**nterference **A**lignment
pBIA	**p**ractical **B**lind **I**nterference **A**lignment
sBIA	**s**tandard **B**lind **I**nterference **A**lignment
BS	**B**ase **S**tation
CAPEX	**Cap**ital **Ex**penditures
CDMA	**C**ode **D**ivision **M**ultiple **A**ccess
CSIR	**C**hannel **S**tate **I**nformation at the **R**eceiver
CSIT	**C**hannel **S**tate **I**nformation at the **T**ransmitter
DoF	**D**egrees of **F**reedom
lDoF	**l**inear **D**egrees of **F**reedom
ECR	**E**nergy **C**onsumption **R**ating
EVDO	**EV**olution **D**ata **O**ptimized
FAP	**F**emtocell **A**ccess **P**oint
FDD	**F**requency **D**ivision **D**uplex
FDMA	**F**requency **D**ivision **M**ultiple **A**ccess
FR	**F**requency **R**euse
FSO	**F**ree **S**pace **O**ptical
GSM	**G**lobal **S**ystem for **M**obile
GPRS	**G**eneral **P**acket **R**adio **A**ccess

HSPA	**H**igh **S**peed **P**acket **A**ccess
IA	**I**nterference **A**lignment
IC	**I**nterference **C**hannel
LTE	**L**ong **T**erm **E**volution
LTE-A	**L**ong **T**erm **E**volution **A**dvance
LZFB	**L**inear **Z**ero **F**orcing **B**eamforming
MAC	**M**ultiple **A**ccess **C**hannel
MIMO	**M**ultiple **I**nput **M**ultiple **O**utput
MISO	**M**ultiple **I**nput **S**ingle **O**utput
OFDM	**O**rthogonal **F**requency **D**ivision **M**ultiplexing
OPEX	**Op**erational **Ex**penditures
RIA	**R**etrospective **I**nterference **A**lignment
SMS	**S**hort **M**essage **S**ervice
SNR	**S**ignal to **N**oise **R**atio
SINR	**S**ignal to **I**nterference plus **N**oise **R**atio
SVD	**S**ingular **V**alue **D**ecomposition
TACS	**T**otal **A**ccess **C**ommunication **S**ystem
TIN	**T**reat **I**nterference as **N**oise
TDD	**T**ime **D**ivision **D**uplex
TDMA	**T**ime **D**ivision **M**ultiple **A**ccess
UMTS	**U**niversal **M**obile **T**elecommunications **S**ystem

Notation

a	Scalar
$\mathbf{a}$	Vector
$\mathbf{A}$	Matrix
$\mathbf{A}^{-1}$	Inverse of the matrix $\mathbf{A}$
$\mathbf{A}^{T}$	Transpose of a matrix
$\mathbf{A}^{H}$	Transpose and complex conjugate of a matrix (Hermitian)
$\mathbf{0}$	Vector/matrix of zeros of the appropriate dimensions
$\mathbf{I}$	Identity matrix of the appropriate dimensions
$\mathrm{Tr}\left(\mathbf{I}\right)$	Identity matrix of the appropriate dimensions
$\mathbf{A} \otimes \mathbf{B}$	Kronecker product of the matrices $\mathbf{A}$ and $\mathbf{B}$
$\mathbb{E}\left\{\cdot\right\}$	Statistical expectation.
$\log\left(\cdot\right)$	Natural (base e) logarithm.
$\log_2\left(\cdot\right)$	Base 2 logarithm.
$[a]^{+}$	$\max\left(0, a\right)$.
$\mathbb{R}$	Field of real numbers.
$\mathbb{R}^{+}$	Set of positive real numbers.
$\mathbb{C}$	Field of complex numbers.

Chapter 1

Introduction

The pressing need to improve the efficiency of wireless systems has led to the intensive study of interference and its effect on communications. Given the increasing demand for high data rates in cellular networks several generations of standards have been developed during the last two decades. Every generation proposes new requirements dictated by the trends in the use of the mobile connectivity. In the early 90s the main motivation was to provide reliable voice service by using Base Stations (BSs) covering a widely geographical area. The effects of the interference between BSs was avoided by using orthogonal Frequency Reuse (FR) and treating the co-channel interference as noise. Nowadays, the research efforts are focused on managing the interference in multiple antenna systems, referred to as Multiple-Input Multiple-Output (MIMO), over a very heterogenous cellular network composed of macro, micro, pico, femto cells and relays. Furthermore, voice service plays a minor role while issues such as achieving higher data rates, low latency, or greater power efficiency are the main motivations of the researchers. The evolution of the mobile communications can be summarized as follows.

Mobile 1G. The first generation of mobile technologies such as Advance Mobile Phone System (AMPS) or Total Access Communication System (TACs) provides analog voice services. Although 1G standards are already extinct, they established the foundation of the actual cellular systems, regulating the licensed spectrum, managing the intercell interference by using FR, and standardizing the mobile network. In this sense, the first generation brought forth a coordinated wireless network for seamless access and mobility. However, the capacity of the analog voice services was quite limited. The available

bandwidth was split in 30 KHz channels by using Frequency Division Multiple Access (FDMA). Since each user consumes 1 channel per slice, a extremely scarce resource such as the available bandwidth was wasted to provide analog voice services.

Mobile 2G. Analog voice services based on FDMA were replaced by digital wireless technologies using Time Division Multiple Access (TDMA). Second generation technologies provide voice and also data services compressed in small digital packages multiplexed in time slots. Hence, more than 1 user can be served per channel. Moreover, the use of digital components instead of analog reduces the costs and weight of the cellular devices. Although there exists several 2G standards, the most successful has been Global System for Mobile communications (GSM) and its extension General Packet Radio Service (GPRS), which is widely used currently with more than 4 billion connections [1, 2]. It is interesting to remark that a secondary service of GSM such as Short Message Service (SMS) has been the most profitable service for the mobile operators. This fact reflects the unpredictable behavior of the users demand. In spite of the GSM achievements, due to the huge increase of the number of cellular devices in the last decades, the channel capacity given by 2G was not enough to satisfy the user demands.

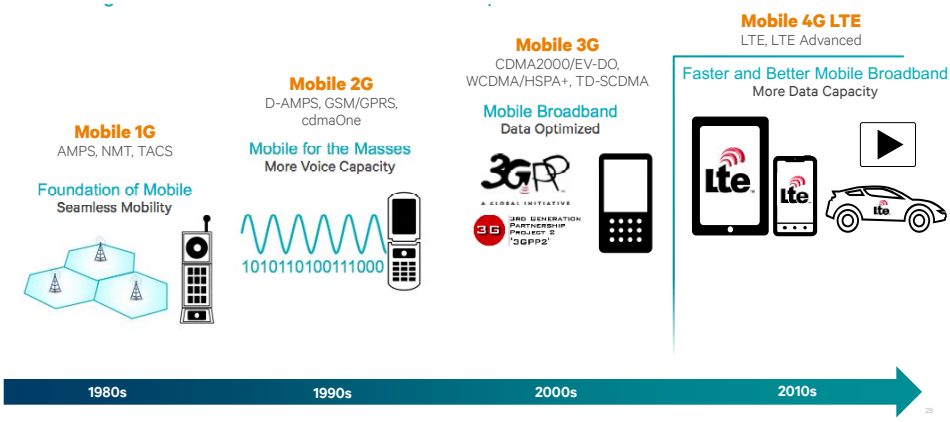

FIGURE 1.1: Evolution of the generations of mobile communications.

Mobile 3G. With the aim of improving the efficiency of the spectral resource, Code Division Multiple Access (CDMA) was proposed to implement the third generation of mobile standards. Basically, CDMA enables the users to share the same frequency and communicate at the same time [3, 4]. Challenging issues such as the near-far problem, cell-edge users and multipath fading were solved by using previous research works on power control, soft/hard handoffs and RAKE receivers (note that RAKE is not an acronym, is the real name for this type of receiver), respectively. However, the first 3G

standards such as Universal Mobile Telecommunications System (UMTS) or CDMA2000 were overwhelmed by the users demand of high data rates. At this time of the evolution of mobile standards, data traffic played a major role in the network design. In consequence, the previous 3G standards evolved to Evolution Data Optimized (EVDO) and High Speed Packet Access (HSPA), which have satisfied the users demand during the last years.

Mobile 4G. Nevertheless, the demand of faster and better broadband capacity have been increasing continually. Besides, nowadays not only the classical mobile devices require cellular service, tablets, laptops, cars, and other home devices can be connected to the cellular network. To satisfy the market demand, the fourth generation of mobile standards such as Long Term Evolution (LTE) or LTE-Advanced (LTE-A) propose to employ Orthogonal Frequency Division Multiplexing (OFDM) transmission joint to advanced MIMO technologies [5, 6]. As occurs in the evolution of previous mobile generations, the foundation of 4G is based on the research advances achieved during the last years.

Mobile 5G. Future generation of mobile standards is still defining accurate requirements to specify the techniques employed to achieve them [7–10]. The challengues to be addressed by the 5G of mobile communications can be summarized as

- Flexibility of all the network parameters; resource allocation, spectrum, antennas, protocols...
- High speed (6 - 50 Gbps) and low-latency (1 msec) services.
- Distributed mobility over a extremely dense radio network.
- Improved utilization of the current frequency bands (800MHz - 6 GHz) and exploration of centimeter/millimeter bands (6 GHz - 100 GHz).
- Better power efficiency. Optimization of the Energy Consumption Rating (ECR).

With the aim of satisfying these requirements in the future cellular networks results useful to analyze the following approximation of the capacity for MIMO systems

$$C \approx W \cdot n \cdot \log_2 (1 + SNR) , \tag{1.1}$$

where W is the available spectrum for transmission, n corresponds to the number of antennas, and SNR denotes the Signal-to-Noise Ratio. Therefore, there exist three ways to improve the network capacity

- *Best use of the spectrum W.* The available spectrum is split according to a fixed regulation that allocates each slice to a predefined service. Traditionally, improve the spectral efficiency involves the development of novel transmission and modulation schemes [10]. Although upgrade these features do not satisfy the actual demand, the use of cognitive approaches has been proposed to enhance the bandwidth utilization. Notice that in spite of the fact that the available spectrum is a scarce resource, it is usually underused due to the fixed bandwidth regulation [11–14]. Other way to achieve better utilization of the spectrum consist in the use of the barely exploited bands. Significant research efforts on the use of higher frequency bands have been carried out during the last years. Millimeter waves (60 GHz systems) [15–17], THz transmission antennas [18, 19], and even the use of Free Space Optimal (FSO) MIMO [20] communications have focused the interest of the researchers.

- *Augment the transmit/receive antennas n.* The use of MIMO systems is already considered in 3G and plays a major role for 4G. Therefore, the research efforts are focused on exploiting the spatial diversity by using multiple antennas [21, 22]. It is interesting to remark the current referred to as Massive MIMO, which is one of the most promising approaches for 5G. Basically, Massive MIMO exploits an excess of transmit antennas, which is assumed to be about 10 times the number of receive antennas, to achieve robustness, power efficiency, and high data rates [23, 24]. Although Massive MIMO is a promising transmission scheme, there are still some open issues such as the need for Time Division Duplex (TDD) transmission instead of Frequency Division Duplex (FDD) or its interaction with heterogeneous cellular networks.

- *Increase the SNR.* Power consumption, is a principal issue to solve for the operators nowadays. Increase the power transmission involves to waste a considerable amount of energy, which taking into consideration the decouple between profits and expenditures results unaffordable by the operators. In this sense, Green Communications is a very actual topic [14], not only because of the obvious environmental

benefits, but also for increasing the mobile operator earnings. Since increasing the transmit power does not seem to be a solution, an affordable approach to improve the SNR is the micro-ization of the cellular network, that is reducing the distance between transmitter and receiver. Heterogeneous networks composed of macro, micro, pico, femto cells and relays according to the user demands have been proposed to improve the SNR, and at the same time, improve the energy efficiency of the cellular network [25–27].

In conclusion, the future cellular network will be characterized by an enormous flexibility of all the parameters. Adaptive power and bandwidth allocation must be carried out while reducing the amount of information necessary to handle a cellular massive multi-antenna heterogeneous network.

1.1 Multiple Antenna techniques for Cellular Systems

The use of MIMO systems has emerged as a means of achieving high-capacity communications. The use of multiple antennas allow to increase the data rate either through diversity or multiplexing gain. Diversity use the fact that independent signal paths have a low probability of experiencing the same channel response, including deep fading, when the antennas are sufficiently far apart. The simplest example of diversity gain is either a transmitter or receiver equipped with 2 antennas that selects the strongest signal from both paths, which contain the same message. In contrast, multiplexing gain exploits the channel structure formed by the signal paths from multiple antennas. Considering the previous case, multiplexing gain would be achieved when different symbols are transmitted by both antennas and the receiver is able to decode them. The multiplexing gain is usually measured by using the Degrees of Freedom metric (DoF). Basically, the DoF metric takes the limit when the total transmit power approaches infinity, whereas the channel coefficients and the local noise power remain unchanged. Denoting the sum-capacity as $C(P)$ with a total transmit power P, the DoF metric η is defined as

$$\text{DoF} : \eta = \lim_{P \to +\infty} \frac{C(P)}{\log(P)}, \tag{1.2}$$

which can be rewritten as

$$C(P) = \eta \log(P) + o\left(\log(P)\right), \tag{1.3}$$

where the $o\left(\log(P)\right)$ term is some function $f(P)$ that satisfies

$$o\left(\log(P)\right) = \lim_{P \to +\infty} \frac{f(P)}{\log(P)} = 0. \tag{1.4}$$

Notice that checking (1.3) we can consider the DoF metric as the number of signaling dimensions, where each dimension corresponds to an interference-free Additive White Gaussian Noise (AWGN) channel where the SNR increases proportionally with P. Besides, taken into consideration a baseband model in a wireless communication system as shown in (1.1), we can consider η as the bandwidth effectivity. Therefore, the DoF metric can be understood as the multiplexing gain, bandwidth, number of signal dimensions, or the capacity pre-log factor.

1.1.1 Parallel Decomposition of the MIMO Channel

For illustrative purposes consider a MIMO channel where the transmitter and receiver are equipped with N_t and N_r antennas, respectively. Thus, the corresponding input-output system can be represented by the following discrete time model

$$\begin{bmatrix} y_1 \\ \vdots \\ y_{N_r} \end{bmatrix} = \begin{bmatrix} h_{11} & \dots h_{1N_t} \\ \vdots & \vdots \\ h_{N_r 1} & \dots h_{N_r N_t} \end{bmatrix} \begin{bmatrix} x_1 \\ \vdots \\ x_{N_t} \end{bmatrix} + \begin{bmatrix} n_1 \\ \vdots \\ n_{N_r} \end{bmatrix}, \tag{1.5}$$

which can be written simply as $\mathbf{y} = \mathbf{H}\mathbf{x} + \mathbf{n}$, where $\mathbf{H}$ denotes the $N_r \times N_t$ channel matrix gain. By using Single Value Decomposition (SVD) we can rewrite the matrix $\mathbf{H}$ as a function of its singular values

$$\mathbf{H} = \mathbf{U}\mathbf{\Sigma}\mathbf{V}^H, \tag{1.6}$$

where $\mathbf{U}$ and $\mathbf{V}$ are $N_r \times N_r$ and $N_t \times N_t$ are unitary matrices, i.e. $\mathbf{U}\mathbf{U}^H = \mathbf{I}$, and Σ the $N_r \times N_t$ diagonal matrix of singular values σ_i of $\mathbf{H}$. The vector σ_i contains the R_H eigenvalues of $\mathbf{H}\mathbf{H}^H$, where R_H is the rank of the matrix $\mathbf{H}$. Hence, taken into consideration the structure of the channel matrix, the rank is upper bounded as

$R_H \leq \min(N_t, N_r)$, which holds with equability for rich scattering channels and $R_H = 1$ for high correlated channels.

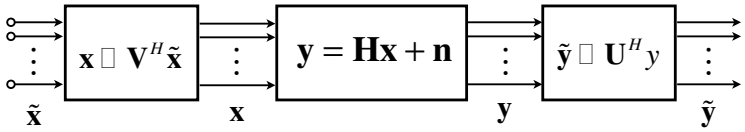

FIGURE 1.2: MIMO parallel decomposition. Transmit precoding and receiver shaping filters

The mathematical process shown above can be applied to obtain a parallel decomposition of the MIMO channel $\mathbf{H}$ as is shown in Figure 1.2. The matrix $\mathbf{V}^H$ is employed as a transmit precoding to transform the input of the MIMO system as $\mathbf{x} = \mathbf{V}^H\tilde{\mathbf{x}}$. Similarly, the receiver decouples the precoded signal by using the matrix $\mathbf{U}^H$ as a receiver shaping matrix. Therefore, the signal received after parallel decomposition is given by

$$\begin{aligned}\tilde{\mathbf{y}} &= \mathbf{U}^H(\mathbf{H}\mathbf{x} + \mathbf{n}) \\ &= \mathbf{U}^H(\mathbf{U}\boldsymbol{\Sigma}\mathbf{V}\mathbf{x} + \mathbf{n}) \\ &= \mathbf{U}^H\left(\mathbf{U}\boldsymbol{\Sigma}\mathbf{V}\mathbf{V}^H\tilde{\mathbf{x}} + \mathbf{n}\right) \\ &= \mathbf{U}^H\mathbf{U}\boldsymbol{\Sigma}\mathbf{V}\mathbf{V}^H\tilde{\mathbf{x}} + \mathbf{U}^H\mathbf{n} \\ &= \boldsymbol{\Sigma}\tilde{\mathbf{x}} + \mathbf{U}^H\mathbf{n},\end{aligned} \tag{1.7}$$

where, since $\mathbf{U}^H$ is a unitary matrix, the distribution of the noise after the multiplication $\mathbf{U}^H\mathbf{n}$ does not change. Notice that Σ is a diagonal matrix. Thus, the $N_t \times N_r$ MIMO system has been transformed into R_H parallel AWGN independent channel where the input and output of the i-th channel is given by $\tilde{x}_i$ and $\tilde{y}_i$, respectively, and the channel gain σ_i. In consequence, the MIMO channel can support R_H times the rate of a single antenna system, i.e. a multiplexing gain of R_H. At this point the question that naturally arises is, *could the MIMO channel decomposition be employed for cellular networks?*.

The first issue to consider is the need for Channel State Information (CSI). Checking (1.7) it can be seen that a knowledge of the channel matrix $\mathbf{H}$ is necessary to calculate the corresponding transmit precoders and receive filters. For the point-to-point MIMO channel, the decomposition described above is doable when CSI is available either at the transmitter (CSIT) or receiver (CSIR). It is interesting to remark that CSIR allow to obtain this decomposition only for the point-to-point MIMO by using joint processing.

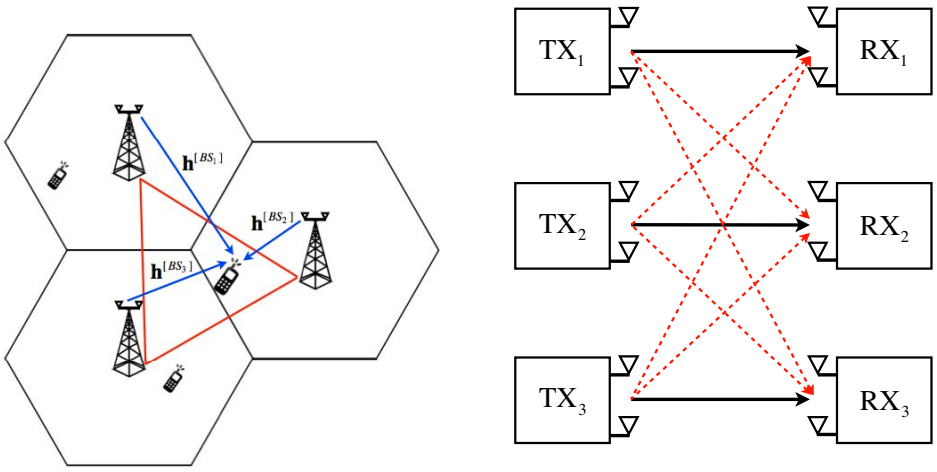

(a) LZFB over a 3-cell MIMO network (b) IA over a 3-user IC

FIGURE 1.3: Cellular network as MIMO network and Interference Channel

However, accurate CSIT is necessary when the MIMO channel is composed of more than one transmitter. Notice that CSIR is quite easy to provide in a wireless network with only consider the use of pilot signals as a preamble of the data signal. In contrast, CSIT involves a more complex methodology; a pilot sequence has to be transmitted orthogonally, the channel is estimated by the receivers, and the CSI has to be sent to the transmitter through feedback channels between transmitter and receivers.

Considering a cellular network with N_{BS} BSs where each BS is equipped with N_t antennas and a single user per cell equipped with N_r antennas[1] as is shown in Figure 1.3(a). The straightforward solution is to consider the cellular scenario as a unique MIMO system where the set of BSs is treated as a single transmitter equipped with $N_{BS}N_t$ antennas that transmit to $N_{BS}N_r$ receive antennas. This concept is usually referred to as a network MIMO. Many techniques such as Linear Zero Forcing Beamforming (LZFB) [28, 29] or Block Diagonalization (BD) [30, 31] have been developed with the aim of exploiting the MIMO channel given by the cellular network. However, considering a multiple BSs system, the network MIMO approach results quite challenging for a realistic implementation. Providing global CSIT does not only involve feedback between receivers and their corresponding BSs, but also very accurate synchronization and high-speed backhaul links among the set of BSs for sharing CSIT and data information.

[1]The single-user model can be considered as a N_r single-antenna users grouped in a single user with N_r antennas.

An alternative approach referred to as Interference Alignment (IA) is proposed in [32–36]. To tackle the interference in a cellular network, it is treated as an Interference Channel (IC) where each transmitter and receiver is equipped with N_t and N_r antennas, respectively, as is shown in Figure 1.3(b). The IA approach applied to a cellular network assumes that the i-th transmitter sends a message W_i to the i-th receiver while the interference because of the transmission of W_i is properly aligned at the remaining receivers $j \neq i$. It is demonstrated in [47] that $\frac{K}{2}$ DoF are achievable by using IA.

1.1.2 Costs of Channel State Information

As we have shown, previous MIMO techniques can achieve an enormous improvement of the achievable data rates. However, the achievability of the aforementioned rates is subject to an accurate and instantaneous knowledge of the CSIT. In cellular networks, providing CSIT involves to waste a considerable amount of the network resources for pilot overheads, feedback channels, high-capacity backhaul links and accurate synchronization [37]. Let us consider a cellular scenario as shown in Figure 1.4. Each BS transmits a pilot sequence that is employed to quantize and feedback the estimation of the CSI to the corresponding BSs via uplink, once the local CSI is obtained, it is shared through backhaul links, which also have to provide precise synchronization and/or data sharing, among the set of BSs.

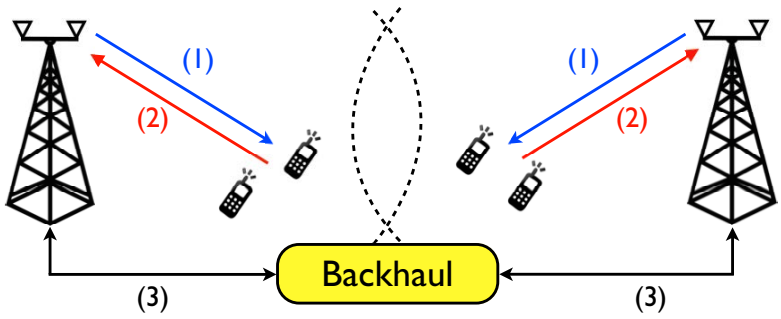

FIGURE 1.4: Achieving CSIT in a cellular network. (1) Pilot transmission, (2) CSI feedback via uplink, (3) backhaul sharing and synchronization

Let us denote θ_{csi} and θ_{cd} as the fraction of the total transmission resources employed for channel estimation and coherence detection required in a scheme based on CSIT, respectively. Similarly, θ_{fb} is denoted as the fraction of downlink resources that has to be re-allocated to the uplink to support the CSI feedback. Assuming that each BS is

equipped with N_t antennas serving K active users, the amount of pilots employed to obtain CSI scales as $N_t\theta_{csi}$. Since each user transmits via uplink the estimation of the CSI, the feedback costs scales as the number of users $K\theta_{fb}$ when the CSI is sent directly to the BS. However, notice that it increases to $KN_t\theta_{fb}$ sending the CSI independently to each transmit antenna of the BS. Once the data frame is transmitted, a pilot overhead $K\theta_{cd}$ is employed for coherence detection.

Consider now the use of blind transmission schemes in the same cellular scenario. Since CSIT is not required $\theta_{csi} = \theta_{fb} = 0$. However, it is necessary to know the channel from the transmitter to each antenna of the corresponding BS. Therefore, the costs of the pilot frames for coherent detection scales as $N_t\theta_{cd'}$, where $\theta_{cd'}$ is the pilot overhead per transmit antenna for blind schemes. Moreover, assuming that the receiver antennas can switch among a set of N_t preset modes, e.g. reconfigurable antennas, this cost increases to $N_t^2\theta_{cd'}$.

Table 1.1 summarizes the overheads for a cellular systems when each BS is equipped with N_t transmit antennas serving K users.

Type	**CSIT**	**Blind**
CSI pilots	$N_t\theta_{csi}$	0
Feedback	$K\theta_{fb}$ to $KN_t\theta_{fb}$	0
Wednesday	$K\theta_{cd}$	$N_t\theta_{cd'}$ to $N_t^2\theta_{cd'}$

TABLE 1.1: CSI overheads for cellular networks

1.2 Analysis of the State of Art

The bulk of this thesis is around interference management for cellular networks. Traditionally, the interference between users within the same cell has been avoided by assigning orthogonal slices of either time or bandwidth to each one, whereas the interference between different cells has been treated by using Frequency Reuse (FR). A survey of these traditional methods to deal with the interference is presented in [38]. An accurate analysis of the efficiency of FR as a function of the reuse distance is presented in [39]. Indeed, the use of smaller cellular coverage areas over a dense deployment was predicted in this work. The evolution of the generations of mobile communications, i.e. from

1G to 5G, can be summarized in [1–10]. Remarkable, a survey of the evolution from homogeneous to heterogeneous cellular networks is described in [14, 25, 27, 40].

Information Theory provides a notion of the theoretical limits of the channel capacity. However, closed-form expressions of the capacity for most of the MIMO configurations are not available. Instead, the ability of multiple signals in the space is measured by the multiplexing gain, i.e. the Degrees of Freedom (DoF) metric. For the MISO BC with N_t antennas at the transmitter and $K = N_t$ users with a single antenna, the achievable DoF are N_t when perfect CSIT knowledge is available [41–43]. Assuming a MISO BC with N_t transmit antennas and 2 users equipped with N_{r_1} and N_{r_2} antennas, respectively, it is shown that the DoF are $\max(N_t, N_{r_1} + N_{r_2})$. Similarly, $\max(N_{t_1} + N_{t_2}, N_r)$ DoF are achievable for the Multiple Access Channel (MAC) with 2 transmitters equipped with N_{t_1} and N_{t_2} antennas, respectively, and N_r antennas at the receiver [44]. As the number of transmitters and/or receivers increases the DoF analysis becomes more complex. The achievable DoF for the MIMO X channel is derived in [45, 46]. In this case, the DoF region depends on the antennas of each transmitter and receiver. As an example, $\frac{4}{3}$ DoF are achievable when the transmitters and receivers are equipped with the same amount of antennas denoted as N_t. The extension of the X channel consist in a Interference Channel (IC) where there exist K pairs transmitter-receiver equipped with N_t and N_r asntennas each, respectively. It is demonstrated in [47] that $\min(N_t, N_r)\, K$ if $K \leq R$ and $\min(N_t, N_r)\, \frac{R}{R+1}$ if $K > R$ DoF are achievable for the IC where $R = \frac{\max(N_t, N_r)}{\min(N_t, N_r)}$. As a remark, $\frac{N_t}{2}$ DoF are achievable in the IC where the transmitters and receivers are equipped with the same amount of antennas.

The achievable DoF described above for different channel configurations assume that perfect CSIT is available. Nevertheless, the main goal of this work is the use of blind transmission schemes with the aim of reducing the amount of information required at the transmitter to reach high data rates. Taking the MISO BC for illustrative purposes, the achievable DoF are only 1 when CSIT is not available and traditional orthogonal resource division is applied. The DoF regions for the BC and IC in absence of CSIT are derived in [48]. An extension of the DoF regions for the previous channel configurations was presented in [49]. However, the CSIT can be partially known. In this sense, the quantization by using codebooks of the channel values is addressed in [50]. Furthermore, because of the limited capacity of the feedback channel, the CSI could not be available at the transmitter on time. Interestingly, in [51] it is demonstrated that even when the

CSI is completely expired it is still useful. The achievable DoF under delayed CSIT for different channel configurations have been widely analyzed in [52–56]. The linear DoF, i.e. by using only linear beamforming, for the X channel with delayed CSIT are derived in [57]. In [58] it is shown that the optimal DoF are achievable when the delay is small enough. The other side of the coin is that maybe CSIT is available but the channel changes at data transmission time. Transmission under channel variations is usually referred to as Compound Channel [59]. The achievable DoF in the compound BC are derived in [60], which conjectures the results of [61], demonstrating that more that more than 1 DoF is achievable when the channel varies among a set of finite states. In [62] an exhaustive analysis of the DoF of the compound BC, X, and IC configurations is carried out. It is demonstrated that $\frac{N_t K}{N_t+K-1}$ are the DoF for the MISO BC with N_t transmit antennas and K single-antenna users even when the channel changes between a finite number of states. Similarly, the DoF for a IC network for the real compound channel are $\frac{K}{2}$.

A point in the middle between CSIT and totally blind techniques consists in the knowledge of network topology. It is interesting to remark that this information is quite easily to provide at the transmitters, and indeed it is a common knowledge in the Media Access Control (MAC) layer. The use of topological interference management is presented initially in [63–65]. The main idea under topological interference management is the optimality of treating interference as noise (TIN) when it is small enough. In [66], it is demonstrated that TIN results optimal in the K user IC when the desired signal strength for each user is no less than the sum of the strengths of the strongest interference from this user and the strongest interference to this user. An analysis for homogeneous hexagonal cellular networks is carried out in [67]. Furthermore, it is demonstrated in [68, 69] that topological interference management for linear, square, and hexagonal cellular arrays results optimal by using three fundamental elements such as aligned frequency reuse, wireless index coding, and interference diversity. Notice that in fact, FR is a simple form of interference alignment without the need for CSIT that allow to reuse network resources. Therefore, knowledge of the network topology is a strong feature for blind transmission techniques.

Once the DoF expressions of each kind of channel have been derived taking into consideration the amount of CSI known at the transmitter side, the question that naturally

arises is *how can this performance be reached in cellular networks?*. The full multiplexing gain when CSIT is available can be easily achieved by using the Linear Zero Forcing Beamforming (LZFB) scheme proposed and analyzed in [28, 29, 70]. When the receivers are equipped with more than one antenna, Block Diagonalization is proposed in [30, 31, 71–73]. As the number of transmitters increases the schemes to achieve the optimal DoF become more complex. There exists a vast bibliography regarding obtaining this optimality by using Interference Alignment (IA). At first, it is necessary to consider the feasibility conditions of IA, which are derived in [74, 75]. The achievability of the optimal DoF in the IC by using IA is proposed in [47, 76–78]. Basically, precoding matrices at the transmitters and shaping filters at the receivers, calculated both by using CSIT and CSIR, can be designed in order to maximize the DoF achieved by the desired receiver while aligning the interference at the remaining receivers. Considering a delay in the CSIT knowledge, Retrospective Interference Alignment (RIA) is proposed in [79] to exploit the outdated CSIT. Furthermore, IA is also feasible in absence of CSIT. It is demonstrated in [80, 81] that the interference can be aligned in the BC by exploiting predefined channel correlations. By using reconfigurable antennas [82–87] to generate these channel variations artificially, Blind Interference Alignment (BIA) is proposed in [88, 89]. It is shown that the proposed BIA scheme achieves the optimal $\frac{N_t K}{N_t+K-1}$ DoF derived for the compound BC [62]. The use of multiple antennas also at the receiver in the BC for BIA transmission is analyzed in [90], and the linear DoF achievable in the MIMO BC with reconfigurable antennas are derived in [91]. However, the use of BIA when there are more than one transmitter is not straightforward. BIA for the 3-user IC is devised in [92] and a BIA scheme for the K-users IC based on exploiting diversity is proposed in [93, 94]. Nevertheless, the DoF achieved in the K-users IC are far from the optimal. It is interesting to remark that, to best of our knowledge, a BIA scheme able to reach the optimal DoF in the general IC has not been developed yet.

The use of BIA in cellular networks is studied in [95]. It is shown that although BIA cancels the intracell interference, the users subject to interference from the neighboring BSs referred to as intercell interference, which is not handled by standard BIA, achieve poor rates. Moreover, a comparison with a transmission technique based on CSIT such as LZFB is carried out in [96]. Taking into consideration the costs of providing accurate CSIT BIA outperforms the sum-rate of LZFB in many scenarios. With the aim of reducing the effects of intercell interference in the two-cell scenario a BIA scheme based

on data sharing is devised in [97]. The set of users is labeled between private users located in the inner cell, and therefore receive a weak signal from the neighboring BSs, and shared users heavily subject to intercell interference. Thus, the same symbol is transmitted to each shared user generating diversity while private users treat intercell interference optimally as noise. The use of diversity for BIA schemes is also proposed in [93, 94, 98]. However, these schemes result sub-optimal in DoF because of the diversity achieved.

Interference management for heterogenous networks is also studied in this work. In [99] and [100] the main issues for the implementation of small cells, femto and pico cells, are discussed. Several schemes based on CSIT such as [101–105] have been developed during the previous years. However, deal with the intracell, intercell, and also inter-tier interference by exploiting the channel knowledge from a set of macro, micro, pico and femto cells involves to manage a huge amount of information through feedback channels and backhaul links. The influence of these limited elements of the cellular network is analyzed in [106], which concludes that, although small cells can improve their performance assuming theoretical cooperative schemes, the costs of its use penalize the global working of an heterogeneous network. With the aim of solving this issue cognitive smalls cell have been proposed in [107–114]. The inherent features of BIA transmission result attractive for its implementation in heterogenous cellular networks. There also exist a few recent schemes that apply BIA for interference management in macro-femto cellular networks. In [115], the authors propose several heuristic schemes that exploit the information of the users and BSs location to reduce the supersymbol length, and therefore achieve more DoF. In [116], the authors use a Kronecker product representation to design a BIA scheme for interference management in a heterogeneous network with one Macro BS and several FAPs, each with one femto user. Although the schemes proposed in [115] and [116] can cancel all the intracell and intercell interference through a coordinated transmission of the Macro BS and the FAPs without CSIT, they are generally sub-optimal in DoF sense.

1.3 Motivation and Contributions

The initial research of the thesis author was focused on developing transmission schemes based on CSIT for heterogeneous networks [101, 104]. Without considering the costs of

providing global CSIT, these schemes achieve a significant improvement of the sum-rates regarding traditional approaches based on orthogonal resource allocation. However, the turning point of the research undertaken during the last 4 years is given by the hardware evaluation of LZFB and BD presented in [117]. It is shown that a considerable amount of the transmission resources are wasted not only for providing instantaneous CSIT, extremely accurate synchronization among the set of transmitters is also required to handle the clock drifts for simultaneous transmission. After obtaining these conclusions, I decided to investigate alternative solutions able to reduce the amount of information required at the transmitters and overcome the performance achieved by orthogonal approaches.

The original BIA scheme for the MISO BC was proposed at the beginning of the research period of this thesis. Obviously, the features of BIA made it attractive for its implementation in cellular networks. Nevertheless, it is necessary to remark that the extension of BIA for systems with more than one transmitter is not straightforward. Therefore, questions such as *how to implement BIA in homogeneous and heterogeneous cellular networks? What are the optimal DoF for cellular networks? Is this optimal achievable?*, or *What is the performance of BIA in practical channels?* motivated this work.

The main contributions are summarized as follows

- First, we evaluate the implementation of standard BIA in cellular networks. It is shown that users subject to intercell interference, which is not handled by standard BIA, attain zero-DoF and the achieved sum-rate in the whole network is heavily limited at finite SNR. Besides, we derive a straightforward extension of the standard BIA scheme for cellular networks based on full cooperation among the BSs. This contribution motivates the development of transmission schemes based on exploiting the network topology for cellular networks.

- Focused on homogenous cellular networks we derive the information theoretic sum-DoF outer bound for cellular networks with partial connectivity in absence of CSIT. For cellular scenarios with partial connectivity, we depict the DoF region without CSIT. It is demonstrated that knowledge of the network topology at the transmitter achieves more DoF than schemes based on cooperation when CSIT is not available. With the aim of developing a transmission scheme that reaches the

derived outer bound we propose a flexible bandwidth BIA scheme that improves the DoF achieved by schemes based on exploiting the diversity given by the multiple transmitters in a cellular network. Nevertheless, the inherent orthogonality due to flexible bandwidth makes this scheme sub-optimal in DoF. After that we devise a network BIA scheme based on exploiting the network topology that attains the optimal DoF for symmetric partially connected networks. It is demonstrated that, by properly combining the BIA supersymbol and the information given by the network topology, the outer bound of the DoF region derived for cellular networks in absence of CSIT is achievable. Moreover, the proposed network BIA obtains a relaxation of the coherence time requirements. For asymmetric partially connected networks in absence of CSIT we design an alternative extension of the network BIA scheme that minimizes the loss of DoF because of asymmetric impairments.

- For two-tier macro-femto heterogeneous networks, we analyze the suitability of the devised network BIA scheme. It is shown that network BIA penalizes the DoF achieved by the upper-tier users, whereas the lower-tier cannot exploit the features of network BIA. As a conclusion, it is demonstrated that the achievable DoF per cell, either upper or lower tier, does no scale as the number of cells in the lower tier increases. Encouraged by this fact, we derive the linear-DoF region for two-tier cellular networks. After analyze this region, it is shown that the upper tier can still attain the optimal DoF given by the compound BC while femto users achieve non-zero DoF. After that, we develop a cognitive BIA scheme that achieves the optimal linear-DoF in the two-tier cellular networks without CSIT, data sharing, or backhaul links between both tiers. Femto users achieve non-zero DoF by stealing an additional dimension from the alignment blocks of macro users. Furthermore, the macro tier achieves the optimal DoF as in a MISO BC transmitting independently of the femtocell deployment within its coverage. Finally, we present an analysis of the achievable performance of several BIA schemes in heterogeneous cellular networks.

- Previous contributions are mainly focused on the DoF for cellular networks, either homogeneous or heterogenous, in absence of CSIT. After that, we analyze the performance of BIA schemes for practical channels. It is shown that coherence time and limited SNR are the main hurdles to overcome for the implementation of BIA. For dealing with both limitations, we devise a practical BIA scheme that,

combined with orthogonal approaches, achieves a trade-off between multiplexing gain, sum-rate at finite SNR, and coherence time. Additionally, we implement a hardware testbed to validate the performance of BIA transmission in comparison with schemes based on CSIT. It is shown that BIA achieves better sum-rate that LZFB when the costs of providing CSIT and also the hardware impairments are taken into consideration.

1.4 Organization

The rest of this dissertation is organized as follows. Chapter 2 presents the BIA scheme for the BC. In Chapter 3 we analyze the implementation of the standard BIA scheme in cellular scenarios. Moreover, an extension of the BIA scheme for the BC based on cooperation among the set of BSs is devised with the aim of managing both intracell and intercell interference. This chapter presents the motivation of developing BIA schemes for cellular networks. In this sense, in Chapter 4 we derive the information theoretic outer bound of the DoF for homogenous cellular networks with partial connectivity and present an achievability BIA scheme that can reach this outer bound. In Chapter 5 BIA for heterogenous networks is considered showing that previous approaches are not suitable because of the particular topology of this kind of networks. This Chapter is devoted to derive the DoF region for two-tier cellular networks and devise a BIA scheme able to reach the outer bound of this region. After that, the use of BIA schemes in practical channels is analyzed in Chapter 6, where an alternative BIA is proposed to handle the limitations of BIA schemes in practical channels, namely coherence time and finite SNR. Addtionaly, an experimental evaluation of BIA in a hardware testbed is presented. Finally, Chapter 7 draws conclusions from the contributions of this dissertation and proposed directions for future work.

Chapter 2

Blind Interference Alignment for the MISO Broadcast Channel

This chapter presents a Blind Interference Alignment scheme for the MISO BC based on reconfigurable antennas at each receiver. After analyzing BIA transmission in several specific examples, the methodology to achieve $\frac{N_t K}{N_t+K-1}$ DoF in the N_t transmit antennas K-users MISO BC is developed in detail. Then, closed form expressions of the achievable rates are obtained depending on the power allocation strategy. Simulation results point out the benefits and drawbacks of BIA in the MISO BC.

2.1 Introduction

The idea of Interference Alignment (IA) for wireless networks lead to an intensive study of the high-capacity potentially achievable by its application [47, 74, 76, 77, 118]. Most of these works are based on perfect knowledge of the Channel State Information at the Transmitter (CSIT). Satisfying this requirement involves high-capacity backhaul links and accurate synchronization, which imply to use a large amount of network resources [37, 119]. Hence, the implementation of IA in realistic wireless networks results challenging or even impossible. However, beyond the costs of providing accurate CSIT, it is necessary to study whether the high-capacity of IA is still achievable under channel uncertainty.

For the MIMO point to point channel it is well known that the absence of CSIT does not affect the achievable DoF. This is because of the combination of joint processing and perfect CSIR is able to compensate the lack of CSIT. Considering the two user MIMO BC where the transmitter is equipped with N_t antennas and there are r_1 and r_2 antennas at each receiver, it is demonstrated in [45, 62] that $\min(N_t, r_1 + r_2)$ DoF are achievable, which is the same as with perfect cooperation at the receiver. However, under lack of CSIT a loss in DoF is expected. For example, under the assumption of i.i.d. fading, it is clear that only 1 DoF is achievable in the absence of CSIT.

The impact on the achievable DoF regarding the channel uncertainty in the MISO BC is widely studied in [120] and [61]. The channel uncertainty is obtained by assuming a space of non-zero probability measured under time-varying channel conditions in [120]. Instead, in [61] the channel uncertainty is modelled by considering each receiver as a compound of states where the channel is drawn among a set of states. Note that the state of each user is unknown to the transmitter. Curiously, both works conjecture the DoF outer bound for the 2-user MISO BC in absence of CSIT. It is known that the outer bound for a 2-user MISO BC where the transmitter is equipped with 2 antennas is $\frac{4}{3}$ DoF. For this setting, [120] conjecture that the DoF collapse to 1. In [61] this conjecture is solved when the channel of each user changes among two states. However, as the number of states for either users increases, the DoF collapse to 1. This conjecture is finally disproved in [62]. Based on interference alignment schemes with asymmetric complex signaling [121] and reciprocity/duality relationship with the interference alignment for the SIMO interference channel [122], it is demonstrated that the number of states does not decrease the achievable DoF. Specifically, it is demonstrated that $\frac{N_t K}{N_t + K - 1}$ DoF are achievable almost surely for the real compound BC with N_t transmit antennas and K single-antenna receivers with $J_k \geq N_t$ states at the k-th receiver.

Once the outer bound of the DoF in absence of CSIT is determined, the natural question is *how can we achieve it?*. The straightforward idea is to use classical blind schemes based on orthogonal resource division, e.g. time or frequency division, which obtain a DoF performance far to the outer bound. Furthermore, it is interesting to remark that the DoF decrease regarding the number of users when orthogonal schemes are employed. In other words, the cake is divided in $\frac{1}{K}$ pieces to each user. However, the outer bound of [62] tends to N_t when the number of users goes to infinity. In [80, 81] it is shown that the outer bound is achievable by employing channel correlations when they are

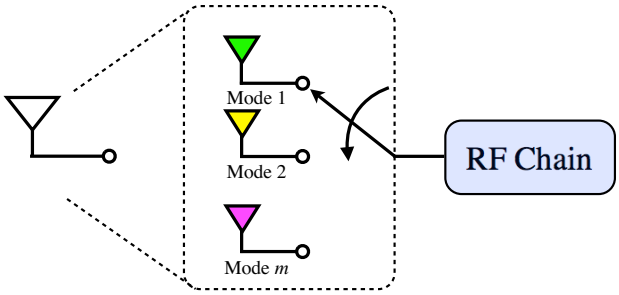

FIGURE 2.1: MISO BC scenario with $N_t = 2$ transmit antennas and K users equipped with reconfigurable antennas.

suitably staggered. These channel correlations form a pattern called *supersymbol* from now on. However, it is clear that we cannot manipulate the channel state at our own whim. Thus, the following question is, *Can we artificially manipulate the channel state of each user with the aim of building a predefined supersymbol?*

The goal of manipulating the channel state of each user can be carried out by using reconfigurable antennas. Basically, reconfigurable antennas can switch their radiation pattern among a set of preset modes by employing only one RF chain as is shown in Figure 2.1. They are constructed through micro-electromechanical switches (MEMS), nano-electromechanical switches (NEMS) that can change the geometry of the antenna or solid state switches able to modify the radiative properties of the antenna [82–87]. Although reconfigurable antennas provide some benefits such as only one RF chain or less space required than multiple conventional antennas, they are not popular in communication signal processing, where in general it is not interesting to use different preset modes. Notice that for implementing beamforming techniques such as LZFB the antennas must use a fixed in a determined channel state. In contrast, the use of reconfigurable antennas have been explored for diversity benefits and they have been widely employed in other fields as RADAR applications [123].

This chapter analyzes in detail the BIA scheme based on reconfigurable antennas that was initially proposed in [88] and developed in [89]. It is shown that $\frac{N_t K}{N_t+K-1}$ DoF are achievable in the MISO BC with N_t transmit antennas and K single-antenna users. Note that it coincides with the outer bound of the maximum DoF achievable in the absence of CSIT. The methodology to create a generic BIA supersymbol and the corresponding beamforming matrices are thoroughly described. Once the BIA scheme has been presented in terms of DoF, the closed-form expression for the achievable rates of each user

is derived. Furthermore, following the power allocation scheme proposed in [95, 96], uniform power per symbol and constant power during the whole supersymbol schemes are described.

2.2 System Model

This section describes the system model for the MISO BC used in this chapter. The transmitter is equipped with N_t antennas and the number of active users is denoted by K. Each user is equipped with a reconfigurable antenna that can switch its radiation pattern among a set of preset modes equals to the number of transmit antennas, i.e. N_t channel modes are available at each receiver. Figure 2.2 shows the 2 transmit antenna K-user MISO BC where each user is equipped with a reconfigurable antenna. The signal transmitted at time t is given by $\mathbf{x}[t] = \left[x_1, \ldots, x_{N_t}\right]^T \in \mathbb{C}^{N_t \times 1}$, where x_τ, $\tau = 1, \ldots, N_t$, is the symbol transmitted by the τ-th antenna. Thus, the signal received by the user k at time t can be written as

$$y^{[k]}[t] = \mathbf{h}^{[k]}\left(l^{[k]}[t]\right)^T \mathbf{x}[t] + z^{[k]}[t] \tag{2.1}$$

where $\mathbf{h}^{[k]}\left(l^{[k]}[t]\right) \in \mathbb{C}^{N_t \times 1}$ is the channel vector between user k and each transmit antenna when the preset mode l, $l \in \{1, 2, \ldots, N_t\}$ is selected and $z^{[k]}[t] \sim \mathcal{CN}(0, 1)$ is additive white Gaussian noise (AWGN).

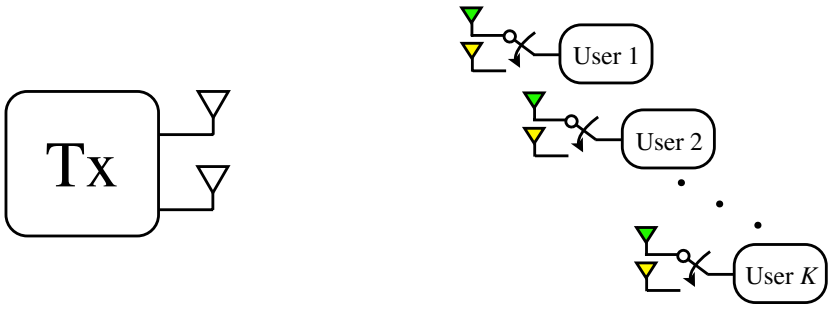

FIGURE 2.2: MISO BC scenario with $N_t = 2$ transmit antennas and K users equipped with reconfigurable antennas.

The transmitted signal is subject to an average power constraint $E\left\{\|\mathbf{x}[t]\|^2\right\} \leq P$ for all $t \geq 1$ and $t \in \mathbb{N}$. Furthermore, the channel coefficients between transmitter and users are drawn from a continuous distribution and, therefore, are linearly independent almost

surely. The transmitter does not have any channel state information (CSIT). Moreover, we assume that the physical channel stays constant across a sufficient number of time or frequency slots. For simplicity, we focus on the temporal dimension, without loss of generality. Hence, from now on each symbol extension t corresponds to a time slot. The application of this system model along frequency slots is straightforward.

2.3 Blind Interference Alignment for the MISO Broadcast Channel. Supersymbol and Beamforming Design

2.3.1 $N_t = 2$, K-user MISO Broadcast Channel

Let us first consider a MISO BC where the transmitter is equipped with $N_t = 2$ antennas serving $K = 2$ active users. Notice that our goal is to achieve the optimal sum-DoF attainable in this scenario, that is $\frac{4}{3}$ DoF [62]. The proposed supersymbol for this toy example is shown in Figure 2.3 and the transmitted signal during the 3 symbol extension that comprise the entire supersymbol $\mathbf{X} = \begin{bmatrix}\mathbf{x}[1]^T & \mathbf{x}[2]^T & \mathbf{x}[3]^T\end{bmatrix}^T \in \mathbb{C}^{3N_t \times 1}$ is given by

$$\mathbf{X} = \begin{bmatrix}\mathbf{x}[1]\\ \mathbf{x}[2]\\ \mathbf{x}[3]\end{bmatrix} = \begin{bmatrix}\mathbf{I}\\ \mathbf{I}\\ \mathbf{0}\end{bmatrix} \mathbf{u}_1^{[1]} + \begin{bmatrix}\mathbf{I}\\ \mathbf{0}\\ \mathbf{I}\end{bmatrix} \mathbf{u}_1^{[2]}, \tag{2.2}$$

where $\mathbf{u}_\ell^{[k]} = \begin{bmatrix}u_{\ell,1}^{[k]} & u_{\ell,2}^{[k]}\end{bmatrix}^T$ is the ℓ-th vector, $\ell = 1$ for this specific example[1], that contains the symbols transmitted to the user k composed by the symbol transmitted by the τ-th antenna, $\tau \in \{1, 2\}$, denoted as $u_{\ell,\tau}^{[k]}$, and $\mathbf{I}$ and $\mathbf{0}$ are the 2×2 identity and zero matrices, respectively. Therefore, the signal received at user 1 during the entire supersymbol can be written as

$$\begin{bmatrix}y^{[1]}[1]\\ y^{[1]}[2]\\ y^{[1]}[3]\end{bmatrix} = \underbrace{\begin{bmatrix}\mathbf{h}^{[1]}(1)^T\\ \mathbf{h}^{[1]}(2)^T\\ \mathbf{0}\end{bmatrix}}_{\text{rank}=2} \mathbf{u}_1^{[1]} + \underbrace{\begin{bmatrix}\mathbf{h}^{[1]}(1)^T\\ \mathbf{0}\\ \mathbf{h}^{[1]}(1)^T\end{bmatrix}}_{\text{rank}=1} \mathbf{u}_1^{[2]} + \begin{bmatrix}z^{[1]}[1]\\ z^{[1]}[2]\\ z^{[1]}[3]\end{bmatrix}. \tag{2.3}$$

[1]For the $N_t = 2$ case, only one symbol with 2 DoF is provided to each user during the entire supersymbol, and therefore, $\ell \in \{1\}$. However, the index $\ell = \{1, 2, \ldots, (N_t - 1)^{K-1}\}$ for the $N_t > 2$ cases.

	1	2	3
User 1	$\mathbf{h}^{[1]}(1)$	$\mathbf{h}^{[1]}(2)$	$\mathbf{h}^{[1]}(1)$
User 2	$\mathbf{h}^{[2]}(1)$	$\mathbf{h}^{[2]}(1)$	$\mathbf{h}^{[2]}(2)$

FIGURE 2.3: The supersymbol structure for the $K = 2$, $N_t = 2$ MISO BC.

It can be easily seen that the interference because of the transmission to user 2 is aligned into one dimension over the vector $\begin{bmatrix} 1 & 0 & 1 \end{bmatrix}^T$ while the desired signal is contained in a full-rank matrix. Besides, note that symbols $\mathbf{u}_1^{[1]}$ and $\mathbf{u}_1^{[2]}$ are transmitted in orthogonal fashion during the second and third symbol extensions, respectively. Thus, notice that the user 1 can employ the signal received during the third symbol extension to measure the interference due to $\mathbf{u}_1^{[2]}$ transmission by using the same preset mode as during the first symbol extension. Therefore, user 1 can remove the interference received in the first symbol extension. In consequence, the signal at user 1 after zero forcing cancellation can be written as

$$\tilde{\mathbf{y}}^{[1]} = \begin{bmatrix} y^{[1]}[1] - y^{[1]}[3] \\ y^{[1]}[2] \end{bmatrix} = \underbrace{\begin{bmatrix} \mathbf{h}^{[1]}(1)^T \\ \mathbf{h}^{[1]}(2)^T \end{bmatrix}}_{\mathbf{H}^{[1]}} \mathbf{u}_1^{[1]} + \underbrace{\begin{bmatrix} z^{[1]}[1] - z^{[1]}[3] \\ z^{[1]}[2] \end{bmatrix}}_{\tilde{\mathbf{z}}^{[k]}}. \tag{2.4}$$

Consequently, denoting $\tilde{\mathbf{y}}^{[k]} \in \mathbb{C}^{N_t \times 1}$ and $\tilde{\mathbf{z}}^{[k]} \in \mathbb{C}^{N_t \times 1}$ as the received signal and noise after zero-forcing interference subtraction at user k, respectively, the user 1 can decode the 2 DoF contained in $\mathbf{u}_1^{[1]}$ by solving the following 2×2 interference-free equation system

$$\tilde{\mathbf{y}} = \mathbf{H}^{[1]}\mathbf{u}_1^{[1]} + \tilde{\mathbf{z}}, \tag{2.5}$$

where $\mathbf{H}^{[1]} = \begin{bmatrix} \mathbf{h}^{[1]}(1)^T & \mathbf{h}^{[1]}(2)^T \end{bmatrix}^T \in \mathbb{C}^{2\times 2}$ is referred to as the channel matrix of user 1. Beyond the DoF metric, it is interesting to remark that the decoded signal at first symbol extension of (2.4) suffers a noise increase because of the interference subtraction.

Similarly, user 2 attains 2 DoF by receiving the desired symbol $\mathbf{u}_1^{[2]}$ during the symbol extensions $\{1, 3\}$, whereas the interference due to transmission of $\mathbf{u}_1^{[1]}$ is measured in symbol extension $\{2\}$. Therefore, each user achieves 2 DoF by using a supersymbol that comprises 3 symbol extensions. In consequence, $\frac{4}{3}$ DoF are achievable in this scenario, which coincide with the information-theoretic sum-DoF in absence of CSIT [62].

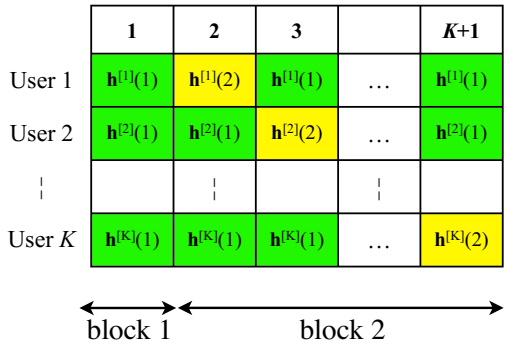

FIGURE 2.4: The supersymbol structure for the K user $N_t = 2$ MISO BC.

For the general case, where K users are served by a transmitter equipped with $N_t = 2$ antennas, the supersymbol is as Figure 2.4 shows. Simultaneous transmission of the symbols desired by each user, $\left\{\mathbf{u}_1^{[1]}, \ldots, \mathbf{u}_1^{[k]}, \ldots, \mathbf{u}_1^{[K]}\right\}$, is carried out during the first symbol extension over the preset mode $\mathbf{h}^{[k]}(1)$ for $k = \{1, 2, \ldots, K\}$. Thus, the signal transmitted during the first symbol extension is

$$\mathbf{x}(1) = \sum_{k=1}^{K} \mathbf{u}_1^{[k]}. \tag{2.6}$$

After that, an additional symbol extension corresponding to the channel mode $\mathbf{h}^{[k]}(2)$ is required to complete a full-rank matrix for each user. The channel mode $\mathbf{h}^{[k]}(2)$ is employed by the k-th user during the symbol extension $k+1$. At the same time, the remaining users take advantage of this additional symbol extension to align the interference by using the same channel mode as during the first symbol extension, i.e. $\mathbf{h}^{[j]}(1)$, $j \neq k$. Hence, the remaining users employ this symbol extension to measure the interference because of the transmission of $\mathbf{u}_1^{[k]}$, $k \neq j$. Consequently, each symbol has to be transmitted independently during the following symbol extensions, that is

$$\mathbf{x}(\rho) = \mathbf{u}_1^{[\rho-1]}, \tag{2.7}$$

for $2 \leq \rho \leq K+1$.

The k-th user can remove the $K-1$ interference terms received in the first symbol extension by measuring them in Block 2. Besides, the symbol extension used to complete the full-rank matrix is free of interference because of (2.7). Thus, the signal received by

the k-th user after zero forcing can be written as

$$\tilde{\mathbf{y}}^{[k]} = \begin{bmatrix} y^{[k]}(1) - \sum_{\substack{\rho=2 \\ \rho \neq k+1}} y^{[k]}(\rho) \\ y^{[k]}(k+1) \end{bmatrix} = \begin{bmatrix} \mathbf{h}^{[k]}(1)^T \\ \mathbf{h}^{[k]}(2)^T \end{bmatrix} \mathbf{u}_1^{[k]} + \begin{bmatrix} z^{[k]}(1) - \sum_{\substack{\rho=2 \\ \rho \neq k+1}} z^{[k]}(\rho) \\ z^{[k]}(k+1) \end{bmatrix}. \tag{2.8}$$

Therefore, the user k can decode 2 DoF by solving the equation system given by

$$\tilde{\mathbf{y}}^{[k]} = \mathbf{H}^{[k]} \mathbf{u}_1^{[k]} + \tilde{\mathbf{z}}^{[k]} \tag{2.9}$$

where $\mathbf{H}^{[k]} = \begin{bmatrix} \mathbf{h}^{[k]}(1)^T & \mathbf{h}^{[k]}(2)^T \end{bmatrix}^T$ and $\tilde{\mathbf{z}}^{[k]} \sim \mathcal{CN}(0, \mathbf{R}_{\tilde{z}})$ where the covariance matrix of the noise is $\mathbf{R}_{\tilde{z}} = \text{diag}(K-1, 1)$.

Therefore, each user attains 1 alignment block providing 2 DoF each when using BIA. Since the supersymbol structure comprises $K+1$ symbol extensions, BIA achieves $\frac{2K}{K-1}$ sum-DoF in the $N_t = 2$, K-user MISO BC. In conclusion, the optimal DoF for this MISO BC case are achieved [62].

2.3.2 $N_t = 3$, K-user MISO Broadcast Channel

As the number of transmit antennas increases the design of the supersymbol is more challenging. The key idea is to create a pattern where the channel state of the desired user changes while the channel state of all other users remains constant within the alignment block of the desired user.

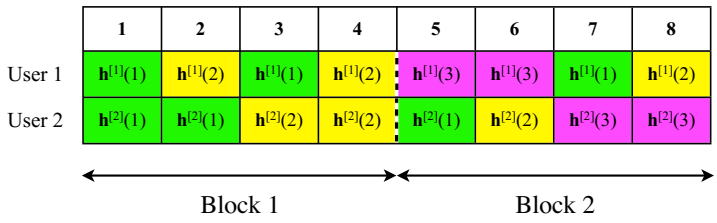

FIGURE 2.5: The supersymbol structure for the $N_t = 2$, $K = 2$ MISO BC.

For illustrative purposes we first consider a toy example where the transmitter is equipped with $N_t = 3$ and there are $K = 2$ active users. The supersymbol for the proposed example is shown in Figure 2.5. Notice that it can be differentiated into Block 1 and Block 2. The alignment between the transmitted symbols in ensured in Block 1 while Block 2 guarantees desired signals do not overlap with interference. For user 1, each set of

symbol extensions $\{1, 2, 5\}$ and $\{3, 4, 6\}$ form an alignment block denoted by the index $\ell = \{1, 2\}$, for user 1. Note that the first two symbol extensions belong to Block 1 and the last symbol extension that completes each alignment block is provided by Block 2. It can be seen that during each of these alignment blocks the channel mode of user 1 changes among $N_t = 3$ preset modes while the channel of user 2 remains constant at preset mode $\mathbf{h}^{[k]}(1)$ and $\mathbf{h}^{[k]}(2)$ during each alignment block. Similarly, the symbol extensions $\{1, 3, 7\}$ and $\{2, 4, 8\}$ form two alignment blocks for user 2. The symbols $\mathbf{u}_\ell^{[k]}$, $k = \{1, 2\}$ and $\ell = \{1, 2\}$, are transmitted during each alignment block. It is interesting to remark that in contrast to the $N_t = 2$ case, each user attains more than one alignment block. To ensure the alignment between the transmitted symbols during Block 1 the channel mode of user 2 must remain constant over each pattern $\left\{\mathbf{h}^{[1]}(1), \mathbf{h}^{[1]}(2)\right\}$ of user 1. Therefore, to maintain this condition the pattern $\left\{\mathbf{h}^{[1]}(1), \mathbf{h}^{[1]}(2)\right\}$ is repeated twice while user 2 employs the pattern $\left\{\mathbf{h}^{[2]}(1), \mathbf{h}^{[2]}(1), \mathbf{h}^{[2]}(2), \mathbf{h}^{[2]}(2)\right\}$. In consequence, two alignment blocks, providing 3 DoF each, have to me assigned to each user due to this periodic repetition. Furthermore, an additional symbol extension from Block 2 is used to complete each alignment block. Orthogonal transmission is used to ensure the independence between the transmitted symbols. Therefore, taking into consideration the supersymbol structure, the transmitted signal is given by

$$\mathbf{X} = \begin{bmatrix} \mathbf{I} & \mathbf{0} \\ \mathbf{I} & \mathbf{0} \\ \mathbf{0} & \mathbf{I} \\ \mathbf{0} & \mathbf{I} \\ \mathbf{I} & \mathbf{0} \\ \mathbf{0} & \mathbf{I} \\ \mathbf{0} & \mathbf{0} \\ \mathbf{0} & \mathbf{0} \end{bmatrix} \begin{bmatrix} \mathbf{u}_1^{[1]} \\ \mathbf{u}_2^{[1]} \end{bmatrix} + \begin{bmatrix} \mathbf{I} & \mathbf{0} \\ \mathbf{0} & \mathbf{I} \\ \mathbf{I} & \mathbf{0} \\ \mathbf{0} & \mathbf{I} \\ \mathbf{0} & \mathbf{0} \\ \mathbf{0} & \mathbf{0} \\ \mathbf{I} & \mathbf{0} \\ \mathbf{0} & \mathbf{I} \end{bmatrix} \begin{bmatrix} \mathbf{u}_1^{[2]} \\ \mathbf{u}_2^{[2]} \end{bmatrix}, \tag{2.10}$$

where $\mathbf{u}_\ell^{[k]} = \left[u_{\ell,1}^{[k]}, \quad u_{\ell,2}^{[k]}, \quad u_{\ell,3}^{[k]}\right]^T$ is the vector that contains the symbols transmitted to the user k during the ℓ-th alignment block, and $\mathbf{I}$ and $\mathbf{0}$ are the 3×3 identity and zero matrices, respectively.

With the proposed scheme the signal received during the first alignment block at user 1 is

$$\begin{bmatrix} y^{[1]}[1] \\ y^{[1]}[2] \\ y^{[1]}[5] \end{bmatrix} = \underbrace{\begin{bmatrix} \mathbf{h}^{[1]}(1)^T \\ \mathbf{h}^{[1]}(2)^T \\ \mathbf{h}^{[1]}(3)^T \end{bmatrix}}_{\text{rank=3}} \mathbf{u}_1^{[1]} + \underbrace{\begin{bmatrix} \mathbf{h}^{[1]}(1)^T \mathbf{u}_1^{[2]} \\ \mathbf{h}^{[1]}(2)^T \mathbf{u}_2^{[2]} \\ \mathbf{0} \end{bmatrix}}_{\text{rank=2}} + \begin{bmatrix} z^{[1]}[1] \\ z^{[1]}[2] \\ z^{[1]}[3] \end{bmatrix}. \tag{2.11}$$

Notice that the desired symbol $\mathbf{u}_1^{[1]}$ is transmitted over a full-rank matrix while the interference is aligned in a rank = 2 matrix. Therefore, the 3 DoF transmitted in the symbol $\mathbf{u}_1^{[1]}$ are decodable without the influence of the interference. Checking the supersymbol structure in Figure 2.5, it can be seen that the interference received in symbol extensions $\{1\}$ and $\{2\}$ can be measured in symbol extensions $\{7\}$ and $\{8\}$, respectively, and therefore, removed afterwards. Thus, the signal after zero-forcing interference cancellation can be written as

$$\tilde{\mathbf{y}}^{[1]} = \begin{bmatrix} y^{[1]}[1] - y^{[1]}[7] \\ y^{[1]}[2] - y^{[1]}[8] \\ y^{[1]}[5] \end{bmatrix} = \underbrace{\begin{bmatrix} \mathbf{h}^{[1]}(1)^T \\ \mathbf{h}^{[1]}(2)^T \\ \mathbf{h}^{[1]}(3)^T \end{bmatrix}}_{\mathbf{H}^{[1]}} \mathbf{u}_1^{[1]} + \underbrace{\begin{bmatrix} z^{[1]}[1] - z^{[1]}[7] \\ z^{[1]}[2] - z^{[1]}[8] \\ z^{[1]}[3] \end{bmatrix}}_{\tilde{\mathbf{z}}^{[1]}}, \tag{2.12}$$

where $\mathbf{H}^{[1]} = \begin{bmatrix} \mathbf{h}^{[1]}(1)^T & \mathbf{h}^{[1]}(2)^T & \mathbf{h}^{[1]}(3)^T \end{bmatrix}^T \in \mathbb{C}^{3\times 3}$ is the channel matrix and $\tilde{\mathbf{z}}^{[1]} \sim \mathcal{CN}(0, \mathbf{R}_{\tilde{z}})$ with $\mathbf{R}_{\tilde{z}} = \text{diag}(3, 1)$.

As we have shown the interference has been completely canceled, and therefore, the 3 DoF of the first alignment block of user 1 can be decoded. Repeating the same procedure with the alignment blocks formed by the sets of symbol extensions $\{3, 4, 6\}$ for user 1, and $\{1, 3, 7\}$ and $\{2, 4, 8\}$ for user 2, 3DoF $\times 2 = 6$ DoF are achieved by each user over 8 symbol extensions. Thus, the proposed BIA scheme attains $\frac{3}{2}$ sum-DoF for the $N_t = 3$ 2-user MISO BC.

As the number of users increases the supersymbol design comprises becomes more complex. The key idea is to replicate periodically the patterns composed of channel modes $\mathbf{h}^{[k]}(1)$ and $\mathbf{h}^{[k]}(2)$ during Block 1 by ensuring the alignment between users. Checking the previous case, it can be seen in Figure 2.5 that the patterns $\left\{\mathbf{h}^{[1]}(1), \mathbf{h}^{[1]}(2)\right\}$ and $\left\{\mathbf{h}^{[2]}(1), \mathbf{h}^{[2]}(1)\mathbf{h}^{[2]}(2), \mathbf{h}^{[2]}(2)\right\}$ are repeated twice and only once for users 1 and 2, respectively. We refer as *building blocks* to each of these patterns. Figure 2.6 shows the structure of the building blocks for the general case where the transmitter is equipped

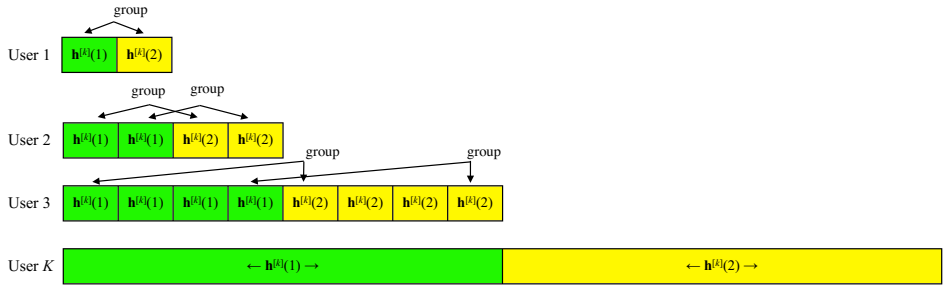

FIGURE 2.6: Building block construction for the $N_t = 3$ MISO BC.

with $N_t = 3$ antennas. The building block of the k-th user comprises 2^k symbol extensions where each preset mode, $\mathbf{h}^{[k]}(1)$ and $\mathbf{h}^{[k]}(2)$, is repeated 2^{k-1} times. It can be seen that the channel of user k changes among 2 preset modes while the channel of all other users, $k+1, \ldots, K$, remains constant. The length of Block 1 is given by the number of symbol extensions that composes the largest building block. Therefore, since Block 1 comprises 2^K symbol extensions, the k-th user repeats its corresponding building block 2^{K-k} times, where the index $p = \left\{1, 2, \ldots, 2^{K-k}\right\}$ is defined to denote the p-th building block of user k.

Once the Block 1 has been designed, the beamforming matrices can be devised by creating *groups* of 2 channel modes within every building block. Therefore, the alignment between groups is ensured because of the building block construction described in Figure 2.6. Since the k-th user contains 2^{K-k} building blocks comprising 2^k symbol extensions each, 2^{k-1} groups can be assembled over each building block. Thus, each user forms $2^{K-k} \times 2^{k-1} = 2^{K-1}$ groups. According to the Block 1 structure proposed in Figure 2.6, the ℓ-group in the p-th building block of the users k corresponds to the symbol extensions

$$\left\{(p-1)2 + 2^{K-1}\right\}, \tag{2.13}$$

where $\ell \in \left\{1, 2, \ldots, 2^{K-1}\right\}$ and $p \in \left\{1, 2, \ldots, 2^{K-k}\right\}$.

Ultimately, Block 2 is easily determined with only annexing an additional symbol extension per each group of each user to complete an alignment block composed of 3 different channel modes. Thus, Block 2 provides 2^{K-1} symbol extensions corresponding to the channel mode $\mathbf{h}^{[k]}(3)$ per each user. In consequence, it comprises $K \times 2^{K-1}$ symbol extensions. To guarantee that each symbol does not overlap with other symbols either desired or interfering, each symbol $\mathbf{u}_\ell^{[k]}$ is transmitted in orthogonal fashion during Block 2. Furthermore, all other users $j \neq k$ take advantage of this strategy to measure the

interference subspace because of transmission to user k and remove it from their desired signal space.

Following the proposed BIA design, each user attains 2^{K-1} alignment blocks providing 3 DoF each. Therefore, $3 \times K \times 2^{K-1}$ DoF are attainable by using BIA. To achieve this goal a supersymbol made up by Block 1 and Block 2, which comprise 2^K and $K \times 2^{K-1}$ symbol extensions, respectively, is required. Since $K \times 2^{K-1}$ symbols providing 3 DoF each are decodable over $2^K + K \times 2^{K-1}$ symbol extensions, the normalized DoF per symbol extension achievable in the $N_t = 3$, K-user MISO BC by using BIA is

$$\text{DoF} = \frac{3 \times K \times 2^{K-1}}{2^K + K \times 2^{K-1}} = \frac{3K}{K+2}. \tag{2.14}$$

2.3.3 N_t K-user MISO Broadcast Channel

So far, the methodology of building a BIA scheme for the MISO BC has been described for some specific cases. For the general case we can consider it as two independent problems.

- **Alignment problem.** The transmission of each desired symbol must be contained in at least one dimension more than the interfering subspace. To ensure this condition a supersymbol based on constructing non-overlapping alignment blocks can be devised. As we have shown previously, the key idea is to create a pattern where the channel state of the desired user changes while the state of all other users remains constant within the alignment block of the desired user. This issue can be solved systematically by creating *building blocks* that are periodically repeated over the Block 1.

- **Linear independence problem.** The BIA design must guarantee the linear independence of each desired symbol and all other desired and interfering symbols. For the set of desired symbols, notice that the signal transmitted over one alignment block must be linearly independent, which is satisfied by using N_t channel modes over each alignment block. Besides, the independence between different alignment blocks for the same user is ensured by orthogonality between them, i.e. the alignment blocks of each user are transmitted over different columns of its

beamforming matrix. Finally, linear independence between the desired and interfering signals is ensured by orthogonality in the las slot of each alignment block. Therefore, each user can measure the interference subspace received because of transmission to all other users.

To tackle both problems separately, Block 1 ensures alignment between the transmitted signals while Block 2 guarantees that the desired signal does not overlap with the interference. This section shows a systematic procedure to build a BIA supersymbol and its corresponding beamforming matrices.

2.3.3.1 Design of Block 1

For the general case where the transmitter is equipped with N_t antennas Block 1 is constructed by generalizing the idea of generate periodic building blocks. For the k-th user each building block is made up by $N_t - 1$ sub-blocks, comprising $(N_t - 1)^{k-1}$ symbol extensions each, where the channel state remains fixed. Thus, the channel state associated to each sub-block corresponds to the channel preset mode selected by the user. The construction of a generic building block is shown in Figure 2.7. Once the

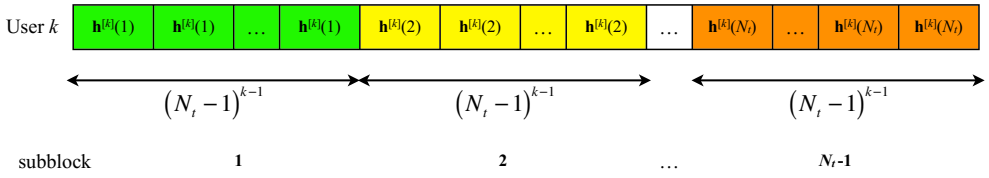

FIGURE 2.7: The building block of user k for the N_t MISO BC.

building block of each user has been defined, the Block 1 is obtained with only repeat the building block of the k-th user $(N_t-1)^{K-k}$ times. In consequence, Block 1 comprises

$$\mathcal{L}_{\text{Block1}} = (N_t - 1)^K \tag{2.15}$$

symbol extensions. Figure 2.8 shows the design of a generic Block 1. As can be seen, the temporal correlation at user k during Block 1 can be written as a function of the channel mode $\{\mathbf{h}^{[k]}(1), \ldots, \mathbf{h}^{[k]}(l), \ldots, \mathbf{h}^{[k]}(N_t)\}$ during a periodic building block. Thus,

the channel mode selected by user k at time t is given by

$$g_k(t) = \begin{cases} \mathbf{h}^{[k]}(1) & t \equiv 1, 2, \ldots, (N_t-1)^{k-1} \left(\mathrm{mod}(N_t-1)^k\right) \\ \vdots & \\ \mathbf{h}^{[k]}(l) & t \equiv (l-1)(N_t-1)^{k-1}+1, \ldots, l(N_t-1)^{k-1} \left(\mathrm{mod}(N_t-1)^k\right) \\ \vdots & \\ \mathbf{h}^{[k]}(N_t-1) & t \equiv (N_t-2)(N_t-1)^{k-1}+1, \ldots, (N_t-1)^k-1 \left(\mathrm{mod}(N_t-1)^k\right) \end{cases} \tag{2.16}$$

where $t \in \left\{1, 2, \ldots, (N_t-1)^K\right\}$.

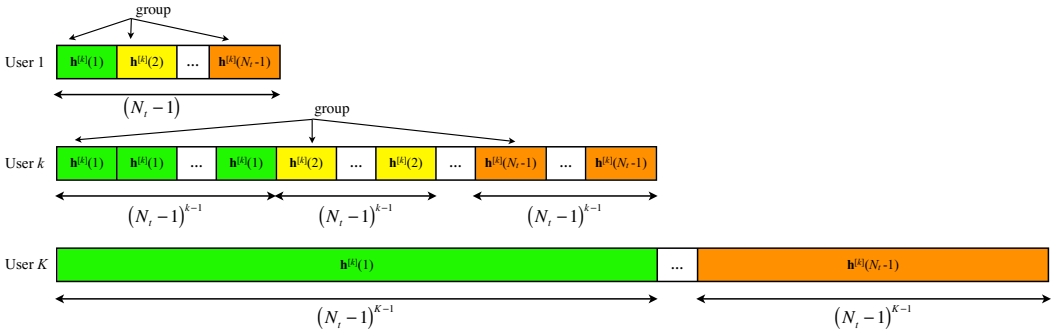

FIGURE 2.8: Staggering of the Building blocks for the N_t, K-user MISO BC.

2.3.3.2 Design of the Beamforming Matrices

With the structure of Block 1 determined, the design of the beamforming matrices can be carried out. The key idea is to create non-overlapping alignment blocks where the channel state of the desired user changes while all the other users remain constant. Taking into consideration the supersymbol structure, it is easy to satisfy this condition with only forming *groups* of symbol extensions within each building block where the channel state changes among $N_t - 1$ preset modes. The last symbol extension to complete each alignment block is provided in Block 2. Besides, the independence between alignment blocks is guaranteed by using orthogonality. For example, checking the equation (2.10), the symbols of the k-th users $\mathbf{u}_\ell^{[k]}$ are orthogonally separated, i.e. they are allocated to different columns in the beamforming matrices. Therefore, the ℓ-th symbol of the k-th user, $\mathbf{u}_\ell^{[k]}$, is transmitted during each alignment block, which corresponds to the ℓ-th column of the beamforming matrix.

Focused on the k-th user, it can be seen that each building block occupies $(N_t-1)^k$ symbol extensions. Since each building block is composed by sub-blocks of $(N_t-1)^{k-1}$ slots, each user k forms a group with each building block during the slots

$$i, i+(N_t-1)^{k-1}, \ldots, i(N_t-2)(N_t-1)^{k-1}, \tag{2.17}$$

where $i \in \left\{1, 2, \ldots, (N_t-1)^{k-1}\right\}$.

As can be seen in Figure 2.8, the building block of user k is repeated $(N_t-1)^{K-k}$ times. Therefore, following the supersymbol structure, the ℓ-th group in the p-th building block of the user k is located in the symbol extensions

$$\left\{(p-1)(N_t-1)+\kappa(N_t-1)^{k-1}\right\}_{\kappa=0}^{N_t-2} \tag{2.18}$$

where $\ell \in \left\{1, 2, \ldots, (N_t-1)^{k-1}\right\}$ and $p \in \left\{1, 2, \ldots, (N_t-1)^{K-k}\right\}$.

2.3.4 Design of Block 2

Block 2 can be easily determined from the design of Block 1. Recall that each group in Block 1 contains N_t-1 symbol extensions corresponding to distinct channel modes. The purpose of Block 2 is to complete each group of each user providing an additional symbol extension with the N_t-th channel mode. Since there are $(N_t-1)^{K-1}$ alignment blocks per user, it comprises

$$\mathcal{L}_{\text{Block2}} = K(N_t-1)^{K-1} \tag{2.19}$$

symbol extensions. Block 2 can be divided in K sub-blocks comprising $(N_t-1)^{K-1}$ symbol extensions each as Figure 2.9 shows. For the k-th user each alignment block is completed by selecting the preset mode $\mathbf{h}^{[k]}(N_t)$ during the symbol extensions

$$\left\{\mathcal{L}_{\text{Block1}} + \frac{(k-1)\mathcal{L}_{\text{Block2}}}{K} + \ell\right\}_{\ell=1}^{\frac{\mathcal{L}_{\text{Block2}}}{K}}, \tag{2.20}$$

where $k = \{1, 2, \ldots, K\}$.

Orthogonal transmission is employed during Block 2 to ensure the independence between the desired symbols and the interference. As we have seen in the previous toy examples,

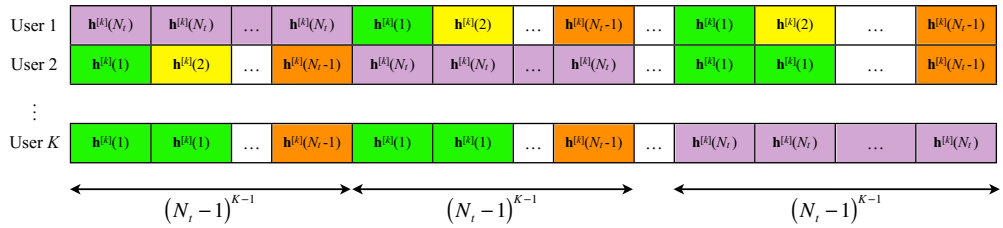

FIGURE 2.9: Block 2 of the BIA supersymbol for the $N_t = 2$ MISO BC.

all other users take advantage of the transmission of the symbols $\mathbf{u}_\ell^{[k]}$, $\ell \in \{1, 2, \ldots, (N_t - 1)^{K-1}\}$, in Block 2 to measure the interference subspace received because of transmission to user k. According to (2.18) the transmission of $\mathbf{u}_\ell^{[k]}$ takes place during the i-th group, $i = 1, \ldots, (N_t - 1)^k$ of the p-th building block, $p = 1, \ldots, (N_t - 1)^{K-k}$, of user k. Thus the channel state of the users $j = 1, \ldots, k-1, k+1, \ldots, K$ in the k-th sub-block in Block 2 equals to

$$g_j\left((p-1)(N_t-1)^k + i\right), \tag{2.21}$$

where $g_j(\cdot)$ is the temporal correlation function of user j given by (2.16).

2.3.5 Achievable Degrees of Freedom

For the general case, where the transmitter is equipped with N_t antennas serving K active users, the BIA scheme described in this chapter generates $(N_t - 1)^{K-1}$ alignment blocks per each user. Since each alignment blocks provides N_t DoF, $N_t \times K \times (N_t - 1)^{K-1}$ DoF are attained by using BIA over a supersymbol that comprises

$$\mathcal{L}_{\text{BIA}} = (N_t - 1)^K + K(N_t - 1)^{K-1} \tag{2.22}$$

symbol extensions. Therefore, the normalized sum-DoF per symbol extension achieved by BIA in the MISO BC is

$$\text{DoF}_{\text{sBIA}} = \frac{N_t K (N_t - 1)^K}{(N_t - 1)^K + K(N_t - 1)^{K-1}} = \frac{N_t K}{N_t + K - 1}. \tag{2.23}$$

Notice that DoF achieved in (2.23) coincides with the information-theoretic outer bound for the MISO BC in absence of CSIT derived in [62].

2.4 Achievable Rates

Until now this chapter has been focused on the achievable DoF in the MISO BC by using BIA. This section is devoted to obtain the closed-form expressions of the achievable rates of BIA at finite SNR. For the general case, each alignment block is composed of N_t symbol extensions where the channel state changes among N_t preset modes. Recall that the first $N_t - 1$ symbol extensions of each alignment block are provided by Block 1, and therefore are subject to $K - 1$ terms of interference. The last element of each alignment block is transmitted in Block 2, where orthogonal transmission of each symbol is carried out. According to the BIA scheme, the $K - 1$ interference terms received in the first $N_t - 1$ symbol extensions of the alignment block can be measured in Block 2 and removed afterwards. Notice that although the interference is completely canceled, a noise increase because of the interference subtraction has to be considered in the first $N_t - 1$ elements of each alignment block. Thus, the signal of the user k after zero forcing during a generic alignment block ℓ can be written as

$$\tilde{\mathbf{y}}^{[k]} = \begin{bmatrix} \tilde{y}^{[k]}[1] \\ \vdots \\ \tilde{y}^{[k]}[N_t - 1] \\ \tilde{y}^{[k]}[N_t] \end{bmatrix} = \begin{bmatrix} \mathbf{h}^{[k]}(1)^T \\ \vdots \\ \mathbf{h}^{[k]}(N_t - 1)^T \\ \mathbf{h}^{[k]}(N_t)^T \end{bmatrix} \mathbf{u}_\ell^{[k]} + \begin{bmatrix} z^{[k]}[1] - \sum_{j=1, j\neq k}^{K} z^{[k]}[j] \\ \vdots \\ z^{[k]}[N_t - 1] - \sum_{j=1, j\neq k}^{K} z^{[k]}[j] \\ z^{[k]}[N_t] \end{bmatrix}. \quad (2.24)$$

Note that for simplicity, the temporal index refers to the position of the symbol extension in the alignment block instead of referring the position in supersymbol. As can be seen, each user can decode N_t DoF by solving a $N_t \times N_t$ equation system given by

$$\tilde{\mathbf{y}}^{[k]} = \mathbf{H}^{[k]} \mathbf{u}_\ell^{[k]} + \tilde{\mathbf{z}}^{[k]}, \quad (2.25)$$

where

$$\mathbf{H}^{[k]} = \begin{bmatrix} \mathbf{h}^{[k]}(1)^T & \mathbf{h}^{[k]}(2)^T & \dots & \mathbf{h}^{[k]}(N_t)^T \end{bmatrix}^T \in \mathbb{C}^{N_t \times N_t} \quad (2.26)$$

is the channel matrix of the user k, $\mathbf{u}_\ell^{[k]} \in \mathbb{C}^{N_t \times 1}$ is the desired symbol, and $\tilde{\mathbf{z}}^{[k]} \sim \mathcal{CN}(0, \mathbf{R}_{\tilde{\mathbf{z}}})$ is the noise vector after the interference subtraction where

$$\mathbf{R}_{\tilde{\mathbf{z}}} = \begin{bmatrix} K\mathbf{I}_{N_t - 1} & \mathbf{0} \\ \mathbf{0} & 1 \end{bmatrix}. \quad (2.27)$$

Besides, the ratio of alignment blocks per user over the entire supersymbol must be taken into consideration. Since there exist $(N_t-1)^{K-1}$ alignment blocks per each user, this ratio is given by

$$B_r = \frac{(N_t-1)^{K-1}}{\mathcal{L}_{\text{BIA}}} = \frac{(N_t-1)^{K-1}}{(N_t-1)^K + K(N_t-1)^{K-1}} = \frac{1}{N_t+K-1}. \tag{2.28}$$

2.4.1 Uniform Power Allocation

Following a logical design, equal power allocation to each symbol in both Block 1 and Block 2 is assumed. Note that during Block 1 N_tK symbols are transmitted in each time slot because of the simultaneous transmission while only N_t symbols per slot are transmitted orthogonally in Block 2. Since the average power constraint in the transmitter is $E\left\{\|\mathbf{x}[t]\|^2\right\} \leq P$, the power allocated to each symbol is

$$\begin{aligned} P_{str} &= \frac{\mathcal{L}_{\text{BIA}}}{N_tK\mathcal{L}_{\text{Block1}} + N_t\mathcal{L}_{\text{Block2}}}P \\ &= \frac{(N_t-1)^K + K(N_t-1)^{K-1}}{N_tK(N_t-1)^K + N_tK(N_t-1)^{K-1}}P = \frac{N_t+K-1}{N_t^2K}P. \end{aligned} \tag{2.29}$$

Therefore, assuming uniform power allocation to each symbol, the normalized rate of the user k is

$$\begin{aligned} R^{[k]} &= B_r\,\mathbb{E}\left[\log\det\left(\mathbf{I} + P_{str}\mathbf{H}^{[k]}{\mathbf{H}^{[k]}}^H{\mathbf{R}_{\tilde{\mathbf{z}}}}^{[k]^{-1}}\right)\right] \\ &= \frac{1}{N_t+K-1}\mathbb{E}\left[\log\det\left(\mathbf{I} + \frac{N_t+K-1}{N_t^2K}P\mathbf{H}^{[k]}{\mathbf{H}^{[k]}}^H{\mathbf{R}_{\tilde{\mathbf{z}}}}^{-1}\right)\right]. \end{aligned} \tag{2.30}$$

2.4.2 Optimizing the Power Allocation

Different amount of symbols are transmitted in each symbol extension of Block 1 and Block 2. In consequence, the power allocation strategy should take into consideration this variation between both blocks. Let us denote π as the ratio of the power allocated to each symbol in Block 1 over the assigned to each symbol in Block 2. This ratio can be modified in order to optimize the power allocation strategy.

For illustrative purposes consider the K-users case where the transmitter is equipped with $N_t = 2$ antennas. The supersymbol is shown in Figure 2.4 and the corresponding beamforming matrices are given by (2.6) and (2.7). The signal received in the first

symbol extension is composed by the sum of K symbols transmitted as $\frac{1}{\sqrt{\pi}}\mathbf{u}_\ell^{[k]}$. Following the described BIA design, the interference in each of the first $N_t - 1$ elements of each alignment block is completely subtracted by using $K-1$ symbol extensions from Block 2. Thus, the signal after zero forcing can be written now as

$$\tilde{\mathbf{y}}^{[k]} = \begin{bmatrix} \tilde{y}^{[k]}(1) \\ \tilde{y}^{[k]}(2) \end{bmatrix} = \begin{bmatrix} \left(\frac{1}{\sqrt{\pi}} y^{[k]}(1) - \sum_{\rho=1,\rho\neq k}^{K} y^{[k]}(\rho) \right) \\ y^{[k]}(k+1) \end{bmatrix}. \tag{2.31}$$

Note that taking into account the power allocation strategy the noise is given by the vector $\tilde{\mathbf{z}}^{[k]} \sim \mathcal{CN}\left(0, \mathbf{R}_{\tilde{\mathbf{z}}}\right)$ where the covariance matrix is $\mathbf{R}_{\tilde{\mathbf{z}}} = \text{diag}\left(\frac{1}{\pi} + K - 1, 1\right)$.

For the general case the interference subtraction follows the same steps as in the example described below. Hence, the covariance matrix of the noise after interference subtraction is

$$\mathbf{R}_{\tilde{\mathbf{z}}} = \begin{bmatrix} \left(\frac{1}{\pi} + K - 1\right) \mathbf{I}_{N_t - 1} & \mathbf{0} \\ \mathbf{0} & 1 \end{bmatrix}. \tag{2.32}$$

Besides, the average power allocated to each symbol is now given by

$$P_{str} = \frac{\mathcal{L}_{BIA}}{N_t K \pi \mathcal{L}_{block1} + N_t \mathcal{L}_{block2}} P = \frac{N_t + K - 1}{N_t K \left((N_t - 1)\pi + 1\right)} P. \tag{2.33}$$

Thus, the normalized rate per symbol extension of user k depending on the ratio π is

$$R^{[k]} = \frac{1}{N_t + K - 1} \mathbb{E}\left[\log\det\left(\mathbf{I} + \frac{N_t + K - 1}{N_t K \left((N_t - 1)\pi + 1\right)} \mathbf{H}^{[k]} \mathbf{H}^{[k]\,H} \mathbf{R}_{\tilde{z}}^{-1} \right) \right]. \tag{2.34}$$

where $\mathbf{H}^{[k]}$ and $\mathbf{R}_{\tilde{\mathbf{z}}}$ are given by (2.26) and (2.32), respectively.

2.4.3 Constant Power Allocation

Constant power allocation is proposed in [95]. It is demonstrated that the optimal[2] power strategy at finite SNR is achieved when the same power is assigned to each slot of the supersymbol, i.e. $\pi^{-1} = K$. In other words, it does not exist power fluctuation between Block 1 and Block 2. For this particular case, the covariance matrix of the noise

[2] Assuming that CSIT is not available also to design the power allocation strategy.

after interference subtraction is given by using $\pi^{-1} = K$ in (2.32)

$$\mathbf{R}_{\tilde{\mathbf{z}}} = \begin{bmatrix} (2K-1)\mathbf{I}_{N_t-1} & \mathbf{0} \\ \mathbf{0} & 1 \end{bmatrix}, \tag{2.35}$$

and the normalized rate per symbol extension of the k-th user reduces to

$$R^{[k]} = \frac{1}{N_t + K - 1}\mathbb{E}\left[\log\det\left(\mathbf{I} + \frac{P}{N_t}\mathbf{H}^{[k]}\mathbf{H}^{[k]H}\mathbf{R}_{\tilde{\mathbf{z}}}{}^{-1}\right)\right], \tag{2.36}$$

with $\mathbf{R}_{\tilde{\mathbf{z}}}$ given by (2.36).

2.5 Simulation Results

The achievable sum-DoF by using BIA depending on the number of active users is depicted in Figure 2.10. First of all, it is interesting to remark that 1 sum-DoF is achievable when basic blind schemes such as orthogonal times or frequency division are employed. Therefore, BIA outperforms clearly the classical blind schemes. Besides, the sum-DoF grows asymptotically to the maximum multiplexing gain $\min(N_t, K)$ as the number of users increases. This effect results more remarkable when the transmitter is equipped with less antennas. Considering that the transmitter serves $K = 10$ users, it can be seen that for the $N_t = 2$ case BIA achieves 1.82 DoF, only 0.18 DoF below the optimal assuming perfect CSIT knowledge, i.e. 2 DoF. However, the achievable sum-DoF is 2 DoF below the maximum achieved with CSIT for $N_t = 6$ when the same amount of users is served. On the other hand, it is 3 DoF above the sum-DoF achievable with orthogonal time or frequency division.

The length of the supersymbols for different values of N_t is shown in Figure 2.11. Note that the length of the supersymbol is directly related with the required coherence time of the system. For $N_t = 2$ the supersymbol grows linearly with the number of active users. Thus, for $N_t = 2$ the coherence time is not a considerable limiting factor. However, as the number of transmit antennas increases, the length of the supersymbol grows exponentially with the number of users. Hence, we conclude that coherence time can be a limiting factor when using BIA. This issue will be discussed in detail in Chapter 6.

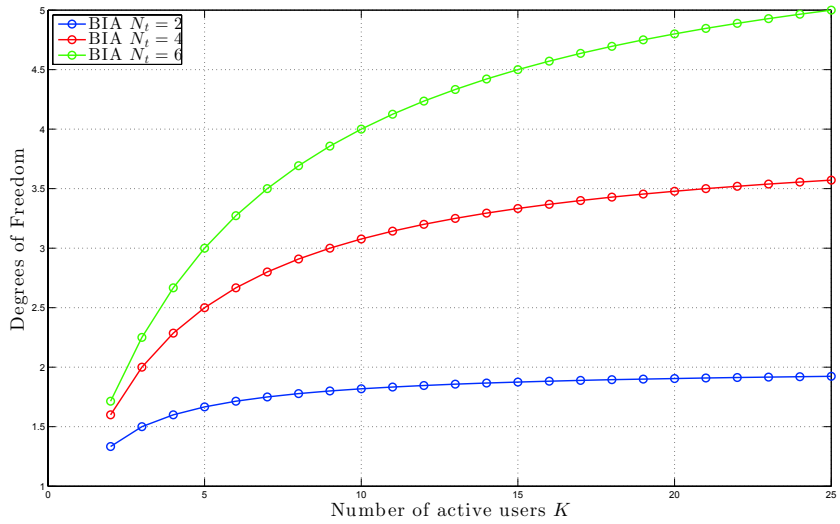

FIGURE 2.10: Achievable sum-DoF by using BIA.

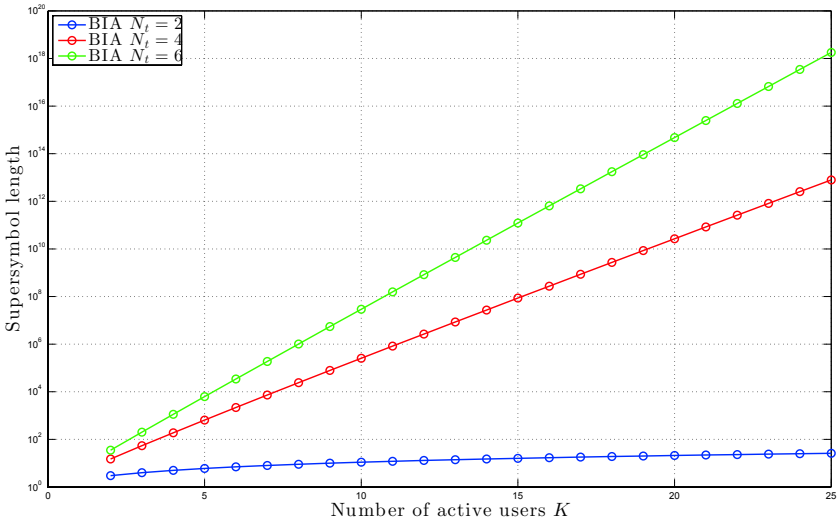

FIGURE 2.11: Supersymbol length of BIA.

Once BIA has been analyzed in DoF terms, we consider the performance of BIA in the medium SNR regime. Figure 2.12 shows the achievable sum-rate of BIA obtained when uniform and constant power allocation are used. Besides, the SU-MISO performance is depicted for comparison purposes. For the same parameters it is shown that constant power allocation outperforms uniform power allocation, which are labeled as improved and original BIA, respectively. Furthermore, it can be seen that the benefits of improved BIA increase with larger N_t and K.

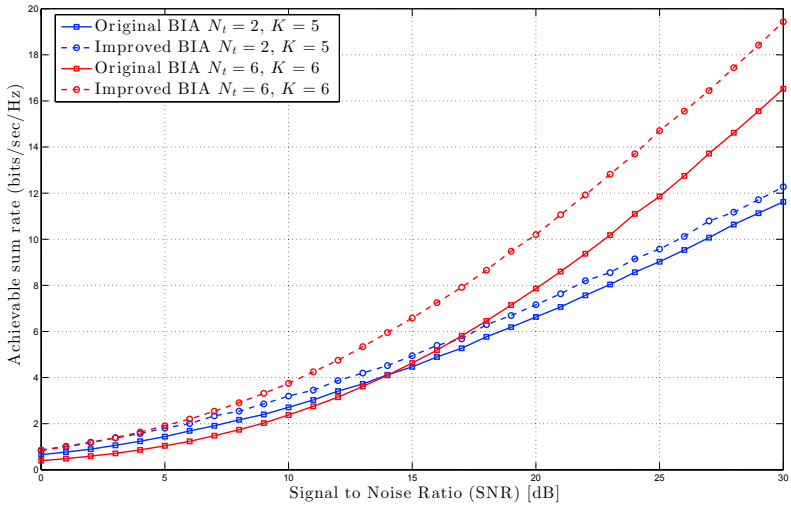

FIGURE 2.12: Achievable sum-rate in the finite SNR regime.

2.6 Conclusions

In this chapter, we describe the BIA transmission scheme for the MISO BC. After analyzing some toy examples in detail, we describe the methodology to build a BIA supersymbol and its corresponding beamforming matrices. We show that the BIA supersymbol can be differentiated between two parts referred to as Block 1 and Block 2, where simultaneous and orthogonal transmission is carried out, respectively. We show that the interference received during Block 1 can be removed by measuring the interference subspace in Block 2. It is proved that the presented BIA scheme achieves $\frac{N_t K}{N_t+K-1}$ DoF when the transmitter is equipped with N_t antennas serving K single-antenna users, which corresponds to the optimal DoF achievable in the compound MISO BC. At this point, recall that traditional blind approaches divide the transmission resource, either time or frequency, in K slices, and therefore they only achieve 1 sum-DoF divided between K users. In contrast, as the numbers of users goes to infinity, the sum-DoF tends to N_t when using BIA. In other words, BIA achieves a growth in DoF with respect to the amount of users.

Although BIA results optimal in sum-DoF for the MISO BC in absence of CSIT, we derive the achievable rates of BIA at finite SNR. Besides, several power allocation strategies are proposed assuming that CSIT is not available. It is shown that constant power

allocation over the entire supersymbol instead of uniform power for each symbols obtains a considerable improvement in the achievable sum-rate. It is interesting to remark that the interference subtraction inherent in the BIA scheme involves a noise increase. Furthermore, it has been assumed that the coherent time is large enough to consider the channel constant during the entire supersymbol. In this sense, limited SNR and channel variations are the two main hurdles to overcome for the implementation of BIA in practical channel. This issue is analyzed in detail during Chapter 6.

Chapter 3

Blind Interference Alignment for Homogeneous Cellular Networks

This chapter evaluates the performance of BIA in cellular networks when the topology is unknown. Although BIA is optimal in DoF for the MISO BC, its implementation in cellular networks is not straightforward. The effects of intercell interference are analyzed in detail for several cellular scenarios. Furthermore, a fully cooperative BIA scheme is proposed to cancel the interference in a straightforward way. It is demonstrated that this approach neither results suitable for cellular networks where users are partially connected to the set of BSs. The influence of the network topology in the achievable DoF is discussed as a conclusion of the features of either isolated or cooperative transmission schemes.

3.1 Introduction

Blind Interference Alignment was originally proposed for the BC. For cellular networks, it can be implemented in a straightforward way with only considering each BS as an isolated transmitter. However, notice that the original BIA scheme does not handle the interference from other transmitters. In other works, although BIA cancels the intracell interference, the effects of intercell interference are still unknown when it is used in cellular environments. The implementation of standard BIA (sBIA) in cellular scenarios is analyzed considering aspects such as power allocation, resource allocation,

and supersymbol mis-alignments in [95]. It is shown that although some quantity of intercell interference can be removed with only synchronizing the supersymbols of each cell, it is not completely canceled, and therefore, users are subject to its influence. In consequence, users located close to the cell edge achieve poor rates because of the transmission in the neighboring BSs. In [96] ways to apply sBIA to cellular networks by using resource allocation such as FR are discussed. The results are compared with the performance achieved by transmission schemes based on CSIT knowledge such as LZFB. Taking into consideration the costs of providing CSIT, it is shown that BIA outperfoms the rates of LZFB in most of the proposed scenarios.

Examining a traditional cellular network, users located close to the cell edge receive a strong signal from several BSs. Therefore, it results obvious that sBIA is sub-optimal in DoF. In order to maximize the achievable DoF over the entire cellular system, a straightforward approach would be to implement BIA over a fully cooperative network (cBIA), i.e. as in a network MIMO. Assuming a cellular scenario where N_{BS} BSs are equipped with N_t antennas each, $M = N_{BS} \times N_t$ transmit antennas are available in the considered network. If K_{tot} active users are located over the coverage area of the whole network, $\frac{MK_{tot}}{M+K_{tot}-1}$ DoF are potentially achievable when using cBIA. Notice that this cooperative approach results costly in practice because of the need for data sharing among the BSs.

In this chapter we analyze the performance of both approaches, each BS transmitting either independently of all other BS or in a cooperative fashion. Several scenarios are considered when each BS transmits independently as in a MISO BC, concluding that intercell interference is one of the main hurdles to overcome for the implementation of BIA in cellular networks. In this sense, this is one of the principal motivations of this work. On the other hand, the drawbacks of fully cooperative approaches are pointed out. The role of the network topology in absence of CSIT is presented at the end of this chapter. Following the idea of [69], it is shown that knowledge of the network topology allows to differentiate the users between subject to intercell interference and users that can treat this interference optimally as noise [66]. This idea motivates the following chapters, where partial connectivity is treated as a resource instead of a limitation.

The contributions of this chapter can be summarized as follows

- The cellular system model based on receivers equipped with reconfigurable antennas is presented in this chapter.
- We evaluate the effects of the intercell interference in cellular scenarios when BIA is implemented in each BS independently of the remaining BSs, i.e. as in MISO BC. It is demonstrated that the achievable rates are heavily limited by the transmission in the neighboring cells.
- A fully cooperative BIA scheme is presented in order to manage the intercell interference. It is demonstrated that cooperative approaches are not DoF optimal for cellular scenarios in absence of CSIT. Indeed, full connectivity between each user and the whole set of BSs jointly to extremely large coherence time are required to implement BIA based on full cooperation among the BSs.
- We present the role of the network topology when CSIT is not available. It is shown that there exists a trade-off between isolated and cooperative transmission depending on connectivity of each user. This conclusion will motivate the following chapters of this work.

3.2 System Model

Consider a cellular network as is shown in Figure 3.1 consisting of N_{BS} BS $\mathcal{N} = \{1, 2, \ldots, N_{BS}\}$. Each BS n, $n \in \mathcal{N}$, is equipped with $N_{t,n}$ transmit antennas and wishes to send data to the set of $\mathcal{K}_{cell,n} = \{1, 2, \ldots, K_{cell,n}\}$ users located within its coverage area. Each user is equipped with one reconfigurable antenna that can switch among $N_{t,n}$ preset modes. Let us denote $l^{[k,n]}[t]$ as the antenna mode selected by user k located in cell n at time t. Assuming that the BSs transmit independently to their corresponding users, the vector $\mathbf{h}^{[k,n,n']}(l) = \left[h_1^{[k,n,n']}(l)^T \quad \cdots \quad h_{N_{t,n'}}^{[k,n,n']}(l)^T\right]^T \in \mathbb{C}^{N_{t,n'} \times 1}$ contains the channel coefficients between the $N_{t,n'}$ antennas of BS n' and the single-antenna user k at preset mode $l^{[k,n]}[t]$ in cell n. Note that since constant channel is assumed, the temporal index has been omitted and the channel only depends on the mode selected by the corresponding user. Thus, the signal received by the user k in cell n at time t

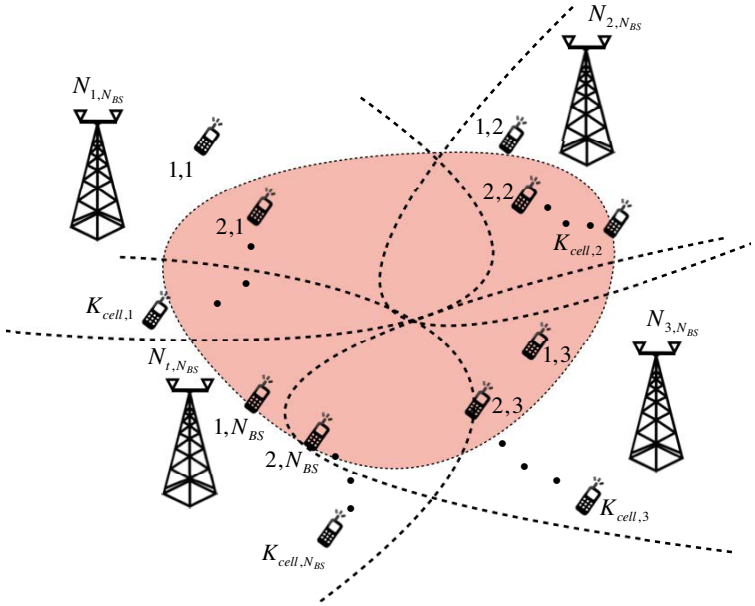

FIGURE 3.1: Cellular system where N_{BS} BSs are deployed transmitting independently. Each BS is equipped with $N_{t,n}$ antennas and sends messages to its corresponding $K_{cell,n}$ users.

can be written as

$$y^{[k,n]}[t] = \mathbf{h}^{[k,n,n]}(l^{[k,n]}[t])^T\mathbf{x}^{[n]}[t] + \underbrace{\sum_{\substack{n'=1\\n'\neq n}}^{N_{BS}} \sqrt{\alpha_{n'}^{[k,n]}}\mathbf{h}^{[k,n,n']}(l^{[k,n]}[t])^T\mathbf{x}^{[n']}[t]}_{\text{intercell interference}} + z^{[k,n]}[t], \quad (3.1)$$

where $\mathbf{x}^{[n]}[t] \in \mathbb{C}^{N_{t,n}\times 1}$ is the signal sent by BS n at time t, $\sqrt{\alpha_{n'}^{[k,n]}}$ is the relative power of the signal of BS n' received at user k,n taking the power of the signal received from BS n as reference, i.e. $\alpha_n^{[k,n]} = 1$, and $z^{[k,n]}[t] \sim \mathcal{CN}(0,1)$ is AWGN.

We also assume that the channel input is subject to an average power constraint for all $t \geq 1$ and $n \in \mathcal{N}$, $E\left\{\|\mathbf{x}^{[n]}[t]\|^2\right\} \leq P$. Furthermore, the channels between each user and the BSs are considered to be drawn from a continuous distribution, so that they are linearly independent almost surely. We also assume that the switching pattern functions $l^{[k,n]}[t]$ are initially predetermined and are known to everyone in the system. On the contrary, we assume that the transmitters do not have any channel state information. Moreover, as in other works addressing the design of BIA schemes in different settings, e.g. [89, 95, 96], we assume that the physical channels stay constant across a sufficient number of time or frequency slots. For simplicity, we focus on the temporal dimension,

without loss of generality. Hence, from now on each symbol extension t corresponds to a time slot. The application of the scheme along frequency slots is straightforward.

3.3 Standard Blind Interference Alignment

Consider a cellular network where each BS n transmits independently of the remaining BSs, $n' \neq n$, to its corresponding $K_{cell,n}$ active users. Besides, it is assumed that transmission by BS $n = 1$ is our cell of interest while the rest of BSs are sources of intercell interference. Under this condition we describe three different scenarios

- The remaining BSs are equipped with the same number of antennas $N_{t,n} = N_t$ serving the same amount of active users K_{cell} in each cell. Furthermore, the supersymbols of each cell are synchronized, and therefore, each BS transmits the same beamforming structure.
- The set of interfering BSs are equipped with N_t antennas and they also transmit to K_{cell} users in each cell. However, the supersymbols are not synchronized and each BS transmits different beamforming in each time slot.
- The interference sources comprise zero-mean i.i.d. vector samples. That is, only the statistics of the inference are known.

3.3.1 Synchronous Aligned Supersymbol

For illustrative purposes consider a two-cell scenario as shown in Figure 3.2. Each BS is equipped with $N_t = 2$ antennas and $K_{cell} = 2$ users are located in the coverage area of each cell. Besides, the supersymbols employed in each cell are synchronized and the signal transmitted by BS n, $n \in \{1, 2\}$ is

$$\mathbf{X}^{[n]} = \begin{bmatrix} \mathbf{x}^{[n]}[1] \\ \mathbf{x}^{[n]}[2] \\ \mathbf{x}^{[n]}[3] \end{bmatrix} = \begin{bmatrix} \mathbf{I} \\ \mathbf{I} \\ \mathbf{0} \end{bmatrix} \mathbf{u}_1^{[1,n]} + \begin{bmatrix} \mathbf{I} \\ \mathbf{0} \\ \mathbf{I} \end{bmatrix} \mathbf{u}_1^{[2,n]}, \tag{3.2}$$

where $\mathbf{x}^{[n]}[t] \in \mathbb{C}^{N_t \times 1}$ is the signal transmitted by the BS n in the time slot t, and $\mathbf{u}_\ell^{[k,n]} \in \mathbb{C}^{N_t \times 1}$ is the symbol, which contains N_t DoF, transmitted to user k in cell n

during its ℓ-th alignment block. Recall that only one alignment block is assigned to each user when $N_t = 2$, therefore, $\ell = \{1\}$ for this particular case.

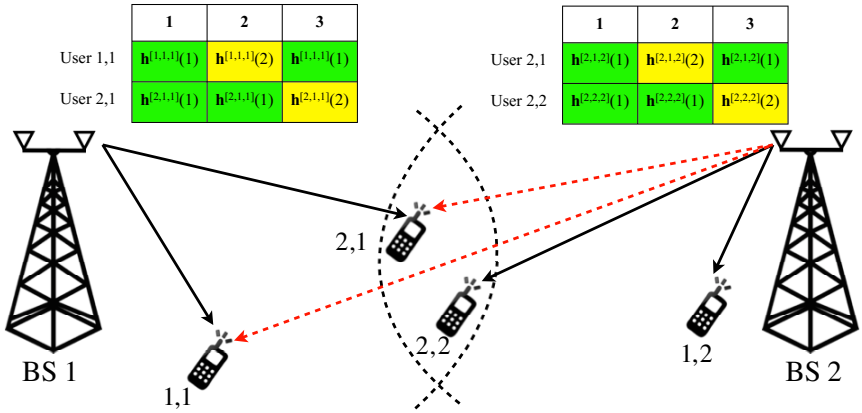

FIGURE 3.2: Toy example: downlink scenario with BSs transmitting aligned super-symbols. The BSs are equipped with $N_t = 2$ antennas and serve $K_{cell} = 2$ users each. For the sake of simplicity only the intercell interference has been depicted from BS 2 to users in cell 1 with red dotted lines.

Under this assumption the signal received at user 1 in cell n can be written as

$$\begin{aligned} y^{[1,n]}[1] &= \mathbf{h}^{[1,n,n]}(1)\left(\mathbf{u}_1^{[1,n]} + \mathbf{u}_1^{[2,n}\right) + \sqrt{\alpha_{n'}^{[1,n]}}\mathbf{h}^{[1,n,n']}(1)\left(\mathbf{u}_1^{[1,n']} + \mathbf{u}_1^{[2,n']}\right) \\ y^{[1,n]}[2] &= \mathbf{h}^{[1,n,n]}(2)\mathbf{u}_1^{[1,n]} + \sqrt{\alpha_{n'}^{[1,n]}}\mathbf{h}^{[1,n,n']}(2)\mathbf{u}_1^{[1,n']} \\ y^{[1,n]}[3] &= \mathbf{h}^{[1,n,n]}(1)\mathbf{u}_1^{[2,n]} + \sqrt{\alpha_{n'}^{[1,n]}}\mathbf{h}^{[1,n,n']}(1)\mathbf{u}_1^{[2,n']}. \end{aligned} \tag{3.3}$$

Following the sBIA scheme described in Chapter 2, user 1 at cell n can remove the intracell interference because of the transmission of $\mathbf{u}^{[2,n]}$. Thus, since each BS transmits independently of all other BSs, i.e. as in a MISO BC, the interference due to $\mathbf{u}_1^{[2,n]}$ is measured in symbol extension 3 and subtracted from symbol extension 1. However, the third symbol extension is also polluted by intercell interference. Curiously, notice that intercell interference because of the transmission of $\mathbf{u}_1^{[2,n']}$, $n' \neq n$, is also measured in symbol extension 3 and, therefore, it is also subtracted. Thus, the signal of user 1 at cell n after zero-forcing is

$$\tilde{\mathbf{y}} = \begin{bmatrix} \mathbf{h}^{[1,n,n]}(1) \\ \mathbf{h}^{[1,n,n]}(2) \end{bmatrix} \mathbf{u}_1^{[1,n]} + \sqrt{\alpha_{n'}^{[1,n]}} \begin{bmatrix} \mathbf{h}^{[1,n,n']}(1) \\ \mathbf{h}^{[1,n,n']}(2) \end{bmatrix} \mathbf{u}_1^{[1,n']} + \begin{bmatrix} z^{[1,n]}[1] - z^{[1,n]}[3] \\ z^{[1,n]}[2] \end{bmatrix}. \tag{3.4}$$

Note that the intercell interference because of the transmission of $\mathbf{u}_1^{[2,n']}$ has been also

canceled, whereas the interference due to $\mathbf{u}_1^{[1,n']}$ still remains. Intuitively, symbol extension 3 takes effect as a *sink of interference* when both supersymbols are synchronized. Although some amount of intercell interference can be removed, the equation system (3.4) shows that the decoding process of each symbol is subject to the strength of the received intercell interference.

Taking into consideration the supersymbol structure and its corresponding beamforming matrices given by (2.16) and (2.18), respectively, it can be seen that Block 2 operates as a sink of interference when the supersymbols of the distinct BSs are aligned. However, intercell interference between users with the same index k still remains. That is, k-th user in cell n is affected by the interference because of transmission of $\mathbf{u}_\ell^{[k,n']}$ from all other BSs $n' \neq n$. Checking the generic BIA alignment block (2.24), the signal $\tilde{\mathbf{y}}^{[k,n]} \in \mathbb{C}^{N_t \times 1}$ after zero-forcing interference cancellation is given by

$$\tilde{\mathbf{y}}^{[k,n]} = \mathbf{H}^{[k,n,n]}\mathbf{u}_\ell^{[k,n]} + \sum_{\substack{n'=1 \\ n' \neq n}}^{N_{BS}} \sqrt{\alpha_{n'}^{[k,n]}}\mathbf{H}^{[k,n,n']}\mathbf{u}_\ell^{[k,n]} + \tilde{\mathbf{z}}^{[k,n]}, \tag{3.5}$$

where

$$\mathbf{H}^{[k,n,n']} = \left[\mathbf{h}^{[k,n,n']}(1)^T \quad \cdots \quad \mathbf{h}^{[k,n,n']}(N_t)^T\right] \in \mathbb{C}^{N_t \times N_t} \tag{3.6}$$

is the channel matrix that contains the channel coefficients between user k located in cell n and BS n', and $\tilde{\mathbf{z}}^{[k,n]} \sim \mathcal{CN}(0, \mathbf{R}_{\tilde{\mathbf{z}}})$ is the noise vector after zero-forcing with $\mathbf{R}_{\tilde{\mathbf{z}}}$ given by the power allocation strategy defined in (2.27), (2.32) or (2.35). Therefore, assuming synchronization among the supersymbols of each cell, the normalized rate per symbol extension of the user k in cell n is

$$R^{[k,n]} = \frac{1}{N_t + K - 1}\mathbb{E}\left[\log\det\left(\mathbf{I} + P_{str}\mathbf{H}^{[k,n,n]}\mathbf{H}^{[k,n,n]H}\mathbf{R}_{\tilde{\mathbf{z}}_\mathbf{I}}{}^{-1}\right)\right], \tag{3.7}$$

where $\mathbf{H}^{[k,n,n']}$ is given by (3.6), P_{str} is the average power allocated to each stream defined in (2.33), and $\mathbf{R}_{\tilde{\mathbf{z}}_\mathbf{I}}$ is the noise plus interference covariance matrix given by

$$\mathbf{R}_{\tilde{\mathbf{z}}_\mathbf{I}} = \mathbf{R}_{\tilde{\mathbf{z}}} + P_{str}\sum_{n=1, n\neq n'}^{N_{BS}} \alpha_{n'}^{[k,n]}\mathbf{H}^{[k,n,n']}\mathbf{H}^{[k,n,n']H}. \tag{3.8}$$

3.3.2 Synchronous Non Aligned Supersymbol

Assume now the same scenario as in the previous case where each BS is equipped with $N_t = 2$ antennas serving $K = 2$ users. In contrast, the supersymbols in each cell are not aligned as is shown in Figure 3.3. For illustrative purposes consider a mis-alignment of 1 slot for users in cell 2. That is, taking the cell 1 as reference, Block 1 transmission occurs in the second symbol extension in cell 2 while Block 2 is transmitted during the first and third symbol extensions. For this specific case, the signal received by user 1 at cell 1 is

$$\begin{aligned} y^{[1,1]}[1] &= \mathbf{h}^{[1,1,1]}(1)\left(\mathbf{u}_1^{[1,1]} + \mathbf{u}_1^{[2,1}\right) + \sqrt{\alpha_2^{[1,1]}}\mathbf{h}^{[1,1,2]}(1)\mathbf{u}_1^{[2,2]} \\ y^{[1,1]}[2] &= \mathbf{h}^{[1,1,1]}(2)\mathbf{u}_1^{[1,1]} + \sqrt{\alpha_2^{[1,1]}}\mathbf{h}^{[1,1,2]}(2)\left(\mathbf{u}_1^{[1,2]} + \mathbf{u}_1^{[2,2]}\right) \\ y^{[1,1]}[3] &= \mathbf{h}^{[1,1,1]}(1)\mathbf{u}_1^{[2,1]} + \sqrt{\alpha_2^{[1,1]}}\mathbf{h}^{[1,1,2]}(1)\mathbf{u}_1^{[1,2]}. \end{aligned} \tag{3.9}$$

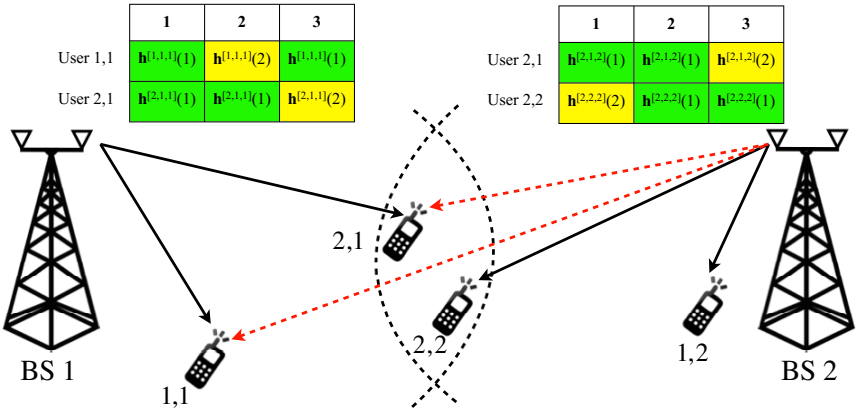

FIGURE 3.3: Toy example: downlink scenario with BSs transmitting not aligned supersymbols. The BSs are equipped with $N_t = 2$ antennas and serve $K_{cell} = 2$ users each. For the sake of simplicity only the intercell interference has been depicted from BS 2 to users in cell 1 with red dotted lines.

Following the sBIA design, user 1 at cell 1 cancels the intracell interference due to transmission of $\mathbf{u}_1^{[2,1]}$ by measuring it during the third symbol extension. Thus, the

signal of user 1 at cell 1 after zero-forcing is given by

$$\tilde{\mathbf{y}}^{[1,1]} = \begin{bmatrix} y^{[1,1]}[1] - y^{[1,1]}[3] \\ y^{[1,1]}[2] \end{bmatrix} = \begin{bmatrix} \mathbf{h}^{[1,1,1]}(1) \\ \mathbf{h}^{[1,1,1]}(2) \end{bmatrix} \mathbf{u}_1^{[1,1]} + \sqrt{\alpha_2^{[1,1]}} \begin{bmatrix} \mathbf{h}^{[1,1,2]}(1) \left(\mathbf{u}_1^{[2,2]} - \mathbf{u}_1^{[1,2]} \right) \\ \mathbf{h}^{[1,1,2]}(2) \left(\mathbf{u}_1^{[1,2]} + \mathbf{u}_1^{[2,2]} \right) \end{bmatrix} + \begin{bmatrix} z^{[1,1]}[1] - z^{[1,1]}[3] \\ z^{[1,1]}[2] \end{bmatrix}. \tag{3.10}$$

As can be seen, the decoding process of the symbol $\mathbf{u}_1^{[1,1]}$ is subject to the strength of the intercell interference. Comparing with (3.4), two terms of interference remain in this case instead of one. Note that the third symbol extension at cell 1 is polluted by interference from the neighboring BS, which employs this symbol extension to transmit the additional symbol extension for completing the alignment block of symbol $\mathbf{u}_1^{[1,2]}$. Therefore, although intracell interference is removed, the subtracting process involves adding another interference term because of $\mathbf{u}_1^{[1,2]}$ transmission[1]. Checking the structure of both supersymbols, it is interesting to remark that the two terms of interference in the second slot of (3.10) are due to the supersymbol mis-alignment. Since Block 1 of cell 2 is transmitted during the second symbol extension, which is employed for the transmission of $\mathbf{u}_1^{[1,1]}$ in Block 2, the sum of $\mathbf{u}_1^{[1,2]} + \mathbf{u}_1^{[2,2]}$ is received in this symbol extension of cell 1.

Similarly, the signal received after zero-forcing for user 2 in cell 1 is given by

$$\tilde{\mathbf{y}}^{[2,1]} = \begin{bmatrix} y^{[2,1]}[1] - y^{[2,1]}[2] \\ y^{[2,1]}[3] \end{bmatrix} = \begin{bmatrix} \mathbf{h}^{[2,1,1]}(1) \\ \mathbf{h}^{[2,1,1]}(2) \end{bmatrix} \mathbf{u}_1^{[2,1]} + \sqrt{\alpha_2^{[2,1]}} \begin{bmatrix} -\mathbf{h}^{[2,1,2]}(1)\mathbf{u}_1^{[1,2]} \\ \mathbf{h}^{[2,1,2]}(2)\mathbf{u}_1^{[1,2]} \end{bmatrix} + \begin{bmatrix} z^{[2,1]}[1] - z^{[2,1]}[2] \\ z^{[2,1]}[3] \end{bmatrix}. \tag{3.11}$$

Notice that in this case, only one term of interference because of transmission from the neighboring BS appears in (3.11). We can check that Block 1 of cell 2 is positioned now in a symbol extension employed by user 2 in cell 1 to measure its intracell interference and remove it from the first symbol extension. Therefore, the interference because of $\mathbf{u}_1^{[2,2]}$ is subtracted in $y^{[2,1]}[1]$ while the term $-\mathbf{u}_1^{[1,2]}$ appears just due to this subtraction.

[1]Note that if transmission of $\mathbf{u}_1^{[2,2]}$ occurs in the same symbol extension the supersymbols would be aligned.

Furthermore, the third symbol extension is employed for transmission of the Block 2 in both cells. Therefore, this symbol extension only contains one term of intercell interference. In consequence, and in contrast to (3.10), the second slot employed to complete the alignment block of $\mathbf{u}_1^{[2,1]}$ only contains one term of interference.

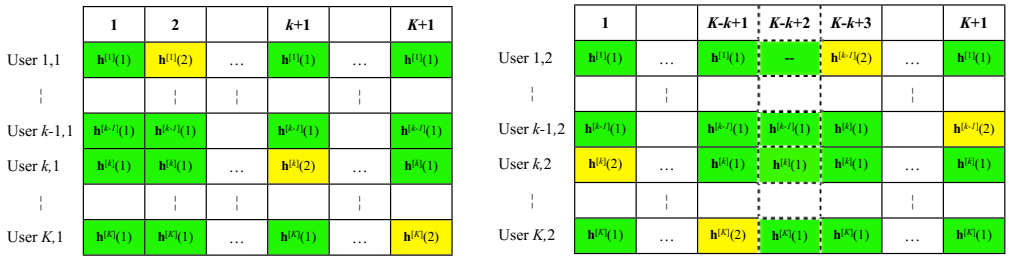

FIGURE 3.4: Supersymbols employed in both cells. Taking the cell 1 as reference, a delay of k symbol extensions is considered in the supersymbol of cell 2. For the sake of simplicity, the channel index refers to the k-th user in each cell.

As we have shown there exist two specific cases for the two-cell scenario when the BSs are equipped with $N_t = 2$ antennas and the supersymbols are not aligned. This idea can be easily extended to the K-users case. Taking the supersymbol of cell 1 as reference, without loss of generality, let us assume a mis-alignment of k symbol extensions in the supersymbol of cell as shown in Figure 3.4. Since each BS is managed independently from all other BSs, the signal transmitted in each cell is given by (2.6) and (2.7) , i.e. as in a MISO BC. Similarly to the case described in (3.10), we can check that Block 1 of cell n' interferes in the symbol extension $k+1$, which is used by user k in cell n to complete its alignment block. Although this additional symbol extension does not contain any term of interference in the MISO BC BIA scheme, for the considered toy example the user k in cell n receives the sum of K terms of interference because of transmission in the neighboring cell during this additional symbol extension. In consequence, the last elements of each alignment block of the user k in cell n are polluted by the aforementioned K terms of interference. Besides, taking into consideration the interference subtraction of sBIA, $K-1$ interference terms appear in the first element of the vector $\tilde{\mathbf{y}}^{[k,n]}$ while the interference received before interference subtraction still remains. In other words, the Block 2 is a *source of interference* because of the subtraction process inherent in BIA schemes, instead of a sink of interferences as occurs when the supersymbols are synchronized. Thus, the received signal after zero-forcing interference

cancellation during a generic alignment block at user k in cell n can be written as

$$\tilde{\mathbf{y}}^{[k,n]} = \mathbf{H}^{[k,n,n]}\mathbf{u}_1^{[k,n]} + \sqrt{\alpha_{n'}^{[k,n]}}\mathbf{H}^{[k,n,n']}\left(\mathbf{u}_1^{[j,n']} - \sum_{k=1}^{K}\mathbf{u}_1^{[k,n']}\right) + \tilde{\mathbf{z}}^{[k,n]}, \tag{3.12}$$

where $\mathbf{H}^{[k,n,n']} = \left[\mathbf{h}^{[k,n,n']}(1)^T \quad \mathbf{h}^{[k,n,n']}(2)^T\right]^T \in \mathbb{C}^{N_t \times N_t}$ is the channel matrix for the $N_t = 2$ case between user k in cell n and BS n'. Thus, the normalized rate per symbol extension of the user k located in BS n is given by

$$R^{[k,n]} = \frac{1}{N_t + K - 1}\mathbb{E}\left[\log\det\left(\mathbf{I} + P_{str}^{[n]}\mathbf{H}^{[k,n,n]}{\mathbf{H}^{[k,n,n]}}^H{\mathbf{R}_{\tilde{\mathbf{z}}_\mathbf{I}}}^{-1}\right)\right], \tag{3.13}$$

where $\mathbf{R}_{\tilde{\mathbf{z}}_\mathbf{I}}$ is the noise plus interference covariance matrix given by

$$\mathbf{R}_{\tilde{\mathbf{z}}_\mathbf{I}} = \mathbf{R}_{\tilde{\mathbf{z}}} + P_{str}^{[n']}K\sqrt{\alpha_{n'}^{[k,n]}}\mathbf{H}^{[k,n,n']}{\mathbf{H}^{[k,n,n']}}^H, \tag{3.14}$$

and $P_{str}^{[n']}$ and $\mathbf{R}_{\tilde{\mathbf{z}}}$ are given by the power allocation defined in Chapter 2, Section 2.4.2.

On the other hand, all other users in cell n receive the transmission of Block 1 from cell n' during the symbol extensions used for interference subtraction. Remind that if it occurs during Block 1 of cell n' the supersymbols would be aligned. Hence, it is possible to ensure that the last element of each alignment block contains only one term of intercell interference from BS n'. Furthermore, the interference cancellation using BIA involves to subtract $K-1$ interference terms, which in contrast to the MISO BC, are polluted by interference from the neighboring BSs in a cellular scenario. Therefore, the term of interference received before subtraction is removed while $K-1$ new terms of interference appear just due to subtraction of the Block 1 from cell n'. Besides, the additional symbol extension from Block 2 employed to complete each alignment block of users $j \neq k$ are polluted by a unique term of intercell interference. Without loss of generality, let us focus on user 1 in cell n, the signal received during the first slot after zero-forcing is given by

$$\tilde{y}^{[1,n]}[1] = \mathbf{h}^{[1,n,n]}(1)\mathbf{u}_1^{[1,n]} + \sqrt{\alpha_{n'}^{[1,n]}}\mathbf{h}^{[1,n,n']}(1)\left(-2\sum_{\substack{j=1\\ j\neq k}}^{K}\mathbf{u}_1^{[j,n]} - \mathbf{u}_1^{[k+1,n]}\right). \tag{3.15}$$

Thus, the signal after zero-forcing for the j-th user, $j \neq k$, in cell n can be written as

$$\tilde{\mathbf{y}}^{[j,n]} = \mathbf{H}^{[j,n,n']}\mathbf{u}_1^{[k,n]} + \sqrt{\alpha_{n'}^{[j,n]}}\mathbf{H}_{\mathbf{I}}^{[j,n,n']}\mathbf{u}_{\mathbf{I}} + \tilde{\mathbf{z}}^{[j,n]}, \tag{3.16}$$

where

$$\mathbf{H}_{\mathbf{I}}^{[j,n,n']} = \begin{bmatrix} \mathbf{h}^{[j,n,n']}(1) & \mathbf{0} \\ \mathbf{0} & \mathbf{h}^{[j,n,n']}(2) \end{bmatrix} \mathbf{B}_{\mathbf{I}}, \tag{3.17}$$

is the channel matrix of the interfering BS n' taking into consideration the permutation given by the supersymbol mis-alignment that can be formulated by the matrix

$$\mathbf{B}_{\mathbf{I}} = \begin{bmatrix} -2\mathbf{I} & \dots & -2\mathbf{I} & -\mathbf{I} & -2\mathbf{I} & \dots & -2\mathbf{I} \\ \mathbf{0} & \dots & \mathbf{0} & \mathbf{I} & \mathbf{0} & \dots & \mathbf{0} \end{bmatrix} \in \mathbb{C}^{4\times 2K}, \tag{3.18}$$

and

$$\mathbf{u}_{\mathbf{I}} = \begin{bmatrix} \mathbf{u}_1^{[1,n]^T} & \dots & \mathbf{u}_1^{[K,n]^T} \end{bmatrix}^T. \tag{3.19}$$

The vector $\tilde{\mathbf{z}}^{[j,n]} \sim \mathcal{CN}(0, \mathbf{R}_{\tilde{\mathbf{z}}})$ is the noise after zero-forcing where $\mathbf{R}_{\tilde{\mathbf{z}}}$ is the covariance matrix given by (2.32) depending on the power allocation strategy.

Thus, the normalized rate per symbol extension at the user $j \neq k$ in cell n can be written as

$$R^{[k,n]} = \frac{1}{N_t + K - 1}\mathbb{E}\left[\log\det\left(\mathbf{I} + P_{str}^{[n]}\mathbf{H}^{[k,n,n]}\mathbf{H}^{[k,n,n]^H}{\mathbf{R}_{\tilde{\mathbf{z}}_{\mathbf{I}}}}^{-1}\right)\right], \tag{3.20}$$

where $\mathbf{R}_{\tilde{\mathbf{z}}_{\mathbf{I}}}$ is the noise plus interference covariance matrix given by

$$\mathbf{R}_{\tilde{\mathbf{z}}_{\mathbf{I}}} = \mathbf{R}_{\tilde{\mathbf{z}}} + P_{str}^{[n']}\sqrt{\alpha_{n'}^{[j,n]}}\mathbf{H}_{\mathbf{I}}^{[j,n,n']}\mathbf{H}_{\mathbf{I}}^{[j,n,n']}, \tag{3.21}$$

and $P_{str}^{[n]}$ is the power assigned to each stream in the n-th cell given by the power allocation strategies in Chapter 2, Section 2.4.2.

As the number of BSs equipped with $N_t = 2$ antennas increases the procedure shown above can be easily extended. Due to the fact that Block 1 comprises only 1 symbol extension for the $N_t = 2$ case, the analysis of the effects of mis-alignments in the supersymbols in a cellular network is analogous. Likewise, all the possible permutations can be analyzed when $N_t > 2$. However, note that Block 1 comprises $(N_t - 1)^K$ symbol extensions, which is greater than 1 when $N_t > 2$. Since the number of possible permutations grows exponentially with N_t and K, this analysis results prohibitive because

of complexity. As a conclusion, we can assert that mis-alignment of the supersymbols in a cellular scenario lead to a considerable penalty in the achievable rates because of intercell interference.

3.3.3 White Isotropic Interference

Consider a scenario where the source of interference is unidentified and only its statistics are known. An example of this case is a neighboring transmitter using BIA with different parameters N_t or K, or even other transmission schemes such as MU-MISO or IA. It is assumed that the intercell interference can be modelled as a zero-mean vector with identity covariance matrix scaled to the interference strength. Besides, it is also assumed that the interfering sources maintain a constant power during the entire supersymbol. Each stream is transmitted with an average power P_{str} in the cell of interest. Thus, the normalized rate of the user k located in cell n can be written as

$$R^{[k,n]} = \frac{1}{N_t + K - 1}\mathbb{E}\left[\log\det\left(\mathbf{I} + \frac{P_{str}}{1 + \sum_{n'=1, n'\neq n}^{N_{BS}} \alpha_{n'}^{k,n} P_I^{[n']}}\mathbf{H}^{[k,n,n]}\mathbf{H}^{[k,n,n]^H}\mathbf{R}_{\tilde{\mathbf{z}}}{}^{-1}\right)\right], \tag{3.22}$$

where $P_I^{[n']}$ is the power of the interference from the transmitter n' and $\mathbf{R}_{\tilde{\mathbf{z}}}$ is the covariance of the noise after zero-forcing given by the power allocation strategy (2.27), (2.32), or (2.35).

3.3.4 Achievable Degrees of Freedom

The question that arises after analyzing the implementation of BIA independently in each BS in a cellular network is what the achievable DoF are. Following the procedure of other works such as [95] a closed form of the rate (3.7), (3.13), (3.20) and (3.22) when $P \to \infty$ can be easily derived. However, considering the DoF definition

$$\text{DoF} = \lim_{P\to\infty} \frac{R_\Sigma(P)}{\log(P)} \tag{3.23}$$

where $R_\Sigma(P)$ is the sum-rate parametrized by the power P, the achievable sum-DoF would be zero as intercell interference still remains because of the $\log(P)$ term in the denominator.

Assume now that the set of users can be differentiated between users that receive a significant signal from the set of BSs and users close to their corresponding BS. Hence, the first group of users is subject to intercell interference and zero-DoF are achieved by them when intercell interference is not managed. In contrast, users close to their BS are characterized by a high SIR and, therefore, it would be optimal to treat the intercell interference as noise [66, 124]. Thus, assuming partial connectivity the achievable sum-DoF in each cell is given by

$$\mathrm{DoF}_{\mathrm{sBIA}} = \frac{N_t K_p}{N_t + K_p - 1}, \tag{3.24}$$

where K_p is the amount of users that can treat the intercell interference optimally as noise in each cell. The achievable DoF and how the topology influences in partially connected networks is analyzed in detail in Section 3.5 and Chapter 4 is devoted to this issue.

3.4 Fully Cooperative Blind Interference Alignment

Until now we have analyzed the performance of BIA when each BS transmits independently of all other BSs. Furthermore, several cases depending on the kind of source of interference have been analyzed. Even when the supersymbols of the whole set of interfering BSs are synchronized it has been shown that intercell interference remains. With the aim of managing the interference in a cellular scenario in a straightforward way, the BIA scheme can be extended to a fully cooperative BIA (cBIA) scheme. Assuming full cooperation among all BSs, the whole set of transmit antennas send messages to the to $K_{tot} = \sum_{n=1}^{N_{BS}} K_{cell,n}$ users as in network MIMO [22, 125–127], i.e. as only one big BS transmitting to all users.

For the system model described in Section 3.2 there exist $M = \sum_{n=1}^{N_{BS}} N_{t,n}$ antennas transmitting to all $K_{tot} = \sum_{n=1}^{N_{BS}} K_{cell,n}$ users. It is assumed that each user can switch among M preset channel modes. Thus, a cBIA supersymbol can be devised with only replacing $N_t = M$ and $K = K_{tot}$ in (2.16). Similarly, we can obtain the corresponding beamforming matrices and Block 2 of cBIA by using the procedure described in

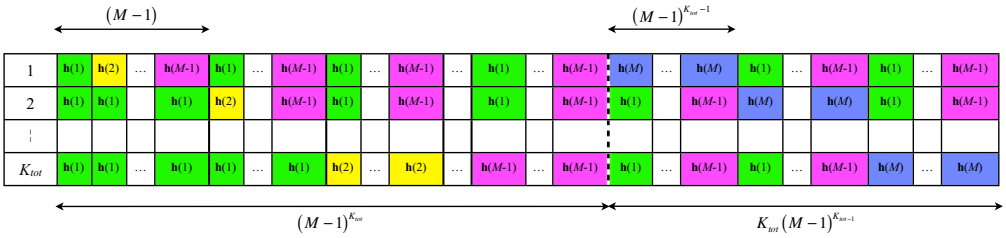

FIGURE 3.5: Supersymbol for the cBIA scheme applied to $M = \sum_{n=1}^{N_{BS}} N_{t,n}$ antennas serving K_{tot} users.

Chapter 2. Hence, the cBIA supersymbol comprises

$$\mathcal{L}_{\text{cBIA}} = (M-1)^{K_{tot}} + K_{tot}(M-1)^{K_{tot}-1} \tag{3.25}$$

symbol extensions.

A generic cBIA supersymbol is shown in Figure 3.5. Note that the user index has been removed from the channel parameter for space issues. It can be seen that each user attains $(M-1)^{K_{tot}-1}$ alignment blocks, each proving M DoF, in the cBIA supersymbol. Note that the channel state of the desired user changes among M channel modes while the state of all other users remains constant during each alignment block. Consider now a generic alignment block for the user k in cell n. Following the BIA scheme, the first $M-1$ symbol extensions of Block 1 are polluted by $K_{tot}-1$ interference terms. Additionally, each alignment block is completed with a symbol extension from Block 2. Hence, the last slot of the alignment block does not contain any interference term. Thus, the signal vector $\mathbf{y}^{[k,n]} = \begin{bmatrix} y^{[k,n]}[1] & \dots & y^{[k,n]}[M] \end{bmatrix}^T \in \mathbb{C}^{M\times 1}$ received by user k in cell n during a given alignment block is

$$\mathbf{y}^{[k]} = \underbrace{\begin{bmatrix} \mathbf{h}^{[k,n]}(1)^T \\ \vdots \\ \mathbf{h}^{[k,n]}(M-1)^T \\ \mathbf{h}^{[k,n]}(M)^T \end{bmatrix}}_{\mathbf{H}^{[k,n]}} \mathbf{u}_{\ell}^{[k,n]} + \underbrace{\begin{bmatrix} \mathbf{h}^{[k,n]}(1)^T \sum_{n'=1}^{N_{BS}} \sum_{\substack{j=1 \\ n'\neq n \& j\neq k}}^{K_{cell,n}} \mathbf{u}_{\ell'}^{[j,n']} \\ \vdots \\ \mathbf{h}^{[k,n]}(M-1)^T \sum_{n'=1}^{N_{BS}} \sum_{\substack{j=1 \\ n'\neq n \& j\neq k}}^{K_{cell,n}} \mathbf{u}_{\ell'}^{[j,n']} \\ \mathbf{0} \end{bmatrix}}_{\text{interference}} + \mathbf{z}^{[k,n]}, \tag{3.26}$$

where

$$\mathbf{h}^{[k,n]}(l) = \left[\sqrt{\alpha_1^{[k,n]}}\mathbf{h}^{[k,n,1]}\left(1\right)^T, \cdots, \sqrt{\alpha_1^{[k,n]}}\mathbf{h}^{[k,n,1]}\left(N_{t,1}\right)^T, \ldots, \mathbf{h}^{[k,n,n]}\left(\sum_{n'=1}^{n} N_{t,n'} + 1\right)^T, \right.$$
$$\left. \ldots, \mathbf{h}^{[k,n,n]}\left(\sum_{n'=1}^{n} N_{t,n'} + N_{t,n}\right)^T, \ldots, \sqrt{\alpha_{N_{BS}}^{[k,n]}}\mathbf{h}^{[k,n,N_{BS}]}(M)^T \right]^T \in \mathbb{C}^{M\times 1}, \tag{3.27}$$

is the channel vector between user k at cell n and the whole set of transmit antennas that form the cooperative network, and $\mathbf{u}_\ell^{[k,n]} \in \mathbb{C}^{M\times 1}$ is the desired symbol to the user k in cell n corresponding to the ℓ-th alignment block. Notice that $\mathbf{u}_\ell^{[k,n]}$ contains M DoF as a contribution from the whole set of BSs. The vector $\mathbf{z}^{[k,n]} \in \mathbb{C}^{M\times 1}$ contains the noise samples received in each slot of the alignment block. For simplicity, the temporal index refers to the position of the symbol extension in the alignment block instead of its position in the supersymbol.

3.4.1 Achievable Rates

Following the BIA scheme described in Chapter 2, the interference terms of (3.26) can be totally removed by measuring them in the appropriate slots in Block 2. Hence, the signal after zero-forcing cancellation at user k in cell n $\tilde{\mathbf{y}}^{[k,n]}$ is given by

$$\tilde{\mathbf{y}}^{[k,n]} = \mathbf{H}^{[k,n]}\mathbf{u}_\ell^{[k,n]} + \tilde{\mathbf{z}}^{[k,n]}, \tag{3.28}$$

where

$$\mathbf{H}^{[k,n]} = \left[\mathbf{h}^{[k,n]}(1)^T \quad \cdots \quad \mathbf{h}^{[k,n]}(M)^T\right]^T \in \mathbb{C}^{M\times M} \tag{3.29}$$

is the channel matrix of user k at cell n when using cBIA, $\mathbf{h}^{[k,n]}(l)$ is defined in (3.27), and $\tilde{\mathbf{z}}^{[k,n]} \sim \mathcal{CN}\left(0, \mathbf{R}_{\tilde{\mathbf{z}}}\right)$ is the noise vector after zero-forcing interference cancellation where

$$\mathbf{R}_{\tilde{\mathbf{z}}} = \begin{bmatrix} K_{tot}\mathbf{I}_{M-1} & \mathbf{0} \\ \mathbf{0} & 1 \end{bmatrix}, \tag{3.30}$$

is the covariance matrix assuming uniform power allocation per symbol. If other power allocation is used, the covariance matrix is given by (2.32) or (2.35) with only replacing $K_{cell} = K_{tot}$. Then as long as the $\{\mathbf{h}^{[k,n]}(l)\}_{l=1}^{M}$ are linearly independent, the M streams

$\mathbf{u}_{\ell}^{[k,n]}$ could be decoded theoretically, assuming full connectivity, by inverting the resulting linear system of (3.28). Therefore, the normalized rate per symbol extension achieved by cBIA for user k in cell n is

$$R^{[k,n]} = \frac{1}{M + K_{tot} - 1} \mathbb{E}\left[\log\det\left(\mathbf{I} + P_{str}\mathbf{H}^{[k,n]}\mathbf{H}^{[k,n]^T}\mathbf{R}_{\tilde{\mathbf{z}}}{}^{-1}\right)\right]. \tag{3.31}$$

It is interesting to remark that $K_{tot} - 1$ interference terms must be subtracted to cancel the interference completely. Recall that only $K_{cell} - 1$ interference terms are subtracted when using sBIA. Therefore, the noise increases $K_{tot} - 1$ times in the first $M - 1$ slots of each alignment block, which penalizes considerably the achievable rates at finite SNR.

3.4.2 Achievable Degrees of Freedom

The described cBIA scheme provides $(M-1)^{K_{tot}-1}$ alignment blocks, containing M DoF each, to each user over a supersymbol that comprises $\mathcal{L}_{\text{cBIA}}$ symbol extensions. Thus, the achievable sum-DoF per symbol extension of cBIA in a cellular network is

$$\text{DoF}_{\text{cBIA}} = \frac{MK_{tot}(M-1)^{K_{tot}-1}}{(M-1)^{K_{tot}} + K_{tot}(M-1)^{K_{tot}-1}} = \frac{MK_{tot}}{M + K_{tot} - 1}. \tag{3.32}$$

It is interesting to remark that the sum-DoF of (3.32) is only achievable assuming full connectivity. That is, each and every user receives a signal strength large enough to decode the messages sent by each BS.

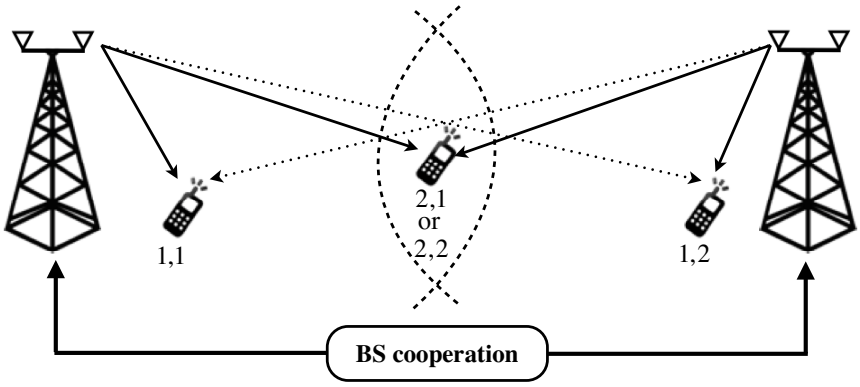

FIGURE 3.6: Two-cell scenario with partial connectivity where each BS is equipped with $N_t = 2$ antennas. Both BSs transmit to $K_{tot} = 3$ users distributed among the network coverage.

For illustrative purposes, consider a toy example as shown in Figure 3.6 where each BS is equipped with $N_t = 2$ antennas. There are $K_{tot} = 3$ users within the coverage area of the whole network. For this setting, and assuming full connectivity of all and each user, cBIA scheme achieves $\frac{4 \cdot 3}{4+3-1} = 2$ DoF by employing a supersymbol comprising $(4-1)^3 + 3 \cdot (4-1)^{3-1} = 54$ symbol extensions.

3.5 Moving to partially connected networks

In this chapter it has been shown that sBIA does not cancel the intercell interference completely. Besides, the achievable DoF per user is limited to only $N_{t,n}$ DoF even if they receive a strong signal from the other BSs, which in fact generate interference at the considered user. On the other hand, the cBIA scheme relies on the assumption of full connectivity, which does not hold in a typical cellular system.

Cellular networks are usually *partially connected* where some users are connected to several BSs, whereas the remaining users located at the inner cell receive a signal from the corresponding BS strong enough to consider the interference from other BSs as noise [66, 124]. Consider now the scenario shown in Figure 3.6, assuming that user 1 within cell n, $n = \{1, 2\}$, cannot decode the signal from the neighboring BS $n' \neq n$. Hence $\frac{2}{4+3-1} = \frac{1}{3}$ DoF are achieved by each inner user while the edge user, which can be labeled as user 2 in either cell 1 or 2, still achieves $\frac{2}{3}$ DoF. In consequence, $\frac{4}{3}$ DoF are achievable in the whole network instead of 2 DoF when partial connectivity is taken into consideration. For a N_{BS} BSs cellular scenario with partial connectivity, the channel of user k in cell n, which can treat the interference from all other BSs $n' \neq n$ optimally as noise, defined in (3.27) can be approximated as

$$\mathbf{h}^{[1,n]}(l) \approx \left[{\mathbf{0}_{a,1}}^T \quad \mathbf{h}^{[k,n,n]}\left(l_{n'}+1\right)^T \quad \dots \quad \mathbf{h}^{[k,n,n]}\left(l_{n'}+N_{t,n}\right)^T \quad {\mathbf{0}_{b,1}}^T \right]^T, \tag{3.33}$$

with $l_{n'} = \sum_{n'=1}^{n} N_{t,n'}$, $a = \sum_{n'=1}^{n-1} N_{t,n'}$, $b = \sum_{n'=n+1}^{N_{BS}} N_{t,n'}$ and $\mathbf{0}_{c,1}$ is a vector of zeros of dimension $c \times 1$. Consequently, the channel matrix that contains the M preset channel modes

$$\mathbf{H}^{[1,n]} = \left[\mathbf{h}^{[1,n]}(1) \quad \dots \quad \mathbf{h}^{[1,n]}(M) \right] \in \mathbb{C}^{M \times 1} \tag{3.34}$$

of the users located close to the BS n is no longer full-rank. Because of this, in (3.28) these users cannot decode the data streams sent by BS n', $n' \neq n$. Therefore, even if

full cooperation between BSs is provided, cBIA fails to achieve the DoF given by (3.32) because of the lack of full connectivity.

Two questions that naturally arise are whether it is possible to devise a scheme that works in a cellular scenario with partial connectivity and what the achievable DoF are. Furthermore, it is interesting to remark that $K_{tot} - 1$ terms of interference must be subtracted when using a full cooperative BIA scheme, which lead to a large noise increment at finite SNR. In the next chapter we propose several schemes based on the knowledge of the network topology. It is shown that the use of the network topology not only allows to devise more suitable BIA schemes for cellular scenarios with partial connectivity, but also attains more DoF than (3.32). In other words, exploiting the topology of the network achieves more DoF than using full cooperation among the BSs. To reach this, we leverage the partial connectivity as a resource that allows to obtain more DoF, and decrease the amount of channel modes required by each user as well as the length of the supersymbol, which is one of the major limitations when applying cBIA in practical systems.

3.6 Simulation Results

The achievable sum-DoF for the sBIA and cBIA schemes in a cellular scenario are depicted in Figures 3.7 and 3.8. As expected, the BIA schemes achieve a growth in the sum-DoF regarding the amount of users. Recall that other traditional blind schemes such as orthogonal resource allocation are subject to sum-DoF equal to 1. For a two-cellular system where each BS is equipped with $N_t = 4$ transmit antennas it can be seen in Figure 3.7 that cBIA overcomes in 0.5 DoF approximately the performance achieved by sBIA. This increase is due to the fact that edge users do not attain zero-DoF by using cooperation among the BSs. However, assuming that only $\frac{1}{3}$ of the users are connected to both BS because of partial connectivity, it can be seen that cBIA is handicapped by the lack of connectivity of private users.

The achievable sum-DoF in a $N_{BS} = 3$ cellular scenario where each BS is equipped with N_t transmit antennas is depicted in Figure 3.8. For this case, it can be seen that cBIA achieve a considerable increase, about 2 DoF, regarding sBIA when full connectivity is assumed. Nevertheless, as occurs in the previous two-cell scenario, this improvement

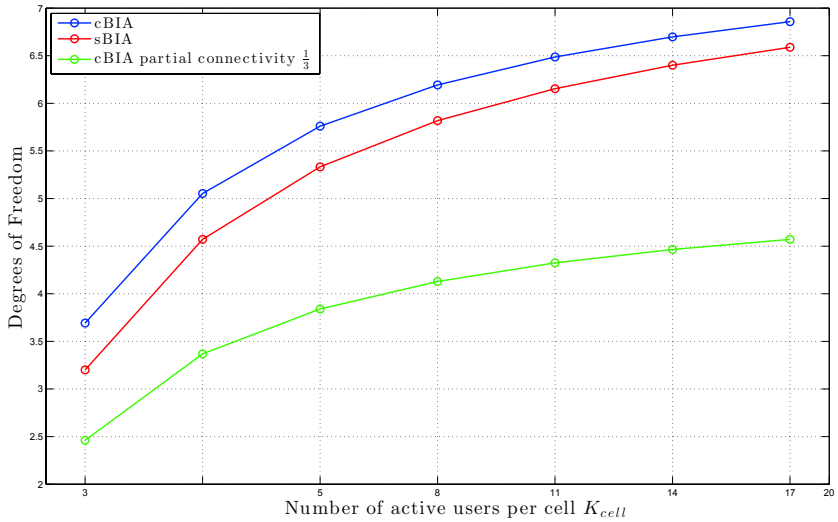

FIGURE 3.7: Achievable sum-DoF for isolated and cooperative BIA schemes. $N_{BS} = 2$ and $N_t = 4$.

results futile when the network topology is taken into consideration. Even if half of the users are connected to the whole set of BSs, the achievable DoF by cBIA are below the performance of treating each cell independently.

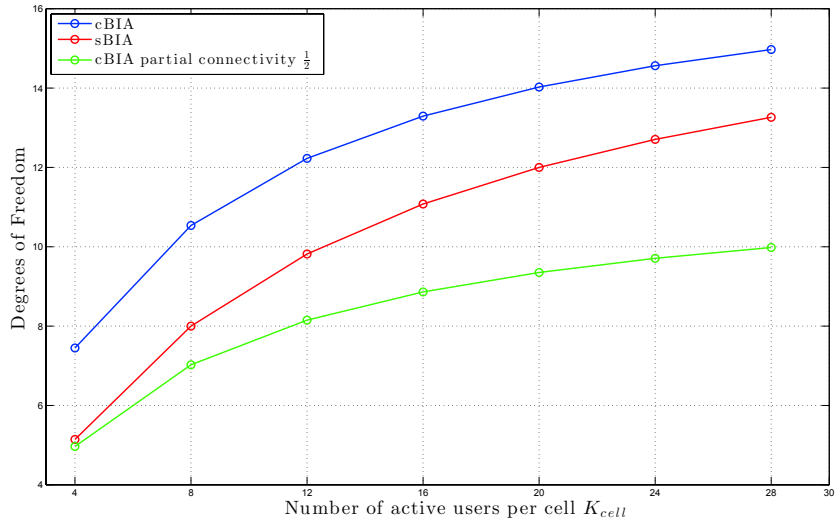

FIGURE 3.8: Achievable sum-DoF for isolated and cooperative BIA schemes. $N_{BS} = 3$ and $N_t = 6$.

Figure 3.9 shows the supersymbol length for sBIA and nBIA in a two-cell scenario when each BS is equipped with $N_t = \{2, 4, 6\}$ transmit antennas. Notice that cBIA requires

extremely large supersymbols. Even if each BS is equipped with only 2 transmit antennas, the supersymbol length is much larger than that of sBIA for 6 transmit antennas. In consequence, cBIA results challenging, or even impossible, to implement in a realistic scenario where the coherence time is a limiting factor.

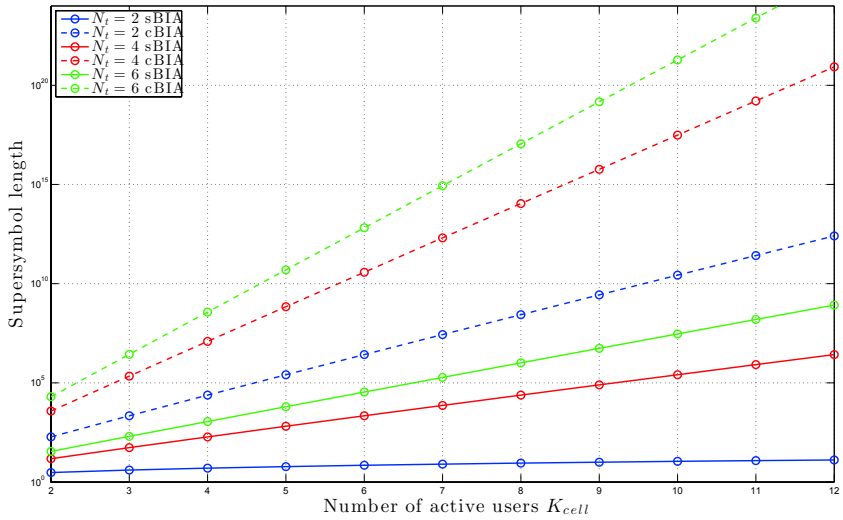

FIGURE 3.9: Supersymbol length for isolated and cooperative BIA schemes.

3.7 Conclusions

The use of BIA schemes in cellular networks has been analyzed in this chapter. It is shown that the achievable DoF and data rates are severely affected by intercell interference when each BS employs BIA transmission independently of the surronding BSs, i.e. as in a MISO BC. In consequence, we can affirm that the implementation of BIA in cellular networks is not straightforward. We have shown that some amount of intercell interference can be canceled when the supersymbols of each cell are aligned. The supersymbols of Block 2 employed for interference measurement are *sinks of interference* when the supersymbols are synchronized. However, the interference because of transmission to users with the same index k in the other cells still remains. Thus, users located in the cell edge achieve a poor performance because of the interference received from the neighboring cells. Furthermore, mis-alignments in the supersymbols of the cells make Block 2 works as source of interference instead of a sink. Thus, the performance of

users subject to intercell interference is heavily limited because of transmission in the neighboring BSs.

With the aim of managing the intercell interference we propose a fully cooperative BIA scheme where the set of BSs transmits as in a cooperative network MIMO. It is shown that full cooperation among the BSs in absence of CSIT results futile because of the lack of full connectivity in cellular networks. Besides, it involves to employ extremely large supersymbols, which require enormous coherence time, and the subtraction of the interference contribution because of transmission to all the other users in the whole network, increasing considerably the noise at finite SNR.

After analyzing both approaches, either isolated or cooperative transmission, the most important conclusion of this chapter is the role of the network topology when CSIT is not available. It has been shown that users located close to their corresponding BSs can treat the intercell interference optimally as noise while users in the cell edge can exploit the multiplexing gain given by the received signal from several BSs. This fact motivates the development of the following chapters.

Chapter 4

Blind Interference Alignment for Homogeneous Cellular Networks based on Network Topology

This chapter analyzes the implementation of BIA in homogeneous cellular scenarios considering the network topology. Assuming partially connected networks, the DoF-region for cellular scenarios in absence of CSIT is derived. It is demonstrated that the knowledge of the network topology is a useful feature that should be treated as a resource instead of a limitation. BIA approaches based on the network topology are devised in this chapter, proving that the outer bound of the DoF region for cellular networks without CSIT is achievable.

4.1 Introduction

The implementation of BIA in cellular networks is not straightforward as we have shown in the previous chapter. On one hand, considering each BS as an isolated transmitter that sends messages only to their corresponding users, i.e. forming a MISO BC, cell edge users achieve a poor performance because of the effects of the intercell interference. On the other hand, the use of full cooperation with the aim of implementing a BIA scheme as in a network MIMO, i.e. the whole set of BSs transmits to each and every user in the network, results futile because of the lack of full connectivity in cellular scenarios.

Besides, both approaches involve several drawbacks such as supersymbol misalignments for sBIA or extremely large supersymbol length and noise increase for cBIA.

Although the DoF in absence of CSIT is well known in many channel configurations such as X channel, BC or IC, the DoF of a cellular network with partial connectivity were still unknown. The DoF of the finite state compound wireless networks are derived in [62]. In [48] the DoF regions for the 2-user MIMO BC and IC are derived when CSIT is not available. A generalization for the K-users case is presented in [49], where the DoF of Broadcast, Interference and Cognitive Channels are derived by using information theory. However, none of these channel configurations corresponds to a cellular network with partial connectivity where transmission to the inner-cell users can be treated as a BC while to the cell-edge users, which receive a strong signal from several BSs, is equivalent to a IC. At this point it is interesting to observe the influence of the network topology in cellular scenarios. For the case considered previously, the whole set of users can be easily differentiated between private users near their corresponding BS who treat intercell interference as noise and shared users at the cell edge who are connected to all BSs in their proximity. In [68, 69] it is demonstrated that the knowledge of the network topology is a powerful tool when CSIT is not available. Indeed, it is shown that interference diversity joint to aligned frequency reuse and index coding provide many opportunities to achieve the optimal DoF in cellular networks.

At first sight, it may appear that partial connectivity lead to a loss in DoF for cellular networks. Interestingly, this is not the case. A major goal of this thesis is to demonstrate that, owing to the partial connectivity, the use of BIA in cellular networks can actually lead to more DoF than if the system were fully connected. In retrospect, this is not surprising. The same way that large path loss can help increase the spectral efficiency by allowing frequency reuse, partial connectivity allows simultaneous transmission of more data streams compared to a fully connected network. As an example, in [66] it is shown that, in a K-users interference channel, there exist scenarios where treating interference as noise achieves all points in the capacity region up to a constant gap, namely it is DoF-optimal.

In this chapter we propose a system model for partially connected cellular networks. We assume that although CSIT is not available, the network topology is known by the BSs. In consequence, the users can be differentiated between private and shared users.

We derive the DoF region in absence of CSIT for partially connected networks. It is demonstrated that, in contrast to orthogonal approaches, a growth in DoF regarding the amount of users deployed in the network is achievable without CSIT. Once we have determined the optimal-DoF achievable in a cellular network in absence of CSIT, the question that arises is, how to reach this performance? At first, we analyze a BIA scheme based on data sharing among the BSs to provide diversity for shared users proposed in [97]. Although intercell interference is canceled for shared users, the sum-DoF is far from the optimal while providing diversity to shared users involves a considerable penalty for the private users. Besides, data sharing requires high-capacity backhaul links among the BSs, which in fact is one of the main issues that BIA schemes try to avoid. In [128], we propose a scheme based on flexible bandwidth allocation to private and shared users that outperforms the sum-rate achieved by BIA providing diversity through data sharing in a wide range of SNR. Basically, the bandwidth is split for each group of users, and therefore, the interference between private and shared users is avoided by transmitting over distinct bandwidth slices. Notice that frequency division is in fact a simple form of interference alignment without CSIT. However, the optimal DoF are not reached because of the orthogonal approach employed to avoid the interference between private and shared users. After that, we develop a network BIA scheme in [129], which is denoted as nBIA, that achieves the optimal-DoF in symmetric cellular networks with partial connectivity. On the other hand, for asymmetric scenarios the achievable sum-DoF are not always the optimal. However, the penalty regarding the optimal is typically small.

The contributions of this chapter can be summarized as follows

- We present the system model for cellular networks with partially connected networks based on reconfigurable antennas at each receiver.
- The information-theoretic DoF region is derived for cellular networks with partial connectivity in absence of CSIT. The converse proof leads to an optimization problem that allows to obtain the sum-DoF in the proposed scenario. Assuming symmetry in the cellular networks, i.e. same amount of users in each cell, we obtain the closed-form expressions of the optimal-DoF.

- The BIA scheme based on data sharing proposed in [97] is analyzed in detail. Besides, we extend this scheme to the N_{BS} BSs cellular scenario. It is demonstrated that the achievable DoF are far from the optimal in partially connected networks.
- With the aim of overcoming the scheme based on data sharing and avoiding the need for high-capacity backhaul links between the BSs, we propose a BIA scheme based on flexible bandwidth allocation [128]. We demonstrate that this approach achieves greater performance than BIA based on data sharing in a wide range of SNR values in several scenarios.
- We develop a network BIA scheme that properly combining the supersymbol structure given by the knowledge of the network topology achieves the optimal-DoF in symmetric scenarios [129]. Moreover, a significant reduction of the supersymbol length is achieved compared to other BIA schemes designed for fully connected networks.
- We propose an extension of the network BIA scheme for asymmetric scenarios that minimizes the loss of DoF because of asymmetric impairments [129].
- We evaluate the performance of the proposed schemes through computer simulations.

4.2 System Model

We consider a partially connected network consisting of N_{BS} BSs $\mathcal{N} = \{1, 2, \ldots, N_{BS}\}$ that want to send a set of messages to K_{tot} users as shown in Figure 4.1. Each BS n, $n \in \mathcal{N}$, has $N_{t,n}$ transmit antennas and wishes to send data to a set of private users $\mathcal{K}_{p,n} = \{p_{1,n}, \ldots, p_{K_{p,n}}\}$ as well as a set of shared users $\mathcal{K}_{sh} = \{sh_1, \ldots, sh_{K_{sh}}\}$ located on the edge of all N_{BS} cells.

Each private user is equipped with one reconfigurable antenna that can switch among $N_{t,n}$ preset modes, whereas each shared user can switch among $M = \sum_{n=1}^{N_{BS}} N_{t,n}$ modes[1]. Therefore, if $l^{[p_{k,n}]}[t]$ denotes the antenna mode of private user $p_{k,n}$ in BS n at time t,

[1] In practice, in a network with user mobility, each user should be able to switch among M preset modes, since it may transition from being private to being shared and vice versa.

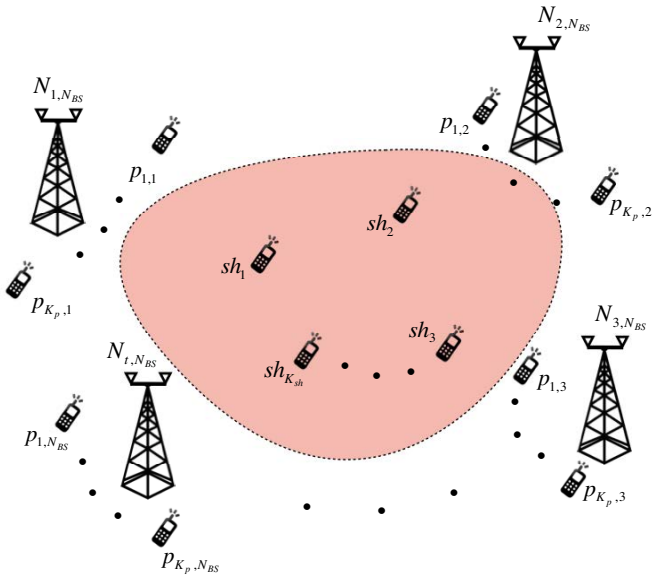

FIGURE 4.1: Cellular system with partial connectivity and N_{BS} BSs. Each BS is equipped with $N_{t,n}$ antennas and serves $K_{p,n}$ private users as well as K_{sh} shared users together with the other BSs.

the signal received by the private user $p_{k,n}$ at time t can be written as

$$y^{[p_{k,n}]}[t] = \mathbf{h}^{[p_{k,n}]}(l^{[p_{k,n}]}[t])^T \mathbf{x}[t] + z^{[p_{k,n}]}[t], \tag{4.1}$$

where $z^{[p_{k,n}]}[t] \sim \mathcal{CN}(0,1)$ is AWGN,

$$\mathbf{x}[t] = \begin{bmatrix} \mathbf{x}^{[1]}[t]^T & \mathbf{x}^{[2]}[t]^T & \cdots & \mathbf{x}^{[N_{BS}]}[t]^T \end{bmatrix}^T \in \mathbb{C}^{M\times 1}, \tag{4.2}$$

and

$$\begin{aligned} \mathbf{h}^{[p_{k,n}]}(l) &= \left[\sqrt{\alpha_1^{[p_{k,n}]}} \mathbf{h}^{[p_{k,n},1]^T}(l) \cdots \quad \mathbf{h}^{[p_{k,n},n]^T}(l) \cdots \quad \sqrt{\alpha_{N_{BS}}^{[p_{k,n}]}} \mathbf{h}^{[p_{k,n},N_{BS}]^T}(l) \right]^T \\ &\approx \begin{bmatrix} \mathbf{0}_{a,1}{}^T & \mathbf{h}^{[p_{k,n},n]^T} & \mathbf{0}_{b,1}{}^T \end{bmatrix}^T \in \mathbb{C}^{M\times 1}, \end{aligned} \tag{4.3}$$

with $M = \sum_{n=1}^{N_{BS}} N_{t,n}$, $a = \sum_{n'=1}^{n-1} N_{t,n'}$, $b = \sum_{n'=n+1}^{N_{BS}} N_{t,n'}$ and $\mathbf{0}_{c,1}$ is a vector of zeros of dimension $c \times 1$. In (4.2), $\mathbf{x}^{[n]}[t] \in \mathbb{C}^{N_{t,n}\times 1}$ is the signal sent by BS n at time t, whereas in (4.3), $\mathbf{h}^{[p_{k,n},n]}(l) = \begin{bmatrix} h_1^{[p_{k,n},n]}(l)^T & \cdots & h_{N_{t,n}}^{[p_{k,n},n]}(l)^T \end{bmatrix}^T \in \mathbb{C}^{N_{t,n}\times 1}$ contains the coefficients between the $N_{t,n}$ antennas of BS n and the single antenna of private user $p_{k,n}$ when its radiation pattern is set to mode $l \in \{1,2,\ldots,N_{t,n}\}$, and $\alpha_{n'}^{[p_{k,n}]}$ is the relative power of the signal of BS n' received at private user $p_{k,n}$ taking the power of the signal received from BS n as reference, i.e. $\alpha_n^{[p_{k,n}]} = 1$. As can be seen in (4.3), we model the

situation where the $K_{p,n} = |\mathcal{K}_{p,n}|$ private users of cell n are close to BS n, and assume that signals received from any other BS $n' \neq n$ are negligible, i.e. $\alpha_{n'}^{[p_{k,n}]} \approx 0$, $n' \neq n$. Thus, no data sharing among the BSs is required to serve the private users, and $\mathbf{x}^{[n']}[t]$ does not contain data intended to any private user $p_{k,n} \in \mathcal{K}_{p,n}$, $n \neq n'$.

Similar to the model for the private users, the signal received by shared user $sh_{k'}$ at time t can be written as

$$y^{[sh_{k'}]}[t] = \mathbf{h}^{[sh_{k'}]}(l^{[sh_{k'}]}[t])^T \mathbf{x}[t] + z^{[sh_{k'}]}[t], \tag{4.4}$$

where, $\mathbf{x}[t]$ is as defined in (4.2) and

$$\mathbf{h}^{[sh_{k'}]}(l) = \left[\mathbf{h}^{[sh_{k'},1]^T}(l) \quad \cdots \quad \sqrt{\beta_{N_{BS}}^{[sh_{k'}]}}\mathbf{h}^{[sh_{k'},N_{BS}]^T}(l)\right]^T \in \mathbb{C}^{M\times 1}, \tag{4.5}$$

$M = \sum_{n=1}^{N_{BS}} N_{t,n}$, $\mathbf{h}^{[sh_{k'},n]}(l) \in \mathbb{C}^{N_{t,n}\times 1}$ denotes the channel between the $N_{t,n}$ antennas of BS n and shared user $sh_{k'}$ for mode l, and $\beta_n^{[sh_{k'}]}$ denotes the relative power of the signal of BS n received at user $sh_{k'}$ taking the power of the signal received from BS 1 as reference, i.e. $\beta_1^{[sh_{k'}]} = 1$. Similarly, $z^{[sh_{k'}]}[t] \sim \mathcal{CN}(0,1)$ is AWGN. We use the index k' instead of k to distinguish from private users. Note that, unlike the observation model (4.3) for private users, in (4.5) it is assumed that shared users can receive signals from all BSs because of their location in the network. As a result, the task of sending data to the shared users can be jointly undertaken by the N_{BS} BSs.

We also assume that the channel input is subject to an average power constraint given by $E\left\{\|\mathbf{x}^{[n]}[t]\|^2\right\} \leq P$ for all $t \geq 1$ and $n \in \mathcal{N}$. Furthermore, the channels between each user, whether private or shared, and the BSs are considered to be drawn from a continuous distribution, so that they are linearly independent almost surely. We also assume that the switching pattern functions $l^{[p_{k,n}]}[t]$ and $l^{[sh_{k'}]}[t]$ are initially predetermined and are known to everyone in the system. On the contrary, we assume that the transmitters do not have any channel state information. Moreover, as in other works addressing the design of BIA schemes in different settings, e.g. [89, 95, 96], we assume that the physical channels stay constant across a sufficient number of time or frequency slots. For simplicity, we focus on the temporal dimension, without loss of generality. Hence, from now on each symbol extension t corresponds to a time slot. The application of the scheme along frequency slots is straightforward.

4.3 Information-theoretic sum-DoF Outer Bound of the Cellular Scenario with Partial Connectivity

Once the system model of a cellular network with partial connectivity has been determined, we analyze it from the information theory point of view. The goal of this section is to obtain an outer bound of the sum-DoF for the scenario shown in Figure 4.1. The following converse is developed along the lines of [130]. For simplicity, the two-cell scenario is considered. However, the proof can be easily extended to the case of N_{BS} BSs.

Consider two BSs equipped with $N_{t,1}$ and $N_{t,2}$ antennas, which transmit to $K_{p,1}$ and $K_{p,2}$ private users, respectively, while K_{sh} shared users are served simultaneously by both BSs. The messages sent by the transmitter n to their $K_{p,n}$ private users are denoted as $W^{[p_{1,n}]}, W^{[p_{2,n}]}, \ldots, W^{[p_{K_p,n}]}$ generating the rates in each user $R^{[p_{1,n}]}, R^{[p_{2,n}]}, \ldots, R^{[p_{K_p,n}]}$, respectively; the messages and the rates of the shared users are denoted as $W^{[sh_1]}, W^{[sh_2]}$, $\ldots, W^{[sh_{K_{sh}}]}$ and $R^{[sh_1]}, R^{[sh_2]}, \ldots, R^{[sh_{K_{sh}}]}$, respectively. Accordingly, we express the sum-rate as $R_\Sigma = R_{\Sigma p_1} + R_{\Sigma p_2} + R_{\Sigma sh} = \sum_{n=1}^{2} \sum_{k=1}^{K_{p,n}} R^{[p_{k,n}]} + \sum_{k'=1}^{K_{sh}} R^{[sh_{k'}]}$. Similarly, the DoF of the private user k in cell n is denoted as $d^{[p_{k,n}]}$ while the DoF of shared user k' is denoted as $d^{[sh_{k'}]}$. Thus, the sum-DoF of each set of private users in cell n and the shared users is given by $d_{\Sigma p_n} = \sum_{k=1}^{K_{p,n}} d^{[p_{k,n}]}$ and $d_{\Sigma sh} = \sum_{k'=1}^{K_{sh}} d^{[sh_{k'}]}$, respectively.

We also define the message sets

$$\mathcal{W}^{[p_n]} = \left\{ W^{[p_{1,n}]}, W^{[p_{2,n}]}, \ldots, W^{[p_{K_p,n}]} \right\} \tag{4.6}$$

with $n \in \{1, 2\}$, and

$$\mathcal{W}^{[sh]} = \left\{ W^{[sh_1]}, W^{[sh_2]}, \ldots, W^{[sh_{K_{sh}}]} \right\}. \tag{4.7}$$

as the whole set of messages for private users in cell n and shared users, respectively.

Let us focus on private user $p_{1,1}$ in cell 1, who desires to receive the message $W^{[p_{1,1}]}$. In particular, consider $N_{t,1}$ random realizations, each corresponding to a different realization of the channel. Because of the lack of CSIT, and requiring reliable decoding (probability of error approaching zero), each realization of the user should also have probability of error approaching zero. According to(4.1) and (4.3) the signal received

$$
\begin{aligned}
nN_{t,1}R^{[p_{1,1}]} \leq & nN_{t,1}\log(P) - \sum_{l=1}^{N_{t,1}} h\left(\left(y_l^{[p_{1,1}]}\right)^n \mid W^{[p_{1,1}]}\right) + o(n) + n\,o(\log(P)) && (4.10)\\
\leq & nN_{t,1}\log(P) - h\left(\left(y_1^{[p_{1,1}]},\ldots,y_{N_{t,1}}^{[p_{1,1}]}\right)^n \mid W^{[p_{1,1}]}\right) + o(n) + n\,o(\log(P)) && (4.11)\\
\leq & nN_{t,1}\log(P) - h\left(W^{[p_{2,1}]},\ldots,W^{[p_{K_p,1}]},\left(y_1^{[p_{1,1}]},\ldots,y_{N_{t,1}}^{[p_{1,1}]}\right)^n \mid W^{[p_{1,1}]}\right)\\
& + h\left(W^{[p_{2,1}]},\ldots,W^{[p_{K_p,1}]} \mid \left(y_1^{[p_{1,1}]},\ldots,y_{N_{t,1}}^{[p_{1,1}]}\right)^n, W^{[p_{1,1}]}\right)\\
& + o(n) + n\,o(\log(P)) && (4.12)\\
\leq & nN_{t,1}\log(P) - h\left(W^{[p_{2,1}]},\ldots,W^{[p_{K_p,1}]}\right) - h\left(\left(y_1^{[p_{1,1}]},\ldots,y_{N_{t,1}}^{[p_{1,1}]}\right)^n \mid \mathcal{W}^{[p_1]}\right)\\
& + \underbrace{h\left(W^{[p_{2,1}]},\ldots,W^{[p_{K_p,1}]} \mid \left(y_1^{[p_{1,1}]},\ldots,y_{N_{t,1}}^{[p_{1,1}]}\right)^n, W^{[p_{1,1}]}\right)}_{\leq n\,o(\log(P))}\\
& + o(n) + n\,o(\log(P)) && (4.13)\\
\leq & nN_{t,1}\log(P) - n(R_{\Sigma p_1} - R^{[p_{1,1}]}) - h\left(\left(y_1^{[p_{1,1}]},\ldots,y_{N_{t,1}}^{[p_{1,1}]}\right)^n \mid \mathcal{W}^{[p_1]},\mathcal{W}^{[p_2]}\right)\\
& + o(n) + n\,o(\log(P)). && (4.14)
\end{aligned}
$$

by user $p_{1,1}$ during the l-th realization at time t can be written as

$$
y_l^{[p_{1,1}]}[t] = \mathbf{h}_l^{[p_{1,1},1]^T}\mathbf{x}_l^{[1]}[t] + z_l^{[p_{1,1}]}, \tag{4.8}
$$

where $l \in \{1,2,\ldots,N_{t,1}\}$ and the i.i.d Gaussian noise terms have been normalized to have unit variance.

Applying Fano's inequality to codebooks spanning n channel uses, we have

$$
\begin{aligned}
nR^{[p_{1,1}]} \leq & I\left(W^{[p_{1,1}]};\left(y_l^{[p_{1,1}]}\right)^n\right) + o(n)\\
= & h\left(\left(y_l^{[p_{1,1}]}\right)^n\right) - h\left(\left(y_l^{[p_{1,1}]}\right)^n \mid W^{[p_{1,1}]}\right) + o(n)\\
\leq & n\left(\log(P) + o(\log(P))\right) - h\left(\left(y_l^{[p_{1,1}]}\right)^n \mid W^{[p_{1,1}]}\right) + o(n), && (4.9)
\end{aligned}
$$

where P is the total transmit power constraint at each BS. Since this is true for every $l \in \{1,2,\ldots,N_{t,1}\}$, in (4.10) we add the inequalities corresponding to all $N_{t,1}$ realizations. For steps (4.11)-(4.13), we use $h(A,B) \leq h(A)+h(B)$, $h(A,B|C) = h(A|BC)+h(B|C)$ and the independence between any pair of messages. To justify step (4.13)-(4.14), from $\left[y_1^{[p_{1,1}]},\ldots,y_{N_{t,1}}^{[p_{1,1}]}\right]$, first notice that we have $N_{t,1}$ linear equations in the $N_{t,1}$ transmitted symbols $\mathbf{x}^{[1]} = \left[x_{1,1}^{[1]},\ldots x_{1,N_{t,1}}^{[1]}\right]$, each subject to additive noise whose variance does

$$
\begin{aligned}
n(N_{t,1}R^{[p_{1,1}]} + N_{t,2}R^{[p_{1,2}]}) \leq & n(N_{t,1}+N_{t,2})\log(P) - n(R_{\Sigma p_1} + R_{\Sigma p_2} - R^{[p_{1,1}]} - R^{[p_{1,2}]}) \\
& - h\left(\left(y_1^{[p_{1,1}]},\ldots,y_{N_{t,1}}^{[p_{1,1}]}\right)^n, \left(y_1^{[p_{1,2}]},\ldots,y_{N_{t,2}}^{[p_{1,2}]}\right)^n \mid \mathcal{W}^{[p_1]}, \mathcal{W}^{[p_2]}\right) \\
& + o(n) + n\,o(\log(P)) \qquad (4.16) \\
\leq & n(N_{t,1}+N_{t,2})\log(P) - n(R_{\Sigma p_1} + R_{\Sigma p_2} - R^{[p_{1,1}]} - R^{[p_{1,2}]}) \\
& - nR_{\Sigma sh} + o(n) + n\,o(\log(P)). \qquad (4.17)
\end{aligned}
$$

not depend on P. Since the channel realizations are random, these linear equations are almost surely linearly independent, i.e. one can recover $\mathbf{x}^{[1]}$ from these equations, subject to noise distortion. However, from $\mathbf{x}^{[1]}$ and noise the messages intended for the users in cell 1 that originate at BS 1 can be recovered. Thus, the remaining uncertainty is just due to noise, which is no more than $o(\log(P))$ per channel use. Moreover, in (4.13)-(4.14) we use the fact that conditioning cannot increase the entropy.

Proceeding similarly for private user $p_{1,2}$ in cell 2,

$$
\begin{aligned}
nN_{t,2}R^{[p_{1,2}]} \leq & nN_{t,2}\log(P) - n(R_{\Sigma p_2} - R^{[p_{1,2}]}) - h\left(\left(y_1^{[p_{1,2}]},\ldots,y_{N_{t,2}}^{[p_{1,2}]}\right)^n \mid \mathcal{W}^{[p_1]}, \mathcal{W}^{[p_2]}\right) \\
& + o(n) + n\,o(\log(P)).
\end{aligned} \qquad (4.15)
$$

Adding (4.14) and (4.15), we obtain (4.16)-(4.17). Step (4.16)-(4.17) is justified as follows. From $\left(y_1^{[p_{1,1}]},\ldots,y_{N_{t,1}}^{[p_{1,1}]}\right)^n$ and $\left(y_1^{[p_{1,2}]},\ldots,y_{N_{t,2}}^{[p_{1,2}]}\right)^n$ we have $N_{t,1}+N_{t,2}$ generic linear equations subject to noise distortion, which are almost surely linearly independent and can therefore be solved to recover $N_{t,1}+N_{t,2}$ input symbols from both BSs, subject to noise distortion. Thus, within a $n\,o(\log(P))$ term due to noise distortion, we can recover all messages. Moreover, we use $h(A,B) \leq h(A) + h(B)$.

Replacing $p_{1,1}$ and $p_{1,2}$ with any private users $p_{k,1}$ and $p_{j,2}$ in (4.17), respectively, after dividing by $n\log(P)$, taking first the limit $n \to \infty$ and then the limit $P \to \infty$, a rearrangement of the terms yields the following DoF outer bound

$$
(N_{t,1}-1)d^{[p_{k,1}]} + (N_{t,2}-1)d^{[p_{j,2}]} + d_\Sigma \leq N_{t,1} + N_{t,2}. \qquad (4.18)
$$

where $d_\Sigma = d_{\Sigma sh} + d_{\Sigma p_1} + d_{\Sigma p_2}$. Adding all these bounds, after another rearrangement we obtain

$$\begin{aligned} &K_{p,2}(K_{p,1} + N_{t,1} - 1)d_{\Sigma p_1} + K_{p,1}(K_{p,2} + N_{t,2} - 1)d_{\Sigma p_2} + K_{p,1}K_{p,2}d_{\Sigma sh} \\ &\quad \leq K_{p,1}K_{p,2}(N_{t,1} + N_{t,2}). \end{aligned} \tag{4.19}$$

Next, consider the first shared user, who wants the message $W^{[sh_1]}$. Also consider $M = N_{t,1} + N_{t,2}$ realizations for this user. For any realization l, starting with Fano's inequality, we go through a similar series of steps, as follows

$$\begin{aligned} nR^{[sh_1]} \leq& I\left(W^{[sh_1]}; \left(y_l^{[sh_1]}\right)^n\right) + o(n) \\ =& h\left(\left(y_l^{[sh_1]}\right)^n\right) - h\left(\left(y_l^{[sh_1]}\right)^n \mid W^{[sh_1]}\right) + o(n) \\ \leq& n\,\log(P) - h\left(\left(y_l^{[sh_1]}\right)^n \mid W^{[sh_1]}\right) + o(n) + n\,o(\log(P)), \end{aligned} \tag{4.20}$$

where now $l \in \{1, 2, \ldots, M\}$. Adding the bounds for all M realizations,

$$\begin{aligned} nMR^{[sh_1]} \leq& nM\log(P) - h\left(\left(y_1^{[sh_1]}, \ldots, y_M^{[sh_1]}\right)^n \mid W^{[sh_1]}\right) + o(n) + n\,o(\log(P)) \\ \leq& nM\log(P) - n(R_{\Sigma p_1} + R_{\Sigma p_2} + R_{\Sigma sh} - R^{[sh_1]}) + o(n) + n\,o(\log(P)). \end{aligned} \tag{4.21}$$

Dividing by $n\,\log(P)$, talking the limit $n \to \infty$ followed by $P \to \infty$, and rearranging terms, we obtain the DoF outer bound

$$(M-1)d^{[sh_1]} + d_{\Sigma p_1} + d_{\Sigma p_2} + d_{\Sigma sh} \leq M. \tag{4.22}$$

If we now sum (4.22) over all shared users, we obtain

$$(K_{sh} + M - 1)d_{\Sigma sh} + K_{sh}(d_{\Sigma p_1} + d_{\Sigma p_2}) \leq K_{sh}M. \tag{4.23}$$

Therefore, by grouping the outer bounds given by (4.19) and (4.23), the sum-DoF for partially connected networks leads to solving the following equation system

$$\begin{bmatrix} (N_{t,1} + K_{p,1} - 1) & 0 & K_{p,1} & 0 \\ 0 & (N_{t,2} + K_{p,2} - 1) & K_{p,2} & 0 \\ K_{sh} & 0 & (N_{t,1} + K_{sh} - 1) & N_{t,1} \\ 0 & K_{sh} & N_{t,2} & (N_{t,2} + K_{sh} - 1) \end{bmatrix} \begin{bmatrix} d_{\Sigma p_1} \\ d_{\Sigma p_2} \\ d_{\Sigma sh} \\ d_{\Sigma sh} \end{bmatrix} = \begin{bmatrix} K_{p,1}N_{t,1} \\ K_{p,2}N_{t,2} \\ K_{sh}N_{t,1} \\ K_{sh}N_{t,2} \end{bmatrix} \tag{4.24}$$

Specialized to the symmetric setting where $N_{t,1} = N_{t,2} = N_t$ and $K_{p,1} = K_{p,2} = K_p$, we have the sum-DoF outer bound

$$\begin{aligned} &\text{maximize} \quad d_{\Sigma sh} + d_{\Sigma p_1} + d_{\Sigma p_2} \\ &\text{subject to} \\ &K_p\, d_{\Sigma sh} + (K_p + N_t - 1)(d_{\Sigma p_1} + d_{\Sigma p_2}) \leq 2K_p N_t \\ &(2N_t + K_{sh} - 1)d_{\Sigma sh} + K_{sh}(d_{\Sigma p_1} + d_{\Sigma p_2}) \leq 2K_{sh} N_t \end{aligned} \tag{4.25}$$

This linear program is easily solved, to obtain the sum-DoF bound

$$d_\Sigma \leq \frac{M\left[K_{sh}(N_t - 1) + K_p(M-1)\right]}{(M-1)(N_t-1) + K_{sh}(N_t-1) + K_p(M-1)}, \tag{4.26}$$

which is achieved when

$$d_{\Sigma p_n} = \frac{N_t K_p\,(M-1)}{(M-1)(N_t-1) + K_{sh}(N_t-1) + K_p(M-1)} \tag{4.27}$$

$$d_{\Sigma sh} = \frac{M K_{sh}\,(N_t-1)}{(M-1)(N_t-1) + K_{sh}(N_t-1) + K_p(M-1)} \tag{4.28}$$

Once the DoF achievable in cellular networks with partial connectivity have been determined, the goal of the following sections will be focused on developing BIA schemes that reach the outer bound (4.26). For simplicity, we first consider symmetric cellular scenarios. A scheme able to achieve the optimal DoF in symmetric cellular networks by exploiting the network topology is presented in this chapter. For asymmetric cellular networks it is shown that the outer bound of (4.24) is not achievable in general due to asymmetric impairments.

4.4 Blind Interference Alignment based on Data Sharing

Let us consider a partially connected network as shown in Figure 4.1. Notice that a portion of the amount of users are subject to intercell interference while the remaining users can treat this interference as noise. It is assumed now that each BS shares the messages to the users limited by intercell interference with the rest of BSs. A BIA scheme based on exploiting the diversity given by data sharing among the set of BSs is proposed in [97]. The key idea is to duplicate the users subject to intercell interference, which will be referred to as shared users from now on, so that the whole set of BSs sends

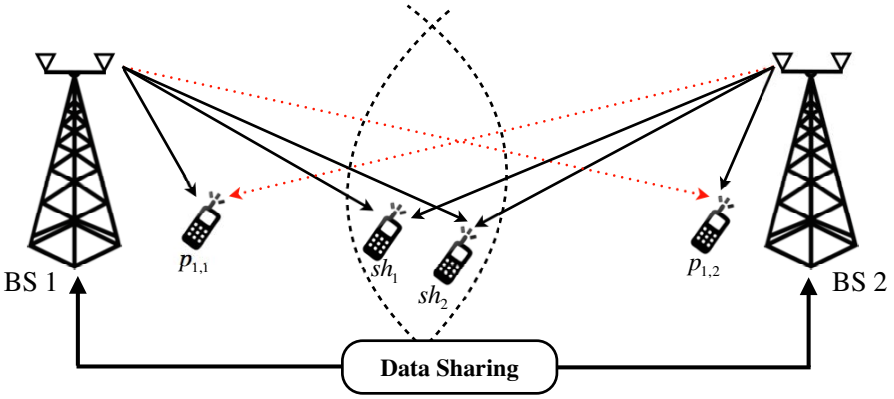

FIGURE 4.2: Toy example: downlink two-cell scenario with transmission based on auBIA. The BSs are equipped with $N_t = 2$ antennas and serve $K_p = 1$ and $K_{sh} = 2$ private and shared users, respectively. Both BSs transmit the same symbol to each shared user.

the same message to each shared user. In other words, each BS n transmits the same symbol as well as other BSs n', $n' \neq n$, to a virtual replica of each shared user, which is assumed to belong to the coverage area of the cell n.

For illustrative purposes, let us assume a two-cell toy example as shown in Figure 4.2. Each BS is equipped with $N_t = 2$ antennas and there are 2 users located in each cell. More specifically, each cell contains a private user that receives a weak signal from the neighboring BSs and a shared user located in the cell edge of both BSs, i.e. one shared user per cell. For this particular case the supersymbol structure is as shown in Figure 4.2. Note that in contrast to the $N_t = 2$, $K_{cell} = 2$ sBIA case shown in Figure 3.2, the length of the supersymbol has increased to 4 symbol extensions instead of 3. As can be seen, this augmented code BIA scheme (auBIA) is based on aligning the interference of the shared users considering all of them as users served by each BS. Thus, BS 1 transmits to its users $p_{1,1}$ and sh_1, and also to user sh_2, which is located in the cell edge of BS 2 and receives a strong signal from BS 1. That is, the BS n transmits to user $p_{1,n}$ and also sh_1 and sh_2 as in a $N_t = 2$, $K_{cell} = 3$ sBIA scenario. According to the supersymbol proposed in Figure 4.3, the signal transmitted by the n-th BS is given by

$$\mathbf{X}^{[n]} = \begin{bmatrix} \mathbf{x}[1]^n \\ \mathbf{x}[2]^{[n]} \\ \mathbf{x}[3]^{[n]} \\ \mathbf{x}[4]^{[n]} \end{bmatrix} = \begin{bmatrix} \mathbf{I} \\ \mathbf{I} \\ \mathbf{0} \\ \mathbf{0} \end{bmatrix} \mathbf{u}_1^{[p_{1,n}]} + \begin{bmatrix} \mathbf{I} \\ \mathbf{0} \\ \mathbf{I} \\ \mathbf{0} \end{bmatrix} \mathbf{u}_1^{[sh_1]} + \begin{bmatrix} \mathbf{I} \\ \mathbf{0} \\ \mathbf{0} \\ \mathbf{I} \end{bmatrix} \mathbf{u}_1^{[sh_2]}, \tag{4.29}$$

	1	2	3	4
$p_{1,n}$	$\mathbf{h}^{[p_{1,n}]}(1)$	$\mathbf{h}^{[p_{1,n}]}(2)$	$\mathbf{h}^{[p_{1,n}]}(1)$	$\mathbf{h}^{[p_{1,n}]}(1)$
sh_1	$\mathbf{h}^{[sh_1]}(1)$	$\mathbf{h}^{[sh_1]}(1)$	$\mathbf{h}^{[sh_1]}(2)$	$\mathbf{h}^{[sh_1]}(1)$
sh_2	$\mathbf{h}^{[sh_2]}(1)$	$\mathbf{h}^{[sh_2]}(1)$	$\mathbf{h}^{[sh_2]}(1)$	$\mathbf{h}^{[sh_2]}(2)$

FIGURE 4.3: The supersymbol for the auBIA scheme in a two-cell scenario with $K_p = 1$ private users close to each BS and $K_{sh} = 2$ shared users in the edge of both cells.

where $\mathbf{x}[t] \in \mathbb{C}^{2\times 1}$ is the signal transmitted during the symbol extension t, each symbol sent to user k, either private or shared, $\mathbf{u}_1^{[k]} \in \mathbb{C}^{2\times 1}$ contains 2 DoF, and $\mathbf{I}$ and $\mathbf{0}$ are 2×2 identity and zero matrix, respectively.

Let us focus on the private user located close to the BS n. To send $N_t = 2$ distinguishable streams in absence of CSIT, the BS n sends the same symbol $\mathbf{u}_1^{[p_{1,n}]}$ during 2 symbol extensions where the channel of the desired user changes between $N_t = 2$ preset modes while the channel state of all the other users remains constant. Notice that the alignment block for each private user comprises the symbol extensions $\{1, 2\}$. It can be seen in Figure 4.3 that the alignment blocks of all other users, which comprise the symbol extensions $\{1, 3\}$ and $\{1, 4\}$ for shared users sh_1 and sh_2, respectively, are aligned over the channel mode $\mathbf{h}(1)$ during the alignment block of the private users. Besides, due to the partial connectivity of the network, it is assumed that transmission from the BS 2 does not affect user $p_{1,1}$ and it can be treated as noise instead of being managed as interference. Thus, the private user $p_{1,2}$ can *reuse* the same radiation pattern and beamforming matrix as the user $p_{1,1}$ because of the partial connectivity. We can check that the pair of symbol extensions $\{1, 2\}$ forms an alignment block for each private user. Therefore, the signal received by the private user $p_{1,n}$ during its alignment block is

$$\begin{bmatrix} y^{[p_{1,n}]}[1] \\ y^{[p_{1,n}]}[2] \end{bmatrix} = \begin{bmatrix} \mathbf{h}^{[p_{1,n},n]}(1)^T \\ \mathbf{h}^{[p_{1,n},n]}(2)^T \end{bmatrix} \mathbf{u}_1^{[p_{1,n}]} + \begin{bmatrix} \mathbf{h}^{[p_{1,n},n]}(1)^T \left(\mathbf{u}_1^{[sh_1]} + \mathbf{u}_1^{[sh_2]} \right) \\ \mathbf{0} \end{bmatrix} + \begin{bmatrix} z^{[p_{1,1}]}[1] \\ z^{[p_{1,1}]}[2] \end{bmatrix}. \tag{4.30}$$

Note that the interference because of transmission to shared users is aligned at channel mode $\mathbf{h}(1)$. On the other hand, the signal received from BS 2 is not considered in (4.30) due to the partial connectivity. Thus, the private user can apply zero-forcing based on measuring the interference because of transmission of the BS 1 to sh_1 and sh_2 in Block

2. The signal after removing the interference can be written as

$$\tilde{\mathbf{y}} = \underbrace{\begin{bmatrix} \mathbf{h}^{[p_{1,n},n]}(1)^T \\ \mathbf{h}^{[p_{1,n},n]}(2)^T \end{bmatrix}}_{\mathbf{H}^{[p_{1,n},n]}} \mathbf{u}_1^{[p_{1,n}]}. + \begin{bmatrix} z^{[p_{1,1}]}[1] - z^{[p_{1,1}]}[3] - z^{[p_{1,1}]}[4] \\ z^{[p_{1,1}]}[2] \end{bmatrix} \tag{4.31}$$

Therefore, since the channels $\mathbf{h}^{[p_{1,n},n]}(l)$, $l \in \{1,2\}$ are generic, the 2 DoF sent in $\mathbf{u}_1^{[p_{1,n}]}$ are decodable by solving the equation system given by (4.31). Remarkably, the terms of interference because of transmission to users sh_1 and sh_2 are subtracted, which increase the noise at finite SNR. Furthermore, the signal received from the BS $n' \neq n$ is treated optimally as noise because of the partial connectivity.

The same methodology can be carried out for each shared user. It can be seen in Figure 4.3 that the desired signal is aligned regarding the rest of users over the channel mode $\mathbf{h}(1)$. Shared users sh_1 and sh_2 exploit an alignment block that comprises the pair of symbol extensions $\{1,3\}$ and $\{1,4\}$, respectively. However, according to the beamforming strategy in (4.29) each shared user $sh_{k'}$ receives the same symbol $\mathbf{u}^{[sh_{k'}]}$, which contains 2 DoF, from each BS. For illustrative purposes, the signal received during the alignment block of user sh_1 can be written as

$$\begin{aligned} \begin{bmatrix} y^{[sh_1]}[1] \\ y^{[sh_1]}[3] \end{bmatrix} = & \underbrace{\begin{bmatrix} \mathbf{h}^{[sh_1,1]}(1)^T + \sqrt{\beta_2^{[sh_1]}}\mathbf{h}^{[sh_1,2]}(1)^T \\ \mathbf{h}^{[sh_1,1]}(2)^T + \sqrt{\beta_2^{[sh_1]}}\mathbf{h}^{[sh_1,2]}(2)^T \end{bmatrix}}_{\text{rank}=2} \mathbf{u}_1^{[sh_1]} \\ & + \underbrace{\begin{bmatrix} \left(\mathbf{h}^{[sh_1,1]}(1)^T + \sqrt{\beta_2^{[sh_1]}}\mathbf{h}^{[sh_1,2]}(1)^T\right)\left(\mathbf{u}_1^{[p_{1,1}]} + \mathbf{u}_1^{[p_{1,2}]} + \mathbf{u}_1^{[sh_1]}\right) \\ \mathbf{0} \end{bmatrix}}_{\text{rank}=1}. \end{aligned} \tag{4.32}$$

We can observe that the two dimensions of $\mathbf{u}_1^{[sh_1]}$ are aligned into one dimension at the remaining users. Hence, the three terms of interference of (4.32) can be canceled. Notice that the sum of the interference because of the transmission to both private users, $\mathbf{u}_1^{[p_{1,1}]} + \mathbf{u}_1^{[p_{1,2}]}$ can be measured in symbol extension $\{2\}$ and removed afterwards from the first slot of (4.32). Similarly, the transmission of $\mathbf{u}_1^{[sh_2]}$ can be measured in symbol extension $\{4\}$. Thus, the received signal at the user sh_1 after zero-forcing interference

cancellation is

$$\tilde{\mathbf{y}}^{[sh_1]} = \underbrace{\begin{bmatrix} \mathbf{h}^{[sh_1,1]}(1)^T + \sqrt{\beta_2^{[sh_1]}}\mathbf{h}^{[sh_1,2]}(1)^T \\ \mathbf{h}^{[sh_1,1]}(2)^T + \sqrt{\beta_2^{[sh_1]}}\mathbf{h}^{[sh_1,2]}(2)^T \end{bmatrix}}_{\mathbf{H}^{[sh_1]}} \mathbf{u}_1^{[sh_1]} + \begin{bmatrix} z[1]^{sh_1} - z[2]^{sh_1} - z[4]^{sh_1} \\ z[3]^{sh_1} \end{bmatrix}, \tag{4.33}$$

where

$$\mathbf{H}^{[sh_1]} = \left[\mathbf{h}^{[sh_1,1]}(1)^T + \sqrt{\beta_2^{[sh_1]}}\mathbf{h}^{[sh_1,2]}(1)^T \quad \mathbf{h}^{[sh_1,1]}(2)^T + \sqrt{\beta_2^{[sh_1]}}\mathbf{h}^{[sh_1,2]}(2)^T\right]^T \in \mathbb{C}^{2\times 2}, \tag{4.34}$$

is the channel matrix of the shared user sh_1. As $\mathbf{H}^{[sh_1]}$ is a full-rank matrix, user sh_1 can decode 2 DoF by solving the equation system given by (4.33).

In summary, intracell and also intercell interference can be canceled when it is optimal to manage it. For the proposed toy example it has been shown that 2 DoF are attainable by each user, either private or shared, by employing a supersymbol that comprises 4 symbol extensions. Hence, $\frac{2\text{DoF}\times 4}{4} = 2$ DoF per symbol extension are achievable in the proposed scenario by using auBIA based on data sharing. It is interesting to remark that the use of sBIA in the same cellular scenario achieves zero-DoF for users subject to intercell interference. In consequence, only private users attain 2 DoF per alignment block over a supersymbol comprising 3 symbol extensions, i.e. $\frac{2\text{DoF}\times 2}{3} = \frac{4}{3}$ DoF are achievable in the whole network by using sBIA.

4.4.1 Achievable Degrees of Freedom

For the general case, a cellular deployment with N_{BS} BSs equipped with N_t antennas is assumed. The users are differentiated between K_p private users located close to each BS and K_{sh} shared users in the cell-edge of the whole set of BSs. As we have shown, intercell interference is treated optimally as noise for private users, which are characterized by a high SIR. In contrast, auBIA cancels the intracell and also the intercell interference for shared users by using diversity among the BSs. Basically, data sharing among the BSs is used to transmit the same symbols to each shared user in the whole network. That is, auBIA replicates each shared user N_{BS} times so that each BS sends data to its private users and to all shared users in a coordinated fashion. Due to this replication of the

shared users, a supersymbol that comprises

$$\mathcal{L}_{\text{auBIA}} = (N_t - 1)^{K'_{cell}} + K'_{cell}(N_t - 1)^{K'_{cell}-1} \tag{4.35}$$

symbol extensions is devised for auBIA, where $K'_{cell} = K_p + K_{sh}$. Note that K_{sh} are the total shared users located in the whole network. Since the auBIA supersymbol contains $(N_t - 1)^{K'_{cell}-1}$ alignment blocks per user, either private or shared, providing N_t DoF each, the normalized sum-DoF per symbol extension is

$$\text{DoF}_{\text{auBIA}} = \frac{N_t \left(N_{BS}K_p + K_{sh}\right)(N_t - 1)^{K'_{cell}-1}}{(N_t - 1)^{K'_{cell}} + K'_{cell}(N_t - 1)^{K'_{cell}-1}} = \frac{N_t \left(N_{BS}K_p + K_{sh}\right)}{N_t + K_p + K_{sh} - 1}. \tag{4.36}$$

It can be easily seen that the set of private users in each cell achieves a sum-DoF per symbol extension given by

$$\text{DoF}_{\text{auBIA}_{\text{pri}}} = \frac{N_t K_p}{N_t + K_p + K_{sh} - 1}, \tag{4.37}$$

whereas the sum-DoF attained by the whole set of K_{sh} shared users is

$$\text{DoF}_{\text{auBIA}_{\text{sh}}} = \frac{N_t K_{sh}}{N_t + K_p + K_{sh} - 1}. \tag{4.38}$$

4.4.2 Achievable Rates

The closed-form expressions of the achievable rates are derived in this section. For simplicity, it is assumed that all users are distributed symmetrically, i.e. the same amount of private users is distributed in each cell. The expressions for the asymmetric scenario can be derived using the same procedure.

As we have shown, focused on private users the intracell interference is completely canceled while intercell interference is approximated as zero due to partial connectivity (4.3). Since intercell interference is treated optimally as noise, this assumption holds for the DoF analysis carried out during the previous section. However, at the finite SNR regime intercell interference must be considered as a source of noise. Furthermore, synchronization between the supersymbols of each cell is assumed. For the private user $p_{k,n}$ the signal received during a generic alignment block after zero-forcing interference

cancellation $\tilde{\mathbf{y}}^{[p_{k,n}]} = \left[\tilde{y}^{[p_{k,n}]}[1] \quad \dots \quad \tilde{y}^{[p_{k,n}]}[N_t]\right]^T$ is given by

$$\tilde{\mathbf{y}}^{[p_{k,n}]} = \mathbf{H}^{[p_{k,n},n]}\mathbf{u}_\ell^{[p_{k,n}]} + \sum_{n'=1,n'\neq n}^{N_{BS}} \sqrt{\alpha_{n'}^{[p_{k,n}]}}\mathbf{H}^{[p_{k,n},n']}\mathbf{u}_\ell^{[p_{k,n'}]} + \tilde{\mathbf{z}}^{[p_{k,n}]}, \tag{4.39}$$

where

$$\mathbf{H}^{[p_{k,n},n']} = \left[\mathbf{h}^{[p_{k,n},n']}(1)^T \quad \dots \quad \mathbf{h}^{[p_{k,n},n']}(N_t)^T\right]^T \in \mathbb{C}^{N_t \times N_t} \tag{4.40}$$

is the channel matrix that contains the coefficients between the private user $p_{k,n}$ and BS n', and $\tilde{\mathbf{z}}^{[p_{k,n}]} \in \mathbb{C}^{N_t \times 1}$ is the noise vector after interference subtraction. Note that due to the replication of each shared user in each cell, the interference cancellation involves to subtract $K_p + K_{sh} - 1$ terms of interference. Thus, the first $N_t - 1$ elements of the vector $\tilde{\mathbf{z}}^{[p_{k,n}]}$ are given by

$$\tilde{z}^{[p_{k,n}]}[t] = z^{[p_{k,n}]}[t] - \sum_{\tau=1}^{K_p} z^{[p_{k,n}]}[\tau] - \sum_{\tau=1}^{K_{sh}} z^{[p_{k,n}]}[\tau'], \tag{4.41}$$

where τ and τ' refer to the position of the symbol extension employed to subtract the interference from transmission of private and shared users, respectively. Besides, since the N_t-th element is obtained from Block 2, it does not suffer noise increment so that $\tilde{z}^{[p_{k,n}]}[N_t] = z^{[p_{k,n}]}[N_t]$. Therefore, and assuming uniform power allocation, the covariance matrix of the noise after zero-forcing cancellation for auBIA is

$$\mathbf{R}_{\tilde{\mathbf{z}}\text{au}} = \begin{bmatrix} (K_p + K_{sh})\,\mathbf{I} & \mathbf{0} \\ \mathbf{0} & 1 \end{bmatrix}. \tag{4.42}$$

Furthermore, auBIA provides $(N_t - 1)^{K'_{cell}-1}$ alignment blocks over a supersymbol that comprises $\mathcal{L}_{\text{auBIA}}$ symbol extensions. Hence, the ratio of alignment blocks per user over the entire supersymbol is $\frac{1}{N_t+K_p+K_{sh}-1}$. Therefore, the normalized rate per symbol extension of the private user $p_{k,n}$ for auBIA is

$$R_{\text{auBIA}}^{[p_{k,n}]} = \frac{1}{N_t + K_p + K_{sh} - 1}\mathbb{E}\left[\log\det\left(\mathbf{I} + P_{str}\mathbf{H}^{[p_{k,n},n]}\mathbf{H}^{[p_{k,n},n]H}\mathbf{R}_{\mathbf{I}\tilde{\mathbf{z}}_{\text{au}}}^{[p_{k,n}]-1}\right)\right] \tag{4.43}$$

where $\mathbf{R}_{\mathbf{I}\tilde{\mathbf{z}}_{\text{au}}}^{[p_{k,n}]}$ is the noise plus interference covariance matrix given by

$$\mathbf{R}_{\mathbf{I}\tilde{\mathbf{z}}_{\text{au}}}^{[p_{k,n}]} = \mathbf{R}_{\tilde{\mathbf{z}}\text{au}} + P_{str}\sum_{n'=1,n'\neq=n}^{N_{BS}} \alpha_{n'}^{[p_{k,n}]}\mathbf{H}^{[p_{k,n},n']}\mathbf{H}^{[p_{k,n},n']H}, \tag{4.44}$$

and P_{str} is the average power assigned to each stream. Since uniform power allocation has been assumed, P_{str} is given by (2.33). The use of other power allocation strategies results straightforward and is analyzed in detail in the Section 2.4.2 of Chapter 2.

In contrast, shared users manage the signal received from the neighboring BSs, which is assumed to be strong enough, to obtain diversity gain due to data sharing among the BSs. Hence, the intercell interference is not treated as a source of interference. The signal during a generic alignment block after zero-forcing interference cancellation for shared user $sh_{k'}$, $\tilde{\mathbf{y}}^{[sh_{k'}]} = \left[\tilde{y}^{[sh_{k'}]}[1] \quad \dots \quad \tilde{y}^{[sh_{k'}]}[N_t]\right]^T$, can be written as

$$\tilde{\mathbf{y}}^{[sh_{k'}]} = \sum_{n=1}^{N_{BS}} \sqrt{\beta_n^{[sh_{k'}]}} \mathbf{H}^{[sh_{k'},n]} \mathbf{u}_\ell^{[sh_{k'}]} + \tilde{\mathbf{z}}^{sh_{k'}}, \tag{4.45}$$

where

$$\mathbf{H}^{[sh_{k'},n]} = \left[\mathbf{h}^{[sh_{k'},n]}(1)^T \quad \dots \quad \mathbf{h}^{[sh_{k'},n]}(N_t)^T\right]^T \in \mathbb{C}^{N_t \times N_t} \tag{4.46}$$

is a full-rank matrix that contains the N_t vectors corresponding to the channel modes between user $sh_{k'}$ and BS n. The vector $\tilde{\mathbf{z}}^{[sh_{k'}]}$ contains the noise elements after interference subtraction following the same structure as (4.41), where the first $N_t - 1$ elements suffer an increment due to the subtraction of $K_p + K_{sh} - 1$ terms while the last element is not affected by any noise increment. Thus, the normalized rate per symbol extension achieved by the shared user $sh_{k'}$ is given by

$$R_{\text{auBIA}}^{[sh_{k'}]} = \frac{1}{N_t + K_p + K_{sh} - 1} \mathbb{E}\left[\log\det\left(\mathbf{I} + P_{str} \widetilde{\mathbf{H}}^{[sh_{k'}]} \widetilde{\mathbf{H}}^{[sh_{k'}]^H} \mathbf{R}_{\tilde{\mathbf{z}}\text{au}}^{-1}\right)\right], \tag{4.47}$$

where

$$\widetilde{\mathbf{H}}^{[sh_{k'}]} = \sum_{n=1}^{N_{BS}} \sqrt{\beta_n^{[sh_{k'}]}} \mathbf{H}^{[sh_{k'},n]} \tag{4.48}$$

is the equivalent channel matrix after adding the contribution of the N_{BS} BSs. Recall that the whole set of BSs sends the same symbol to each shared user. Besides, notice that in contrast to private users, the noise covariance matrices do not contain any term due to treating intercell interference as noise. Therefore, the noise covariance matrix is as (4.42) and the average power assigned to each stream P_{str} is defined by the power allocation strategy (2.33).

4.5 Blind Interference Alignment based on Bandwidth Division

Although the auBIA scheme based on augmented code allows to cancel the intercell interference of the users subject to it, some features of auBIA must be discussed.

- Data sharing involves to use high-capacity backhaul links among the BSs, which is one of the main issues that BIA schemes try to avoid. Besides, synchronization among the BSs is required.
- Although shared users manage the intercell interference by exploiting diversity, they only achieve N_t DoF per alignment block. Notice that, since the signal from $M = N_{BS}N_t$ antennas can reach each shared user, M DoF are potentially achievable during each alignment block of each shared user.
- Private users suffer a considerable penalty because of the replication of each shared user N_{BS} times.
- Since each BS transmits to all shared users in the whole network, the supersymbol length increases with respect to sBIA transmission.

Motivated by the provision of flexible bandwidth allocation in the latest-generation of mobile communication standards such as LTE or LTE-A [131, 132] and the development of reconfigurable antennas [82–87], we propose in [128] a cooperative BIA based on flexible bandwidth allocation, to which we refer as fbwBIA in the following. The key idea is to employ different parts of the available spectrum for transmission to private and shared users as is shown in Figure 4.4. In fact, note that orthogonal resource allocation is, although sub-optimal, a simple form of interference alignment in absence of CSIT.

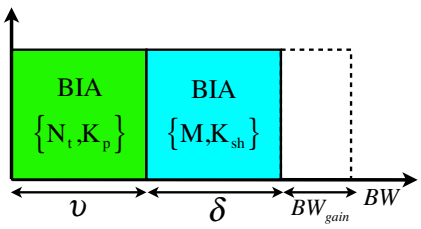

FIGURE 4.4: Flexible bandwidth BIA . Transmission to private and shared users occurs in distinct bandwidth slices υ and δ, respectively. BW_{gain} is the bandwidth improvement regarding the auBIA scheme.

In order to avoid the interference between both groups of users, a portion υ and δ of the available bandwidth is allocated for private and shared users, respectively. Thus, the whole used bandwidth $\upsilon + \delta$ suffices to attain the same performance as BIA with augmented code, $BW_{gain} \geq 0$ is the amount of bandwidth that can be used to improve the user rates. In other words, BW_{gain} corresponds to the improvement of the bandwidth efficiency achieved by fbwBIA regarding auBIA. Since transmission to K_p and K_{sh} private and shared users, respectively, is carried out in distinct bandwidth slices, $\{N_t, K_p\}$ and $\{M, K_{sh}\}$ BIA codes are designed for each group. In consequence, the interference between private and shared users is avoided by using distinct parts of the available bandwidth. A supersymbol comprising $\mathcal{L}_{\text{sBIA}}(N_t, K_p)$ and $\mathcal{L}_{\text{sBIA}}(M, K_{sh})$ symbol extensions is employed in each cell. Therefore, a considerable reduction in the supersymbol length can be achieved with fbwBIA. In contrast to auBIA, each BS transmits N_t different symbols to each shared user instead of sending the same symbol as the other BSs. Hence, assuming reconfigurable antennas with enough preset modes, $N_{BS}N_t$ DoF are achievable to each shared user in each alignment block. Nevertheless, the use of orthogonal resource allocation involves a penalty in the DoF achieved by fbwBIA. As an example, the achievable DoF in each group of users, either private or shared, are divided by two when the bandwidth is halved in two equal slices.

4.5.1 They key to Blind Interference Alignment based on flexible bandwidth

For illustrative purposes consider a two-cell scenario as shown in Figure 4.5. Each BS is equipped with $N_t = 2$ antennas that serve $K_p = 1$ private user each and there are $K_{sh} = 3$ shared users located in the cell-edge of both BSs. It can be easily checked from (4.36) that auBIA achieves 2 sum-DoF per symbol extension by employing data sharing among the BSs in the proposed scenario.

Consider now that instead of using data sharing to create an augmented BIA code based on replicating the shared users, the interference between private an shared users is avoided by dividing the available bandwidth in two proportional slices $\upsilon = \frac{1}{4}$ and $\delta = \frac{3}{4}$ for private and shared users, respectively. Therefore, each BS transmits the same BIA code for $N_t = 2$ and $K_p = 1$ over a fraction of bandwidth $\upsilon = \frac{1}{4}$. Notice that private users reuse the same BIA code assuming that the intercell interference can

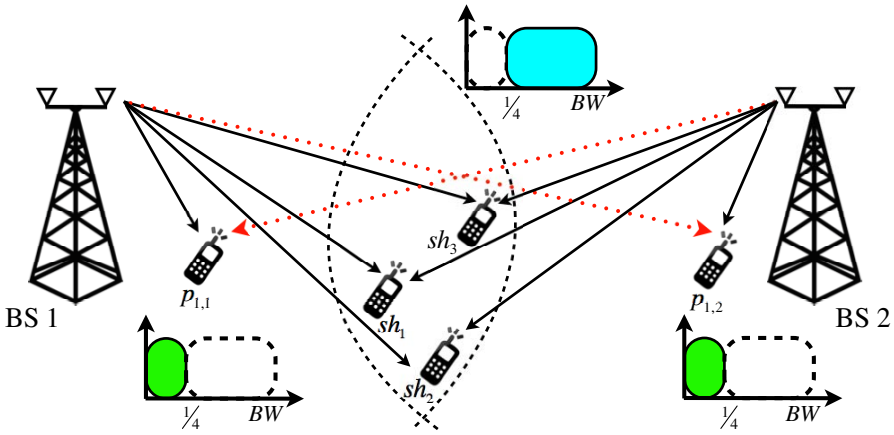

FIGURE 4.5: Toy example: downlink two-cell scenario with transmission based on fbwBIA. The BSs are equipped with $N_t = 2$ antennas and serve $K_p = 1$ and $K_{sh} = 3$ private and shared users. Proportional bandwidth $\upsilon = \frac{1}{4}$ and $\delta = \frac{3}{4}$ is allocated to each group of users.

be treated optimally as noise. For the proposed toy example, since there is only one inner user in each cell, 1 DoF is attained by each private user. Assume now that the set of BSs cooperate to transmit N_t streams to each shared user forming an alignment block of 4 DoF. This approach corresponds to a cBIA scheme for $M = 4$ antennas and $K_{sh} = 3$ users devised to serve these users independently of the private users. The task of sending data to the shared users can be jointly undertaken by the 2 BSs. That is, no data sharing is required to implement the proposed scheme. Since full connectivity is assumed for shared users and according to (3.32), the set of shared users achieves $\frac{4 \cdot 3}{4+3-1} = 2$ DoF over a fraction $\delta = \frac{3}{4}$ of the available bandwidth. Therefore, the sum-DoF achievable in the proposed scenario is $1\text{DoF} \times \upsilon \times 2 + 2\text{DoF} \times \delta = 2$ DoF. It can be seen that it coincides with the sum-DoF achievable by using auBIA in the same scenario. Moreover, the attainable sum-DoF increases for larger number of shared users. Notice that in contrast to auBIA a backhaul link to provide data sharing between both BSs is not required. Furthermore, since private and shared users are served independently over distinct bandwidth slices, fbwBIA allows to reduce the supersymbol length and the noise increment due to interference subtraction.

4.5.2 Supersymbol and Beamforming Construction for the General case

For the general case a BIA code for N_t antennas and K_p users is devised for serving the private users of each cell over a portion υ of the available bandwidth. This code is reused in each cell assuming that private users treat the intercell interference as noise optimally. In consequence, private users are not affected by transmission from the neighboring BSs. Therefore, the supersymbol construction and the corresponding beamforming matrices are given by (2.16) and (2.18), respectively. On the other hand, cBIA tranmission with $M = N_{BS}N_t$ antennas is employed to serve K_{sh} users over a portion δ of the overall bandwidth. Analogously, to obtain the supersymbol and beamforming matrices it is only necessary to replace $N_t = M$ and $K = K_{sh}$ in (2.16) and (2.18), respectively.

Notice that the required coherence time in the system is given by the maximum length between the supersymbols used for transmission to shared and private users, that is

$$\mathcal{L}_{\text{fbwBIA}} = \max\left\{\mathcal{L}_{\text{BIA}}\left(N_t, K_p\right), \mathcal{L}_{\text{cBIA}}\left(M, K_{sh}\right)\right\}, \tag{4.49}$$

where $\mathcal{L}_{\text{BIA}}$ and $\mathcal{L}_{\text{cBIA}}$ are given by (2.22) and (3.25), respectively.

4.5.3 Achievable Degrees of Freedom

Since different slices of bandwidth are employed for transmission to private and shared users, the achievable sum-DoF can be analyzed independently for each group of users. A BIA code for N_t and K_p users is employed to serve the private users of each cell over a bandwidth υ. Therefore, the sum-DoF attained by the set of K_p users located in the inner cell of each BS is given by

$$\text{DoF}_{\text{fbwBIA}_{\text{pri}}} = \upsilon \cdot \frac{N_t K_p}{N_t + K_p - 1}. \tag{4.50}$$

Furthermore, cBIA transmission for $M = N_{BS}N_t$ antennas and K_{sh} users over a bandwidth δ is used to serve the set of shared users that receives similar signal strength from the whole set of BS. Thus, the achievable sum-DoF for shared users is

$$\text{DoF}_{\text{fbwBIA}_{\text{sh}}} = \delta \cdot \frac{M K_{sh}}{M + K_{sh} - 1}. \tag{4.51}$$

As we have shown, the interference between each group of users is avoided by splitting the available bandwidth in two slices of size υ and δ for private and shared users, respectively. Therefore, the achievable sum-DoF per symbol extension when fbwBIA is used in a partially connected network is

$$\begin{aligned}\mathrm{DoF}_{\mathrm{fbwBIA}} &= \upsilon \cdot \frac{N_{BS}N_tK_p}{N_t+K_p-1} + \delta \cdot \frac{N_{BS}N_tK_{sh}}{N_{BS}N_t+K_{sh}-1} \\ &= N_{BS}N_t\left[\frac{\upsilon K_p}{N_t+K_p-1} + \frac{\delta K_{sh}}{N_{BS}N_t+K_{sh}-1}\right].\end{aligned} \tag{4.52}$$

It is interesting to remark that in contrast to the strategy employed in the toy example of Figure 4.5, the achievable bandwidth division does not need to be proportional to the total number of users. In consequence, fbwBIA can be flexible to penalize or reward any group of users, either private or shared.

4.5.4 Achievable Rates

To begin with the analysis of the performance of fbwBIA at finite SNR, recall that υ is defined as the portion the total bandwidth that it is allocated to private users. This group of users employs a BIA code for N_t and K_p users, while the intercell interference because of transmission in the neighbor BSs is treated as noise. Thus, following the steps described to obtain the rates of sBIA in Chapter 3, the achievable rate normalized per symbol extension of the private user k within the cell n is given by

$$R_{\mathrm{fbwBIA}}^{[p_{k,n}]} = \upsilon \cdot \frac{1}{N_t+K_p-1}\mathbb{E}\left[\log\det\left(\mathbf{I} + P_{str}\mathbf{H}^{[p_{k,n},n]}\mathbf{H}^{[p_{k,n},n]^H}\mathbf{R}_{\mathbf{I}\tilde{\mathbf{z}}_{\mathrm{fbw}}}^{[p_{k,n}]^{-1}}\right)\right] \tag{4.53}$$

where $\mathbf{H}^{[p_{k,n},n]} \in \mathbb{C}^{N_t\times N_t}$ is given by (4.40), P_{str} is the average power allocated to each stream, and $\mathbf{R}_{\mathbf{I}\tilde{\mathbf{z}}_{\mathrm{fbw}}}$ is given by

$$\mathbf{R}_{\mathbf{I}\tilde{\mathbf{z}}_{\mathrm{fbw}}}^{[p_{k,n}]} = \mathbf{R}_{\tilde{\mathbf{z}}_{\mathrm{fbw}}^{[p]}} + P_{str}\sum_{n'=1,n'\neq=n}^{N_{BS}} \alpha_{n'}^{[p_{k,n}]}\mathbf{H}^{[p_{k,n},n']}\mathbf{H}^{[p_{k,n},n']^H}. \tag{4.54}$$

In contrast to (4.44), transmission to shared users does not affect to the signal received by private users. Therefore, private users only have to subtract K_p terms of interference

when using fbwBIA transmission. Thus, the covariance matrix of the noise after zero-forcing interference subtraction is

$$\mathbf{R}_{\underset{\text{fbw}}{\tilde{\mathbf{z}}^{[p]}}} = \begin{bmatrix} K_p\mathbf{I}_{N_t-1} & \mathbf{0} \\ \mathbf{0} & 1 \end{bmatrix}. \tag{4.55}$$

Similarly, as we have shown previously, δ is defined as the portion of the total bandwidth allocated to the shared users. A BIA code with M transmit antennas and K_{sh} users is employed over this slice of bandwidth. Thus, each shared user attains M DoF per alignment block by using cBIA transmission. Following the steps of cBIA, the achievable rate normalized per symbol extension by the shared user $sh_{k'}$ can be written as

$$R_{\text{fbwBIA}}^{[sh_{k'}]} = \delta \cdot \frac{1}{M+K_{sh}-1}\mathbb{E}\left[\log\det\left(\mathbf{I} + P_{str}\mathbf{H}^{[sh_{k'}]}{\mathbf{H}^{[sh_{k'}]}}^H \mathbf{R}_{\underset{\text{fbw}}{\tilde{\mathbf{z}}^{[sh]}}}{}^{-1}\right)\right] \tag{4.56}$$

where the channel matrix is now a $M \times M$ full-rank matrix

$$\mathbf{H}^{[sh_{k'}]} = \left[\mathbf{h}^{[sh_{k'}]}(1)^T \quad \dots \quad \mathbf{h}^{[sh_{k'}]}(l)^T \quad \dots \quad \mathbf{h}^{[sh_{k'}]}(M)^T\right]^T \in \mathbb{C}^{M\times M} \tag{4.57}$$

and $\mathbf{h}^{[sh_{k'}]}(l)$ is given by (4.5) with $M = N_{BS}N_t$, i.e., the reconfigurable antennas of the shared users now need $N_{BS}N_t$ preset modes. Since the interference from the neighboring BSs is managed to provide multiplexing gain for shared users, note that intercell interference does not appear in (4.56) as a source of interference. Besides, the shared users are served in the slice δ independently of the private users, and therefore, only K_{sh} terms of interference are subtracted by using fbwBIA. In consequence, the covariance matrix of the noise after zero-forcing interference for shared users is given by

$$\mathbf{R}_{\underset{\text{fbw}}{\tilde{\mathbf{z}}^{[sh]}}} = \begin{bmatrix} K_{sh}\mathbf{I}_{M-1} & \mathbf{0} \\ \mathbf{0} & 1 \end{bmatrix}. \tag{4.58}$$

4.5.5 Theoretical analysis of BIA based on flexible bandwidth

It has been shown that the proposed fbwBIA allows to reduce the length of the supersymbol and the noise after interference subtraction. The following two theorems demonstrate that the use of BIA joint to an orthogonal approach based on the network topology outperforms the sum-rate of auBIA in a wide range of SNR values (SNR_{min}, ∞)

when the condition $K_{sh} \geq 2N_t - 1$ is satisfied. Despite the fact that the fbwBIA scheme has been developed for a N_{BS} BSs network, in order to compare with the auBIA scheme proposed in [97] we will focus on the two-cell scenario from now on. The extension to the N_{BS} BSs case is straightforward.

Theorem 4.1. *In the two-cell scenario with K_p private users per cell and K_{sh} cell-edge users in total in both cells, when SNR $\to \infty$, flexible bandwidth BIA achieves larger sum-rate than using data sharing with augmented BIA code if $K_{sh} \geq 2N_t - 1$.*

Proof. Because the variance of the noise is finite, SNR $\to \infty$ corresponds to $P \to \infty$. The achievable sum-rate for the shared users in a two-cell scenario can be written in terms of the DoF metric [133], in view of the fact that the interference is fully canceled. Let us define $R_{\text{auBIA}}^{\Sigma_{sh}} = \sum_{k'=1}^{K_{sh}} R_{\text{auBIA}}^{[sh_{k'}]}$ and $R_{\text{fbwBIA}}^{\Sigma_{sh}} = \sum_{k'=1}^{K_{sh}} R_{\text{fbwBIA}}^{[sh_{k'}]}$ as the sum-rate achieved by auBIA and fbwBIA for the shared users, respectively. From (4.43) and (4.56) we can re-write these sum-rates in terms of the DoF metric as

$$R_{\text{auBIA}}^{\Sigma_{sh}}(P \to \infty) = \frac{N_t K_{sh}}{N_t + K_p + K_{sh} - 1} \log(P) + o\left(\log(P)\right) \tag{4.59}$$

$$R_{\text{fbwBIA}}^{\Sigma_{sh}}(P \to \infty) = \delta \frac{2N_t K_{sh}}{2N_t + K_{sh} - 1} \log(P) + o\left(\log(P)\right). \tag{4.60}$$

The term $o\left(\log(P)\right)$ corresponds to some function $f(P)$ that satisfies $\lim_{P\to\infty} \frac{f(P)}{\log(P)} = 0$. Therefore, the two approaches achieve the same sum-DoF for the shared users when

$$\delta = \frac{2N_t + K_{sh} - 1}{2(N_t + K_p + K_{sh} - 1)}. \tag{4.61}$$

Although the intercell interference to which the private users are subject is small enough to be treated as noise, at the limit $P \to \infty$ transmission to private users becomes interference-limited. Analogously, given the achievable rate of private user $p_{k,n}$ for auBIA and fbwBIA in (4.47) and (4.56), respectively, $R_{\text{auBIA}}^{\Sigma_p} = \sum_{k=1}^{K_p} R_{\text{auBIA}}^{[p_{k,n}]}$ and $R_{\text{fbwBIA}}^{\Sigma_p} = \sum_{k=1}^{K_p} R_{\text{fbwBIA}}^{[p_{k,n}]}$ are the sum-rate of the private users located in the inner cell of BS n for auBIA and fbwBIA, respectively. Letting $P \to \infty$ while keeping the SIR of private users fixed to α_{pri}, if $\breve{\mathbf{R}}_{\mathbf{I}}^{[p_{k,n}]} = \mathbb{E}\left[\mathbf{H}^{[p_{k,n},n']}\mathbf{H}^{[p_{k,n},n']^H}\right]$, $n' \neq n$, the sum-rate of the private

users in cell n can be written as

$$R_{\text{auBIA}}^{\Sigma_p}(P \to \infty) = \frac{K_p}{N_t + K_p + K_{sh} - 1} \mathbb{E}\left[\log\det\left(\mathbf{I} + \frac{1}{\alpha_{pri}} \mathbf{H}^{[p_{k,n},n]} \mathbf{H}^{[p_{k,n},n]^H} \left(\breve{\mathbf{R}}_{\mathbf{I}}^{[p_{k,n}]}\right)^{-1}\right)\right] \tag{4.62}$$

$$R_{\text{fbwBIA}}^{\Sigma_p}(P \to \infty) = \upsilon \cdot \frac{K_p}{N_t + K_p - 1} \mathbb{E}\left[\log\det\left(\mathbf{I} + \frac{1}{\alpha_{pri}} \mathbf{H}^{[p_{k,n},n]} \mathbf{H}^{[p_{k,n},n]^H} \left(\breve{\mathbf{R}}_{\mathbf{I}}^{[p_{k,n}]}\right)^{-1}\right)\right]. \tag{4.63}$$

Thus, the same sum-rate is achieved for private users by both methods when fbwBIA assigns the following portion of the bandwidth to the private users

$$\upsilon = \frac{N_t + K_p - 1}{N_t + K_p + K_{sh} - 1}. \tag{4.64}$$

If the bandwidth gain is defined as $BW_{gain} = 1 - (\upsilon + \delta)$, the use of fbwBIA is favorable compared to the auBIA scheme if

$$\begin{aligned} &\upsilon + \delta < 1 \Rightarrow \frac{2N_t + K_{sh} - 1}{2(N_t + K_p + K_{sh} - 1)} + \frac{N_t + K_p - 1}{N_t + K_p + K_{sh} - 1} < 1 \Rightarrow \\ &\frac{4N_t + K_{sh} + 2K - 3}{2(N_t + K_p + K_{sh} - 1)} < 1 \Rightarrow K_{sh} > 2N_t - 1, \end{aligned} \tag{4.65}$$

which concludes the proof. □

Theorem 4.2. *For the two-cell scenario, assuming that the power received by the shared users is large enough so that* $\log(1+\text{SNR}) \approx \log(\text{SNR})$*, if* $K_{sh} \geq 2N_t - 1$*, fbwBIA scheme achieves a larger sum-rate than auBIA with augmented code if*

$$\text{SNR} > N_t \frac{1 + \beta_{sh}}{\beta_{sh}} \left(\frac{2K_{sh} - 1}{2(K_p + K_{sh}) - 1}\right)^{\frac{N_t - 1}{N_t}} \frac{2K_{sh} - 1}{e^{\frac{1}{N_t}\sum_{l=0}^{N_t-1} \psi(2N_t - 1)}}, \tag{4.66}$$

where β_{sh} *is the SIR of the shared users (assumed equal for all) and* $\psi(\cdot)$ *is the Euler digamma function.*

Proof. For private users it is easy to see that if $\upsilon = \frac{N_t + K_p - 1}{N_t + K_p + K_{sh} - 1}$ as in (4.64), it suffices to compare the expectation terms in (4.43) and the evaluation of (4.53) at $N_{BS} = 2$.

The only difference between the terms is the noise covariance matrix, which is larger in (4.43) because the augmented code involves the subtraction of $K_p + K_{sh}$ terms of interference for each user either private or shared, whereas in fbwBIA the noise is only proportional to K_p for private users. Therefore, if $K_{sh} \geq 2N_t - 1$, $BW_{gain} \geq 0$ still holds when (4.64) and (4.61) are satisfied, and fbwBIA achieves a larger sum-rate at any SNR value for the private users of each cell.

Note that N_t and M DoF are achieved in each alignment block for auBIA and fbwBIA, respectively. That is, auBIA provides diversity gain while fbwBIA increases the multiplexing gain sacrificing that diversity gain. Hence, the analysis for shared users results more complex. Let A_{AU} and A_{FBW} denote the value of the determinants in (4.47) and (4.56), respectively. Using the assumption $\log(1 + \text{SNR}) \approx \log(\text{SNR})$,

$$R_{\text{auBIA}}^{\Sigma_{sh}} \approx \kappa\, \mathbb{E}\left[\log A_{AU}\right] = \kappa\, \mathbb{E}\left[\log\det\left(\frac{P}{N_t}\widetilde{\mathbf{H}}^{[sh_{k'}]}\widetilde{\mathbf{H}}^{[sh_{k'}]^H}\mathbf{R}_{\tilde{\mathbf{z}}\text{au}}^{-1}\right)\right]. \tag{4.67}$$

where $\kappa > 0$ equals a strictly positive constant and $\widetilde{\mathbf{H}}^{[sh_{k'}]}$ is given by (4.48). Since $\widetilde{\mathbf{H}}^{[sh_{k'}]}$ and $\mathbf{R}_{\tilde{\mathbf{z}}\text{au}}$ are $N_t \times N_t$ matrices, and the entries of $\widetilde{\mathbf{H}}^{[sh_{k'}]}$ are i.i.d. Gaussian with zero mean and variance $(1 + \beta_{sh})g^{[sh_{k'}]}$, where $g^{[sh_{k'}]}$ is the channel gain at shared user $sh_{k'}$,

$$A_{AU} = \left(\frac{P}{N_t}\right)^{N_t} \det\left(\mathbf{R}_{\tilde{\mathbf{z}}\text{au}}^{-1}\right) \det\left(\boldsymbol{\Sigma}\overline{\mathbf{H}}_{N_t}\boldsymbol{\Phi}\overline{\mathbf{H}}_{N_t}{}^H\right), \tag{4.68}$$

where $\overline{\mathbf{H}}_{N_t} \sim \mathcal{CN}(0, \mathbf{I}_{N_t})$, $\boldsymbol{\Sigma} = g^{[sh_{k'}]}(1+\beta_{sh})\mathbf{I}_{N_t}$, $\boldsymbol{\Phi} = \mathbf{I}_{N_t}$ and $\beta_{sh} = \beta^{[sh_{k'}]}$, $\forall sh_k \in \mathcal{K}_{sh}$. Thus, since $\boldsymbol{W} = \overline{\mathbf{H}}_{N_t}\overline{\mathbf{H}}_{N_t}{}^H$ is a Wishart matrix $\boldsymbol{W} \sim W_{N_t}(N_t, \mathbf{I})$, applying [134, Theorem 2.11]

$$\mathbb{E}\left[\log\det\left(\overline{\mathbf{H}}_{N_t}\overline{\mathbf{H}}_{N_t}{}^H\right)\right] = \sum_{l=0}^{N_t-1}\psi\left(N_t - l\right) \tag{4.69}$$

where $\psi(\cdot)$ is the Euler digamma function. Finally, since $\mathbf{R}_{\tilde{\mathbf{z}}\text{au}}$ is a diagonal matrix,

$$\begin{aligned}\mathbb{E}\left[\log A_{AU}\right] =& \log\left(\left(\frac{P}{N_t}\right)^{N_t}\left(\frac{1}{2(K_p+K_{sh})-1}\right)^{N_t-1}\left(g^{[sh_{k'}]}(1+\beta_{sh})\right)^{N_t}\right)\\ &+\mathbb{E}\left[\log_e\det\left(\overline{\mathbf{H}}_{N_t}{\overline{\mathbf{H}}_{N_t}}^H\right)\right]\\ =& \log\left(\left(\frac{P}{N_t}\right)^{N_t}\left(\frac{1}{2(K_p+K_{sh})-1}\right)^{N_t-1}\left(g^{[sh_{k'}]}(1+\beta_{sh})\right)^{N_t}\right)\\ &+\sum_{l=0}^{N_t-1}\psi\left(N_t-l\right).\end{aligned} \tag{4.70}$$

Similarly, the achievable sum-rate obtained with fbwBIA can be approximated as

$$R_{\text{fbwBIA}}^{\Sigma_{sh}} \approx \kappa\,\mathbb{E}\left[\log A_{FBW}\right] = \kappa\,\mathbb{E}\left[\log\det\left(\frac{P}{N_t}\mathbf{H}^{[sh_{k'}]}{\mathbf{H}^{[sh_{k'}]}}^H{\mathbf{R}_{\tilde{\mathbf{z}}_{\text{fbw}}^{[sh]}}}^{-1}\right)\right]. \tag{4.71}$$

Because BIA over the antennas of both BSs is used for FBW, the size of the matrices $\mathbf{H}^{[sh_{k'}]}$ is full-rank $2N_t \times 2N_t$ matrix and $\mathbf{R}_{\tilde{\mathbf{z}}_{\text{fbw}}^{[sh]}}$ is a is $2N_t \times 2N_t$ diagonal matrix. Hence, it is possible to re-write A_{FBW} as

$$A_{FBW} = \left(\frac{P}{N_t}\right)^{2N_t}\det\left({\mathbf{R}_{\tilde{\mathbf{z}}_{\text{fbw}}^{[sh]}}}^{-1}\right)\det\left(\mathbf{\Sigma}'\overline{\mathbf{H}}_{2N_t}\mathbf{\Phi}{\overline{\mathbf{H}}_{2N_t}}^H\right), \tag{4.72}$$

where $\overline{\mathbf{H}}_{2N_t} \sim \mathcal{CN}(0, \mathbf{I}_{2N_t})$, $\mathbf{\Sigma}' = g^{[sh_{k'}]}\begin{bmatrix}\mathbf{I}_{N_t} & \mathbf{0}\\ \mathbf{0} & \beta_{sh}\mathbf{I}_{N_t}\end{bmatrix}$ and $\mathbf{\Phi} = \mathbf{I}_{2N_t}$. Thus, since $\boldsymbol{W_{sh}} = \overline{\mathbf{H}}_{2N_t}{\overline{\mathbf{H}}_{2N_t}}^H$ is a Wishart Matrix $\boldsymbol{W} \sim W_{2N_t}(2N_t, \mathbf{I})$, applying, again, [134, Theorem 2.11].

$$\mathbb{E}\left[\log\det\left(\overline{\mathbf{H}}_{2N_t}{\overline{\mathbf{H}}_{2N_t}}^H\right)\right] = \sum_{l=0}^{2N_t-1}\psi\left(2N_t-l\right). \tag{4.73}$$

Finally,

$$\begin{aligned}\mathbb{E}\left[\log A_{FBW}\right] =& \log\left(\left(\frac{P}{N_t}\right)^{2N_t}\left(\frac{1}{2K_{sh}-1}\right)^{2N_t-1}\left(g^{[sh_{k'}]}\right)^{2Nt}(\beta_{sh})^{N_t}\right)\\ &+\mathbb{E}\left[\log\det\left(\overline{\mathbf{H}}_{2N_t}{\overline{\mathbf{H}}_{2N_t}}^H\right)\right]\\ =& \log\left(\left(\frac{P}{N_t}\right)^{2N_t}\left(\frac{1}{2K_{sh}-1}\right)^{2N_t-1}\left(g^{[sh_{k'}]}\right)^{2Nt}(\beta_{sh})^{N_t}\right)\\ &+\sum_{l=0}^{2N_t-1}\psi\left(2N_t-l\right).\end{aligned} \tag{4.74}$$

Hence, FBW leads to a larger sum-rate for the shared users if $\mathbb{E}\left[\log A_{FBW}\right] > \mathbb{E}\left[\log A_{AU}\right]$, or

$$\begin{aligned}
&\log\left(\left(\frac{P}{N_t}\right)^{2N_t}\left(g^{[sh_{k'}]}\right)^{2Nt}(\beta_{sh})^{N_t}\left(\frac{1}{2K_{sh}-1}\right)^{2N_t-1}\right)+\sum_{l=0}^{2N_t-1}\psi\left(2N_t-l\right)\\
&>\log\left(\left(\frac{P}{N_t}\right)^{N_t}\left(g^{[sh_{k'}]}(1+\beta_{sh})\right)^{N_t}\left(\frac{1}{2(K_p+K_{sh})-1}\right)^{N_t-1}\right)+\sum_{l=0}^{N_t-1}\psi\left(N_t-l\right)\Rightarrow\\
&\text{SNR}>N_t\frac{1+\beta_{sh}}{\beta_{sh}}\left(\frac{2K_{sh}-1}{2(K_p+K_{sh})-1}\right)^{\frac{N_t-1}{N_t}}\frac{2K_{sh}-1}{e^{\frac{1}{N_t}\sum_{l=0}^{N_t-1}\psi(2N_t-l)}}.
\end{aligned} \tag{4.75}$$

where $\text{SNR}=Pg^{[sh_{k'}]}$. □

4.6 Network Blind Interference Alignment

So far, we have proposed the use of either data sharing (auBIA) or orthogonal approaches (fbwBIA) as a way to implement BIA in cellular networks. Although these schemes obtain some benefits, they are sub-optimal in DoF. In this section we propose a network BIA (nBIA) scheme based on the partially connected topology that achieves the optimal DoF for symmetric scenarios. Moreover, an extension of the nBIA scheme for the asymmetric case is devised in order to minimize the loss of DoF because of asymmetric impairments. It is demonstrated that this penalty in DoF is typically small, and the proposed scheme outperforms other BIA schemes amply. In this section, we first describe the key idea of nBIA using the toy examples of previous sections. Then, for the sake of an easy exposition we describe nBIA for the symmetric scenario with N_{BS} BSs, each equipped with N_t antennas serving K_p private users and K_{sh} shared users. After that, we derive the closed-form expressions of the achievable rates for nBIA. Finally, we analyze the asymmetric cases in detail.

4.6.1 The key to Blind Interference Alignment in cellular systems

Consider again the two-cell example shown in Figure 4.6. Each BS is equipped with $N_t = 2$ antennas, $K_p = 1$ private user is located in the inner cell of each BS, and $K_{sh} = 1$ shared user is in the cell edge of both BSs. The shared user receives data from

both BS. On the contrary, each private user, i.e. $p_{1,1}$ and $p_{1,2}$, can only be served by its corresponding BS, BS 1 and BS 2, respectively. Thus, user $p_{k,n}$ does not decode the data sent by any other BS n', $n \neq n'$. As a positive counterpart of this lack of connectivity, private users of a given BS are not subject to interference by any other BS.

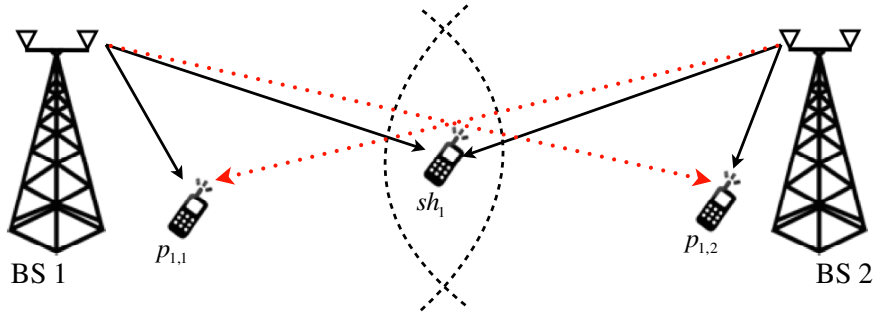

FIGURE 4.6: Toy example: downlink two-cell scenario with partial connectivity. The BSs are equipped with $N_t = 2$ antennas and serve $K_p = 1$ and $K_{sh} = 1$ private and shared users, respectively.

Since cBIA does not take into account the lack of full connectivity, it does not achieve (3.32). For the toy example, cBIA achieves $\frac{4}{3}$ DoF when there is partial connectivity, which is less than the 2 DoF attained in a fully connected system. As an alternative to cBIA, consider the supersymbol of Figure 4.7 and the beamforming matrices

$$\mathbf{X} = \begin{bmatrix} \mathbf{x}[1] \\ \mathbf{x}[2] \\ \mathbf{x}[3] \\ \mathbf{x}[4] \\ \mathbf{x}[5] \\ \mathbf{x}[6] \\ \mathbf{x}[7] \end{bmatrix} = \underbrace{\begin{bmatrix} \mathbf{I} & \mathbf{0} & \mathbf{0} \\ \mathbf{0} & \mathbf{I} & \mathbf{0} \\ \mathbf{0} & \mathbf{0} & \mathbf{I} \\ \mathbf{I} & \mathbf{0} & \mathbf{0} \\ \mathbf{0} & \mathbf{I} & \mathbf{0} \\ \mathbf{0} & \mathbf{0} & \mathbf{I} \\ \mathbf{0} & \mathbf{0} & \mathbf{0} \end{bmatrix}}_{p_{1,1}} \begin{bmatrix} \mathbf{u}_1^{[p_{1,1}]} \\ \mathbf{u}_2^{[p_{1,1}]} \\ \mathbf{u}_3^{[p_{1,1}]} \end{bmatrix} + \underbrace{\begin{bmatrix} \mathbf{I} & \mathbf{0} & \mathbf{0} \\ \mathbf{0} & \mathbf{I} & \mathbf{0} \\ \mathbf{0} & \mathbf{0} & \mathbf{I} \\ \mathbf{I} & \mathbf{0} & \mathbf{0} \\ \mathbf{0} & \mathbf{I} & \mathbf{0} \\ \mathbf{0} & \mathbf{0} & \mathbf{I} \\ \mathbf{0} & \mathbf{0} & \mathbf{0} \end{bmatrix}}_{p_{1,2}} \begin{bmatrix} \mathbf{u}_1^{[p_{1,2}]} \\ \mathbf{u}_2^{[p_{1,2}]} \\ \mathbf{u}_3^{[p_{1,2}]} \end{bmatrix} + \underbrace{\begin{bmatrix} \mathbf{I} \\ \mathbf{I} \\ \mathbf{I} \\ \mathbf{0} \\ \mathbf{0} \\ \mathbf{0} \\ \mathbf{I} \end{bmatrix}}_{sh_1} \mathbf{u}_1^{[sh_1]}, \tag{4.76}$$

where $\mathbf{x}[t] \in \mathbb{C}^{4\times 1}$,

$$\begin{aligned} \mathbf{u}_1^{[sh_1]} &= \begin{bmatrix} \mathbf{u}_1^{[sh_1,1]^T} & \mathbf{u}_1^{[sh_1,2]^T} \end{bmatrix}^T \\ \mathbf{u}_\ell^{[p_{1,1}]} &= \begin{bmatrix} \mathbf{u}_\ell^{[p_{1,1},1]^T} & \mathbf{0}_{2,1}{}^T \end{bmatrix}^T \\ \mathbf{u}_\ell^{[p_{1,2}]} &= \begin{bmatrix} \mathbf{0}_{2,1}{}^T & \mathbf{u}_\ell^{[p_{1,2},2]^T} \end{bmatrix}^T. \end{aligned} \tag{4.77}$$

	1	2	3	4	5	6	7
$p_{1,1}/p_{1,2}$	$\mathbf{h}^{[p_{1,n}]}(1)$	$\mathbf{h}^{[p_{1,n}]}(1)$	$\mathbf{h}^{[p_{1,n}]}(1)$	$\mathbf{h}^{[p_{1,n}]}(2)$	$\mathbf{h}^{[p_{1,n}]}(2)$	$\mathbf{h}^{[p_{1,n}]}(2)$	$\mathbf{h}^{[p_{1,n}]}(1)$
sh_1	$\mathbf{h}^{[sh_1]}(1)$	$\mathbf{h}^{[sh_1]}(2)$	$\mathbf{h}^{[sh_1]}(3)$	$\mathbf{h}^{[sh_1]}(1)$	$\mathbf{h}^{[sh_1]}(2)$	$\mathbf{h}^{[sh_1]}(3)$	$\mathbf{h}^{[sh_1]}(4)$

FIGURE 4.7: Supersymbol of the nBIA scheme for the toy example. $N_t = 2$, $K_{sh} = 1$, and $K_{p,1} = K_{p,2} = 1$.

The vectors $\mathbf{u}_\ell^{[p_{1,n},n]} \in \mathbb{C}^{2\times 1}$, $\ell \in \{1,2,3\}$ and $\mathbf{u}_1^{[sh_1,n]} \in \mathbb{C}^{2\times 1}$ contain the symbols transmitted by BS n to $p_{1,n}$ and sh_1, respectively, and $\mathbf{I}$ and $\mathbf{0}$ are the 4×4 identity and zero matrix, respectively.

Let us first focus on the transmission of data to shared user sh_1. As is explained in [88], since sh_1 is served by both BSs, to send $M = N_{t,1} + N_{t,2} = 4$ distinguishable data streams, the BSs need to transmit $\mathbf{u}_1^{[sh_1]} \in \mathbb{C}^{4\times 1}$ repetitively during 4 symbol extensions over which the antenna of sh_1 switches through $M = 4$ different modes. At the same time, the beams need to be aligned into one dimension at the users that are subject to interference by the signal sent to sh_1. Therefore, during these symbol extensions, $p_{1,1}$ and $p_{1,2}$ maintain the same mode. For instance, by looking at the supersymbol of Figure 4.7 and the beamforming matrix of (4.76), we can check that symbol extensions 1, 2, 3 and 7 constitute an alignment block for sh_1. Thus, the signal received at user sh_1 during its alignment block is given by

$$\begin{aligned}\begin{bmatrix} y^{[sh_1]}[1] \\ y^{[sh_1]}[2] \\ y^{[sh_1]}[3] \\ y^{[sh_1]}[7] \end{bmatrix} &= \begin{bmatrix} \mathbf{h}^{[sh_1]}(1)^T\mathbf{x}[1] \\ \mathbf{h}^{[sh_1]}(2)^T\mathbf{x}[2] \\ \mathbf{h}^{[sh_1]}(3)^T\mathbf{x}[3] \\ \mathbf{h}^{[sh_1]}(4)^T\mathbf{x}[7] \end{bmatrix} \\ &= \underbrace{\begin{bmatrix} \mathbf{h}^{[sh_1]}(1)^T \\ \mathbf{h}^{[sh_1]}(2)^T \\ \mathbf{h}^{[sh_1]}(3)^T \\ \mathbf{h}^{[sh_1]}(4)^T \end{bmatrix}}_{\mathbf{H}^{[sh_1]}} \mathbf{u}_1^{[sh_1]} + \underbrace{\begin{bmatrix} \mathbf{h}^{[sh_1]}(1)^T\left(\mathbf{u}_1^{[p_{1,1}]} + \mathbf{u}_1^{[p_{1,2}]}\right) \\ \mathbf{h}^{[sh_1]}(2)^T\left(\mathbf{u}_2^{[p_{1,1}]} + \mathbf{u}_2^{[p_{1,2}]}\right) \\ \mathbf{h}^{[sh_1]}(3)^T\left(\mathbf{u}_3^{[p_{1,1}]} + \mathbf{u}_3^{[p_{1,2}]}\right) \\ 0 \end{bmatrix}}_{\text{interference}} + \begin{bmatrix} z^{[sh_1]}[1] \\ z^{[sh_1]}[2] \\ z^{[sh_1]}[3] \\ z^{[sh_1]}[7] \end{bmatrix},\end{aligned} \tag{4.78}$$

where

$$\mathbf{H}^{[sh_1]} = \begin{bmatrix} \mathbf{h}^{[sh_1]}(1)^T & \mathbf{h}^{[sh_1]}(2)^T & \mathbf{h}^{[sh_1]}(3)^T & \mathbf{h}^{[sh_1]}(4)^T \end{bmatrix}^T \in \mathbb{C}^{4\times 4} \tag{4.79}$$

is the channel matrix of user sh_1. Since the channels $\mathbf{h}^{[sh_1]}(l)$, $l \in \{1,2,3,4\}$ are generic, once the second term of (4.78) associated with the interference has been removed, user sh_1 can decode the 4 data streams $\mathbf{u}_1^{[sh_1]}$. Now, if we consider the signal received at the private user 1 in cell n

$$\begin{aligned}
\begin{bmatrix} y^{[p_{1,n}]}[1] \\ y^{[p_{1,n}]}[2] \\ y^{[p_{1,n}]}[3] \\ y^{[p_{1,n}]}[7] \end{bmatrix} &= \begin{bmatrix} \mathbf{h}^{[p_{1,n},n]}(1)^T\mathbf{x}^{[n]}[1] + \mathbf{0}_{2,1}^T\mathbf{x}^{[n']}[1] \\ \mathbf{h}^{[p_{1,n},n]}(1)^T\mathbf{x}^{[n]}[2] + \mathbf{0}_{2,1}^T\mathbf{x}^{[n']}[2] \\ \mathbf{h}^{[p_{1,n},n]}(1)^T\mathbf{x}^{[n]}[3] + \mathbf{0}_{2,1}^T\mathbf{x}^{[n']}[3] \\ \mathbf{h}^{[p_{1,n},n]}(1)^T\mathbf{x}^{[n]}[7] + \mathbf{0}_{2,1}^T\mathbf{x}^{[n']}[7] \end{bmatrix} \\
&= \underbrace{\begin{bmatrix} \mathbf{h}^{[p_{1,n},n]}(1)^T\mathbf{u}_1^{[p_{1,n},n]} \\ \mathbf{h}^{[p_{1,n},n]}(1)^T\mathbf{u}_2^{[p_{1,n},n]} \\ \mathbf{h}^{[p_{1,n},n]}(1)^T\mathbf{u}_3^{[p_{1,n},n]} \\ 0 \end{bmatrix}}_{\text{desired signals}} + \underbrace{\begin{bmatrix} \mathbf{h}^{[p_{1,n},n]}(1)^T \\ \mathbf{h}^{[p_{1,n},n]}(1)^T \\ \mathbf{h}^{[p_{1,n},n]}(1)^T \\ \mathbf{h}^{[p_{1,n},n]}(1)^T \end{bmatrix}}_{\text{interference}} \mathbf{u}_1^{[sh_1,n]} + \begin{bmatrix} z^{[p_{1,n}]}[1] \\ z^{[p_{1,n}]}[2] \\ z^{[p_{1,n}]}[3] \\ z^{[p_{1,n}]}[7] \end{bmatrix},
\end{aligned} \tag{4.80}$$

$n \in \{1,2\}$, we can observe that the four transmissions of $\mathbf{u}_1^{[sh_1]} = \begin{bmatrix} \mathbf{u}_1^{[sh_1,1]^T} & \mathbf{u}_1^{[sh_1,2]^T} \end{bmatrix}^T$ are aligned into one dimension corresponding to preset mode 1 when transmitting data to the private users. This way, since during symbol extension 7 the set of BS n, $n \in \{1,2\}$, only transmits $\mathbf{u}_1^{[sh_1,n]}$, private user $p_{1,n}$ can subtract the interference during symbol extensions 1, 2 and 3 by applying zero-forcing based on the measurement of $y^{[p_{1,n}]}[7]$.

Next, we concentrate on the transmission to private user $p_{1,1}$. Unlike shared user sh_1, the private user $p_{1,1}$ can only be served by BS 1. To send $N_{t,1} = 2$ distinguishable symbols, $\mathbf{u}_\ell^{[p_{1,1},1]}$, to user $p_{1,1}$ in the absence of CSIT, BS 1 employs a repetition code to transmit $\mathbf{u}_\ell^{[p_{1,1},1]}$ during 2 symbol extensions over which the antenna of $p_{1,1}$ switches through $N_{t,1} = 2$ modes. Moreover, to align the two transmissions of $\mathbf{u}_\ell^{[p_{1,1},1]}$ into one dimension at the users subject to interference because of the transmission to user $p_{1,1}$, the affected users should keep the same radiation pattern. However, due to the partial connectivity of the network, sh_1 is now the only user subject to this interference. Therefore, the radiation pattern of its antenna is the only one that has to be kept constant to project the interference caused by the transmissions of $\mathbf{u}_\ell^{[p_{1,1},1]}$ into one dimension. From the supersymbol of Figure 4.7, we can easily check that the pairs of symbol extensions $\{1,4\}$, $\{2,5\}$ and $\{3,6\}$ satisfy all the previous conditions. Each of these pairs constitutes an alignment block ℓ, $\ell = \{1,2,3\}$, for private user $p_{1,1}$. For instance, consider the first alignment block formed by symbol extensions $\{1,4\}$. The signal received by the private

user $p_{1,1}$ during its first alignment block is

$$\begin{bmatrix} y^{[p_{1,1}]}[1] \\ y^{[p_{1,1}]}[4] \end{bmatrix} = \begin{bmatrix} \mathbf{h}^{[p_{1,1},1]}(1)^T \mathbf{x}^{[1]}[1] + \mathbf{0}_{2,1}^T \mathbf{x}^{[2]}[1] \\ \mathbf{h}^{[p_{1,1},1]}(2)^T \mathbf{x}^{[1]}[4] + \mathbf{0}_{2,1}^T \mathbf{x}^{[2]}[4] \end{bmatrix}$$
$$= \underbrace{\begin{bmatrix} \mathbf{h}^{[p_{1,1},1]}(1)^T \\ \mathbf{h}^{[p_{1,1},1]}(2)^T \end{bmatrix}}_{\mathbf{H}^{[p_{1,1},1]}} \mathbf{u}_1^{[p_{1,1},1]} + \underbrace{\begin{bmatrix} \mathbf{h}^{[p_{1,1},1]}(1)^T \mathbf{u}_1^{[sh_1,1]} \\ 0 \end{bmatrix}}_{\text{interference}} + \begin{bmatrix} z^{[p_{1,1}]}[1] \\ z^{[p_{1,1}]}[4] \end{bmatrix}. \tag{4.81}$$

Private user $p_{1,1}$ applies zero-forcing based on $y^{[p_{1,1}]}[7]$ to remove the interference at time instants 1, 2 and 3 (see (4.80)). Thus, the signal at user $p_{1,n}$ after interference subtraction is given by

$$\begin{bmatrix} y^{[p_{1,1}]}[1] \\ y^{[p_{1,1}]}[4] \end{bmatrix} = \underbrace{\begin{bmatrix} \mathbf{h}^{[p_{1,1},1]}(1)^T \\ \mathbf{h}^{[p_{1,1},1]}(2)^T \end{bmatrix}}_{\mathbf{H}^{[p_{1,1},1]}} \mathbf{u}_1^{[p_{1,1},1]} + \begin{bmatrix} z^{[p_{1,1}]}[1] - z^{[p_{1,1}]}[3] \\ z^{[p_{1,1}]}[4] \end{bmatrix}, \tag{4.82}$$

where

$$\mathbf{H}^{[p_{1,1},1]} = \begin{bmatrix} \mathbf{h}^{[p_{1,1},1]}(1)^T & \mathbf{h}^{[p_{1,1},1]}(2)^T \end{bmatrix}^T \in \mathbb{C}^{2\times 2}, \tag{4.83}$$

is the channel matrix of user $p_{1,1}$. Consequently, due to the fact that the channels $\mathbf{h}^{[p_{1,1},1]}(l)$, $l \in \{1,2\}$, are generic, the 2 symbols in $\mathbf{u}_1^{[p_{1,1},1]}$ can be decoded by inverting the full-rank matrix $\mathbf{H}^{[p_{1,1},1]}$. The same procedure can be followed to decode the data streams $\mathbf{u}_2^{[p_{1,1},1]}$ and $\mathbf{u}_3^{[p_{1,1},1]}$ transmitted repetitively over the pairs of symbol extensions $\{2,5\}$ and $\{3,6\}$, respectively.

Recall that, as can be seen from (4.81), the transmission of data to private users of a specific cell does not cause interference to private users of other cells. Consequently, $p_{1,2}$ can *reuse* the same radiation pattern and the same beamforming matrix as $p_{1,1}$, which can also be verified from (4.76). This way, each pair of symbol extensions $\{1,4\}$, $\{2,5\}$ and $\{3,6\}$ also constitutes an alignment block of $p_{1,2}$. Moreover, in (4.78) note that the interference associated with the repeated transmissions of $\mathbf{u}_\ell^{[p_{1,2},2]}$ by BS 2 along the ℓ-th alignment block of $p_{1,2}$ is aligned into the same single dimension as the transmission of $\mathbf{u}_\ell^{[p_{1,1},1]}$ by the BS 1 along the ℓ-th alignment block of $p_{1,1}$. Hence, in (4.78) the interference term associated with the transmissions of $\mathbf{u}_\ell^{[p_{1,1},1]}$ and $\mathbf{u}_\ell^{[p_{1,2},2]}$ can be removed if user sh_1 applies zero-forcing based on the signals received during the time slot over which is not receiving data. For instance, if sh_1 applies zero-forcing based on

$y^{[sh_1]}[4] = \mathbf{h}^{[sh_1]}(1)^T \left(\mathbf{u}_1^{[p_{1,1}]} + \mathbf{u}_1^{[p_{1,2}]}\right)$, it can remove all this interference during symbol extension 1. Similarly, sh_1 can remove the interference during symbol extensions 2 and 3 by applying zero-forcing based on $y^{[sh_1]}[5]$ and $y^{[sh_1]}[6]$, respectively. Hence, the terms of interference received during the transmission of $\mathbf{u}_1^{[sh_1]}$ can be subtracted afterwards. The signal at shared user sh_1 after zero-forcing interference cancellation is

$$\begin{bmatrix} y^{[sh_1]}[1] - y^{[sh_1]}[4] \\ y^{[sh_1]}[2] - y^{[sh_1]}[5] \\ y^{[sh_1]}[3] - y^{[sh_1]}[6] \\ y^{[sh_1]}[7] \end{bmatrix} = \underbrace{\begin{bmatrix} \mathbf{h}^{[sh_1]}(1)^T \\ \mathbf{h}^{[sh_1]}(2)^T \\ \mathbf{h}^{[sh_1]}(3)^T \\ \mathbf{h}^{[sh_1]}(4)^T \end{bmatrix}}_{\mathbf{H}^{[sh_1]}} \mathbf{u}_1^{[sh_1]} + \begin{bmatrix} z^{[sh_1]}[1] - z^{[sh_1]}[4] \\ z^{[sh_1]}[2] - z^{[sh_1]}[5] \\ z^{[sh_1]}[3] - z^{[sh_1]}[6] \\ z^{[sh_1]}[7] \end{bmatrix}. \tag{4.84}$$

In summary, using a reconfigurable antenna with $N_t = 2$ modes, each private user achieves 6 DoF, 2 DoF per alignment block. At the same time, using a single antenna with 4 modes, shared user sh_1 achieves 4 DoF over only one alignment block. Therefore, a total of 16 DoF are achieved along 7 symbol extensions, which yields 16/7 DoF per symbol extension. Notice that in comparison with the cBIA proposed in Figure 3.6, the proposed scheme improves upon the 2 DoF per symbol extension achieved by cBIA in a cellular network even when there is full connectivity and all BSs share data intended to every user of the system. Furthermore, this improvement is achieved using a supersymbol of 7 instead of 54 symbol extensions. Consequently, the nBIA scheme can be used over channels with smaller coherence time or bandwidth than cBIA.

To conclude, we remark that the key of nBIA lies on the generalization of the definition of alignment block for a communication system with partial connectivity. If a user k can be served by N_k transmit antennas, then an alignment block for this user consists of N_k symbol extensions over which it can receive N_k distinguishable data streams. At the same time, these beams are aligned into one dimension at all users subject to interference. On one hand, to decode N_k distinguishable data streams, the channel state of user k has to switch through N_k different modes, one per symbol extension of the alignment block. As we checked in the toy example and as is described in [88], to align the aforementioned beams into one dimension at all users subject to interference, their channel state has to be maintained constant over the N_k symbol extensions that form the alignment block of the desired user k. Moreover, the data streams intended to a specific user need to be only aligned into one dimension at those users where the power of the

interference created by the aforementioned data streams is high enough, and therefore cannot be treated as noise.

4.6.2 The network Blind Interference Alignment scheme

We now describe the nBIA scheme for the general symmetric scenario of a partially connected network. To construct the corresponding supersymbol and the beamforming matrices for each user, we can follow a systematic procedure that allows to generalize the alignment blocks to networks with partial connectivity. An sBIA scheme is implemented by each BS to send data to its set of K_p private users. As shown in [88], this strategy allows each private user to remove interference caused by transmission to all other private users in its cell. The sBIA scheme is reused by all N_{BS} BSs owing to the partial connectivity. Furthermore, all BSs of the system jointly implement a cBIA scheme to send data to the K_{sh} shared users of the system and to let them cancel the interference among them. Finally, to obtain the supersymbol shown in Figure 4.8(a), the two schemes are combined appropriately in order to remove the interference that the transmission of data to private users causes to the shared users and vice-versa.

4.6.2.1 Design of S-Block 1 of nBIA

We first consider the design of Block 1 of the supersymbol of the nBIA scheme, which will be denoted as Super-Block 1 (S-Block 1). As shown in Figure 4.8(a), the symbol extensions of the shared users are formed by repeating an identical Block 1 of a cBIA scheme for K_{sh} shared users $(N_t-1)^{K_p}$ times. Block 1 that is repeated is shown in Figure 4.8(b). As in [88], the building block of $sh_{k'}$ is formed by $M-1$ sub-blocks comprising $(M-1)^{k'-1}$ symbol extensions (see Figure 4.9(a)). Hence, it comprises

$$\mathcal{L}_{\mathrm{S-Block1}} = (M-1)^{K_{sh}} (N_t-1)^{K_p} \tag{4.85}$$

symbol extensions. During the l-th sub-block, $l \in \{1,2,\ldots,M-1\}$, the receiver of $sh_{k'}$ maintains the l-th reconfigurable mode. Hence, the temporal correlation function of $sh_{k'}$ in the entire S-Block 1 is given by

$$g_{sh_{k'}}(t) = \mathbf{h}^{[sh_{k'}]}(l) \text{ if mod } \left(t, (M-1)^{k'}\right) \in \mathcal{I}_{sh}(l), \tag{4.86}$$

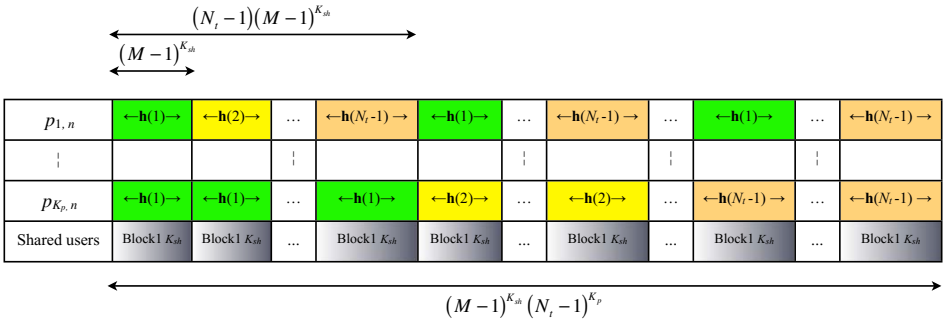

(a) S-Block 1 of the nBIA scheme for a symmetric cellular scenario with partial connectivity. Block1 K_{sh} is shown in Figure 4.8(b)

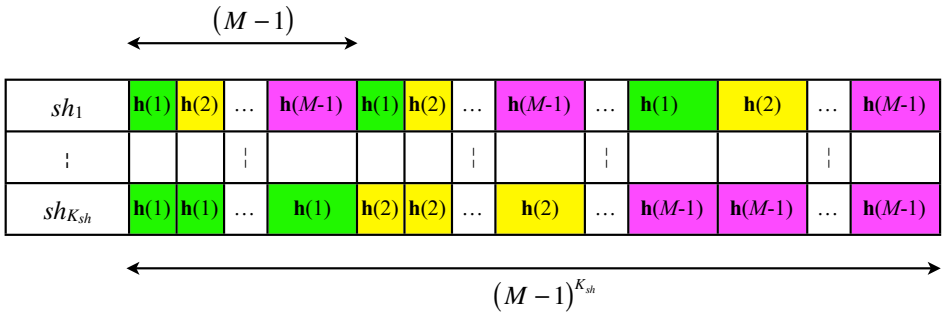

(b) Block 1 of the cBIA scheme for transmission to the K_{sh} shared users.

FIGURE 4.8: S-Block 1 of the nBIA scheme.

with $t \in \{1, 2, \ldots, (M-1)^{K_{sh}}(N_t-1)^{K_p}\}$, and

$$\mathcal{I}_{sh}(l) = \Big\{ (l-1)(M-1)^{k'-1} + 1 \\ , \ldots, l\,(M-1)^{k'-1} - 1, \mathrm{mod}\left(l\,(M-1)^{k'-1}, (M-1)^{k'}\right) \Big\}.$$

As can be seen in Figure 4.8(a), Block-1 of the private users is closely based on Block 1 of a cBIA scheme aimed at transmitting to K_p users using N_t antennas. The mode of $p_{k,n}$ is periodic with the building block shown in Figure 4.9(b), which is repeated $(N_t-1)^{K_p-k}$ times to form S-Block 1. The building block is now composed of N_t-1 sub-blocks, each with length $b_{sh}(N_t-1)^{k-1}$, where $b_{sh} = (M-1)^{K_{sh}}$. As in the sub-blocks associated with $sh_{k'}$, the l-th mode is used in the l-th sub-block, $l \in \{1, ..., N_t-1\}$. This way, during each Block 1 of Figure 4.8(b), each private user maintains a fixed mode. Hence, the temporal correlation function for private user $p_{k,n}$ for any cell $n \in \{1, 2, \ldots, N_{BS}\}$ is

$$g_{p_{k,n}}(t) = \mathbf{h}^{[p_{k,n}]}(l) \text{ if } \mathrm{mod}\left(t, (M-1)^{K_{sh}}\,(N_t-1)^{k}\right) \in \mathcal{I}_p(l) \tag{4.87}$$

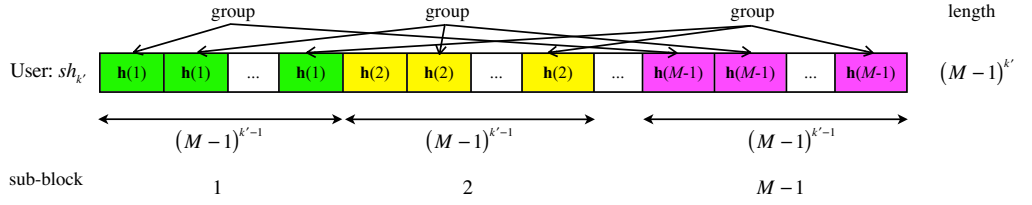

(a) Building block of shared user $sh_{k'}$.

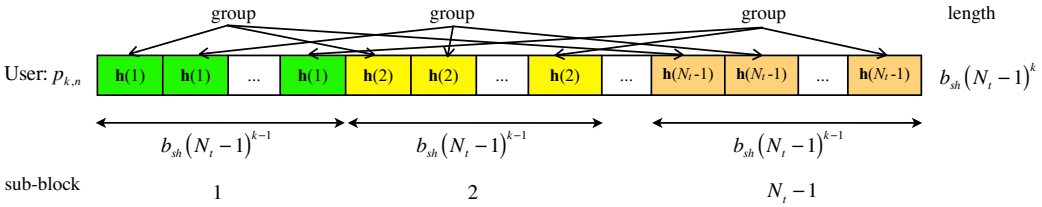

(b) Building block of private user $p_{k,n}$.

FIGURE 4.9: Building blocks of the private and the shared users.

	1	2	3	4	5	6	7	8	9	10
$p_{1,n}$	$\mathbf{h}^{[p1,n]}(1)$	$\mathbf{h}^{[p1,n]}(1)$	$\mathbf{h}^{[p1,n]}(1)$	$\mathbf{h}^{[p1,n]}(1)$	$\mathbf{h}^{[p1,n]}(1)$	$\mathbf{h}^{[p1,n]}(2)$	$\mathbf{h}^{[p1,n]}(2)$	$\mathbf{h}^{[p1,n]}(2)$	$\mathbf{h}^{[p1,n]}(2)$	$\mathbf{h}^{[p1,n]}(2)$
sh_1	$\mathbf{h}^{[sh1]}(1)$	$\mathbf{h}^{[sh1]}(2)$	$\mathbf{h}^{[sh1]}(3)$	$\mathbf{h}^{[sh1]}(4)$	$\mathbf{h}^{[sh1]}(5)$	$\mathbf{h}^{[sh1]}(1)$	$\mathbf{h}^{[sh1]}(2)$	$\mathbf{h}^{[sh1]}(3)$	$\mathbf{h}^{[sh1]}(4)$	$\mathbf{h}^{[sh1]}(5)$

FIGURE 4.10: Structure of S-Block 1 when $K_p = 1$ and $K_{sh} = 1$ in a two-cell scenario where each BS is equipped with $N_t = 3$ antennas.

with $t \in \{1, 2, \ldots, (M-1)^{K_{sh}}(N_t-1)^{K_p}\}$ and

$$\mathcal{I}_p(l) = \Big\{ (l-1)\, b_{sh}\, (N_t-1)^{k-1} + 1 \\ , \ldots, l\, b_{sh}\, (N_t-1)^{k-1} - 1, \mathrm{mod}\left(l\, b_{sh}\, (N_t-1)^{k-1}, b_{sh}\, (N_t-1)^{k} \right) \Big\},$$

where recall that $b_{sh} = (M-1)^{K_{sh}}$.

For instance, in a two-cell scenario where $N_t = 3$, $K_p = 1$ and $K_{sh} = 1$ S-Block 1 has the form shown in Figure 4.10.

4.6.2.2 Transmission strategy and beamforming matrices for S-Block 1

The key to designing the beamforming matrices is to create alignment blocks that take into account the partial connectivity of the network. Each alignment block of a shared or private user corresponds to one block column in the corresponding beamforming matrix. Since each shared user $sh_{k'}$ is served by all BSs, i.e. M antennas, each block column

of its beamforming matrix is obtained by placing an $M \times M$ identity matrix, $\mathbf{I}_M$, at the rows corresponding to the symbol extensions of the alignment block. The remaining blocks are filled with $M \times M$ zero matrices, $\mathbf{0}_M$. To obtain the signals transmitted from the BSs to shared user $sh_{k'}$, the beamforming matrix is multiplied by

$$\mathbf{u}_{\ell'}^{[sh_{k'}]} = \left[\mathbf{u}_{\ell'}^{[sh_{k'},1]^T} \cdots \quad \mathbf{u}_{\ell'}^{[sh_{k'},n]^T} \cdots \quad \mathbf{u}_{\ell'}^{[sh_{k'},N_{BS}]^T}\right]^T \tag{4.88}$$

where $\mathbf{u}_{\ell'}^{[sh_{k'}]} \in \mathbb{C}^{N_{BS}N_t \times 1}$, $\ell' = 1, 2, \ldots, (M-1)^{K_{sh}-1}(N_t-1)^{K_p}$ and $\mathbf{u}_{\ell'}^{[sh_{k'},n]} \in \mathbb{C}^{N_t \times 1}$ contains the N_t symbols transmitted from BS n to $sh_{k'}$ during alignment block ℓ'.

The same procedure is applied to obtain the beamfroming matrix for each private user at any cell n. However, $p_{k,n}$ is only served by the N_t antennas of BS n. Recall that the signals $\mathbf{x}^{[n]}[t]$ transmitted by BSs n do not contain data intended to any private user $p_{k,n'}$, $n' \neq n$. Therefore, each block column ℓ of the beamforming matrix is formed in the same way as for the shared users. However, to obtain the signals transmitted from the BSs to $p_{k,n}$ the corresponding beamforming matrix is multiplied by

$$\mathbf{u}_{\ell}^{[p_{k,n}]} = \left[\mathbf{0}_{N_t(n-1),1}{}^T \quad \mathbf{u}_{\ell}^{[p_{k,n},n]^T} \quad \mathbf{0}_{N_t(N_{BS}-1),1}{}^T\right]^T \tag{4.89}$$

and $\ell = 1, 2, \ldots, (N_t-1)^{K_p-1}(M-1)^{K_{sh}}$.

To maintain the data beams of one alignment block distinguishable at the user for which they are intended, the channel between the transmit antennas and the user should change at each symbol extension of each alignment block. Moreover, during these symbol extensions, each of the affected users should maintain a constant channel so that interference be aligned. As is shown in Sections 4.6.2.3 and 4.6.2.4, in S-Block 1 both decodability and interference alignment requirements can be satisfied by using *groups*. Each *group* consists of the first $M-1$ or N_t-1 symbol extensions of the alignment block of a shared or private user, respectively. In particular, we can group the ℓ'-th symbol extension in each one of the $M-1$ sub-blocks within one building block as shown in Figure 4.9(a) for shared user $sh_{k'}$. Since each sub-block consists of $(M-1)^{k'-1}$ symbol extensions, a total of $(M-1)^{k'-1}$ *groups* can be built within one building block. As was mentioned above, each of these *groups* will be associated with a specific alignment block of $sh_{k'}$. Similarly, as shown in Figure 4.9(b), for private user $p_{k,n}$, the ℓ-th symbol extension in each of the N_t-1 sub-blocks of one building block can be grouped. Since each sub-block of $p_{k,n}$

is now composed of $b_{sh}(N_t-1)^{k-1}$ symbol extensions, a total of $b_{sh}(N_t-1)^{k-1}$ *groups* can be formed within one building block. Recalling that S-Block 1 of $sh_{k'}$ consists of $(N_t-1)^{K_p}(M-1)^{K_{sh}-k'}$ building blocks of $(M-1)^{k'}$ symbol extensions, the ℓ'-th *group* in the p'-th building block of $sh_{k'}$ comprises symbol extensions

$$\{(p'-1)(M-1)^{k'}+\kappa(M-1)^{k'-1}+\ell'\}_{\kappa=0}^{M-2} \tag{4.90}$$

where $\ell' \in \{1,2,\ldots,(M-1)^{k'-1}\}$ and

$$p' \in \{1,2,\ldots,(M-1)^{K_{sh}-k'}(N_t-1)^{K_p}\}.$$

Analogously, taking into account that S-Block 1 of $p_{k,n}$, $n \in \{1,2,\ldots,N_{BS}\}$ is formed by $(N_t-1)^{K_p-k}$ building blocks of $b_{sh}(N_t-1)^k$ symbol extensions, the ℓ-th *group* in its p-th building block consists of symbol extensions

$$\{(p-1)\,b_{sh}\,(N_t-1)^k+\kappa\,b_{sh}\,(N_t-1)^{k-1}+\ell\}_{\kappa=0}^{N_t-2}, \tag{4.91}$$

where $p \in \{1,2,\ldots,(N_t-1)^{K_p-k}\}$, $\ell \in \{1,\ldots,b_{sh}(N_t-1)^{k-1}\}$, and $b_{sh}=(M-1)^{K_{sh}}$.

For instance, particularizing to our illustrative scenario with two cells, $N_t=3$, $K_p=1$ and $K_{sh}=1$, corresponding to the supersymbol shown in Figure 4.10, the signal transmitted during S-Block 1 is given by

$$\mathbf{X}=\underbrace{\begin{bmatrix}\mathbf{I}_{30}\\ \mathbf{I}_{30}\end{bmatrix}\begin{bmatrix}\mathbf{u}_1^{[p_{1,1}]}\\ \mathbf{u}_2^{[p_{1,1}]}\\ \mathbf{u}_3^{[p_{1,1}]}\\ \mathbf{u}_4^{[p_{1,1}]}\\ \mathbf{u}_5^{[p_{1,1}]}\end{bmatrix}}_{\text{to } p_{1,1}}+\underbrace{\begin{bmatrix}\mathbf{I}_{30}\\ \mathbf{I}_{30}\end{bmatrix}\begin{bmatrix}\mathbf{u}_1^{[p_{1,2}]}\\ \mathbf{u}_2^{[p_{1,2}]}\\ \mathbf{u}_3^{[p_{1,2}]}\\ \mathbf{u}_4^{[p_{1,2}]}\\ \mathbf{u}_5^{[p_{1,2}]}\end{bmatrix}}_{\text{to } p_{1,2}}+\underbrace{\begin{bmatrix}\mathbf{I}_6 & \mathbf{0}_6\\ \mathbf{I}_6 & \mathbf{0}_6\\ \mathbf{I}_6 & \mathbf{0}_6\\ \mathbf{I}_6 & \mathbf{0}_6\\ \mathbf{I}_6 & \mathbf{0}_6\\ \mathbf{0}_6 & \mathbf{I}_6\\ \mathbf{0}_6 & \mathbf{I}_6\\ \mathbf{0}_6 & \mathbf{I}_6\\ \mathbf{0}_6 & \mathbf{I}_6\end{bmatrix}}_{\text{to } sh_1}\begin{bmatrix}\mathbf{u}_1^{[sh_1]}\\ \mathbf{u}_2^{[sh_1]}\end{bmatrix}, \tag{4.92}$$

where

$$\begin{aligned}\mathbf{u}_{\ell}^{[p_{1,1}]} &= \left[\mathbf{u}_{\ell}^{[p_{1,1},1]^T} \quad \mathbf{0}_{2,1}{}^T\right]^T, \\ \mathbf{u}_{\ell}^{[p_{1,2}]} &= \left[\mathbf{0}_{2,1}{}^T \quad \mathbf{u}_{\ell}^{[p_{1,2},2]^T}\right]^T, \\ \mathbf{u}_{\ell'}^{[sh_1]} &= \left[\mathbf{u}_{\ell'}^{[sh_1,1]^T} \quad \mathbf{u}_{\ell'}^{[sh_1,2]^T}\right]^T.\end{aligned} \tag{4.93}$$

Each private user has 5 *groups* formed by 2 symbol extensions. Specifically, for both private users these *groups* are formed by the pairs of symbol extensions $\{1,6\}$, $\{2,7\}$, $\{3,8\}$, $\{4,9\}$ and $\{5,10\}$. On the contrary, shared user sh_1 has two *groups*, each composed of 5 symbol extensions, i.e. $\{1,2,3,4,5\}$ and $\{6,7,8,9,10\}$.

4.6.2.3 Achieving decodability and interference alignment at the shared users

First, recall that the channel switching pattern for each shared user is created by concatenating $(N_t-1)^{K_p}$ identical Blocks 1 associated with a cBIA scheme aimed at transmitting data to K_{sh} users. This way, based on the results in [89], it is straightforward to show that each *group* ℓ' of each user $sh_{k'}$ is formed by $M-1$ symbol extensions over which the mode of its antenna changes while the state of all other shared users remains constant. Consequently, the data sent by all BSs to each user $sh_{k'}$ over each of its alignment blocks can be decoded and the interference induced to the other shared users is aligned into one dimension of their signal space.

Note that the private users are also subject to interference because of the data sent by the BSs to the shared users. To also align this interference, the $M-1$ data streams sent to a shared user over one of its *groups* also need to be contained into one dimension at all private users. As is also shown in Figures 4.8(a) and 4.11(a), the channel mode of all private users does not change during an entire Block 1 of shared users. Moreover, recall that each group of shared user $sh_{k'}$ is composed of symbols within a specific building block, which belongs to one of the Blocks 1 of $sh_{k'}$. Hence, within each *group* of any shared user $sh_{k'}$ the reconfigurable modes of the antennas of all private users remain the same state. In conclusion, the interference caused by transmission to $sh_{k'}$ during each one of its *groups* is aligned into one dimension at all private users.

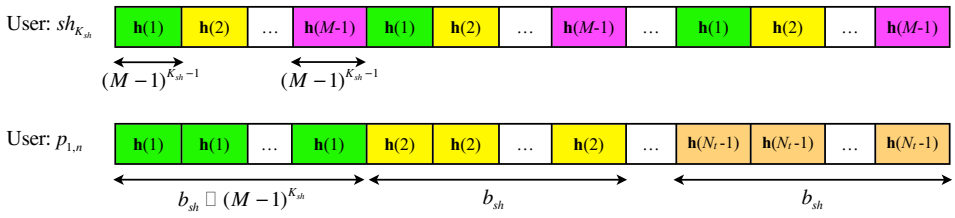

(a) The building blocks of shared users $sh_{K_{sh}}$ and $p_{1,n}$.

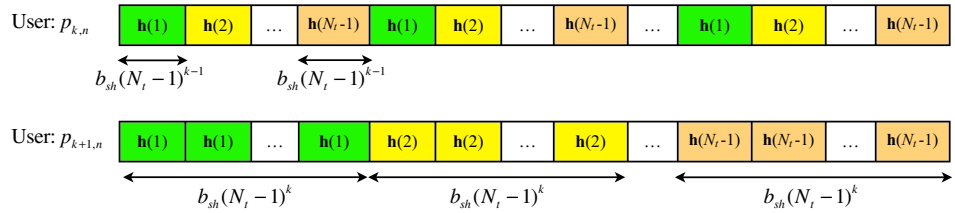

(b) The building blocks of private users $p_{k,n}$ and $p_{k+1,n}$.

FIGURE 4.11: Building blocks of the private and shared users.

4.6.2.4 Achieving decodability and interference alignment at the private users

We now concentrate on the private users. First, we check that the channel state of each private user changes at each symbol extension within any of its *groups*. Note that (4.91) specifies the symbol extensions of the ℓ-th group in the p-th building block of private user $p_{k,n}$. Now, it can be easily seen that, for all $p \in \{1, 2, \ldots, (N_t-1)^{K_p-k}\}$, the modulus of these symbol extensions with $b_{sh}(N_t-1)^k$ yields

$$\{\kappa\, b_{sh}\,(N_t-1)^{k-1} + \ell\}_{\kappa=0}^{N_t-2} \tag{4.94}$$

with $\ell \in \{1, 2, \ldots, b_{sh}(N_t-1)^{k-1}\}$. Hence, from (4.87), the channel states of $p_{k,n}$ are $\mathbf{h}^{[p_{k,n}]}(1), \mathbf{h}^{[p_{k,n}]}(2), \ldots, \mathbf{h}^{[p_{k,n}]}(N_t-1)$ during the symbol extensions that form each one of its *groups*.

Next, we focus on proving that the interference caused by the transmission to private user $p_{k,n}$ is aligned into one dimension at the signal space of the other private users in cell n. First, consider private users $\{p_{j,n}\}_{j=1}^{k-1}$. Note that the remainder of the division of the symbol extensions in (4.91) by $b_{sh}(N_t-1)^j$ is the same, i.e. $\mathrm{mod}(\ell, b_{sh}\,(N_t-1)^j)$, for a specific *group* ℓ in the p-th building block of $p_{k,n}$ and any $j \in \{1, 2, \ldots, k-1\}$. Hence, from (4.87), within each *group* of $p_{k,n}$, the channel state of all other private users

$\{p_{j,n}\}_{j=1}^{k-1}$ remains constant. Now, consider private users $\{p_{j,n}\}_{j=k+1}^{K_p}$. Notice that the lengths of the sub-blocks of the private users in S-Block 1 are larger than $b_{sh}\,(N_t-1)^k$, i.e. the length of a building block associated with private user $p_{k,n}$. Hence, as is shown in Figure 4.11(b), because the boundaries of the building blocks of $p_{k,n}$ are aligned with those of the sub-blocks of $p_{j,n},\ j \in \{k+1, k+2, \ldots, K_p\}$, the channels of this last sub-group of private users are the same within each *group* of $p_{k,n}$. Therefore, from the structure of S-Block 1 we can conclude that the data streams transmitted over the N_t-1 symbol extensions of the ℓ-th *group* of user $p_{k,n}$ are aligned into one dimension at all other private users of cell n.

Ultimately, we show that interference caused by transmission to user $p_{k,n}$ is also aligned at the K_{sh} shared users. Recall that because of the partial connectivity, the transmission of data from a BS to any of its private users does not create interference to the private users of the other cells. Therefore, we only need to verify that for each *group* of users $p_{k,n}$ the channel state of all shared users remains constant. Consider any shared user $sh_{k'}$ and the symbol extensions in (4.91), which form the ℓ-th group in the p-th building block of $p_{k,n}$. Since $b_{sh} = (M-1)^{K_{sh}}$ is an integer multiple of $(M-1)^{k'}$, the remainders of the indices of the symbol extensions in (4.91) divided by $(M-1)^{k'}$ are the same, i.e. $\mathrm{mod}(\ell, (M-1)^{k'})$. Consequently, from (4.86), within each *group* of $p_{k,n}$, the channel state of any user $sh_{k'}$ is constant. Hence, the requirements of decodability and alignment are satisfied in each *group* of each private user.

As explained previously, due to the partial connectivity, the transmission of data from BS n', $n' \neq n$, to its private users does not impose any constraints on the design of the channel pattern and the beamforming matrices of private user $p_{k,n}$. Thus, private users $\{p_{k,n}\}_{n=1}^{N_{BS}}$ can *reuse* the same beamforming matrix and the same channel pattern in S-Block 1 when receiving data from their corresponding BSs. This can be seen in our illustrative two-cell scenario in (4.92) and Figure 4.10. More generally, the same fact can be verified in Figure 4.8(a) and in (4.91) where the symbol extensions of the *groups* associated with private users $\{p_{k,n}\}_{n=1}^{N_{BS}}$ are the same. As a result, not only are the N_t data beams transmitted within each *group* of one private user $p_{k,n}$ aligned into one dimension at each shared user, but also all data beams transmitted to all private users $\{p_{k,n}\}_{n=1}^{N_{BS}}$ within each *group* specified in (4.91) are projected into the *same* single dimension at each shared user.

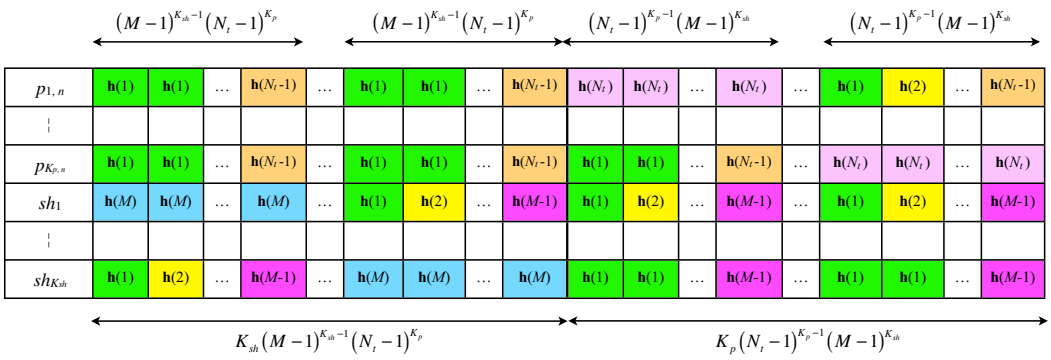

FIGURE 4.12: S-Block 2 of the nBIA supersymbol.

4.6.2.5 Design of S-Block 2

From the design of S-Block-1 and the corresponding beamforming matrices, we can undertake the design of the switching pattern of all users during Block 2 of the nBIA scheme, which will be called Super-Block 2 (S-Block 2). The purpose of S-Block 2 is to complete the alignment blocks of all users so that each user can decode the data received along its *groups* and cancel the interference caused by the transmission of data to other users during S-Block 1. From (4.90) notice that the number of alignment blocks associated with each shared user is equal to $(M-1)^{K_{sh}-1}(N_t-1)^{K_p}$. Consequently, to complete the alignment blocks of the K_{sh} shared users, a total of

$$t_{sh} = K_{sh}\left[(M-1)^{K_{sh}-1}(N_t-1)^{K_p}\right] \tag{4.95}$$

symbol extensions are needed in S-Block 2. As shown in Figure 4.12, these symbol extensions are $\mathcal{L}_{\text{S-Block1}}+1, \mathcal{L}_{\text{S-Block1}}+2, \ldots, \mathcal{L}_{\text{S-Block1}}+t_{sh}$, where $\mathcal{L}_{\text{S-Block1}} = (M-1)^{K_{sh}}(N_t-1)^{K_p}$ is the length of S-Block 1. Within the aforementioned symbol extensions, sub-block

$$\{\mathcal{L}_{\text{S-Block1}}+(k'-1)\,t_{sh}/K_{sh}+\ell'\}_{\ell'=1}^{t_{sh}/K_{sh}} \tag{4.96}$$

with $k' \in \{1,2,\ldots,K_{sh}\}$, provides the last symbol extensions of the alignment blocks of $sh_{k'}$. In particular, each symbol extension specified in (4.96) constitutes the last element of the ℓ'-th alignment block of $sh_{k'}$. Hence, in order to be able to decode the signals of interest over the alignment block, user $sh_{k'}$ employs the M-th preset mode during each symbol extension in (4.96). This way, if the N_{BS} BSs repetitively transmit

$\mathbf{u}_{\ell'}^{[sh_{k'}]} \in \mathbb{C}^{M\times 1}$ within each symbol extension of the ℓ'-th alignment block of $sh_{k'}$, it can decode $\mathbf{u}_{\ell'}^{[sh_{k'}]}$ after removing the interference.

Since the interference caused by the first $M-1$ transmissions of $\mathbf{u}_{\ell'}^{[sh_{k'}]}$ during the ℓ'-th *group* of $sh_{k'}$ in S-Block 1 is aligned into one dimension at all other shared and private users, zero-forcing can be applied to remove it. Due to the fact that only $\mathbf{u}_{\ell'}^{[sh_{k'}]}$, $\ell' \in \{1, 2, \ldots, \frac{t_{sh}}{K_{sh}}\}$, are transmitted during each symbol extension of (4.96), any shared user $sh_{j'} \neq sh_{k'}$ and all private users $p_{k,n}$ can measure the interference caused by the transmission of $\mathbf{u}_{\ell'}^{[sh_{k'}]}$. Therefore, they can subtract the interference received in S-Block 1 if, during the symbol extensions given in (4.96), they maintain the same channel state as the one used during the ℓ'-th alignment *group* of $sh_{k'}$. From (4.90) notice that the symbol extensions that form the ℓ'-th *group* of shared user $sh_{k'}$ are

$$\{p_{sh}(\ell', k')\,(M-1)^{k'} + \kappa(M-1)^{k'-1} + l_{sh}(\ell', k')\}_{\kappa=0}^{M-2} \tag{4.97}$$

where

$$l_{sh}(\ell, k') = \mathrm{mod}(\ell' - 1, (M-1)^{k'-1}) + 1$$

and $p_{sh}(\ell', k') = \left\lfloor \frac{\ell'-1}{(M-1)^{k'-1}} \right\rfloor$. Consequently, during the ℓ'-th symbol extension specified in (4.96) the channel state of shared users $sh_{j'} \neq sh_{k'}$ equals

$$g_{sh_{j'}}\left(p_{sh}(\ell', k')\,(M-1)^{k'} + l_{sh}(\ell', k')\right),$$

whereas the channel state for all private users $\{p_{k,n}\}_{k=1}^{N_{BS}}$ is

$$g_{p_{k,n}}\left(p_{sh}(\ell', k')\,(M-1)^{k'} + l_{sh}(\ell', k')\right),$$

with $g_{sh_{j'}}$ and $g_{p_{k,n}}$ given in (4.86) and (4.87), respectively.

Next, we consider the design of S-Block 2 for the private users. As we have seen in (4.91), the number of alignment blocks per private user equals $b_{sh}(N_t - 1)^{K_p - 1}$. Due to the partial connectivity, BSs n and n' can transmit simultaneously the data associated with a specific alignment block of $p_{k,n}$ and $p_{k,n'}$, respectively, without interfering with each other. Thus, one symbol extension of S-Block 2 can be *reused* by private users $\{p_{k,n}\}_{n=1}^{N_{BS}}$ to complete one of their alignment blocks. Thus, since there are K_p private users per

cell, a total of

$$t_p = K_p \left[(M-1)^{K_{sh}} (N_t - 1)^{K_p - 1} \right] \tag{4.98}$$

symbol extensions are needed in S-Block 2 for all private users. Therefore, the entire length of S-Block 2 is

$$\mathcal{L}_{\text{S-Block2}} = t_{sh} + t_p = K_{sh} \left[(M-1)^{K_{sh}-1} (N_t - 1)^{K_p} \right] + K_p \left[(M-1)^{K_{sh}} (N_t - 1)^{K_p - 1} \right] \tag{4.99}$$

In order not to create any interference, similar to the symbol extensions of S-Block 2 for the shared users, each BS n only transmits data to one specific user in its cell. However, this time the BSs do not transmit data to a specific shared user. Instead, each BS n only transmits data to a specific private user $p_{k,n}$ during each of the t_p symbol extensions. As shown in Figure 4.12, the t_p symbol extensions of S-Block 2 are $\mathcal{L}_{\text{S-Block1}} + t_{sh} + 1, \mathcal{L}_{\text{S-Block1}} + t_{sh} + 2, \ldots, \mathcal{L}_{\text{S-Block1}} + t_{sh} + t_p$. Within these symbol extensions, the sub-block

$$\{\mathcal{L}_{\text{S-Block1}} + t_{sh} + (k-1)\, t_p/K_p + \ell\}_{\ell=1}^{t_p/K_p} \tag{4.100}$$

$k \in \{1, 2, \ldots, K_p\}$, provides the last symbol extensions of the alignment blocks of private users $\{p_{k,n}\}_{n=1}^{N_{BS}}$. Hence, during each symbol extension in (4.100) the private users have to keep the N_t-th preset mode. This way, if each BS n applies a repetition code to send $\mathbf{u}_\ell^{[p_{k,n}]} \in \mathbb{C}^{N_t \times 1}$ during each symbol extension within the ℓ-th alignment block of $\{p_{k,n}\}_{n=1}^{N_{BS}}$, each user $p_{k,n}$ at any cell n can use the signals received during its ℓ-th alignment block to decode $\mathbf{u}_\ell^{[p_{k,n}]}$.

Continuing the design of the symbol extensions of S-Block 2, notice that the simultaneous transmissions of $\{\mathbf{u}_\ell^{[p_{k,n}]}\}_{n=1}^{N_{BS}}$ during the ℓ-th *group* of private users $\{p_{k,n}\}_{n=1}^{N_{BS}}$ are aligned into the same single dimension of the signal space of each shared user $sh_{k'}$. Hence, to remove the interference caused by these transmissions, $sh_{k'}$ can apply zero-forcing based on the interference signal measured in S-Block 2. To do so, the preset mode of $sh_{k'}$ during the ℓ-th symbol extension in (4.100) has to be equal to the mode of $sh_{k'}$ during the ℓ-th alignment *group* of private users $\{p_{k,n}\}_{n=1}^{N_{BS}}$, which consists of symbol extensions

$$\{p_b(\ell, k)\, b_{sh}\, (N_t - 1)^k + \kappa\, b_{sh}\, (N_t - 1)^{k-1} + l_p(\ell, k)\}_{\kappa=0}^{N_t - 2} \tag{4.101}$$

with $l_p(\ell,k) = \mathrm{mod}(\ell-1, b_{sh}\,(N_t-1)^{k-1}) + 1$ and $p_p(\ell,k) = \left\lfloor \frac{\ell-1}{b_{sh}\,(N_t-1)^{k-1}} \right\rfloor$. Mathematically, during the ℓ-th symbol extension in (4.100) the channel state of $sh_{k'}$ equals $g_{sh_{k'}}\left(p_p(\ell,k)\,b_{sh}\,(N_t-1)^k + l_p(\ell,k)\right)$, where $g_{sh_{k'}}$ is given in (4.86).

Due to the fact that the transmitted symbols $\mathbf{u}_\ell^{[p_{k,n}]}$ during the symbol extensions of S-Block 1 are aligned into one dimension at the signal space of any private user $p_{j,n} \neq p_{k,n}$, each private user of cell n can apply the same technique as shared user $sh_{k'}$ to remove the interference caused by the transmission of $\mathbf{u}_\ell^{[p_{k,n}]}$. Specifically, at private user $p_{j,n} \neq p_{k,n}$, the interference is removed by applying zero-forcing based on the signal received during the ℓ-th symbol extension in (4.100) with the mode of its antenna equal to $g_{p_{j,n}}\left(p_p(\ell,k)\,b_{sh}\,(N_t-1)^k + l_p(\ell,k)\right)$, where $g_{p_{j,n}}$ is given in (4.87). Finally, due to the partial connectivity, the transmission of $\mathbf{u}_\ell^{[p_{k,n}]}$ to any private user $p_{k,n}$ at cell n does not interfere with the communication between BS n' and any user $p_{j,n'}$ at cell $n' \neq n$. As a result, users $p_{j,n'} \neq p_{k',n}$ do not need to cancel the interference caused by the transmission of data to $p_{k,n}$ during S-Block 1.

4.6.3 Alternative Supersymbol Design

An alternative design of the supersymbol of the nBIA scheme can also be obtained. As shown in Figure 4.13, a Block 1 associated with an sBIA scheme aimed at transmitting data to K_p users is repeated $(M-1)^{K_{sh}}$ times to construct S-Block 1 for the K_p private users of each cell n. For the shared users, S-Block 1 is formed by augmenting the length of the sub-blocks that form Block 1 of a cBIA scheme for a system with K_{sh} shared users and M transmit antennas. This time, the length of the sub-block of a shared user equals $(N_t-1)^{K_p}\,(M-1)^{k'-1}$ symbol extensions. Similarly to S-Block 2 of Figure 4.12, the alternative design for S-Block 2 is obtained by completing the alignment blocks whose groups form S-Block 1. It can be easily verified that the same DoF as in (4.102) can also be achieved by the alternative structure of the supersymbol.

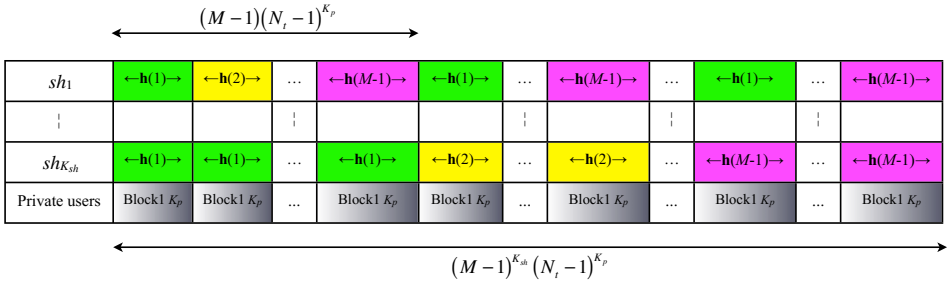

FIGURE 4.13: Alternative design of S-Block 1 of the nBIA supersymbol.

4.6.4 Achievable Degrees of Freedom

With the nBIA scheme, each shared user achieves M DoF per alignment block, whereas each private user attains N_t DoF per alignment block. Since the total number of alignment blocks of each shared user is equal to $t_{sh}/K_{sh} = (M-1)^{K_{sh}-1}(N_t-1)^{K_p}$ in the supersymbol of the nBIA scheme, a total of $M\,t_{sh}/K_{sh}$ DoF per supersymbol are achieved for each shared user. Following a similar reasoning and recalling that each private user employs $(M-1)^{K_{sh}}(N_t-1)^{K_p-1}$ alignment blocks per supersymbol, a total $N_t\,t_p/K_p$ DoF are attained by each private user in a supersymbol. Thus, since the length of the supersymbol equals $\mathcal{L}_{\text{S-Block1}} + \mathcal{L}_{\text{S-Block2}}$ symbol extensions where $\mathcal{L}_{\text{S-Block2}} = t_{sh} + t_p$ is the number of symbol extensions in S-Block 2 (see Figs. 4.8(a), 4.8(b) and 4.12), when nBIA is used for the symmetric scenario the achievable sum-DoF per symbol extension are

$$\begin{aligned}\text{DoF}_{\text{nBIA}} &= \frac{K_{sh}\,M\,\frac{t_{sh}}{K_{sh}} + N_{BS}\,K_p\,N_t\,\frac{t_p}{K_p}}{\mathcal{L}_{\text{S-Block1}} + \mathcal{L}_{\text{S-Block2}}} \\ &= \frac{M\left[K_{sh}\,(N_t-1) + K_p\,(M-1)\right]}{(M-1)(N_t-1) + K_{sh}\,(N_t-1) + K_p\,(M-1)}.\end{aligned} \tag{4.102}$$

Notice that the achievable DoF can be split between

$$\text{DoF}_{\text{nBIA}_{\text{pri}}} = \frac{N_t K_p (M-1)}{(M-1)(N_t-1) + K_{sh}\,(N_t-1) + K_p\,(M-1)}, \tag{4.103}$$

in each group of private users and

$$\text{DoF}_{\text{nBIA}_{\text{sh}}} = \frac{M K_{sh} (N_t-1)}{(M-1)(N_t-1) + K_{sh}\,(N_t-1) + K_p\,(M-1)}, \tag{4.104}$$

for the set of shared users located between the set of BSs. Checking the information-theoretic sum-DoF outer bound derived for private and shared users in (4.27) and (4.28),

respectively, it is demonstrated that the proposed nBIA scheme results DoF-optimal in symmetric cellular networks with partial connectivity.

4.6.5 Asymmetric Partially Connected Cellular Networks

So far, a symmetric scenario has been considered. In this section, the nBIA scheme is extended to asymmetric cellular networks where the number of private users can be different at each cell. Moreover, it will be shown that there exist some settings for which the extension of the proposed scheme achieves the sum-DoF outer bound of Section 4.3. However, this is not generally the case, and therefore, the DoF optimality of the proposed approach for asymmetric cellular networks is still an open problem.

For illustrative purposes, we consider a toy example where $N_t = 2$, $K_{sh} = 1$, $K_{p,1} = 2$ and $K_{p,2} = 1$ (see Figure 4.14). Note that the number of private users is now different at each cell. By solving the optimization problem of (4.18) and (4.22), it is found that the outer bound of the achievable DoF is 2.5 DoF. The supersymbol of the nBIA scheme

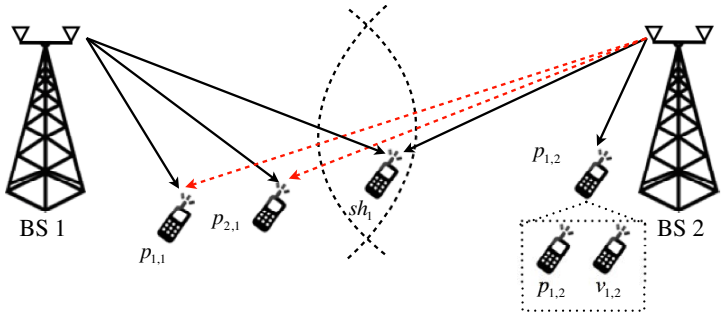

FIGURE 4.14: Asymmetric toy example. BS 1 and BS 2 transmit to $K_{p,1} = 2$ and $K_{p,2} = 1$, respectively, and both transmit to $K_{sh} = 1$ shared user. For the sake of simplicity only the intercell interference has been depicted from BS 2 to users in cell 1 with red dotted lines.

of Section 4.6.2 is shown in Figure 4.15. Each private user exploits 3 alignment blocks, providing $N_t = 2$ DoF each, whereas the shared user attains $M = 4$ DoF during 10 symbol extensions. Therefore, the proposed scheme attains $\frac{2\times3\times3+4}{10} = \frac{22}{10}$ DoF in total, which is $\frac{3}{10}$ below the outer bound.

In Figure 4.15, the pairs of symbol extensions {1,4}, {2,5} and {3,6} constitute alignment blocks of private user $p_{1,2}$. During each of the aforementioned alignment blocks, private user $p_{1,2}$ achieves 2 DoF. Moreover, symbol extension {10} is used by $p_{1,2}$ to remove the interference caused by the transmission to the shared user sh_1. Note also that

	1	2	3	4	5	6	7	8	9	10
$p_{1,1}$	$\mathbf{h}^{[p_{1,1}]}(1)$	$\mathbf{h}^{[p_{1,1}]}(1)$	$\mathbf{h}^{[p_{1,1}]}(1)$	$\mathbf{h}^{[p_{1,1}]}(2)$	$\mathbf{h}^{[p_{1,1}]}(2)$	$\mathbf{h}^{[p_{1,1}]}(2)$	$\mathbf{h}^{[p_{1,1}]}(1)$	$\mathbf{h}^{[p_{1,1}]}(1)$	$\mathbf{h}^{[p_{1,1}]}(1)$	$\mathbf{h}^{[p_{1,1}]}(1)$
$p_{2,1}$	$\mathbf{h}^{[p_{2,1}]}(1)$	$\mathbf{h}^{[p_{2,1}]}(1)$	$\mathbf{h}^{[p_{2,1}]}(1)$	$\mathbf{h}^{[p_{2,1}]}(1)$	$\mathbf{h}^{[p_{2,1}]}(1)$	$\mathbf{h}^{[p_{2,1}]}(1)$	$\mathbf{h}^{[p_{2,1}]}(2)$	$\mathbf{h}^{[p_{2,1}]}(2)$	$\mathbf{h}^{[p_{2,1}]}(2)$	$\mathbf{h}^{[p_{2,1}]}(1)$
$p_{1,2}$	$\mathbf{h}^{[p_{1,2}]}(1)$	$\mathbf{h}^{[p_{1,2}]}(1)$	$\mathbf{h}^{[p_{1,2}]}(1)$	$\mathbf{h}^{[p_{1,2}]}(2)$	$\mathbf{h}^{[p_{1,2}]}(2)$	$\mathbf{h}^{[p_{1,2}]}(2)$	$\mathbf{h}^{[p_{1,2}]}(1)$	$\mathbf{h}^{[p_{1,2}]}(1)$	$\mathbf{h}^{[p_{1,2}]}(1)$	$\mathbf{h}^{[p_{1,2}]}(1)$
sh_1	$\mathbf{h}^{[sh_1]}(1)$	$\mathbf{h}^{[sh_1]}(2)$	$\mathbf{h}^{[sh_1]}(3)$	$\mathbf{h}^{[sh_1]}(1)$	$\mathbf{h}^{[sh_1]}(2)$	$\mathbf{h}^{[sh_1]}(3)$	$\mathbf{h}^{[sh_1]}(1)$	$\mathbf{h}^{[sh_1]}(2)$	$\mathbf{h}^{[sh_1]}(3)$	$\mathbf{h}^{[sh_1]}(4)$

FIGURE 4.15: Supersymbol for the asymmetric scenario with $N_t = 2$, $K_{p,1} = 2$, $K_{p,2} = 1$ and $K_{sh} = 1$. Dashed lines represent the idle slots that can be used for transmission of $v_{1,2}$.

symbol extensions {7,8,9}, which are employed by BS 1 to transmit to $p_{2,1}$ and complete its alignment blocks, are used by shared user sh_1 in order to remove the interference caused by the transmission from BS 1 to user $p_{2,1}$. On the contrary, symbol extensions {7,8,9} are idle for private user $p_{1,2}$ since it is not subject to interference caused by the transmission to $p_{2,1}$, and therefore, does not need to remove it. In order to exploit them, we can devise a virtual user $v_{1,2}$, which is the same physical user as $p_{1,2}$. Since no changes are required at BS 1, we only consider transmission of BS 2. Taking virtual user $v_{1,2}$ into account, the symbols sent by BS 2 are now

$$\mathbf{X} = \underbrace{\begin{bmatrix} \mathbf{I} & \mathbf{0} & \mathbf{0} \\ \mathbf{0} & \mathbf{I} & \mathbf{0} \\ \mathbf{0} & \mathbf{0} & \mathbf{I} \\ \mathbf{I} & \mathbf{0} & \mathbf{0} \\ \mathbf{0} & \mathbf{I} & \mathbf{0} \\ \mathbf{0} & \mathbf{0} & \mathbf{I} \\ \mathbf{0} & \mathbf{0} & \mathbf{0} \\ \mathbf{0} & \mathbf{0} & \mathbf{0} \\ \mathbf{0} & \mathbf{0} & \mathbf{0} \\ \mathbf{0} & \mathbf{0} & \mathbf{0} \end{bmatrix}}_{p_{1,2}} \begin{bmatrix} \mathbf{u}_1^{[p_{1,2}]} \\ \mathbf{u}_2^{[p_{1,2}]} \\ \mathbf{u}_3^{[p_{1,2}]} \end{bmatrix} + \underbrace{\begin{bmatrix} \mathbf{I} & \mathbf{0} & \mathbf{0} \\ \mathbf{0} & \mathbf{I} & \mathbf{0} \\ \mathbf{0} & \mathbf{0} & \mathbf{I} \\ \mathbf{0} & \mathbf{0} & \mathbf{0} \\ \mathbf{0} & \mathbf{0} & \mathbf{0} \\ \mathbf{0} & \mathbf{0} & \mathbf{0} \\ \mathbf{I} & \mathbf{0} & \mathbf{0} \\ \mathbf{0} & \mathbf{I} & \mathbf{0} \\ \mathbf{0} & \mathbf{0} & \mathbf{I} \\ \mathbf{0} & \mathbf{0} & \mathbf{0} \end{bmatrix}}_{v_{1,2}} \begin{bmatrix} \mathbf{u}_1^{[v_{1,2}]} \\ \mathbf{u}_2^{[v_{1,2}]} \\ \mathbf{u}_3^{[v_{1,2}]} \end{bmatrix} + \underbrace{\begin{bmatrix} \mathbf{I} \\ \mathbf{I} \\ \mathbf{I} \\ \mathbf{0} \\ \mathbf{0} \\ \mathbf{0} \\ \mathbf{0} \\ \mathbf{0} \\ \mathbf{0} \\ \mathbf{I} \end{bmatrix}}_{sh_1} \mathbf{u}_1^{[sh_1]}, \tag{4.105}$$

where

$$\begin{aligned} \mathbf{u}_1^{[sh_1]} &= \begin{bmatrix} \mathbf{0}_{2,1}{}^T & \mathbf{u}_1^{[sh_1,2]^T} \end{bmatrix}^T \\ \mathbf{u}_\ell^{[p_{1,2}]} &= \begin{bmatrix} \mathbf{0}_{2,1}{}^T & \mathbf{u}_\ell^{[p_{1,2},2]^T} \end{bmatrix}^T \\ \mathbf{u}_\ell^{[v_{1,2}]} &= \begin{bmatrix} \mathbf{0}_{3,1}{}^T & u_\ell^{[p_{1,2},2]^T} \end{bmatrix}^T . \end{aligned} \tag{4.106}$$

The private users $p_{1,1}$ and $p_{2,1}$ served by BS 1 are not subject to interference by the transmission of BS 2 to $v_{1,2}$. The shared user can measure the sum of interference from transmission to both $p_{2,1}$ and $v_{1,2}$ during symbol extensions {7,8,9} and remove it from symbol extensions $\{1, 2, 3\}$. Note that, since only the sum of the interference terms caused by the transmission to $v_{1,2}$ and $p_{2,1}$ can be measured, this scheme requires to retransmit the symbols $\{\mathbf{u}_\ell^{[v_{1,2}]}\}_{\ell=1}^{3}$ not only during symbol extensions {7,8,9}, but also during symbol extensions {1,2,3}, respectively. Furthermore, transmission of BS 2 to private user $p_{1,2}$ is carried out using the nBIA scheme of Section 4.6.2. However, private user $p_{1,2}$ is now subject to interference caused by the transmission from BS 2 to virtual user $v_{1,2}$ during symbol extensions {1,2,3}. In order to remove it, private user $p_{1,2}$ only needs to measure it during symbol extensions {7,8,9} with the same channel mode as in symbol extensions {1,2,3}, respectively. After removing this interference, the DoF attained by $p_{1,2}$ are not affected.

During symbol extensions {7,8,9}, BS 2 only transmits to $v_{1,2}$. Additionally, similar to private user $p_{1,2}$, due to the partial connectivity of the network, notice that virtual user $v_{1,2}$ is not subject to interference caused by the transmission from BS 1 to private user $p_{2,1}$. Hence, the virtual user attains 3 additional DoF, one per symbol extension. Since the supersymbol consists of 10 slots, an improvement of $\frac{3}{10}$ DoF is achieved compared to the $\frac{22}{10}$ DoF achieved by the nBIA scheme of previous sections for symmetric networks. As a result, by adding the virtual user, the outer bound of (4.24) is attained despite the asymmetric impairments.

Next, we consider the same scenario as in Figure 4.14, but now with $N_t = 3$ antennas per BS. After solving the optimization problem (4.18) and (4.22) for this setting, we can check that the DoF outer bound is $\frac{17}{6}$ DoF. The supersymbol of the nBIA scheme for the symmetric case is shown in Figure 4.16. Similar to the case where $N_t = 2$, if we implement the beamforming matrices of Section 4.6.2, symbol extensions {31-40} of user $p_{1,2}$ are idle. Therefore, as in the previous toy example, we can design new beamforming matrices that include transmission to a virtual user $v_{1,2}$ in order to get an additional DoF during each idle symbol extension. This way, the 3 private users achieve 3 DoF in each of the 10 alignment blocks plus 10 additional DoF for virtual user $v_{1,2}$, which is the same physical user as $p_{1,2}$. Additionally, shared user sh_1 achieves 6 DoF in each of the 4 alignment blocks. In other words, the scheme attains $\frac{31}{11}$ DoF, which is only $\frac{1}{66}$ DoF below the outer bound. On the contrary, since cBIA does not leverage the partial

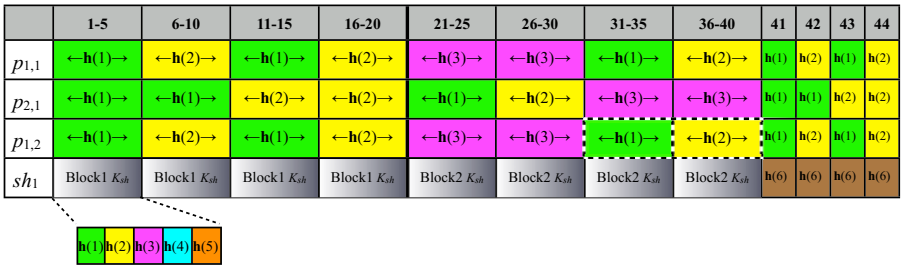

FIGURE 4.16: Supersymbol for asymmetric scenario with $N_t = 3$, $K_{p,1} = 2$, $K_{p,2} = 1$ and $K_{sh} = 1$. Dashed lines represent the idle slots that can be used for transmission of $v_{1,2}$.

connectivity of the system, it only achieves $\frac{5}{3}$ DoF, which is considerably smaller than the DoF attained by the proposed nBIA scheme.

For the general case, the construction of the supersymbol is the same as in a symmetric setting where $K_p = K_{p,n_{\max}}$ with $K_{p,n_{\max}} = \max_n \{K_{p,n}\}$. S-Block 1 consists of $\mathcal{L}_{\text{S-Block1}} = (M-1)^{K_{sh}}(N_t-1)^{K_{p,n_{\max}}}$ slots, whereas S-Block 2 contains $\mathcal{L}_{\text{S-Block2}} = t_{sh,\max} + t_{p,\max}$ symbol extensions where

$$t_{p,\max} = K_{p,n_{\max}} \left[(M-1)^{K_{sh}}(N_t-1)^{K_{p,n_{\max}}-1}\right]$$

and

$$t_{sh,\max} = K_{sh} \left[(M-1)^{K_{sh}-1}(N_t-1)^{K_{p,n_{\max}}}\right].$$

Thus, there are

$$\frac{t_{p,\max}}{K_{p,n_{\max}}} \sum_{n=1}^{N_{BS}} K_{p,n}$$

alignment blocks during which the nBIA scheme for symmetric networks is applied. Moreover,

$$\frac{t_{p,\max}}{K_{p,n_{\max}}} \sum_{n=1}^{N_{BS}} (K_{p,n_{\max}} - K_{p,n})$$

additional DoF are attained by taking advantage of the idle slots of S-Block 2. To do so, as in the toy examples, the beamforming matrices have to be modified in order to include transmission to virtual users. The sum-DoF per symbol extension that are attained by

the extension of the nBIA to the asymmetric setting are given by (4.107).

$$\begin{aligned}\mathrm{DoF}_{\mathrm{nBIA,asymm}} =& \frac{M\,\frac{t_{sh,\max}}{K_{sh}}\,K_{sh} + N_t\frac{t_{p,\max}}{K_{p,n_{\max}}}\sum_{n=1}^{N_{BS}}K_{p,n} + \frac{t_{p,\max}}{K_{p,n_{\max}}}\sum_{n=1}^{N_{BS}}(K_{p,n_{\max}} - K_{p,n})}{\mathcal{L}_{\mathrm{S-Block1}} + \mathcal{L}_{\mathrm{S-Block2}}} \\ =& \frac{MK_{sh}\,(N_t-1) + (M-1)\,\left[(N_t-1)\sum_{n=1}^{N_{BS}}K_{p,n} + N_{BS}\,K_{p,n_{\max}}\right]}{(M-1)(N_t-1) + K_{sh}\,(N_t-1) + K_{p,n_{\max}}\,(M-1)}.\end{aligned} \tag{4.107}$$

4.6.6 Achievable Rates

So far, this work has focused on the high SNR regime and on the achievable DoF. To complement the previous sections, we derive closed-form expressions for the achievable rates of the nBIA scheme in the symmetric scenario for finite SNR. Expressions for the asymmetric scenario can be derived using the same procedure.

Due to the symmetry of the setting with respect to the private users, we analyze a generic alignment block for private user $p_{k,n}$. For simplicity, the index refers to the position of the symbol extension in the alignment block of $p_{k,n}$. First, recall that the supersymbol of $p_{k,n}$ contains t_p/K_p alignment blocks, each formed by N_t symbol extensions. The first N_t-1 symbol extensions are contained in S-Block 1 and are subject to interference from the signals sent to K_p-1 private and K_{sh} shared users. On the contrary, the last symbol extensions of the alignment blocks are in S-Block 2, are free of interference, and are used to achieve decodability and measure the interference. Furthermore, since the beamforming matrix and the pattern of the channel modes are *reused* by the private users across the cells, the interference due to transmission to users $\{p_{j,n'}\}_{n'=1,n'\neq n}^{N_{BS}}$ with $j \neq k$ is also removed together with the interference generated by the transmission to $p_{j,n}$. However, due to the *reuse*, the transmission to user $p_{k,n'}$ generates a weak interference term that cannot be canceled, and is treated as noise. Hence, the received signal

$$\tilde{\mathbf{y}}_\ell^{[p_{k,n}]} = \mathbf{H}^{[p_{k,n},n]}\mathbf{u}_\ell^{[p_{k,n},n]} + \sum_{n'=1,n'\neq n}^{N_{BS}} \sqrt{\alpha_{n'}^{[p_{k,n},n]}}\,\mathbf{H}^{[p_{k,n},n']}\mathbf{u}_\ell^{[p_{k,n},n']} + \tilde{\mathbf{z}}^{[p_{k,n}]}, \tag{4.108}$$

where $\alpha_{n'}^{[p_{k,n},n]}$ is the relative power of the signal of BS n' received at user $p_{k,n}$ taking the power of the signal received from BS n as reference, i.e. $\alpha_n^{[p_{k,n},n]} = 1$. In (4.108),

$$P_{str} = \frac{(N_t-1)(M-1)+K_p(M-1)+K_{sh}(N_t-1)}{N_t\left[(K_p+K_{sh})(N_t-1)(M-1)+K_p(M-1)+K_{sh}(N_t-1)\right]}P. \tag{4.110}$$

$\mathbf{H}^{[p_{k,n},n']} = \left[\mathbf{h}^{[p_{k,n},n']}(1)^T \quad \dots \quad \mathbf{h}^{[p_{k,n},n']}(N_t)^T\right]^T \in \mathbb{C}^{N_t\times N_t}$ contains the channel coefficients between $p_{k,n}$ and BS n' normalized by $\sqrt{\alpha_{n'}^{[p_{k,n},n]}}$ and $\tilde{\mathbf{z}}^{[p_{k,n}]} \in \mathbb{C}^{N_t\times 1}$ is the noise vector after interference subtraction. Consequently, the N_t-th element of $\tilde{\mathbf{z}}^{[p_{k,n}]}$ is $\tilde{z}_{N_t}^{[p_{k,n}]} = z^{[p_{k,n}]}[N_t]$, while

$$\tilde{z}_i^{[p_{k,n}]} = z^{[p_{k,n}]}[t] - \sum_{\substack{j=1\\ j\neq k}}^{K_p} z^{[p_{j,n}]}[t] - \sum_{k'=1}^{K_{sh}} z^{[sh_{k'}]}[t] \tag{4.109}$$

for any $t \in \{1,2,\dots,N_t-1\}$. From now on, we will assume that the noise terms $z^{[p_{k,n}]}[t]$ and $z^{[sh_{k'}]}[t]$ are independent and that $z^{[p_{k,n}]}[t], z^{[sh_{k'}]}[t] \sim \mathcal{CN}(0,1)$ for all $p_{k,n} \in \mathcal{K}_{p,n}$, $sh_k \in \mathcal{K}_{sh}$ and $n \in \{1,2,\dots,N_{BS}\}$.

Since the length of S-Block 1 is $(N_t-1)^{K_p}(M-1)^{K_{sh}}$ and each BS serves K_p+K_{sh} users at each slot, $N_t\,(K_p+K_{sh})\,(N_t-1)^{K_p}(M-1)^{K_{sh}}$ symbols are sent over S-Block 1. On the other hand, to allow decodability and interference cancellation, S-Block 2 provides an additional symbol extension per alignment block in an orthogonal fashion. Since there are t_{sh} and t_p alignment blocks per K_p private and per K_{sh} shared users, respectively, to exploit the partial connectivity each BS needs to transmit $N_t(t_p+t_{sh})$ symbols during S-Block 2. Therefore, assuming equal power transmission to each stream, the allocated power per symbol is given by (4.110). Moreover, since each supersymbol contains t_p/K_p alignment blocks per private user (see (4.98)), the ratio of alignment blocks per private user over the total number of slots is

$$B_p = \frac{M-1}{(M-1)(N_t+K_p-1)+K_{sh}(N_t-1)}. \tag{4.111}$$

Thus, the normalized rate per slot for $p_{k,n}$ is

$$R^{[p_{k,n}]} = B_p\mathbb{E}\left[\log\det\left(\mathbf{I}+P_{str}\mathbf{H}^{[p_{k,n},n]}\mathbf{H}^{[p_{k,n},n]H}\mathbf{R}_{\tilde{\mathbf{z}}}^{[p_{k,n}]^{-1}}\right)\right], \tag{4.112}$$

where the covariance matrix of the noise plus interference subtraction after interference subtraction is given by

$$\mathbf{R}_{\tilde{\mathbf{z}}}^{[p_{k,n}]} = \mathbf{R}_{\tilde{\mathbf{z}}}^{[p_{k,n}]} + P_{str} \sum_{n'=1, n' \neq n}^{N_{BS}} \alpha_{n'}^{[p_{k,n}]} \mathbf{H}^{[p_{k,n},n]} \mathbf{H}^{[p_{k,n},n]^H}, \tag{4.113}$$

and

$$\mathbf{R}_{\tilde{\mathbf{z}}}^{[p_{k,n}]} = \begin{bmatrix} (K_p + K_{sh})\mathbf{I}_{N_t-1} & \mathbf{0} \\ \mathbf{0} & 1 \end{bmatrix}. \tag{4.114}$$

Similarly, to obtain the rate expression for the shared users, recall that each alignment block of $sh_{k'}$ is made up of M symbol extensions. The first $M-1$ symbol extensions are subject to interference by the signals sent to $N_{BS}\,K_p$ private users and $K_{sh}-1$ shared users, whereas the last slot of each alignment block is free of interference. In this case, BIA codes are not reused among shared users, and therefore interference from transmission to the private and the remaining shared users can be canceled entirely. Thus, the signal

$$\tilde{\mathbf{y}}_{\ell'}^{[sh_{k'}]} = \mathbf{H}^{[sh_{k'}]} \mathbf{u}_{\ell'}^{[sh_{k'}]} + \tilde{\mathbf{z}}^{[sh_{k'}]}, \tag{4.115}$$

where $\mathbf{H}^{[sh_{k'}]} = \left[\mathbf{h}^{[sh_{k'}]}(1)^T \quad \dots \quad \mathbf{h}^{[sh_{k'}]}(M)^T \right]^T \in \mathbb{C}^{M \times M}$ and

$$\mathbf{h}^{[sh_{k'}]}(l) = \left[h_1^{[sh_{k'},1]}(l)^T, \dots, \sqrt{\beta_n^{[sh_{k'}]}} h_t^{[sh_{k'},n]}(l)^T, \dots, \sqrt{\beta_{N_{BS}}^{[sh_{k'}]}} h_{N_t}^{[sh_{k'},N_{BS}]}(l)^T \right]^T \in \mathbb{C}^{M \times 1}$$

contains the coefficients of the channel between user $sh_{k'}$ and the $N_t N_{BS}$ antennas for mode l, $\beta_n^{[sh_{k'}]}$ denotes the relative power of the signal of BS n received at user $sh_{k'}$ taking the power of the signal received from BS 1 as reference, i.e. $\beta_1^{[sh_{k'}]} = 1$, and $\tilde{\mathbf{z}}^{[sh_{k'}]} \in \mathbb{C}^{M \times 1}$ is the noise vector after zero forcing, whose structure is similar to $\tilde{\mathbf{z}}^{[p_{k,n}]}$. Notice that the first $(M-1)$ terms are subject to a noise increment $K_p + K_{sh} - 1$ due to interference subtraction, while the M-th term only contains the noise term $z^{[sh_{k'}]}[N_t]$.

The power allocated to each symbol is also given by (4.110). Moreover, t_{sh}/K_{sh} alignment blocks are used to transmit to each shared user (see (4.95)). Hence, the ratio of alignment blocks per shared user over the supersymbol length is

$$B_{sh} = \frac{N_t - 1}{(M-1)(N_t + K_p - 1) + K_{sh}(N_t - 1)}. \tag{4.116}$$

Therefore, the normalized rate of $sh_{k'}$ is

$$R^{[sh_{k'}]} = B_{sh}\mathbb{E}\left[\log\det\left(\mathbf{I} + P_{srt}\mathbf{H}^{[sh_{k'}]}\mathbf{H}^{[sh_{k'}]^H}\mathbf{R}_{\tilde{\mathbf{z}}}^{[sh_{k'}]^{-1}}\right)\right], \tag{4.117}$$

where the noise covariance matrix is

$$\mathbf{R}_{\tilde{\mathbf{z}}}^{[sh_{k'}]} = \begin{bmatrix} (K_p + K_{sh})\mathbf{I}_{M-1} & \mathbf{0} \\ \mathbf{0} & 1 \end{bmatrix}. \tag{4.118}$$

4.7 Simulation Results

As we discussed in Chapter 3, there exits a trade-off between private and shared users when either isolated or cooperative BIA transmission is taken into consideration in a cellular network. The region of the DoF achievable for private users regarding the achieved by shared is depicted in Figure 4.17. Notice that the DoF achieved by the shared users when private users obtain zero-DoF corresponds to the fully cooperative solution (3.32), whereas private users achieve the DoF given by the use of sBIA in the MISO BC (2.23) subject to zero-DoF for shared users. Assuming a symmetric scenario, it can be seen that nBIA obtains the outer bound derived in section 4.3. In other words, the proposed nBIA scheme results DoF-optimal. Therefore, the optimal DoF for partially connected cellular networks with K_p private users and K_{sh} shared users is achievable by using nBIA. For auBIA based on augmented code by using data sharing among the BSs, the optimal DoF for private users is achievable when there are not any shared users. However, since shared users obtain diversity gain instead of multiplexing gain, they are limited to attain N_t DoF per alignment block. In consequence, shared users are far from the optimal. Last but not least, the use of augmented code BIA supersymbols, which provides diversity gain for shared users, involves a considerable penalty in DoF for private users. In fact, the use of sBIA and cBIA together with an orthogonal approach as is proposed by the fbwBIA scheme overcomes the performance of auBIA. The slope of the region for fbwBIA is given by the portion of bandwidth allocated to each group of users.

The achievable DoF for different transmission schemes over a symmetric partially connected network are depicted in Fig. 4.18. A two-cell scenario where each BS is equipped with $N_t = 3$ antennas is assumed; there are 3 private users per each shared user in

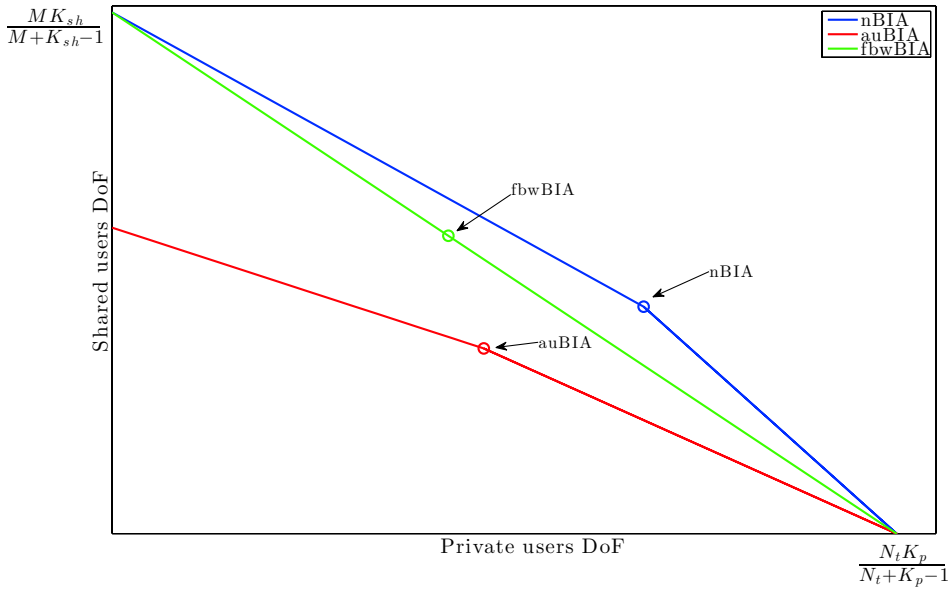

FIGURE 4.17: Degrees of Freedom region for homogeneous cellular networks with partial connectivity.

each cell, i.e. in the first iteration $K_{p,1} = K_{p,2} = 3$ and $K_{sh} = 2$. As expected, the proposed nBIA scheme achieves the information-theoretic outer bound of Section 4.3. In contrast, although the DoF grow with the number of users, the performance of cBIA is inferior due to the lack of connectivity. Besides, since in the augmented code solution proposed in [97] the shared users are not subject to intercell interference, the scheme attains more DoF compared to the case where sBIA is implemented in each cell. However, its performance is inferior to the proposed nBIA scheme.

In Fig. 4.19 we show the achievable DoF for an asymmetric two-cell scenario where one cell contains $\frac{4}{3}$ times the private users of the other cell. As pointed out in Section 4.6.5, the nBIA scheme does not always achieve the outer bound of Section 4.3. However it is close to the sum-DoF outer bound. Moreover, it can be seen that nBIA attains more DoF than other schemes.[2] In contrast with nBIA, cBIA attains significantly fewer DoF since it does not exploit the lack of full connectivity.

The length of the supersymbols of the different transmission schemes is shown in Fig. 4.20 for the same parameters as in Fig. 4.18. As can be seen, the implementation of cBIA requires a prohibitive supersymbol length. This is due to the fact that the supersymbol length of cBIA depends exponentially on the total number of users in the network,

[2]Since auBIA was devised for symmetric networks, its performance is not depicted.

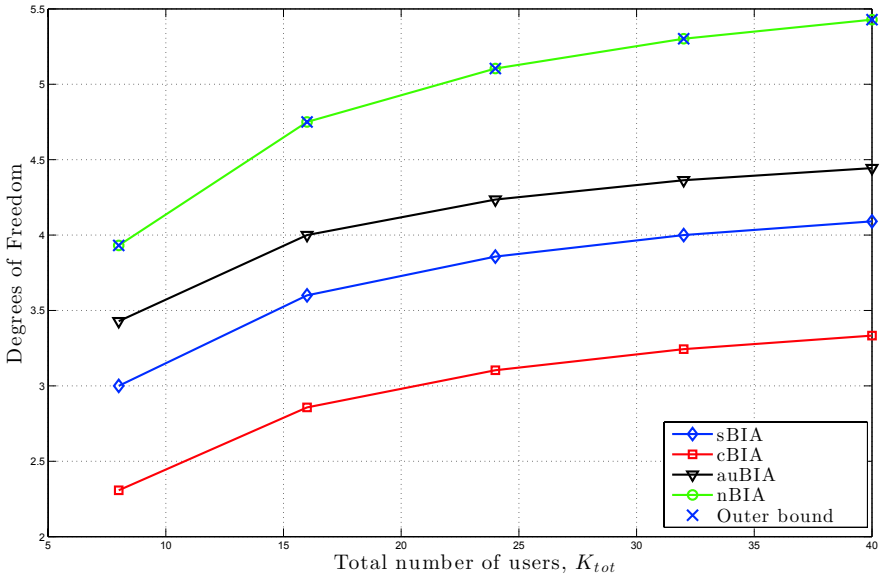

FIGURE 4.18: Achievable DoF over a symmetric partially connected network. $N_{BS} = 2$, $N_t = 3$, and $K_{p,1} = K_{p,2} = \frac{3}{2}K_{sh}$.

K_{tot}. On the other hand, the shortest supersymbol corresponds to an independent implementation of the sBIA scheme at each cell, which does not deal with the intercell interference. The proposed nBIA scheme has an acceptable supersymbol length with similar slope as sBIA and augmented code. This advantage is more remarkable taking into account the DoF achieved by nBIA in comparison with other schemes.

The achievable sum-rate of the users in each cell, i.e. $K_{cell} = K_p + \frac{K_{sh}}{2}$ in a two-cell scenario is plotted in Fig. 4.21. Each BS is equipped with $N_t = 3$ antennas that serve a fixed number of private users, $K_p = 6$. The transmission power is fixed at 25 dB and the average Signal-to-Interference Ratio (SIR) is assumed to be 10 dB and 2 dB for the private and the shared users, respectively. The nBIA scheme achieves a larger sum-rate than the other schemes. Furthermore, the sum-rate increases with the number of shared users. Notice that the cBIA scheme achieves a poor sum-rate in comparison with the other schemes because many interference terms have to be subtracted. Therefore, in addition to other disadvantages, cBIA requires a high SNR for good performance. In comparison with augmented code and sBIA, it can be seen that nBIA has better performance, especially when the number of shared users, K_{sh}, is large.

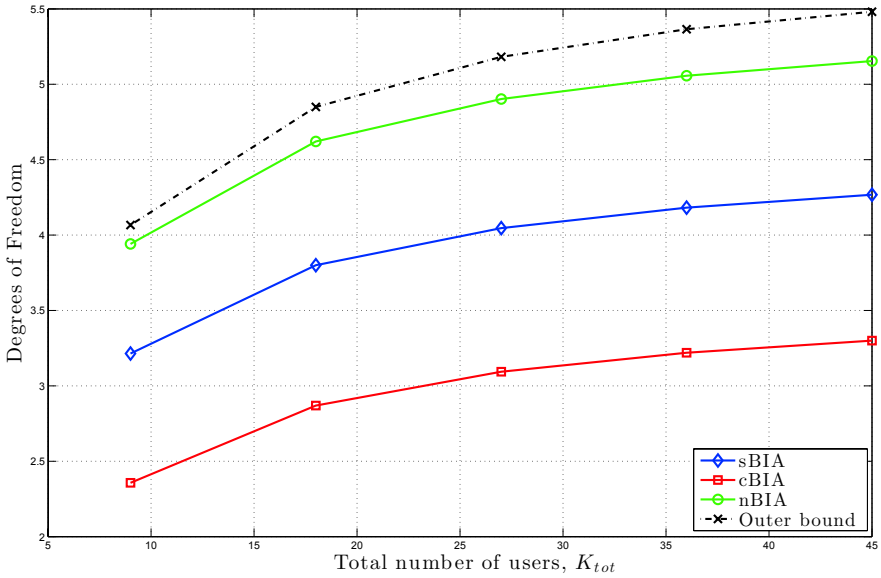

FIGURE 4.19: Achievable DoF for an asymmetric partially connected network. $N_{BS} = 2$, $N_t = 3$, and $K_{p,1} = \frac{4}{3}K_{p,2} = 2K_{sh}$.

4.8 Conclusions

In this chapter, we develop the use of BIA in homogeneous cellular networks assuming that the network topology is known by the transmitters. By using information theory the DoF region for cellular networks with partial connectivity in absence of CSIT has been derived. As a main conclusion, it is demonstrated that the use of the knowledge of the network topology can attain more DoF than fully cooperative schemes, even if full connectivity is assumed when CSIT is not available. The key idea is that the lack of connectivity in cellular networks should be treated as an inherent resource instead of a limitation.

Although the DoF of cellular networks were derived, its achievability was an open issue. In this chapter we analyze the auBIA schemes based on exploiting diversity for users subject to intercell interference, which requires data sharing among the set of BSs. It has been shown that BIA based on augmented code scheme results sub-optimal in DoF. Besides, providing diversity to shared users involves a larger supersymbol, penalizing considerable the performance achieved by private users. With the aim of improving the achievable DoF we proposed the use of an orthogonal approach such as flexible bandwidth allocation joint to either standard or cooperative BIA for private and shared

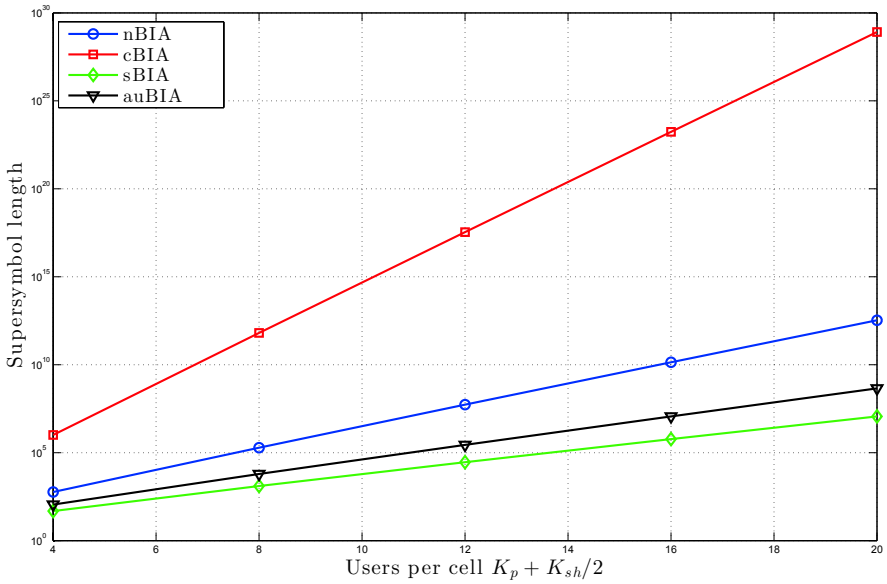

FIGURE 4.20: Comparison of the supersymbol length. $N_{BS} = 2$, $N_t = 3$, and $K_{p,1} = K_{p,2} = \frac{3}{2}K_{sh}$.

users, respectively. It has been demonstrated that this scheme overcomes the DoF achieved by using data sharing to provide BIA with diversity for shared users when $K_{sh} \geq 2N_t - 1$ where each BS is equipped with N_t antennas. Furthermore, at finite SNR, BIA based on flexible bandwidth provides two useful features; it reduces the noise increment and also the supersymbol length. We have shown that this approach outperforms the sum-rate achieved by augmented code BIA in many scenarios. The use of orthogonal approaches joint to BIA will be discussed in detail in Chapter 6. Nonetheless, flexible bandwidth BIA is not still DoF-optimal. We develop a network BIA scheme that provides the optimal-DoF in symmetric cellular networks with partial connectivity. By properly combining the BIA supersymbols according to the network topology knowledge, private and shared users obtain a non-optimal DoF considering each group isolate, but sum-DoF optimal when the whole network is considered. For asymmetric scenarios we propose an extension of the network BIA scheme that minimizes the penalty in DoF because of the impairments between the amount of users in each cell. By using computer simulations it is shown that network BIA achieves better sum-rates that other schemes, based or not in the network topology.

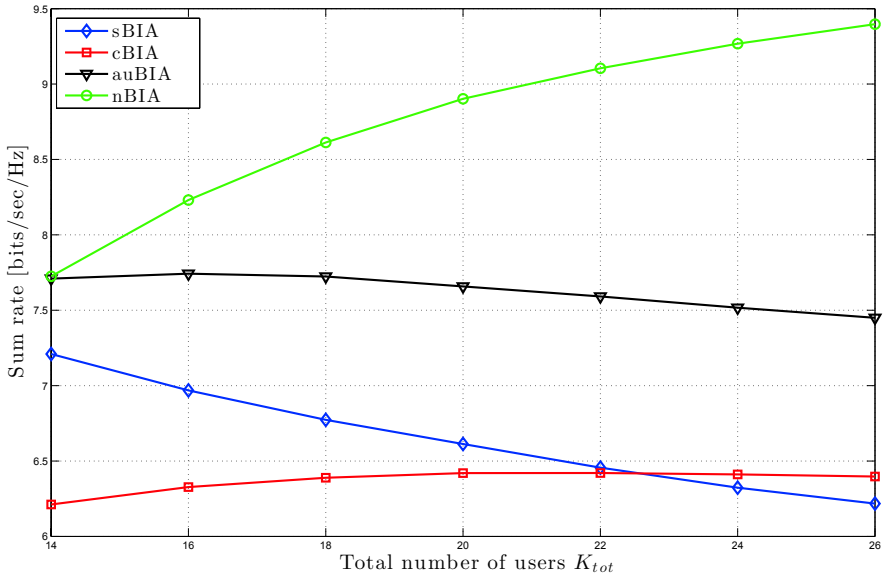

FIGURE 4.21: Average achievable sum-rates per cell versus the number of shared users K_{sh}. The SNR is fixed to 25 dB for all users, whereas the average SIR is 10 dB and 2 dB for private and shared users, respectively. $N_{BS} = 2$, $N_t = 3$, and $K_p = 6$.

Chapter 5

Blind Interference Alignment for Heterogeneous Celluar Networks

This chapter evaluates the use of BIA schemes in heterogenous cellular networks. An extension of the network BIA devised in the previous chapter is proposed in order to reach the optimal sum-DoF in the whole network. However, it is demonstrated that this is not achievable because of the particular topology of the heterogeneous cellular networks. Indeed, it is shown that the sum-DoF decreases as the amount of femtocells grows. With the aim of providing a sum-DoF goal for heterogeneous networks, the information theoretic DoF-region of the two-tier cellular networks is derived in this chapter. After that, a BIA scheme based on a cognitive approach is devised to attain the sum-DoF outer bound derived previously. Simulation results show that this cognitive BIA approach outperforms other transmission schemes such as standard BIA or orthogonal resource allocation.

5.1 Introduction

The increasing demand for high data rates in cellular networks has encouraged the development of multiple antenna transmission schemes [22]. This work is focused on transmission schemes in absence of CSIT. In this sense, BIA for homogeneous cellular networks has been investigated so far. We have shown that the use of the network topology joint to BIA schemes allow to obtain the optimal DoF without CSIT. However,

BIA or other transmission schemes such as FR or IA based on CSIT do not suffice to satisfy the actual demand of high data rates [135]. At this point, it is interesting to consider whether the homogeneous cellular deployment results efficient in the actual cellular network. Traditionally, the cellular mobile network has been based on outdoor BSs covering a fairly large geographical area serving a relatively large number of users. Taking into consideration the increasing demand of high data rates, the continuous deployment of BSs generating a more dense network results unaffordable from the point of view of the mobile operators. On the other hand, users are still penalyzed by the costs of providing high data rates in the actual cellular network. In consequence, a decoupling between the data rates and the revenues of mobile operators occurs just due to the capital expenditures (CAPEX) of deploying a dense homogeneous cellular network based on traditional BSs and also because of the operational expenditures (OPEX) of an excessive consumption of energy.

Taking into consideration the approximation of the capacity for MIMO channels provided in(1.1), there exist ways to improve the area spectral efficiency in a wireless network such as the use of a wider spectrum, better modulation schemes, or reducing the distance between user and transmitter. Since bandwidth is a very scarce resource and better transmission schemes are not enough to satisfy the future demand of high data rates, a possible solution lies in reducing the cell radius [14, 27, 40]. As predicted in [39], a micro-ization of the actual cellular network is required to increase the data rates while reducing the power consumption of the whole network. Thus, macro and micro cells should reduce their coverage radius continuously creating a dense cellular deployment. This solution, which also could moderate the energy costs, is nonetheless inefficient reducing the CAPEX of the mobile operators.

At this point, small cells, usually referred to as femto and pico cells, have been proposed as a key element in the future cellular network. Femtocell Access Points (FAPs) are BSs with a reduced radius of coverage operating in the licensed cellular band and usually backhauled onto IP networks through conventional subscriber lines (DSL). They are devised to be self-user installed in houses, small offices, etc. Similarly, dense femtocell networks can be also deployed in wide public buildings such as airports or shopping centres. Therefore, smalls cells can solve the lack of mobile coverage in indoor environments. However, other benefits beyond this issue are obtained with the use of small cells. Since the distance between receiver and transmitter is lessened to a few meters,

small cells improve the capacity of the end-user while the power consumption is also reduced considerably. Although the aforementioned benefits make the use of femtocells an attractive element for the future cellular network, there still exist some open issues to be solved. Notice that FAPs are end-user installed in arbitrary locations, and therefore, their deployment is unpredictable. In consequence, the management of the interference in heterogenous cellular networks composed by traditional BSs, i.e. macro and micro cells, and smalls cells results quite challenging. Figure 5.1 shows the interaction of the macro-femto tiers in a heterogeneous cellular network.

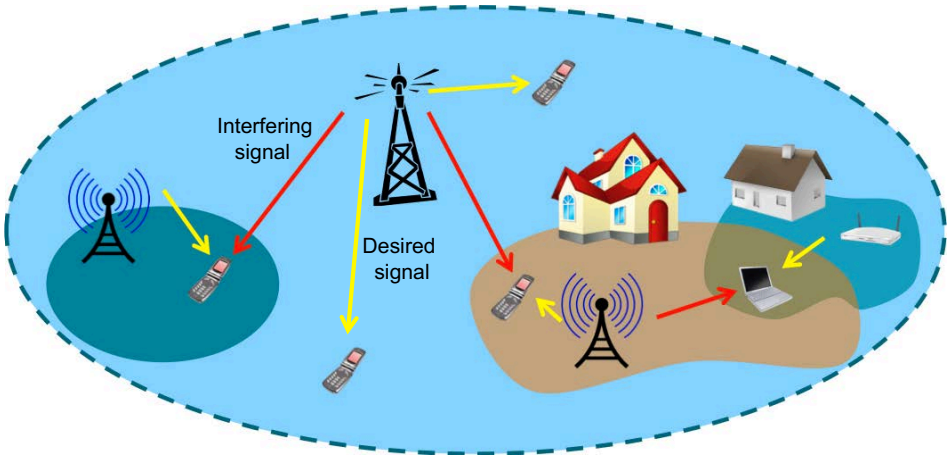

FIGURE 5.1: Two-tier macro-femto cellular network. The rates achieved by femtocell users are limited by interference from the macro BS.

Several techniques such as LZFB or IA can be easily extended to their application in heterogeneous cellular networks. However, providing CSIT and accurate synchronization results even more challenging in multiple-tier networks where a large amount of small cells coexist with the traditional deployments. On the other hand, the use of orthogonal interference management such as FR may reduce the performance of the system considerably [136, 137]. Following the lines of the previous chapter, we focus on exploiting the network topology. Notice that for heterogeneous cellular networks where several femtocells are spread over the coverage area of a macro BS, femto users generally receive a strong signal from the macro BS. On the other hand, macro users are not subject to femtocell transmission, and they can handover to the femtocell of interest when it is optimal to do it [138–140]. Beyond traditional approaches, several schemes have been proposed to manage the interference in macro-femto cellular networks. Cooperation between macro BS and FAPs is generally avoided since they waste a large amount of

the network resources for signalling when a large number of FAPs are installed within the macro BS [100]. On the other hand, without requiring any cooperation between the two tiers, and therefore without bringing additional intercell overhead, some transmission schemes based on fractional frequency reuse, distributed power control and static resource partition are proposed in [141–143]. However, the performance of these techniques is suboptimal in general. Alternatively, with the aim of increasing the achievable data rates, other kind of approaches allow some coordination between the macro BSs and the FAPs. Within this category, cognitive schemes based on different techniques (e.g., opportunistic transmission or hybrid division duplexing) have become popular for small cell networks limited by macro/micro BSs transmission [114, 144].

In this chapter, we evaluate the use of BIA in heterogeneous cellular networks. Indeed, there exist a few recent schemes [115]-[116] that apply BIA for interference management in macro-femto cellular networks. In [115], the authors propose several heuristic schemes that exploit the location information of the users and the BSs to reduce the supersymbol length, and therefore achieve more DoF. In [116], the authors use a Kronecker product representation to design a BIA scheme for interference management in a heterogeneous network with one macro BS and several FAPs, each with one femto user. Although the schemes proposed in [115] and [116] can cancel all the intracell and inter-tier interference through a coordinated transmission of the macro BS and the FAPs without CSIT, they are generally suboptimal in DoF sense. We propose to maximize the sum-DoF of the whole network by extending the nBIA scheme developed in [129] and presented in Chapter 4. In this sense, macro users can be considered as *private* users that only receive signal from their macro BS while femto users can be treated as *shared* users receiving signal from their corresponding FAP and also from the interfering macro BS. Note that this approach involves cooperation between both tiers in order to transmit to femto users. That is, macro BS transmission penalyzes their macro users for transmitting to femto users. Furthermore, it is demonstrated that this cooperative approach does not scale with the number of femtocells. Thus, we can conclude that the nBIA scheme is not suitable for heterogeneous cellular networks.

At first sight, without CSIT knowledge or cooperation between both tiers, the maximization of the sum-DoF for macro users involves to obtain zero-DoF in the femto tier. Interestingly, in this chapter we demonstrate that this is not the case. Based on the

definition of linear DoF (lDoF) [57, 91], i.e. the achievable DoF for linear coding strategies, we derive the lDoF region of a two-tier heterogeneous cellular network subject to maximization of the sum-DoF in the macro tier. It is shown that the femto tier can align their transmission with the interfering macro BS by "stealing" one dimension from macro tier transmission. After that, we develop a cognitive BIA scheme that achieves the optimal lDoF in macro-femto cellular networks subject to maximizing the DoF in the macro tier. Moreover, due to its cognitive nature, the proposed scheme does not depend on the number of FAPs located within the macro coverage. Besides reducing the intercell overhead, for settings with a dense deployment of FAPs, this feature of the proposed cognitive BIA scheme allows to achieve more DoF than cooperative BIA schemes where both tiers jointly transmit data to femto users.

The contributions of this chapter can be summarized as follows

- We present the system model of the macro-femto cellular network based on reconfigurable antennas.
- We derive the lDoF region of the two-tier heterogeneous networks subject to maximizing the DoF in the upper tier without CSIT. It is demonstrated that in absence of CSIT, the lower tier achieves non zero-DoF while the upper tier obtains the same optimal DoF as when the lower tier is not considered.
- We develop an extension of the network BIA scheme of Chapter 4 based on cooperation between both tiers. It is shown that the sum-DoF achieved with this approach does not scale with the number of femtocells.
- We devise a cognitive BIA scheme that reaches the optimal lDoF in the two-tier cellular network. Remarkably, the sum-DoF scales with the amount of femtocells deployed within the macro coverage.

5.2 System Model

We consider a macro-femto cellular network as is shown in Figure 5.2. In the considered cellular network, the macro BS is equipped with N_m antennas that serve a set of single-antenna macro users $\mathcal{K}_m = \{m_1, \ldots, m_{K_m}\}$, which are not subject to interference by any other macro BS or access point. Additionally, a set of FAPs $\mathcal{F} = \{\varphi_1, \ldots, \varphi_F\}$, each

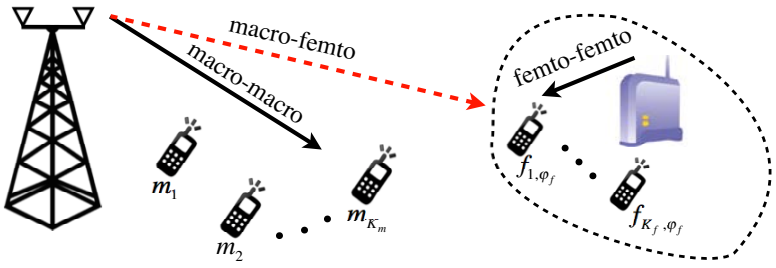

FIGURE 5.2: Two-tier macro-femto cellular network. The macro BS is equipped with N_m antennas and K_m are deployed within its coverage. FAP φ_f is equipped with N_f antennas and there exists K_f femto users.

equipped with N_f antennas, have been deployed randomly over the coverage area of the macro BS. It is assumed that each FAP φ_f transmits to a set $\mathcal{K}_F = \{f_{1,\varphi_f}, \ldots, f_{K_f,\varphi_f}\}$ of K_f single-antenna femto users[1]. Following the lines of Chapter 4, the set of FAPs and their users[2], can be categorized as either femtocells subject to interference from the macro BS or femtocells that can treat interference as noise because of path loss [66]. It is assumed that users are equipped with reconfigurable antennas, which can switch among different preset modes. Without loss of generality, since it is assumed that the FAPs do not cause interference to other femtocells, only one generic FAP φ_f will be analyzed from now on. We will focus on a generic FAP that is subject to interference from the macro BS. Since FAPs that treat interference from the macro BS as noise can be considered as isolated cells, note that they can manage their intracell interference by simply applying the BIA scheme derived in [89] for the MISO BC channel.

The symbols transmitted by the macro BS can be written in vector form as $\mathbf{x}^{[M]} = \left[x_1^{[M]}, \ldots, x_{N_m}^{[M]}\right]^T$. Due to the low power transmission of the FAPs, it is assumed that the macro users are not subject to interference caused by the transmission from the FAPs. As result, we will consider that the macro users can treat the femto-macro interference as noise. In case that one macro user receives a strong signal from a FAP, it proceeds to handover to the corresponding femtocell. Thus, the signal received by macro user m_k at time t can be expressed as

$$y^{[m_k]}[t] = \mathbf{h}^{[m_k]}\left(l^{[m_k]}[t]\right)^T \mathbf{x}^{[M]}[t] + z^{[m_k]}[t], \tag{5.1}$$

[1]Without loss of generality and for the sake of simplicity in the derivations, it is assumed that all FAPs have the same number of femto users.

[2]Due to the reduced radius of coverage of the femtocells, it is assumed that all femto users in a given femtocell receive the same power of interference from the macro BS.

where $\mathbf{h}^{[m_k]}\left(l^{[m_k]}[t]\right) \in \mathbb{C}^{N_m \times 1}$ is the vector that contains the channel coefficients between the macro BS and user m_k corresponding to the l-th preset antenna mode at macro user m_k, and $z^{[m_k]}[t]$ is AWGN with zero mean and unit variance.

Similarly, FAP φ_f transmits a symbol vector $\mathbf{x}^{[\varphi_f]} = \left[x_1^{[\varphi_f]}, \ldots, x_{N_f}^{[\varphi_f]}\right]^T$. However, the femto users are subject to interference from the macro BS. Thus, the signal received at femto user f_{k',φ_f} at time t can be written as

$$y^{[f_{k',\varphi_f}]}[t] = \mathbf{h}^{[f_{k',\varphi_f},\varphi_f]}\left(l^{[f_{k',\varphi_f}]}[t]\right)^T \mathbf{x}^{[\varphi_f]}[t] + \underbrace{\mathbf{h}^{[f_{k',\varphi_f},M]}\left(l^{[f_{k',\varphi_f}]}[t]\right)^T \mathbf{x}^{[M]}[t]}_{\text{inter-tier interference}} + z^{[f_{k',\varphi_f}]}[t], \tag{5.2}$$

where $\mathbf{h}^{[f_{k',\varphi_f},\varphi_f]}\left(l^{[f_{k',\varphi_f}]}[t]\right) \in \mathbb{C}^{N_f \times 1}$ is the channel vector between the FAP φ_f and user f_{k',φ_f} associated with the l-th antenna mode, $\mathbf{h}^{[f_{k',\varphi_f},M]}\left(l^{[f_{k',\varphi_f}]}[t]\right) \in \mathbb{C}^{N_m \times 1}$ denotes the channel between the macro BS and femto user f_{k',φ_f} with the l-th antenna mode of the femto user f_{k',φ_f}. Moreover, $z^{[f_{k',\varphi_f}]}[t]$ denotes AWGN noise with zero mean and unit variance. Here, notice that we use index k' instead of k to distinguish from macro users in further derivations.

We assume that the transmitted signals are subject to an average power constraint $E\left\{\|\mathbf{x}^{[M]}[t]\|^2\right\} \leq P_m$ and $E\left\{\|\mathbf{x}^{[\varphi_f]}[t]\|^2\right\} \leq P_f$. Moreover, we assume that the switching pattern functions $l^{[m_k]}[t]$ and $l^{[f_{k',\varphi_f}]}[t]$ are predetermined and known beforehand. On the contrary, we assume that the transmitters do not have any CSIT. We also assume that the channel coefficients between each user and the transmitter, macro or femto, are drawn from a continuous distribution, and therefore, are linearly independent almost surely. Additionally, we assume that the channels stay constant for a sufficient number of time or frequency slots. For simplicity, we focus on the temporal dimension without loss of generality. Therefore, each symbol extension corresponds to a time slot t. Nevertheless, all results can be applied easily to the frequency domain.

5.3 Information-theoretic sum-DoF Outer Bound of the Macro-Femto Cellular Network

In this section, we derive the outer bound for the DoF achieved by each FAP in the absence of CSIT and subject to optimal sum-DoF in the macro tier. Toward this goal, we will build upon the approaches taken in [57] and [91] by employing the definition of linear DoF (lDoF) without CSIT, i.e. the symbols decoded by the users when there is not CSIT and when linear precoding schemes are employed by the macro and femto transmitters.

Considering the scenario described in Section II, a n-time extended model is proposed to derive the outer bound for the sum-DoF of the femto users[3]. For the considered n-time extended model, let us define $\gamma^{[m_k]}[n] \in \mathbb{C}^{1\times N_m}$ as the vector consisting of zero values except for a single element that selects the corresponding channel mode used by user m_k at symbol extension n. Moreover, we define

$$\mathbf{H}^{[m_k]} = \left[\mathbf{h}^{[m_k]}(1)^T \quad \dots \quad \mathbf{h}^{[m_k]}(N_m)^T\right]^T \in \mathbb{C}^{N_m\times N_m} \tag{5.3}$$

as the channel matrix that contains the coefficients between the N_m antennas of the macro BS and the macro user m_k for the N_m preset modes of its single reconfigurable antenna. Given the previous definitions, if we also assume that the macro BS sends the information symbols of each macro user m_k, denoted by $\mathbf{u}^{[m_k]} \in \mathbb{C}^{a_n^{[m_k]}}$, through the n-time extended matrix $\mathbf{V}_n^{[m_k]} \in \mathbb{C}^{n\,N_m\times a_n^{[m_k]}}$, the n-time extended signal vector transmitted by the macro BS is

$$\mathbf{x}^{[M]} = \sum_{j=1}^{K_m} \mathbf{V}_n^{[m_j]}\mathbf{u}^{[m_j]} \tag{5.4}$$

and the n-time extended signal received by the macro user m_k can be written as

$$\mathbf{y}^{[m_k]} = \sum_{j=1}^{K_m} \mathbf{\Gamma}_n^{[m_k]}\mathbf{H}_n^{[m_k]}\mathbf{V}_n^{[m_j]}\mathbf{u}^{[m_j]} + \mathbf{z}_n^{[m_k]} \tag{5.5}$$

[3]The macro-femto two-tier cellular network is considered for simplicity. Notice that the derived bound is also valid for other two-tier networks, e.g. macro-pico cells, that satisfy the proposed system model.

where

$$\mathbf{\Gamma}_n^{[m_k]} = \text{diag}\left(\gamma^{[m_k]}[1] \quad ,\ldots, \quad \gamma^{[m_k]}[n]\right) \tag{5.6}$$

$$\mathbf{H}_n^{[m_k]} = \mathbf{I}_n \otimes \mathbf{H}^{[m_k]} \tag{5.7}$$

$$\mathbf{y}_n^{[m_k]} = \left[y^{[m_k]}[1] \quad \ldots \quad y^{[m_k]}[n]\right]^T \tag{5.8}$$

$$\mathbf{x}_n^{[M]} = \left[\mathbf{x}^{[M]}[1]^T \quad \ldots \quad \mathbf{x}^{[M]}[n]^T\right]^T \tag{5.9}$$

$$\mathbf{z}_n^{[m_k]} = \left[z^{[m_k]}[1] \quad \ldots \quad z^{[m_k]}[n]\right]^T. \tag{5.10}$$

Similarly, $\gamma^{[f_{k'},\varphi_f]}[n] \in \mathbb{C}^{1\times N_f}$ is the vector that selects the corresponding channel mode used by femto user f_{k',φ_f} at symbol extension n.

The channel matrix between the N_f antennas of FAP φ_f and the femto user f_{k',φ_f} for the N_f preset modes of its single reconfigurable antenna is given by

$$\mathbf{H}^{[f_{k'}]} = \left[\mathbf{h}^{[f_{k',\varphi_f},\varphi_f]}(1)^T \quad \ldots \quad \mathbf{h}^{[f_{k',\varphi_f},\varphi_f]}(N_f)^T\right]^T \in \mathbb{C}^{N_f\times N_f}, \tag{5.11}$$

as well as the channel matrix between the N_m antennas of the macro BS and the femto user f_{k',φ_f} for the N_f preset modes is defined as

$$\mathbf{G}^{[f_{k'}]} = \left[\mathbf{h}^{[f_{k',\varphi_f},M]}(1)^T \quad \ldots \quad \mathbf{h}^{[f_{k',\varphi_f},M]}(N_f)^T\right]^T \in \mathbb{C}^{N_f\times N_m} \tag{5.12}$$

with $f \in \{1,2,\ldots,F\}$ and $k' \in \{1,2,\ldots,K_f\}$, respectively. Since we aim at obtaining an outer bound for the sum-lDoF, i.e. $P \to \infty$, note that the interfering signal strength from the macro BS to each femto user does not depend on the femtocell φ_f where the user f_{k',φ_f} is located. As a result, for the sake of simplicity, the index φ_f has been omitted. Moreover, as we considered for the macro BS, we assume that each FAP sends the information symbols of each femto user $f_{k'}$, denoted by $\mathbf{u}^{[f_{k'}]} \in \mathbb{C}^{a_n^{[f_{k'}]}}$, through the n-time extended matrix $\mathbf{V}_n^{[f_{k'}]} \in \mathbb{C}^{n\,N_f\times a_n^{[f_{k'}]}}$. Therefore, the n-time extended signal vector transmitted by the each FAP is

$$\mathbf{x}^{[\varphi_f]} = \sum_{j'=1}^{K_f} \mathbf{V}_n^{[f_{j'}]}\mathbf{u}^{[f_{j'}]} \tag{5.13}$$

and the received signal vector during n time slots for femto user $f_{k'}$ located at a generic FAP φ_f can be written as

$$\mathbf{y}^{[f_{k'}]} = \sum_{j'=1}^{K_f} \mathbf{\Gamma}_n^{[f_{k'}]} \mathbf{H}_n^{[f_{k'}]} \mathbf{V}_n^{[f_{j'}]} \mathbf{u}^{[f_{j'}]} + \sum_{j=1}^{K_m} \mathbf{\Gamma}_n^{[f_{k'}]} \mathbf{G}_n^{[f_{k'}]} \mathbf{V}_n^{[m_j]} \mathbf{u}^{[m_j]} + \mathbf{z}_n^{[f_{k'}]}, \tag{5.14}$$

where

$$\mathbf{\Gamma}_n^{[f_{k'}]} = \operatorname{diag}\left(\gamma^{[f_{k'}]}[1] \quad , \ldots, \quad \gamma^{[f_{k'}]}[n]\right) \tag{5.15}$$

$$\mathbf{H}_n^{[f_{k'}]} = \mathbf{I}_n \otimes \mathbf{H}^{[f_{k'}]} \tag{5.16}$$

$$\mathbf{G}_n^{[f_{k'}]} = \mathbf{I}_n \otimes \mathbf{G}_n^{[f_{k'}]} \tag{5.17}$$

$$\mathbf{y}_n^{[f_{k'}]} = \left[y^{[f_{k'}]}[1] \quad \ldots \quad y^{[f_{k'}]}[n]\right]^T \tag{5.18}$$

$$\mathbf{x}_n^{[\varphi_f]} = \left[\mathbf{x}^{[\varphi_f]}[1]^T \quad \ldots \quad \mathbf{x}^{[\varphi_f]}[n]^T\right]^T \tag{5.19}$$

$$\mathbf{z}_n^{[f_{k'}]} = \left[z^{[f_{k'}]}[1] \quad \ldots \quad z^{[f_{k'}]}[n]\right]^T. \tag{5.20}$$

According to [91], the linear DoF (lDoF) of the K_m-tuple $\left(d^{[m_1]}, \ldots, d^{[m_{K_m}]}\right)$ are achievable if there exist a set of beamforming matrices $\left\{\mathbf{V}_n^{[m_k]}\right\}_{k=1}^{K_m}$ and selection matrices $\left\{\mathbf{\Gamma}_n^{[m_k]}\right\}_{k=1}^{K_m}$ that satisfy almost surely

$$\begin{aligned} &\dim\left(\operatorname{Proj}_{\mathcal{I}_c^{[m_k]}} \mathcal{R}\left[\mathbf{\Gamma}_n^{[m_k]} \mathbf{H}_n^{[m_k]} \mathbf{V}_n^{[m_k]}\right]\right) = a_n^{[m_k]} \\ &d^{[m_k]} = \lim_{n \to +\infty} \frac{a_n^{[m_k]}}{n}, \end{aligned} \tag{5.21}$$

for $k \in \{1, \ldots, K_m\}$, where the interference subspace received by the macro user m_k is

$$\mathcal{I}_c^{[m_k]} = \mathcal{R}\left[\mathbf{\Gamma}_n^{[m_k]} \mathbf{H}_n^{[m_k]} \mathbf{V}_n^{[m_{-k}]}\right] \tag{5.22}$$

with

$$\mathbf{V}_n^{[m_{-k}]} = \left[\mathbf{V}_n^{[m_1]} \ \ldots \ \mathbf{V}_n^{[m_{k-1}]} \, \mathbf{V}_n^{[m_{k+1}]} \ \ldots \ \mathbf{V}_n^{[m_{K_f}]}\right]. \tag{5.23}$$

and $\operatorname{Proj}_{\mathcal{A}_c}\mathcal{B}$ denoting the vector space induced by projecting the vector space $\mathcal{B}$ onto the orthogonal complement of the vector space $\mathcal{A}$.

For femtocell users, the lDoF given by the K_f-tuple $\left(d^{[f_1]}, \ldots, d^{[f_{K_f}]}\right)$ are achievable if there exist two sets of beamforming matrices, $\left\{\mathbf{V}_n^{[f_{k'}]}\right\}_{k'=1}^{K_f}$ and $\left\{\mathbf{V}_n^{[m_k]}\right\}_{k=1}^{K_m}$, as well as

a set of selection matrices $\left\{\mathbf{\Gamma}_n^{[f_{k'}]}\right\}_{k'=1}^{K_f}$ that verify almost surely

$$\begin{aligned}&\dim\left(\mathrm{Proj}_{\mathcal{I}_c^{[f_{k'}]}}\mathcal{R}\left[\mathbf{\Gamma}_n^{[f_{k'}]}\mathbf{H}_n^{[f_{k'}]}\mathbf{V}_n^{[f_{k'}]}\right]\right)=a_n^{[f_{k'}]}\\&d^{[f_{k'}]}=\lim_{n\to+\infty}\frac{a_n^{[f_{k'}]}}{n},\end{aligned}\tag{5.24}$$

for $k'\in\{1,\ldots,K_f\}$. The interference subspace of the femto user $f_{k'}$ is given by the intracell interference from the own FAP transmission and also from the other-tier interference caused by the transmission of the macro BS, i.e.

$$\mathcal{I}_c^{[f_{k'}]}=\mathcal{R}\left[\mathbf{\Gamma}_n^{[f_{k'}]}\mathbf{H}_n^{[f_{k'}]}\mathbf{V}_n^{[f_{-k'}]}\quad\mathbf{\Gamma}_n^{[f_{k'}]}\mathbf{G}_n^{[f_{k'}]}\mathbf{V}_n^{[M]}\right],\tag{5.25}$$

where

$$\mathbf{V}_n^{[f_{-k'}]}=\left[\mathbf{V}_n^{[f_1]}\ \ldots\ \mathbf{V}_n^{[f_{k'-1}]}\,\mathbf{V}_n^{[f_{k'+1}]}\ \ldots\ \mathbf{V}_n^{[f_{K_f}]}\right]\tag{5.26}$$

and

$$\mathbf{V}_n^{[M]}=\left[\mathbf{V}_n^{[m_1]}\ \ldots\ \mathbf{V}_n^{[m_{K_m}]}\right].\tag{5.27}$$

In the following, we characterize the outer bound for the sum-lDoF achieved by a generic FAP in the absence of CSIT and subject to optimal sum-DoF in the macro tier.

Theorem 5.1. *For a macro-femto cellular network where the macro BS has N_m antennas that serve K_m macro users and the transmitter of the femtocell is equipped with $N_f\leq N_m$ antennas serving K_f users, in the absence of CSIT, the maximum sum-lDoF achievable for each FAP are*

$$d_{\Sigma_{low}}=\frac{N_fK_f(N_m-1)}{(N_m+K_m-1)(N_f+K_f-1)},\tag{5.28}$$

subject to optimal sum-DoF in the macro tier, i.e.

$$d_{\Sigma_{upper}}=\frac{N_mK_m}{N_m+K_m-1}.\tag{5.29}$$

Proof. Consider an extended macro-femto setting as is shown in Figure 5.3 were each macro user m_k and each femto user $f_{j'}$ is equipped with N_m and N_f conventional

antennas with $k \in \{1, 2, \ldots, K_m\}$ and $j' \in \{1, 2, \ldots, K_f\} \setminus \{k'\}$, respectively. In the considered macro-femto setting, we also assume that femto user $f_{k'}$ is equipped with one single reconfigurable antenna with N_f preset modes. Obviously, in this extended setting, subject to optimal sum-DoF for the macro users, the sum-lDoF achieved by the femto users constitutes an upper bound of the sum-lDoF achieved by femto users equipped with one reconfigurable antenna with N_f preset modes.

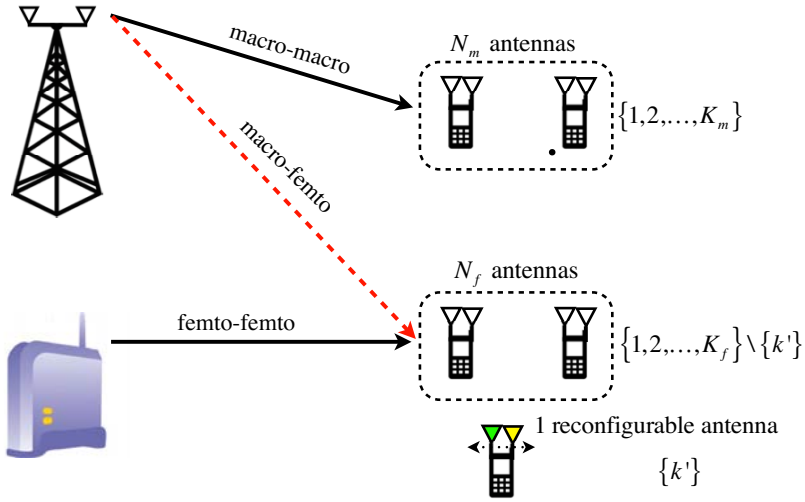

FIGURE 5.3: Extended macro-femto scenario. Each macro user and femto user is equipped with N_m and N_f receive antennas, respectively, but the femto user f_{k',φ_f} is equipped with a single reconfigurable antenna that can switch among N_f preset modes.

Without loss of generality, let us now consider femto user $f_{k'}$. From definition of lDoF, we have that

$$a_n^{[f_{k'}]} = \dim\left(\mathrm{Proj}_{\mathcal{I}_c^{[f_{k'}]}}\mathcal{R}\left[\mathbf{\Gamma}_n^{[f_{k'}]}\mathbf{H}_n^{[f_{k'}]}\mathbf{V}_n^{[f_{k'}]}\right]\right) \tag{5.30}$$

Since the following equality

$$\mathrm{Proj}_{\mathcal{R}(\mathbf{A})^c}\mathcal{R}(\mathbf{B}) = \mathrm{rank}\left(\begin{bmatrix}\mathbf{A} & \mathbf{B}\end{bmatrix}\right) - \mathrm{rank}(\mathbf{A}) \tag{5.31}$$

is verified for two matrices $\mathbf{A}$, $\mathbf{B}$ of the same size [57], we can show that

$$\begin{aligned} a_n^{[f_{k'}]} = &\mathrm{rank}\left(\begin{bmatrix}\mathbf{\Gamma}_n^{[f_{k'}]}\mathbf{H}_n^{[f_{k'}]}\mathbf{V}_n^{[\varphi_f]} & \mathbf{\Gamma}_n^{[f_{k'}]}\mathbf{G}_n^{[f_{k'}]}\mathbf{V}_n^{[M]}\end{bmatrix}\right) \\ &- \mathrm{rank}\left(\begin{bmatrix}\mathbf{\Gamma}_n^{[f_{k'}]}\mathbf{H}_n^{[f_{k'}]}\mathbf{V}_n^{[f_{-k'}]} & \mathbf{\Gamma}_n^{[f_{k'}]}\mathbf{G}_n^{[f_{k'}]}\mathbf{V}_n^{[M]}\end{bmatrix}\right) \end{aligned} \tag{5.32}$$

where the set of all the beamfoming matrices in the corresponding FAP is

$$\mathbf{V}_n^{[\varphi_f]} = \left[\mathbf{V}_n^{[f_1]} \quad \dots \quad \mathbf{V}_n^{[f_{K_f}]}\right] \tag{5.33}$$

and where $\mathbf{\Gamma}_n^{[f_{k'}]}$, $\mathbf{G}_n^{[f_{k'}]}$, $\mathbf{H}_n^{[f_{k'}]}$, $\mathbf{V}_n^{[f_{-k'}]}$ and $\mathbf{V}_n^{[M]}$ are defined in (5.15), (5.16), (5.17), (5.26) and (5.27), respectively.

Next, note that

$$\begin{aligned}&\operatorname{rank}\left[\mathbf{\Gamma}_n^{[f_{k'}]}\mathbf{H}_n^{[f_{k'}]}\mathbf{V}_n^{[f_{-k'}]} \quad \mathbf{\Gamma}_n^{[f_{k'}]}\mathbf{G}_n^{[f_{k'}]}\mathbf{V}_n^{[M]}\right]\\ &\qquad = \operatorname{rank}\left[\mathbf{\Gamma}_n^{[f_{k'}]}\left[\mathbf{H}_n^{[f_{k'}]} \quad \mathbf{G}_n^{[f_{k'}]}\right]\begin{bmatrix}\mathbf{V}_n^{[f_{-k'}]} & \mathbf{0}\\ \mathbf{0} & \mathbf{V}_n^{[M]}\end{bmatrix}\right]\end{aligned} \tag{5.34}$$

By applying Lemma 2 of [91] based on the previous expression, we can show that mode switching in a femto user does not decrease the dimension of its interference space. In particular, we can prove that

$$\begin{aligned}&\operatorname{rank}\left[\mathbf{\Gamma}_n^{[f_{k'}]}\left[\mathbf{H}_n^{[f_{k'}]} \quad \mathbf{G}_n^{[f_{k'}]}\right]\begin{bmatrix}\mathbf{V}_n^{[f_{-k'}]} & \mathbf{0}\\ \mathbf{0} & \mathbf{V}_n^{[M]}\end{bmatrix}\right]\\ &\qquad \overset{a.s.}{\geq} \operatorname{rank}\left[\left[\overline{\mathbf{H}}_n^{[f_{k'}]} \quad \overline{\mathbf{G}}_n^{[f_{k'}]}\right]\begin{bmatrix}\mathbf{V}_n^{[f_{-k'}]} & \mathbf{0}\\ \mathbf{0} & \mathbf{V}_n^{[M]}\end{bmatrix}\right]\end{aligned} \tag{5.35}$$

where $a.s.$ denotes that the inequality holds almost surely and where $\overline{\mathbf{H}}_n^{[f_{k'}]} = \mathbf{I}_n \otimes \mathbf{H}^{[f_{k'}]}$ and $\overline{\mathbf{G}}_n^{[f_{k'}]} = \mathbf{I}_n \otimes \mathbf{G}^{[f_{k'}]}$ with $\mathbf{H}^{[f_{k'}]}$ and $\mathbf{G}^{[f_{k'}]}$ denoting the sub-matrices that consist of the first row of $\mathbf{H}^{[f_{k'}]}$ and $\mathbf{G}^{[f_{k'}]}$, respectively. Moreover, we can easily check that

$$\operatorname{rank}\left(\left[\mathbf{\Gamma}_n^{[f_{k'}]}\mathbf{H}_n^{[f_{k'}]}\mathbf{V}_n^{[\varphi_f]} \quad \mathbf{\Gamma}_n^{[f_{k'}]}\mathbf{G}_n^{[f_{k'}]}\mathbf{V}_n^{[M]}\right]\right) \leq n. \tag{5.36}$$

Thus, by using (5.35) and (5.36), (5.32) can now be re-written as follows

$$a_n^{[f_{k'}]} \overset{a.s.}{\leq} n - \operatorname{rank}\left(\left[\overline{\mathbf{H}}_n^{[f_{k'}]}\mathbf{V}_n^{[f_{-k'}]} \quad \overline{\mathbf{G}}_n^{[f_{k'}]}\mathbf{V}_n^{[M]}\right]\right). \tag{5.37}$$

Intuitively, step (5.37) is given by the fact that the use of reconfigurable antennas always provides the same or greater rank channel matrices than using fixed antennas.

For convenience, we now rearrange the users so that the new network-wide index λ for each femto user j' is

$$\lambda = \varsigma_f(j') = \begin{cases} 1 & \text{if } j' = k', \\ j' & \text{if } j' < k', \\ j'-1 & \text{otherwise.} \end{cases} \tag{5.38}$$

while the new index for macro user k is

$$\lambda = \varsigma_m(k) = K_f + k. \tag{5.39}$$

From now on, we will employ the user index λ to denote the re-arranged index for a macro or a femto user, respectively.

According to the new rearrangement of the users, the number of antennas at each user λ, denoted as Δ_λ, is increasing with the new user index λ, i.e.,

$$\Delta_\lambda = \begin{cases} 1 & \text{if } \lambda = 1 \\ N_f & \text{if } \lambda \in \{2, \ldots, K_f\} \\ N_m & \text{if } \lambda \in \{K_f+1, K_f+2, \ldots, K_f+K_m\} \end{cases} \tag{5.40}$$

with $N_m > N_f$. After verifying this property, we can check that Lemma 3 in [91] can be applied to obtain the relation of the dimensions of the interference space between users $\lambda - 1$ and λ in the considered extended macro-femto setting. In particular, from Lemma 3 in [91] and several algebraic manipulations, we can easily show that

$$\begin{aligned} \frac{1}{\Delta_{\lambda-1}}\text{rank}\left(\mathbf{Z}_n^{[\lambda-1]}\left[\mathbf{U}_n^{[\lambda]} \quad \ldots \quad \mathbf{U}_n^{[K_f+K_m]}\right]\right) &\overset{a.s.}{\geq} \frac{1}{\Delta_\lambda}\text{rank}\left(\mathbf{Z}_n^{[\lambda]}\left[\mathbf{U}_n^{[\lambda+1]} \quad \ldots \quad \mathbf{U}_n^{[K_f+K_m]}\right]\right) \\ &\quad + \dim\left(\text{Proj}_{\mathcal{I}_c^{[\lambda]}}\mathcal{R}\left(\mathbf{Z}_n^{[\lambda]}\mathbf{U}_n^{[\lambda]}\right)\right), \end{aligned} \tag{5.41}$$

for $\lambda \in \{2, 3, \ldots, K_f + K_m\}$ and

$$\begin{aligned} &\frac{1}{\Delta_{K_f+K_m-1}}\text{rank}\left(\mathbf{Z}_n^{[K_f+K_m-1]}\left[\mathbf{U}_n^{[K_f+K_m]}\right]\right) \\ &\qquad \overset{a.s.}{\geq} \dim\left(\text{Proj}_{\mathcal{I}_c^{[K_f+K_m]}}\mathcal{R}\left(\mathbf{Z}_n^{[K_f+K_m]}\mathbf{U}_n^{[K_f+K_m]}\right)\right) \end{aligned} \tag{5.42}$$

where

$$\mathbf{Z}_n^{[\lambda]} = \begin{cases} \left[\overline{\mathbf{H}}_n^{[f_{k'}]}\ \overline{\mathbf{G}}_n^{[f_{k'}]}\right] & \text{if } \lambda = 1, \\ \left[\mathbf{H}_n^{[f_{\varsigma_f^{-1}(\lambda)}]}\ \mathbf{G}_n^{[f_{\varsigma_f^{-1}(\lambda)}]}\right] & \text{if } \lambda = 2, \ldots, K_f, \\ \left[\mathbf{0}_{n\,N_m \times n\,N_f}\ \mathbf{H}_n^{[m_{\lambda - K_f}]}\right] & \text{otherwise,} \end{cases} \tag{5.43}$$

$$\mathbf{U}_n^{[\lambda]} = \begin{cases} \left[\left[\mathbf{V}_n^{[f_{\varsigma_f^{-1}(\lambda)}]}\right]^T \mathbf{0}_{a_n^{[\lambda]} \times n\,N_m}\right]^T & \text{if } \lambda = 1, \ldots, K_f, \\ \left[\mathbf{0}_{a_n^{[\lambda]} \times n\,N_f}\ \left[\mathbf{V}_n^{[m_{\lambda - K_f}]}\right]^T\right]^T & \text{otherwise} \end{cases} \tag{5.44}$$

and

$$\mathcal{I}_c^{[\lambda]} = \begin{cases} \mathcal{I}_c^{[f_{\varsigma_f^{-1}(\lambda)}]} & \text{if } \lambda = 1, \ldots, K_f, \\ \mathcal{I}_c^{[m_{\lambda - K_f}]} & \text{otherwise} \end{cases} \tag{5.45}$$

with $\lambda \in \{1, 2, \ldots, K_f + K_m\}$ and

$$a_n^{[\lambda]} = \begin{cases} a_n^{[f_{\varsigma_f^{-1}(\lambda)}]} & \text{if } \lambda = 2, \ldots, K_f, \\ a_n^{[m_{\lambda - K_f}]} & \text{otherwise.} \end{cases} . \tag{5.46}$$

Recalling that $\lambda = 1$ for femto user $f^{[k']}$, note that a recursive application of (5.41) and (5.42) to the last term in the right hand side of (5.37) allows to obtain the subsequent inequality

$$\begin{aligned} a_n^{[f_{k'}]} \leq & n - \sum_{k'=1}^{K_f} \frac{1}{N_f} \dim\left(\mathrm{Proj}_{\mathcal{I}_c^{[f_{k'}]}} \mathcal{R}\left[\overline{\mathbf{H}}_n^{[f_{k'}]} \mathbf{V}_n^{[f_{k'}]}\right]\right) \\ & - \sum_{k=1}^{K_m} \frac{1}{N_m} \dim\left(\mathrm{Proj}_{\mathcal{I}_c^{[m_k]}} \mathcal{R}\left[\overline{\mathbf{G}}_n^{[f_k]} \mathbf{V}_n^{[f_k]}\right]\right). \end{aligned} \tag{5.47}$$

If we now divide both sides of (5.47) by n and take the limit as n goes to infinity, from the definitions provided in (5.24) and (5.30) we can check that

$$d^{[f_{k'}]} \leq 1 - \sum_{j'=2}^{K_f} \frac{d^{[f_{j'}]}}{N_f} - \sum_{k=1}^{K_m} \frac{d^{[m_k]}}{N_f} \tag{5.48}$$

for each $k' \in \{1, 2, \ldots, K_f\}$. Therefore, the sum-lDoF over all femto users verifies

$$d_{\Sigma_{low}} \leq K_f - \frac{(K_f - 1) d_{\Sigma_{low}}}{N_f} - K_f \sum_{k=1}^{K_m} \frac{d^{[m_k]}}{N_f}. \tag{5.49}$$

Since macro users are subject to reach the optimal sum-DoF as in an isolated MISO BC, from (2.23) we have that

$$\sum_{k=1}^{K_m} \frac{d^{[m_k]}}{N_f} = \frac{N_m K_m}{N_m + K_m - 1}. \tag{5.50}$$

After substituting (5.50) into (5.49), we can therefore see that

$$d_{\Sigma_{low}} \leq \frac{N_f K_f (N_m - 1)}{(N_m + K_m - 1)(N_f + K_f - 1)}, \tag{5.51}$$

In this way, the proof is concluded. □

From Theorem 5.1 it is demonstrated that, for a macro-femto cellular network and in absence of CSIT, femto users can achieve non zero-DoF subject to optimal sum-DoF in the macro tier when $N_m \geq N_f$. As a result, we obtain an outer bound of the DoF achievable by using linear coding strategies for femtocell users while the macro BS transmits independently of the femtocell deployment within its coverage. From now on, the following sections of this chapter are devoted to devise a transmission scheme able to achieve the outer-bound derived in Theorem 5.1.

5.4 Network Blind Interference Alignment for the macro-femto network

In this section we analyze the use of the network BIA (nBIA) scheme proposed in Chapter 4 for heterogeneous cellular networks. In summary, the key idea lies on the

	1	2	3	4	5	6	7	8	9	10
m_1	$\mathbf{h}^{[m_1]}(1)$	$\mathbf{h}^{[m_1]}(1)$	$\mathbf{h}^{[m_1]}(1)$	$\mathbf{h}^{[m_1]}(2)$	$\mathbf{h}^{[m_1]}(2)$	$\mathbf{h}^{[m_1]}(2)$	$\mathbf{h}^{[m_1]}(1)$	$\mathbf{h}^{[m_1]}(1)$	$\mathbf{h}^{[m_1]}(1)$	$\mathbf{h}^{[m_1]}(1)$
m_2	$\mathbf{h}^{[m_2]}(1)$	$\mathbf{h}^{[m_2]}(1)$	$\mathbf{h}^{[m_2]}(1)$	$\mathbf{h}^{[m_2]}(1)$	$\mathbf{h}^{[m_2]}(1)$	$\mathbf{h}^{[m_2]}(1)$	$\mathbf{h}^{[m_2]}(2)$	$\mathbf{h}^{[m_2]}(2)$	$\mathbf{h}^{[m_2]}(2)$	$\mathbf{h}^{[m_2]}(1)$
f_{1,φ_1}	$\mathbf{h}^{[f_1,\varphi_1]}(1)$	$\mathbf{h}^{[f_1,\varphi_1]}(2)$	$\mathbf{h}^{[f_1,\varphi_1]}(3)$	$\mathbf{h}^{[f_1,\varphi_1]}(1)$	$\mathbf{h}^{[f_1,\varphi_1]}(2)$	$\mathbf{h}^{[f_1,\varphi_1]}(3)$	$\mathbf{h}^{[f_1,\varphi_1]}(1)$	$\mathbf{h}^{[f_1,\varphi_1]}(2)$	$\mathbf{h}^{[f_1,\varphi_1]}(3)$	$\mathbf{h}^{[f_1,\varphi_1]}(4)$

FIGURE 5.4: Supersymbol of the nBIA scheme applied to macro-femto scenario for $F = 1$, $N_m = N_f = 2$, $K_m = 2$, and $K_f = 1$.

construction of a supersymbol considering that macro users are *private* users since they only receive signal from the N_m antennas of the macro BS. On the other hand, femto users are considered *shared* users since they receive signals from more than one BS in the network, i.e. from the N_f antennas of their corresponding FAP and the N_m antennas from the macro BS. Moreover, since the macro BS transmits data to both the macro users and the femto users, the transmission of data to a femto or a macro user creates interference to the rest of users in the network. As a result, the beams transmitted to any of the users in the network, need to be aligned into one dimension at the rest of the users.

5.4.1 The key idea of network Blind Interference Alignment for macro-femto networks

To illustrate the key idea of nBIA in our macro-femto network, let us consider a toy example where the macro BS has $N_m = 2$ transmit antennas and $K_m = 2$ macro users. Moreover, there is one FAP, i.e. $F = 1$, with $N_f = 2$ antennas and $K_f = 1$ femto user. Following the generalization of alignment block provided in Chapter 4 for partially connected networks, the supersymbol has the structure shown in Figure 5.4

and the corresponding beamforming matrices are

$$\mathbf{X} = \begin{bmatrix} \mathbf{I} & \mathbf{0} & \mathbf{0} \\ \mathbf{0} & \mathbf{I} & \mathbf{0} \\ \mathbf{0} & \mathbf{0} & \mathbf{I} \\ \mathbf{I} & \mathbf{0} & \mathbf{0} \\ \mathbf{0} & \mathbf{I} & \mathbf{0} \\ \mathbf{0} & \mathbf{0} & \mathbf{I} \\ \mathbf{0} & \mathbf{0} & \mathbf{0} \\ \mathbf{0} & \mathbf{0} & \mathbf{0} \\ \mathbf{0} & \mathbf{0} & \mathbf{0} \\ \mathbf{0} & \mathbf{0} & \mathbf{0} \end{bmatrix} \begin{bmatrix} \mathbf{u}_1^{[m_1]} \\ \mathbf{u}_2^{[m_1]} \\ \mathbf{u}_3^{[m_1]} \end{bmatrix} + \begin{bmatrix} \mathbf{I} & \mathbf{0} & \mathbf{0} \\ \mathbf{0} & \mathbf{I} & \mathbf{0} \\ \mathbf{0} & \mathbf{0} & \mathbf{I} \\ \mathbf{0} & \mathbf{0} & \mathbf{0} \\ \mathbf{0} & \mathbf{0} & \mathbf{0} \\ \mathbf{0} & \mathbf{0} & \mathbf{0} \\ \mathbf{I} & \mathbf{0} & \mathbf{0} \\ \mathbf{0} & \mathbf{I} & \mathbf{0} \\ \mathbf{0} & \mathbf{0} & \mathbf{I} \\ \mathbf{0} & \mathbf{0} & \mathbf{0} \end{bmatrix} \begin{bmatrix} \mathbf{u}_1^{[m_2]} \\ \mathbf{u}_2^{[m_2]} \\ \mathbf{u}_3^{[m_2]} \end{bmatrix} + \begin{bmatrix} \mathbf{I} \\ \mathbf{I} \\ \mathbf{I} \\ \mathbf{0} \\ \mathbf{0} \\ \mathbf{0} \\ \mathbf{0} \\ \mathbf{0} \\ \mathbf{0} \\ \mathbf{I} \end{bmatrix} \mathbf{u}_1^{[f_{1,\varphi_1}]}, \tag{5.52}$$

where $\mathbf{u}_1^{[f_{1,\varphi_1}]} = \begin{bmatrix} \mathbf{u}_1^{[f_{1,\varphi_1},M]^T} & \mathbf{u}_1^{[f_{1,\varphi_1},\varphi_1]^T} \end{bmatrix}^T \in \mathbb{C}^{4\times 1}$, $\mathbf{u}_\ell^{[m_k]} = \begin{bmatrix} \mathbf{u}_\ell^{[m_k,M]^T} & \mathbf{0}_{2,1}^T \end{bmatrix} \in \mathbb{C}^{4\times 1}$ and $\mathbf{X} = \text{col}\{\mathbf{x}[i]\}_{i=1}^{10}$ with $\mathbf{x}[i] = \text{col}\{\mathbf{x}^{[M]}[i], \mathbf{x}^{[\varphi_1]}[i]\}$ formed by the signals $\mathbf{x}^{[M]}[i] \in \mathbb{C}^{2\times 1}$ and $\mathbf{x}^{[\varphi_1]}[i] \in \mathbb{C}^{2\times 1}$ transmitted by the antennas of the macro BS and FAP, respectively. The vectors $\mathbf{u}_1^{[f_{k',\varphi_1},M]}$ and $\mathbf{u}_1^{[f_{k',\varphi_1},\varphi_1]}$ contain the symbols transmitted to femto user f_{k',φ_1} from the macro BS and FAP φ_1, respectively, whereas $\mathbf{u}_\ell^{[m_k,M]} \in \mathbb{C}^{2\times 1}$ are the symbols transmitted by the macro BS to macro user m_k. Additionally, $\mathbf{I}$ and $\mathbf{0}$ are the 4×4 identity and the zero matrix, respectively.

At each symbol extension, femto users are served by the $N_m = 2$ and $N_f = 2$ antennas of the macro BS and the FAP, respectively. To send $M = N_m + N_f = 4$ distinguishable data streams, both the macro BS and the FAP jointly transmit $\mathbf{u}_1^{[f_{1,\varphi_1}]}$ at 4 different symbol extensions over which the antenna of f_{1,φ_1}, switches through $M = 4$ different modes. At the same time, these 4 beams need to be aligned into one dimension at the users subject to interference because of transmission to user f_{1,φ_1}. Toward this goal, all the macro users set the same channel mode during the entire alignment block of the femto user f_{1,φ_1}, which corresponds to symbol extensions $\{1, 2, 3, 10\}$ according to the supersymbol shown in Figure 5.4 and the beamforming matrices given in (5.52). For

example, if we ignore the noise, the signal received by user f_{1,φ_1} is

$$\begin{aligned}\begin{bmatrix} y^{[f_{1,\varphi_1}]}[1] \\ y^{[f_{1,\varphi_1}]}[2] \\ y^{[f_{1,\varphi_1}]}[3] \\ y^{[f_{1,\varphi_1}]}[10] \end{bmatrix} &= \begin{bmatrix} \mathbf{h}^{[f_{1,\varphi_1}]}(1)^T\mathbf{x}[1] \\ \mathbf{h}^{[f_{1,\varphi_1}]}(2)^T\mathbf{x}[2] \\ \mathbf{h}^{[f_{1,\varphi_1}]}(3)^T\mathbf{x}[3] \\ \mathbf{h}^{[f_{1,\varphi_1}]}(4)^T\mathbf{x}[10] \end{bmatrix} \\ &= \begin{bmatrix} \mathbf{h}^{[f_{1,\varphi_1}]}(1)^T \\ \mathbf{h}^{[f_{1,\varphi_1}]}(2)^T \\ \mathbf{h}^{[f_{1,\varphi_1}]}(3)^T \\ \mathbf{h}^{[f_{1,\varphi_1}]}(4)^T \end{bmatrix} \mathbf{u}_1^{[f_{1,\varphi_1}]} + \underbrace{\begin{bmatrix} \mathbf{h}^{[f_{1,\varphi_1}]}(1)^T\left(\mathbf{u}_1^{[m_1]}+\mathbf{u}_1^{[m_1]}\right) \\ \mathbf{h}^{[f_{1,\varphi_1}]}(2)^T\left(\mathbf{u}_2^{[m_1]}+\mathbf{u}_2^{[m_2]}\right) \\ \mathbf{h}^{[f_{1,\varphi_1}]}(3)^T\left(\mathbf{u}_3^{[m_1]}+\mathbf{u}_3^{[m_3]}\right) \\ 0 \end{bmatrix}}_{\text{macroBS interference}}. \end{aligned} \tag{5.53}$$

where $\mathbf{h}^{[f_{1,\varphi_1}]}(l) = \left[\mathbf{h}^{[f_{1,\varphi_1},M]}(l)^T \quad \mathbf{h}^{[f_{1,\varphi_1},\varphi_1]}(l)^T\right]^T \in \mathbb{C}^{4\times 1}$ contains the channel coefficients between the transmit antennas of macro BS and FAP φ_1 to user f_{1,φ_1} at channel mode l. The interference created by the transmission from the macro BS to the macro users m_1 and m_2 can be measured in symbol extensions {4,5,6} and {7,8,9}, respectively. Since the channels $\mathbf{h}^{[f_{1,\varphi_1}]}(l)$, $l \in \{1,2,3,4\}$, are generic, the femtocell user f_{1,φ_1} can decode the 4 symbols contained in $\mathbf{u}_1^{[f_{1,\varphi_1}]}$ after applying zero-forcing based on the signals received during the aforementioned symbol extensions. Additionally, we can observe that the four transmissions of $\mathbf{u}_1^{[f_{1,\varphi_1}]}$ are aligned into one dimension at all the macro users, by checking the signal received at any macro user m_k

$$\begin{bmatrix} y^{[m_k]}[1] \\ y^{[m_k]}[2] \\ y^{[m_k]}[3] \\ y^{[m_k]}[7] \end{bmatrix} = \underbrace{\begin{bmatrix} \mathbf{h}^{[m_k]}(1)^T\mathbf{u}_1^{[m_k]} \\ \mathbf{h}^{[m_k]}(1)^T\mathbf{u}_2^{[m_k]} \\ \mathbf{h}^{[m_k]}(1)^T\mathbf{u}_3^{[m_k]} \\ 0 \end{bmatrix}}_{\text{desired signals}} + \underbrace{\begin{bmatrix} \mathbf{h}^{[m_k]}(1)^T \\ \mathbf{h}^{[m_k]}(1)^T \\ \mathbf{h}^{[m_k]}(1)^T \\ \mathbf{h}^{[m_k]}(1)^T \end{bmatrix}}_{\text{interference}} \mathbf{u}_1^{[f_{1,\varphi_1}]} \tag{5.54}$$

where $\mathbf{h}^{[m_1]}(l) \approx \left[\mathbf{h}^{[m_1,M]}(l)^T \quad \mathbf{0}_{2,1}{}^T\right]^T \in \mathbb{C}^{4\times 1}$ contains the channel coefficients between the antennas of the macro BS and the macro user. As a result, since the macro BS only transmits $\mathbf{u}_1^{[f_{1,\varphi_1}]}$ during symbol extension 7, the macro users can apply zero-forcing based on measuring $y^{[m_k]}[7]$ to remove the interference during symbol extensions $\{1,2,3\}$.

Unlike the femto users, macro user m_k only receives signals from the $N_m = 2$ antennas of the macro BS. To send $N_m = 2$ distinguishable data streams, which are contained in

the symbol $\mathbf{u}_{\ell}^{[m_k,M]}$, macro BS repeatedly transmits $\mathbf{u}_{\ell}^{[m_k,M]}$ during 2 symbol extensions over which the antenna of macro user m_k switches among 2 preset modes. Additionally, to align the two transmissions of $\mathbf{u}_{\ell}^{[m_k,M]}$ into one dimension at the users subject to interference, the affected users should keep the same radiation pattern. In this case, due to the considered connectivity of the network, note that all users, macro and femto, are subject to interference when the macro BS transmits to any macro user. From the supersymbol shown in Figure 5.4, we can check that the pairs of symbol extensions $\{1, 4\}$ satisfy all these conditions. For instance, if we ignore the noise, the signal received at user m_1 during the first alignment block is

$$\begin{bmatrix} y^{[m_1]}[1] \\ y^{[m_1]}[4] \end{bmatrix} = \begin{bmatrix} \mathbf{h}^{[m_1]}(1)^T \\ \mathbf{h}^{[m_1]}(2)^T \end{bmatrix} \mathbf{u}_1^{[m_1]} + \underbrace{\begin{bmatrix} \mathbf{h}^{[m_1]}(1)^T(\mathbf{u}_1^{[m_1]} + \mathbf{u}_1^{[f_{1.\varphi_1},M]}) \\ 0 \end{bmatrix}}_{\text{interference}}. \tag{5.55}$$

The interference term caused by transmission from the macro BS to macro user m_1 and femto user f_{1,φ_1} can be cancelled by applying zero-forcing based on the signal received at symbol extensions 7 and 10, respectively. Thus, since $\mathbf{h}^{[m_k]}(l)$, $l \in \{1, 2\}$, are generic, user m_1 can decode 2 data streams. Note that a similar procedure can be followed to decode the data streams $\mathbf{u}_2^{[m_1]}$ and $\mathbf{u}_3^{[m_1]}$ transmitted repetitively over the pairs of symbol extensions $\{2, 5\}$ and $\{3, 6\}$, respectively.

In summary, the key idea of nBIA lies on the construction of a supersymbol formed by alignment blocks for communication systems with partial connectivity, as it happens in the considered macro-femto cellular network. If a user k can be served by N_k transmit antennas, then its alignment block consists of N_k symbol extensions over which its antenna switches over N_k different preset modes in order to receive N_k distinguishable data streams. At the same time, to align the aforementioned N_k beams into one dimension at all the users subject to interference due to the transmission to user k, their channel state has to be maintained constant over the symbol extensions that form the alignment block of user k.

5.4.2 Achievable Degrees of Freedom of network Blind Interference Alignment in two-tier networks

The network BIA scheme developed in the previous chapter has been extended to its implementation in heterogeneous cellular networks. In this way, macro users are managed as private users that only receive signal from a BS in the network, in this case from the N_m antennas of the macro BS. On the other hand, femto users are considered shared users receiving a useful signal from both the macro BS and its corresponding FAP. In consequence, each femto user receives data from $M = N_m + N_f$ antennas. Moreover, since the macro BS transmits data to both the macro users and the femto users, it creates interference to the rest of users in the network. As a result, the beams transmitted to any of the users in the network, need to be aligned into one dimension at the rest of the users. Taking all these features into account, from the Section 4.6 of Chapter 4 we can build the supersymbol for a macro-femto cellular network that has one macro BS with N_m antennas and K_m macro users as well as F FAPs, each with N_f antennas and K_f femto users (e.g., see the supersymbol shown in Figure 5.5 for an heterogeneous network with $F = 2$ FAPs). Therefore, for the described macro-femto cellular network, the Block 1 consists of

$$\mathcal{L}_{\text{SB1,nBIA}} = (N_m - 1)^{K_m} (M - 1)^{K_f} \tag{5.56}$$

symbol extensions over which simultaneous transmission takes place. Since each alignment block of a macro user comprises (N_m-1) symbol extensions of the Block 1, a total of $(N_m-1)^{K_m-1}(M-1)^{K_f}$ alignment blocks are distributed over the supersymbol for each macro user. Similarly, since $(M-1)$ symbol extensions of the alignment block of each femto user belong to Block 1, the proposed supersymbol contains $(N_m-1)^{K_m}(M-1)^{K_f-1}$ alignment blocks for each femto user.

To complete the alignment block of any user and let the other users measure the interference created within the alignment block, each user employs one additional symbol extension of Block 2 over which the beams associated with the considered alignment block are transmitted free of interference. Therefore,

$$\mathcal{L}_{\text{SB2}_\text{m},\text{nBIA}} = K_m \left[(N_m - 1)^{K_m - 1} (M - 1)^{K_f} \right] \tag{5.57}$$

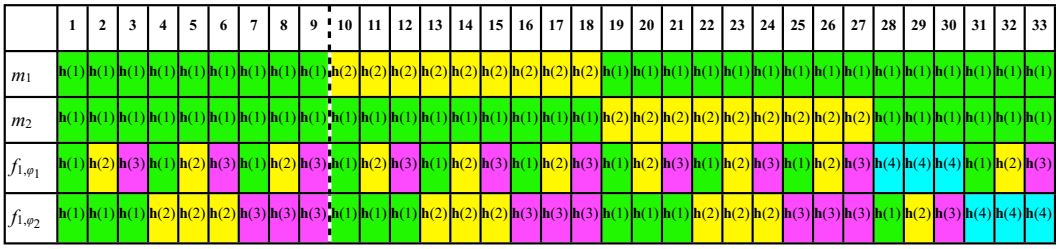

FIGURE 5.5: Supersymbol of the nBIA scheme applied to the macro-femto scenario for $F = 2$, $N_m = N_f = 2$, $K_m = 2$, and $K_f = 1$.

and

$$\mathcal{L}_{\mathrm{SB2_f,nBIA}} = F\,K_f\left[(M-1)^{K_f-1}\,(N_m-1)^{K_m}\right] \tag{5.58}$$

symbol extensions are required in Block 2 to complete the alignment blocks of all the macro and femto users, respectively. Notice that each macro and femto user achieves N_m and M DoF per alignment block, respectively. Therefore, we can now verify that the achievable sum-DoF per symbol extension in the macro tier are

$$\mathrm{DoF_{m,nBIA}} = \frac{N_m K_m (M-1)}{(M-1)(N_m+K_m-1)+F\,K_f(N_m-1)}, \tag{5.59}$$

whereas the sum-DoF per symbol extension achieved in each femtocell are

$$\mathrm{DoF_{f,nBIA}} = \frac{M K_f (N_m-1)}{(M-1)(N_m+K_m-1)+F\,K_f(N_m-1)}. \tag{5.60}$$

It is interesting to remark that for the toy example analyzed in Section 5.4.1, the proposed extension of the nBIA scheme for heterogeneous cellular networks achieves $\frac{6}{5}$ DoF and $\frac{2}{5}$ DoF for macro and femto users, respectively. That is, $\frac{8}{5}$ DoF are achievable in the whole network. Note that according to the theoretic outer bound derived in (5.51) and (5.51), $\frac{4}{3}$ DoF and $\frac{1}{3}$ DoF are achievable in the macro and femto tiers, respectively. Notice that $\frac{5}{3}$ DoF are potentially achievable in the proposed scenario, and nevertheless, the performance of nBIA in this case is $\frac{1}{15}$ DoF below the optimal. Besides, it can be seen in (5.60) and (5.59) that the achievable DoF decrease as a large amount of femtocells within the macro coverage are deployed. Last but not least, cooperation among both tiers involves to penalyze the macro users, which do not receive any data from the femtocell tier.

5.5 Cognitive Blind Interference Alignment

Although the previous approach based on the nBIA scheme proposed in Chapter 4 cancels the intracell interference and also the inter-tier interference, it requires cooperation among macro BS and FAPs when transmitting to the femto users. Due to the features of a typical femtocell deployment, i.e. several FAPs randomly spread over the macrocell coverage area, cooperation requires a large amount of network resources. Furthermore, the DoF achieved by macro and femto users in each cell decrease with the number of FAPs F as can be seen in (5.59) and (5.60). In this section we propose a cognitive BIA (cogBIA) scheme where the macro users achieve the optimal sum-DoF in the absence of CSIT and where the FAPs take advantage of the supersymbol structure of the macro users to transmit in a cognitive fashion. Indeed, the macro BS transmits independently of the femtocells deployed within its coverage. Furthermore, in contrast with the nBIA scheme applied in a two-tier network, the achievable sum-DoF in each femtocell does not decrease with F. That is, the achievable sum-DoF in the femto tier scales linearly with the amount of femtocells deployed.

5.5.1 Femtocell Transmission Using Cognitive Blind Interference Alignment

To illustrate the proposed cognitive scheme, we first consider a toy macro-femto network. Let us consider a two-tier cellular network formed by one FAP with $N_f = 1$ antenna and $K_f = 1$ femto user as well as a macro BS that has $N_m = 2$ antennas that only transmits data to $K_m = 2$ femto users. To let the macro users achieve the optimal sum-DoF in the absence of CSIT, the macro BS will implement the sBIA scheme with the supersymbol shown in Figure 5.6(a) and beamforming matrix provided in (5.61).

$$\mathbf{X} = \begin{bmatrix} \mathbf{x}[1] \\ \mathbf{x}[2] \\ \mathbf{x}[3] \end{bmatrix} = \begin{bmatrix} \mathbf{I} \\ \mathbf{I} \\ \mathbf{0} \end{bmatrix} \mathbf{u}_1^{[m_1]} + \begin{bmatrix} \mathbf{I} \\ \mathbf{0} \\ \mathbf{I} \end{bmatrix} \mathbf{u}_1^{[m_2]} \tag{5.61}$$

Due to the reduced radius of coverage of the FAP, in the aforementioned supersymbol the FAP can leverage the symbols extensions of Block 1, referred to as m-Block 1 from now on, to transmit data to the femto user without creating interference in the macro

	1	2	3
m_1	$\mathbf{h}^{[m_1]}(1)$	$\mathbf{h}^{[m_1]}(2)$	$\mathbf{h}^{[m_1]}(1)$
m_2	$\mathbf{h}^{[m_2]}(1)$	$\mathbf{h}^{[m_2]}(1)$	$\mathbf{h}^{[m_2]}(2)$

(a)

	1	2	3
f_{1,φ_f}	$\mathbf{h}^{[f_1,\varphi_1]}(1)$	$\mathbf{h}^{[f_1,\varphi_1]}(2)$	$\mathbf{h}^{[f_1,\varphi_1]}(1)$
f_{2,φ_f}	$\mathbf{h}^{[f_2,\varphi_1]}(1)$	$\mathbf{h}^{[f_2,\varphi_1]}(1)$	$\mathbf{h}^{[f_2,\varphi_1]}(2)$

(b)

FIGURE 5.6: Supersymbol of the sBIA scheme for a) $N_m = 2$ transmit antennas serving $K_m = 2$ macro users and for b) $N_f = 2$ and $K_f = 2$ femto users.

cell. However, notice that the received signal of the femto users is subject to interference because of the transmission of the macro BS to the macro users during m-Block 1. At first sight, this interference could hamper the femto user f_{1,φ_1} when decoding the signals transmitted from its corresponding FAP. Nonetheless, by inspecting the sBIA supersymbol in Figure 5.6(a) as well as the beamforming matrices provided in (5.61), femto user f_{1,φ_1} can remove the macro-femto interference by applying zero-forcing based on the signals received during the symbol extensions of Block 2, which will be referred to as m-Block 2. To do so, the femto user f_{1,φ_1} only needs to measure the interference associated with the transmission of a specific data stream, $\mathbf{u}_\ell^{[m_k]}$, with the same preset mode as in the symbol extensions of m-Block 1 over which that data stream $\mathbf{u}_\ell^{[m_k]}$ interferes its desired signals. Following all this reasoning, we can now design the supersymbol shown in Figure 5.7 and the following beamforming matrices

$$\mathbf{X} = \begin{bmatrix} \mathbf{x}[1] \\ \mathbf{x}[2] \\ \mathbf{x}[3] \end{bmatrix} = \begin{bmatrix} \mathbf{I} \\ \mathbf{I} \\ \mathbf{0} \end{bmatrix} \mathbf{u}_1^{[m_1]} + \begin{bmatrix} \mathbf{I} \\ \mathbf{0} \\ \mathbf{I} \end{bmatrix} \mathbf{u}_1^{[m_2]} + \begin{bmatrix} \mathbf{I} \\ \mathbf{0} \\ \mathbf{0} \end{bmatrix} \mathbf{u}_1^{[f_{1,\varphi_1}]} \tag{5.62}$$

where, for $k \in \{1, 2\}$, $\mathbf{x}[t] = \left[\mathbf{x}^{[M]^T}[t] \;\; x^{[\varphi_1]}[t]\right]^T$, $\mathbf{u}_1^{[m_k]} = \left[\mathbf{u}_1^{[m_k,M]^T} \;\; 0\right]^T$ and $\mathbf{u}_1^{[f_{1,\varphi_1}]} = \left[\mathbf{0}_{2,1}^T \;\; u_1^{[f_{1,\varphi_1},\varphi_1]^T}\right]^T$ with $\mathbf{u}_1^{[m_k,M]} \in \mathbb{C}^{2\times 1}$ and $u_1^{[f_{1,\varphi_1},\varphi_1]} \in \mathbb{C}$ denoting the symbols transmitted from the macro BS and the FAP to the macro user m_k and femto user f_{1,φ_1}, respectively.

From the supersymbol shown in Figure 5.7 and the beamforming matrix in (5.62), if we ignore the noise we can observe that

$$y^{[f_{1,\varphi_1}]}[1] = h^{[f_{1,\varphi_1},\varphi_1]}(1) u_1^{[f_{1,\varphi_1},\varphi_1]} + \underbrace{\mathbf{h}^{[f_{1,\varphi_1},M]}(1)^T \left(\mathbf{u}_1^{[m_1]} + \mathbf{u}_1^{[m_2]}\right)}_{\text{macro-femto interference}}. \tag{5.63}$$

	1	2	3
m_1	$\mathbf{h}^{[m_1]}(1)$	$\mathbf{h}^{[m_1]}(2)$	$\mathbf{h}^{[m_1]}(1)$
m_2	$\mathbf{h}^{[m_2]}(1)$	$\mathbf{h}^{[m_2]}(1)$	$\mathbf{h}^{[m_1]}(2)$
f_{1,φ_f}	$\mathbf{h}^{[f_{2,\varphi_1}]}(1)$	$\mathbf{h}^{[f_{2,\varphi_1}]}(1)$	$\mathbf{h}^{[f_{2,\varphi_1}]}(1)$

FIGURE 5.7: Supersymbol of the proposed cognitive BIA scheme for $N_m = 2$, $K_m = 2$, $N_f = 1$, and $K_f = 1$.

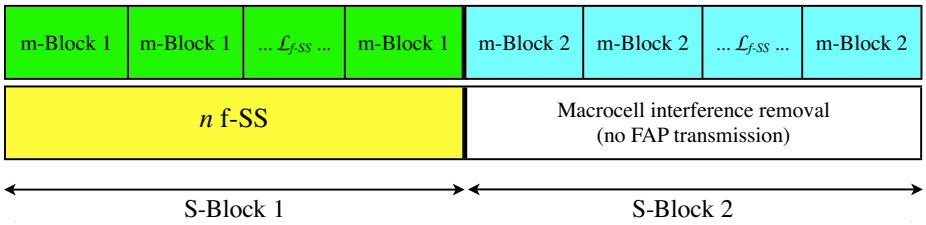

FIGURE 5.8: Macro and femto supersymbols for cognitive BIA.

	1	2	3	4	5	6	7	8	9
m_1	$\mathbf{h}^{[m_1]}(1)$	$\mathbf{h}^{[m_1]}(1)$	$\mathbf{h}^{[m_1]}(1)$	$\mathbf{h}^{[m_1]}(2)$	$\mathbf{h}^{[m_1]}(2)$	$\mathbf{h}^{[m_1]}(2)$	$\mathbf{h}^{[m_1]}(1)$	$\mathbf{h}^{[m_1]}(1)$	$\mathbf{h}^{[m_1]}(1)$
m_2	$\mathbf{h}^{[m_2]}(1)$	$\mathbf{h}^{[m_2]}(1)$	$\mathbf{h}^{[m_2]}(1)$	$\mathbf{h}^{[m_2]}(1)$	$\mathbf{h}^{[m_2]}(1)$	$\mathbf{h}^{[m_2]}(1)$	$\mathbf{h}^{[m_2]}(2)$	$\mathbf{h}^{[m_2]}(2)$	$\mathbf{h}^{[m_2]}(2)$
f_{1,φ_f}	$\mathbf{h}^{[f_{1,\varphi_1}]}(1)$	$\mathbf{h}^{[f_{1,\varphi_1}]}(2)$	$\mathbf{h}^{[f_{1,\varphi_1}]}(1)$	$\mathbf{h}^{[f_{1,\varphi_1}]}(1)$	$\mathbf{h}^{[f_{1,\varphi_1}]}(2)$	$\mathbf{h}^{[f_{1,\varphi_1}]}(1)$	$\mathbf{h}^{[f_{1,\varphi_1}]}(1)$	$\mathbf{h}^{[f_{1,\varphi_1}]}(2)$	$\mathbf{h}^{[f_{1,\varphi_1}]}(1)$
f_{2,φ_f}	$\mathbf{h}^{[f_{2,\varphi_1}]}(1)$	$\mathbf{h}^{[f_{2,\varphi_1}]}(1)$	$\mathbf{h}^{[f_{2,\varphi_1}]}(2)$	$\mathbf{h}^{[f_{2,\varphi_1}]}(1)$	$\mathbf{h}^{[f_{2,\varphi_1}]}(1)$	$\mathbf{h}^{[f_{2,\varphi_1}]}(2)$	$\mathbf{h}^{[f_{2,\varphi_1}]}(1)$	$\mathbf{h}^{[f_{2,\varphi_1}]}(1)$	$\mathbf{h}^{[f_{2,\varphi_1}]}(2)$

FIGURE 5.9: Supersymbol for cognitive BIA with $N_m = N_f = 2$ and $K_m = K_f = 2$.

Since femto user f_{1,φ_1} has the same preset mode in all symbol extensions, it can remove the interference in symbol extension 1 by applying zero-forcing based on its received signal during symbol extensions $\{2\}$ and $\{3\}$. Hence, the signal after zero-forcing cancellation is

$$\tilde{y}^{[f_{1,\varphi_1}]}[1] - \left(\tilde{y}^{[f_{1,\varphi_1}]}[2] + \tilde{y}^{[f_{1,\varphi_1}]}[3]\right) = h^{[f_{1,\varphi_1},\varphi_1]}(1) u_1^{[f_{1,\varphi_1},\varphi_1]}. \tag{5.64}$$

In consequence, the femto user f_{1,φ_f} achieves 1 DoF over 3 symbol extensions. Moreover, since the macro users are not subject to interference by the transmission of the FAP, each macro user still achieves 2 DoF over 3 symbol extensions, which corresponds to the maximum achievable without CSIT (See (2.23) for the MISO BC).

Assume now that the FAP has $N_f = 2$ transmit antennas and $K_f = 2$ femto users. With the aim of achieving as many DoF as possible without CSIT, we also assume that the FAP employs the BIA scheme to transmit data to its femto users and manage the intracell interference. Hence, the supersymbol of the FAP (f-SS) is as shown in Figure 5.6(b). Analogously to the supersymbol of the macro users, the supersymbol f-SS consists of two blocks, referred to as f-Block 1 and f-Block 2. To follow the idea of cognitive BIA illustrated in the previous example, the FAP would need to implement f-SS during the only symbol extension that forms m-Block 1. However, since the supersymbol f-SS comprises now 3 symbol extensions, one of them belonging to f-Block 1 and the rest belonging to f-Block 2, such an implementation is not straightforward.

For the considered toy example and for the general case, the length of m-Block 1, referred to as q, is not generally equal to the length of the f-SS supersymbol, denoted as $\mathcal{L}_{\text{f-SS}}$. In the case that the macro BS implements a sBIA scheme for K_m macro users served by N_m antennas, from (2.15) notice that

$$q = (N_m - 1)^{K_m}. \tag{5.65}$$

On the contrary, if each FAP transmits data to K_f femto users by employing N_f antennas, from (2.22) we can also check that the length of the f-SS supersymbol equals

$$\mathcal{L}_{\text{f-SS}} = (N_f - 1)^{K_f} + K_f(N_f - 1)^{K_f - 1}, \tag{5.66}$$

which is not necessarily equal to q. As a result, a FAP might not be able to implement a f-SS supersymbol within one m-Block 1 so that the antenna switching pattern of each femto user aligns into the same dimension the macro-femto interference caused by the repeated transmission of a specific data stream $\mathbf{u}_\ell^{[m_k]}$. As shown in Figure 5.8, this issue can be handled by forming a supersymbol whose Block 1, referred to as S-Block 1, consists of q identical f-SS supersymbols and m-Blocks 1 repeated $\mathcal{L}_{\text{f-SS}}$ times for the femto and macro users, respectively.

As a result, Block 2 in the new supersymbol, referred to as S-Block 2 from now on, is formed by $\mathcal{L}_{\text{f-SS}}$ identical m-Blocks 2 for the macro users. Besides letting each macro user to complete its alignment blocks and remove the intracell interference created by the transmission from the macro BS to any other macro user, notice that the symbol

extensions in S-Block 2 allow the femto users to measure the macro-femto interference caused because of transmission in S-Block 1. However, to fully remove the macro-femto interference based on the measurement performed during S-Block 2, each femto user needs to keep the same channel mode along all the symbol extensions over which a specific data stream $\mathbf{u}_\ell^{[m_k]}$ is repeatedly transmitted. This condition determines how the $\mathcal{L}_{\mathrm{f-SS}}$ m-Blocks 1 and the q f-SS supersymbols should be combined to form S-Block 1. Moreover, it allows to determine the preset mode of the femto users in S-Block 2 given a specific distribution of the $\mathcal{L}_{\mathrm{f-SS}}$ m-Blocks 2 over S-Block 2. For instance, for our toy example considering the supersymbol shown in Figure 5.9, the following beamforming matrices

$$\mathbf{X} = \begin{bmatrix} \mathbf{I} & \mathbf{0} & \mathbf{0} \\ \mathbf{0} & \mathbf{I} & \mathbf{0} \\ \mathbf{0} & \mathbf{0} & \mathbf{I} \\ \mathbf{I} & \mathbf{0} & \mathbf{0} \\ \mathbf{0} & \mathbf{I} & \mathbf{0} \\ \mathbf{0} & \mathbf{0} & \mathbf{I} \\ \mathbf{0} & \mathbf{0} & \mathbf{0} \\ \mathbf{0} & \mathbf{0} & \mathbf{0} \\ \mathbf{0} & \mathbf{0} & \mathbf{0} \end{bmatrix} \begin{bmatrix} \mathbf{u}_1^{[m_1]} \\ \mathbf{u}_2^{[m_1]} \\ \mathbf{u}_3^{[m_1]} \end{bmatrix} + \begin{bmatrix} \mathbf{I} & \mathbf{0} & \mathbf{0} \\ \mathbf{0} & \mathbf{I} & \mathbf{0} \\ \mathbf{0} & \mathbf{0} & \mathbf{I} \\ \mathbf{0} & \mathbf{0} & \mathbf{0} \\ \mathbf{0} & \mathbf{0} & \mathbf{0} \\ \mathbf{0} & \mathbf{0} & \mathbf{0} \\ \mathbf{I} & \mathbf{0} & \mathbf{0} \\ \mathbf{0} & \mathbf{I} & \mathbf{0} \\ \mathbf{0} & \mathbf{0} & \mathbf{I} \end{bmatrix} \begin{bmatrix} \mathbf{u}_1^{[m_2]} \\ \mathbf{u}_2^{[m_2]} \\ \mathbf{u}_3^{[m_2]} \end{bmatrix} + \begin{bmatrix} \mathbf{I} & \mathbf{I} \\ \mathbf{I} & \mathbf{0} \\ \mathbf{0} & \mathbf{I} \\ \mathbf{0} & \mathbf{0} \\ \mathbf{0} & \mathbf{0} \\ \mathbf{0} & \mathbf{0} \\ \mathbf{0} & \mathbf{0} \\ \mathbf{0} & \mathbf{0} \\ \mathbf{0} & \mathbf{0} \end{bmatrix} \begin{bmatrix} \mathbf{u}_1^{[f_{1,\varphi_1}]} \\ \mathbf{u}_1^{[f_{2,\varphi_1}]} \end{bmatrix} \tag{5.67}$$

where $\mathbf{u}_1^{[f_{1,\varphi_1}]} = \begin{bmatrix} \mathbf{0}_{2,1}^T & \mathbf{u}_1^{[f_{1,\varphi_1},\varphi_1]^T} \end{bmatrix}^T \in \mathbb{C}^{4\times 1}$, $\mathbf{u}_\ell^{[m_k]} = \begin{bmatrix} \mathbf{u}_\ell^{[m_k,M]^T} & \mathbf{0}_{2,1}{}^T \end{bmatrix}^T \in \mathbb{C}^{4\times 1}$ and $\mathbf{X} = \mathrm{col}\{\mathbf{x}[t]\}_{t=1}^9$ with $\mathbf{x}[t] = \mathrm{col}\{\mathbf{x}^{[M]}[i], \mathbf{x}^{[\varphi_1]}[t]\}$ formed by the signals $\mathbf{x}^{[M]}[t] \in \mathbb{C}^{2\times 1}$ and $\mathbf{x}^{[\varphi_1]}[t] \in \mathbb{C}^{2\times 1}$ are transmitted by the antennas of the macro BS and FAP, respectively.

By inspecting the supersymbol in Figure 5.9 and the corresponding beamforming matrices in (5.67), note that the antenna switching pattern of the macro users during S-Block 1 and S-Block 2 simply consists of the concatenation of the antenna switching pattern associated with $\mathcal{L}_{\mathrm{f-SS}}$ m-Blocks 1 and $\mathcal{L}_{\mathrm{f-SS}}$ m-Blocks 2, respectively. Since the macro BS does not transmit data to the femto users and the transmissions of the FAPs do not cause interference to the macro users, the aforementioned strategy allows each macro user to cancel all the intracell interference, which is created by the transmission from the macro BS to other macro users.

Unlike the nBIA scheme proposed in the previous section, each femto user f_{k,φ_1} only receives the desired signals from the $N_f = 2$ antennas of its FAP φ_1, which only transmits during S-Block 1. To send $N_f = 2$ distinguishable data streams, i.e., $\mathbf{u}_\ell^{[f_{k,\varphi_1},\varphi_1]} \in \mathbb{C}^{2\times 1}$ without CSIT, the FAP repeatedly transmits $\mathbf{u}_\ell^{[f_{k,\varphi_1},\varphi_1]}$ during an alignment block composed of two symbol extensions over which the antenna of femto user f_{k,φ_1} switches between 2 different modes. For instance, from the antenna switching pattern of femto user f_{1,φ_1} in Figure 5.9 and its corresponding beamforming matrices in (5.67), the signal received by femto user f_{1,φ_1} during the first two symbol extensions is given by

$$\begin{bmatrix} y^{[f_{1,\varphi_1}]}[1] \\ y^{[f_{1,\varphi_1}]}[2] \end{bmatrix} = \begin{bmatrix} \mathbf{h}^{[f_{1,\varphi_1},\varphi_1]}(1)^T \\ \mathbf{h}^{[f_{1,\varphi_1},\varphi_1]}(2)^T \end{bmatrix} \mathbf{u}_1^{[f_{1,\varphi_1},\varphi_1]} + \underbrace{\begin{bmatrix} \mathbf{h}^{[f_{1,\varphi_f},M]}(1)^T \left(\mathbf{u}_1^{[m_1,M]} + \mathbf{u}_1^{[m_2,M]}\right) \\ \mathbf{h}^{[f_{1,\varphi_f},M]}(2)^T \left(\mathbf{u}_2^{[m_1,M]} + \mathbf{u}_2^{[m_2,M]}\right) \end{bmatrix}}_{\text{macro-femto interference}} + \underbrace{\begin{bmatrix} \mathbf{h}^{[f_{1,\varphi_1},\varphi_1]}(1)^T \mathbf{u}_1^{[f_{2,\varphi_1},\varphi_1]} \\ 0 \end{bmatrix}}_{\text{intracell femto interference}} \tag{5.68}$$

where $\mathbf{h}^{[f_{1,\varphi_f},M]}(l) \in \mathbb{C}^{2\times 1}$ and $\mathbf{h}^{[f_{1,\varphi_1},\varphi_1]}(l) \in \mathbb{C}^{2\times 1}$ contains the channel coefficients between the transmit antennas of macro BS and FAP φ_1 to femto user f_{1,φ_1} at the preset mode l, respectively. Since the channels $\mathbf{h}^{[f_{1,\varphi_1},\varphi_1]}(l) \in \mathbb{C}^{2\times 1}$, $l \in \{1, 2\}$, are linearly independent almost surely, femto user f_{1,φ_1} can decode the data stream $\mathbf{u}_1^{[f_{1,\varphi_1},\varphi_1]} \in \mathbb{C}^{2\times 1}$ once all the interference is removed.

As in our first toy example, the femto users employ the symbol extensions of S-Block 2 in order to measure the macro-femto interference in a cognitive fashion. In this sense, note that the FAP remains in silence during S-Block 2 and that the macro BS transmits each data stream $\mathbf{u}_\ell^{[m_k]}$ in an orthogonal fashion. Therefore, if each femto user keeps the same radiation pattern along an alignment block associated with the transmission of the data stream $\mathbf{u}_\ell^{[m_k]}$, then it can remove the macro-femto interference by applying zero-forcing based on the signals received in S-Block 2. For example, if we ignore the noise, during the alignment block of macro user m_1 the signal received by femto user

f_{1,φ_1} is

$$\begin{bmatrix} y^{[f_{1,\varphi_1}]}[1] \\ y^{[f_{1,\varphi_1}]}[4] \end{bmatrix} = \begin{bmatrix} \mathbf{h}^{[f_{1,\varphi_1},\varphi_1]}(1)^T \mathbf{u}_1^{[f_{1,\varphi_1},\varphi_1]} \\ 0 \end{bmatrix} + \underbrace{\begin{bmatrix} \mathbf{h}^{[f_{1,\varphi_f},M]}(1)^T \left(\mathbf{u}_1^{[m_1,M]} + \mathbf{u}_1^{[m_2,M]} \right) \\ \mathbf{h}^{[f_{1,\varphi_f},M]}(1)^T \mathbf{u}_1^{[m_1,M]} \end{bmatrix}}_{\text{macro-femto interference}} + \underbrace{\begin{bmatrix} \mathbf{h}^{[f_{1,\varphi_1},\varphi_1]}(1)^T \mathbf{u}_1^{[f_{2,\varphi_1},\varphi_1]} \\ 0 \end{bmatrix}}_{\text{femto intracell interference}} \tag{5.69}$$

From (5.69), notice that the interference from the macro BS at femto user f_{1,φ_1} is aligned over the channel state $\mathbf{h}^{[f_{1,\varphi_f},M]}(1)$. In consequence, the user f_{1,φ_1} can remove the macro-femto interference caused by the transmission of $\mathbf{u}_1^{[m_1]}$ by applying zero-forcing based on the signal received during symbol extension 4. Similarly, by using the signals received during symbol extensions $\{5, 7, 8\}$, femto user f_{1,φ_1} can remove the rest of the macro-femto interference in its first alignment block, which consists of symbol extensions $\{1, 2\}$. Afterwards, the only remaining interference is caused by the transmission from the FAP to the other femto users. That is, the FAP intracell interference.

To remove the femto intracell interference without CSIT, the FAP applies the same technique as in sBIA. It relies on the idea of aligning the transmission of each data stream, $\mathbf{u}_\ell^{[f_{k,\varphi_1},\varphi_1]}$, into one dimension of all users subject to interference, i.e., the femto users. To achieve the aforementioned alignment, the antenna of each femto user f_{j,φ_1}, with $j \neq k$, needs to keep the same radiation pattern along the alignment block of femto user f_{k,φ_1}. As a result, if the FAP transmits each data stream $\mathbf{u}_\ell^{[f_{k,\varphi_1},\varphi_1]}$ in an orthogonal fashion, then note that the femto users can measure all the femto intracell interference and remove it afterwards. For instance, after ignoring the noise and after subtracting the macro-femto interference, observe that the two transmissions of $\mathbf{u}_1^{[f_{1,\varphi_1},\varphi_1]}$ are aligned into one dimension in the signal space of femto user f_{2,φ_1}

$$\begin{bmatrix} y^{[f_{2,\varphi_1}]}[1] \\ y^{[f_{2,\varphi_1}]}[2] \end{bmatrix} = \begin{bmatrix} \mathbf{h}^{[f_{2,\varphi_1},\varphi_1]}(1)^T \mathbf{u}_1^{[f_{2,\varphi_1},\varphi_1]} \\ 0 \end{bmatrix} + \underbrace{\begin{bmatrix} \mathbf{h}^{[f_{2,\varphi_1},\varphi_1]}(1)^T \mathbf{u}_1^{[f_{1,\varphi_1}]} \\ \mathbf{h}^{[f_{2,\varphi_1},\varphi_1]}(1)^T \mathbf{u}_1^{[f_{1,\varphi_1}]} \end{bmatrix}}_{\text{femto intracell interference}} \tag{5.70}$$

Similarly, we can check that the intracell interference created by the transmission of $\mathbf{u}_1^{[f_{2,\varphi_1},\varphi_1]}$ from the FAP to femto user f_{2,φ_1} is aligned into one dimension in the signal

space of femto user f_{1,φ_1}. Since FAP transmits $\mathbf{u}_1^{[f_{1,\varphi_1},\varphi_1]}$ and $\mathbf{u}_1^{[f_{2,\varphi_1},\varphi_1]}$ in an orthogonal fashion during symbol extensions 2 and 3, respectively, these symbol extensions can be used by femto users f_{1,φ_1} and f_{2,φ_1} to measure the intracell interference and decode their desired symbols afterwards.

In summary, the supersymbol of the proposed cogBIA scheme consists of two blocks of symbol extensions, S-Block 1 and S-Block 2. During S-Block 1, the macro BS and the FAP transmit to macro and femto users using $\mathcal{L}_{\mathrm{f-SS}}$ m-Blocks 1 and q f-SS supersymbols as well as the corresponding beamforming matrices, respectively. On the contrary, during S-Block 2, only the macro BS transmits to its macro users. This transmission is undertaken in an orthogonal fashion by using $\mathcal{L}_{\mathrm{f-SS}}$ m-Blocks 2, which allows the femto users to measure all the macro-femto interference subspace. Hence, along the cogBIA supersymbol, a total of $\mathcal{L}_{\mathrm{f-SS}}$ sBIA supersymbols are distributed to transmit from N_m antennas of a macro BS to K_m users. Moreover, q sBIA supersymbols per FAP are distributed over S-Block 1 in order to transmit from N_f antennas of each FAP to its K_f femto users, respectively. To ensure that all the intracell interference and macro-femto interference is fully cancelled, the key of cogBIA consists on combining the aforementioned supersymbols so that each user k, served by N_k transmit antennas, receives N_k symbols over an alignment block. This alignment block should be formed by N_k symbol extensions over which the antenna of macro or femto user k switches N_k different modes and the antenna of all the other users, macro or femto, keep the same radiation pattern. In the following, we will provide a systematic procedure to combine the supersymbols and build these alignment blocks.

5.5.2 Construction of the supersymbol and the beamforming matrices

5.5.2.1 Antenna switching patterns and beamforming matrices for macro users during S-Block 1

When designing the antenna switching pattern and beamforming matrix of each macro user, one goal is to let the macro users achieve the maximum achievable sum-DoF. Moreover, the resulting antenna switching patterns and beamforming matrices during S-Block 1 should allow each femto user to implement different f-SS supersymbols such that the macro-femto interference caused by the transmission of $\mathbf{u}_\ell^{[m_k]}$ can be aligned into

one dimension of its signal space. To achieve all these goals, assuming that each FAPs has N_f antennas and K_f femto users, the antenna switching pattern and the beamforming matrices of the macro users along S-Block 1 can consist of the concatenation of $\mathcal{L}_{\mathrm{f-SS}}$ m-Blocks 1 and their corresponding beamforming matrices with $\mathcal{L}_{\mathrm{f-SS}}$ defined in (5.66) (see Figure 5.8). Thus, recalling that the length of m-Block 1 equals $q = (N_m - 1)^{K_m}$ symbol extensions when the macro BS has N_m antennas to transmit to K_m macro users, the length of S-Block 1 is

$$\mathcal{L}_{\mathrm{S-Block1}} = q\,\mathcal{L}_{\mathrm{f-SS}}. \tag{5.71}$$

Since m-Block 1 is repeated $\mathcal{L}_{\mathrm{f-SS}}$ times in S-Block 1, following the lines of the super-symbol construction for the MISO BC in Chapter 2, we can verify that the temporal correlation function of the macro user m_k is

$$g_{m_k}(t) = \mathbf{h}^{[m_k]}(l) \text{ if mod}\left(t, (N_m-1)^k\right) \in \mathcal{I}_{m_k}(l) \tag{5.72}$$

where $t \in \{1, 2, \ldots, \mathcal{L}_{\mathrm{S-Block1}}\}$, $l \in \{1, 2, \ldots, N_m - 1\}$ and

$$\begin{aligned}\mathcal{I}_{m_k}(l) = \Big\{&(l-1)(N_m-1)^{k-1}+1, \ldots, l\,(N_m-1)^{k-1}-1 \\ &, \mathrm{mod}\left(l\,(N_m-1)^{k-1}, (N_m-1)^k\right)\Big\}.\end{aligned}$$

Moreover, since each m-Block 1 consists of the first $N_m - 1$ symbol extensions of each alignment block of macro user m_k, the first $N_m - 1$ symbol extensions of the ℓ-th alignment block of macro user m_k are in S-Block 1 and correspond to

$$\left\{p_m(\ell,k)(N_m-1)^k + \kappa(N_m-1)^{k-1} + \varsigma_m(\ell,k)\right\}_{\kappa=0}^{N_m-2}, \tag{5.73}$$

where

$$\varsigma_m(\ell,k) = \mathrm{mod}(\ell-1, (N_m-1)^{k-1}) + 1 \tag{5.74}$$

and

$$p_m(\ell,k) = \left\lfloor \frac{\ell-1}{(N_m-1)^{k-1}} \right\rfloor \tag{5.75}$$

with $\ell \in \{1, 2, \ldots, p(N_m-1)^{K_m-1}\}$ and $k \in \{1, 2, \ldots, K_m\}$.

Since simultaneous transmission takes place at each symbol extension of m-Block 1, the macro BS transmits data to all macro users at each symbol extension of S-Block 1. The signal transmitted to macro user m_k is the result of multiplying its beamforming matrix and the following data vector

$$\mathbf{u}^{[m_k]} = \left[\mathbf{u}_1^{[m_k]^T} \mathbf{u}_2^{[m_k]^T} \cdots \mathbf{u}_{\mathcal{L}_{\text{S-Block1}}/(N_f-1)}^{[m_k]^T} \right]^T \tag{5.76}$$

where $\mathbf{u}_\ell^{[m_k]} \in \left[\mathbf{u}_{\ell'}^{[m_k,M]^T} \mathbf{0}_{N_f\times 1}^T \right]^T \mathbb{C}^{(N_m+N_f)\times 1}$ with $\mathbf{u}_\ell^{[m_k,M]} \in \mathbb{C}^{N_m\times 1}$ containing the N_m symbols transmitted from the macro BS to macro user m_k during its ℓ-th alignment block. As a result, the ℓ-th alignment block of macro user m_k corresponds to the block of columns $\{(N_m+N_f)(\ell-1)+1, (N_m+N_f)(\ell-1)+2, \ldots, (N_m+N_f)\ell\}$ of its beamforming matrix. The structure of each one of the aforementioned block columns is obtained by placing an $(N_m+N_f)\times(N_m+N_f)$ identity matrix, $\mathbf{I}_{(N_f+N_m)}$ at the rows corresponding to the symbol extensions of the alignment block. Hence, by knowing the symbol extensions that constitute each alignment block of each macro user, we can easily determine the beamforming matrix of macro user m_k during S-Block 1.

5.5.2.2 Antenna switching patterns and beamforming matrices for femto users during S-Block 1

As can be seen in Figure 5.10(a), S-Block 1 of the femto users is closely based on the supersymbol of a BIA scheme for the MISO BC aimed at transmitting from N_f antennas to K_f users. In particular, as shown previously, for the femto users S-Block 1 can be divided in two sub-blocks, f-Block 1 and f-Block 2. The first $\mathcal{L}_{\text{f-Block1}} = q(N_f-1)^{K_f}$ symbol extensions belong to f-Block 1 while the last $\mathcal{L}_{\text{f-Block2}} = qK_f(N_f-1)^{K_f-1}$ symbol extensions correspond to f-Block 2, with $q = (N_m-1)^{K_m}$. Recall that both f-Block 1 and f-Block 2 take place in S-Block 1.

During f-Block 1, the mode of a femto user f_{k',φ_f} is periodic with the building block shown in Figure 5.11. For the k'-th femto user, this block is repeated $(N_f-1)^{K_f-k'}$ times to form S-Block 1 where $k' \in \{1,\ldots,K_f\}$ and $f \in \{1,2,\ldots,F\}$ with F equal to the total number of FAPs. Similarly to the supersymbol of a BIA scheme, the building block is composed of N_f-1 sub-blocks. However, for the considered f-Block 1, the

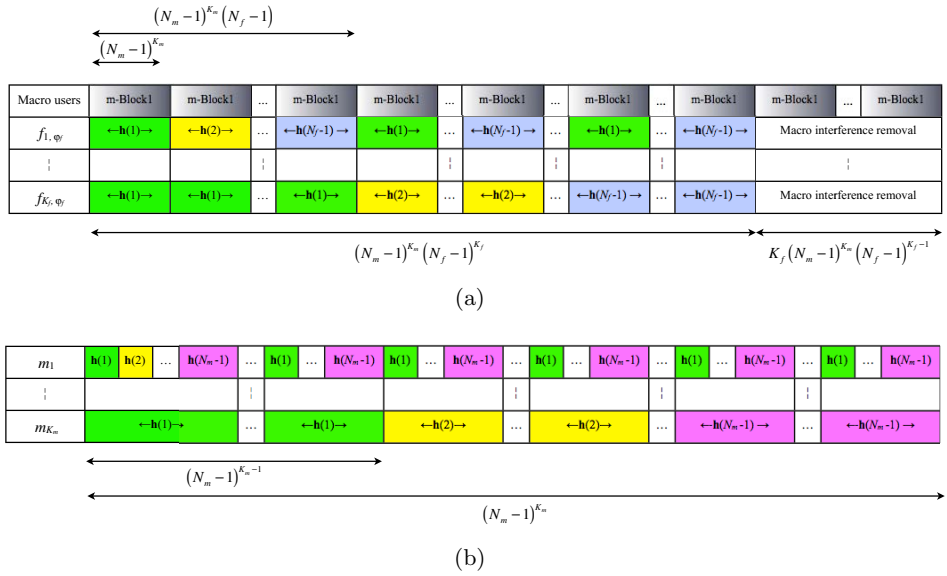

FIGURE 5.10: a) S-Block 1 of the cogBIA scheme and b) m-Block 1 for transmission to K_m macro users

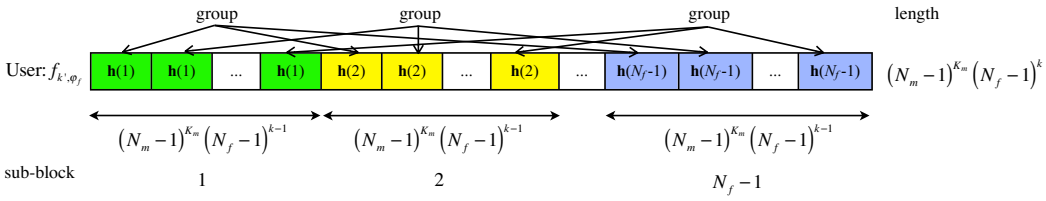

FIGURE 5.11: Building block of femto user f_{k',φ_f}.

length of each sub-block equals $q(N_f-1)^{k'-1}$ with q given in (5.65). As in the sub-blocks associated with the macro user m_k, the l-th mode is used in the l-th sub-block, $l \in \{1,2,\ldots,N_f-1\}$. Thus, during f-Block 1, the temporal correlation function for femto user $f_{k',f}$ for any femto-cell $f \in \{1,2,\ldots,F\}$ is

$$g_{f_{k',\varphi_f}}(t) = \mathbf{h}^{[f_{k',\varphi_f}]}(l) \text{ if } \mathrm{mod}\left(t, q\,(N_f-1)^{k'}\right) \in \mathcal{I}_f(l), \tag{5.77}$$

where $t \in \{1,2,\ldots,\mathcal{L}_{\mathrm{f-Block1}}\}$ and

$$\mathcal{I}_f(l) = \Big\{(l-1)q(N_f-1)^{k'-1}+1,\ldots,l\,q(N_f-1)^{k'-1}-1 \\ ,\mathrm{mod}\left(l\,q(N_f-1)^{k'-1}, q(N_m-1)^{k'}\right)\Big\}.$$

with $l \in \{1,2,\ldots,N_f-1\}$ denoting the preset modes selected by the femto user.

Similarly to Block 1 of the sBIA scheme, simultaneous transmission to all femto users

takes place during the symbol extensions that constitute f-Block 1. The signals transmitted to femto user f_{k',φ_f} are the result of multiplying its beamforming matrix associated and the following data vector

$$\mathbf{u}^{[f_{k',\varphi_f}]} = \left[\mathbf{u}_1^{[f_{k',\varphi_f}]^T} \; \mathbf{u}_2^{[f_{k',\varphi_f}]^T} \cdots \mathbf{u}_{\mathcal{L}_{\text{f-Block2}}/(K_f)}^{[f_{k',\varphi_f}]^T} \right]^T \tag{5.78}$$

where $\mathbf{u}_{\ell'}^{[f_{k',\varphi_f}]} \in \left[\mathbf{0}_{N_m\times 1}^T \; \mathbf{u}_{\ell'}^{[f_{k',\varphi_f},\varphi_f]^T} \right]^T \mathbb{C}^{(N_m+N_f)\times 1}$ with $\mathbf{u}_{\ell'}^{[f_{k',\varphi_f},\varphi_f]} \in \mathbb{C}^{N_f\times 1}$ denoting the N_f symbols transmitted from the f-th FAP to femto user f_{k',φ_f} during its ℓ'-th alignment block. Hence, as it occurs for the macro users, each block of $(N_m + N_f)$ consecutive columns of the beamforming matrix of a femto user corresponds to one different alignment block.

To determine the symbol extensions that constitute the alignment blocks of each femto user, and therefore, determine the rows that should have an identity matrix $\mathbf{I}_{(N_f+N_m)}$ in each block column of the beamforming matrix, two requirements have to be taken into consideration. On the one hand, to maintain the data beams of one alignment block distinguishable at the femto user for which they are intended, the antenna of the femto user sets a different mode at each symbol extension of the alignment block. On the other hand, to align the transmission of the aforementioned data beams into one dimension of the signal space of all users subject to interference, the antenna of the affected users has to keep the same radiation pattern.

The decodability and interference alignment requirements can be satisfied during f-Block 1, by forming *groups* of symbol extensions. For each femto user, each *group* consists of the first $N_f - 1$ symbols extensions of each one of its alignment blocks. Given the antenna switching pattern of the femto users during f-Block 1, to ensure the aforementioned requirements the ℓ'-th *group* in a specific building block is the result of selecting the ℓ'-th symbol extensions of the $(N_f - 1)$ sub-blocks within that particular building block (see Figure 5.11). Recalling that S-Block 1 of femto user $f_{k'\varphi_f}$ consists of $(N_f-1)^{K_f-k'}$ building blocks of $q\,(N_f-1)^{k'}$ symbol extensions, the ℓ'-th *group* in the p'-th building block of femto user f_{k',φ_f} comprises symbol extensions

$$\left\{ p'q(N_f-1)^{k'} + \kappa q(N_f-1)^{k'-1} + \ell' \right\}_{\kappa=0}^{N_f-2} \tag{5.79}$$

where $\ell' \in \{1, 2, \ldots, q(N_f - 1)^{k'-1}\}$ and $p' \in \{1, 2, \ldots, (N_f - 1)^{K_f - k'}\}$. Since each sub-block is composed of $q(N_f - 1)^{k'-1}$, a total of $q(N_f - 1)^{k'-1}$ *groups* can be formed within one building block. Hence, from (5.79) notice that the symbol extensions of the ℓ'-th *group* of femto user f_{k',φ_f} are

$$\left\{ p_f(\ell', k') q(N_f - 1)^{k'} + \kappa (N_f - 1)^{k'-1} + \varsigma_f(\ell', k') \right\}_{\kappa=0}^{N_f - 2}, \tag{5.80}$$

where

$$\varsigma_f(\ell', k') = \mathrm{mod}(\ell' - 1, q(N_f - 1)^{k'-1}) + 1 \tag{5.81}$$

and

$$p_f(\ell', k') = \left\lfloor \frac{\ell' - 1}{q(N_f - 1)^{k'-1}} \right\rfloor \tag{5.82}$$

with $\ell' \in \{1, 2, \ldots, q(N_f - 1)^{K_f - 1}\}$ and $k' \in \{1, 2, \ldots, K_f\}$. By evaluating

$$f_{b-f}(i) = \left\{ iN + i' \right\}_{i'=1}^{N} \tag{5.83}$$

at each symbol extension in (5.80), we can determine the rows of f-Block 1 that should have an identity matrix $\mathbf{I}_N$ in the ℓ' block column of the beamforming matrix of femto user f_{k',φ_f}.

At this point, we only need to design the antenna switching pattern and the beamforming matrix of femto user f_{k',φ_f} during f-Block 2. Following the lines of previous chapters, the symbol extensions within f-Block 2 are employed to complete the alignment blocks of the femto users. Since $q(N_f - 1)^{K_f - 1}$ *groups* are distributed over f-Block 1 for each femto user, a total of $q(N_f - 1)^{K_f - 1}$ symbol extensions are needed to complete the alignment blocks of each femto user. For femto user f_{k',φ_f}, these symbol extensions are

$$\left\{ \mathcal{L}_{\mathrm{f-Block1}} + (k' - 1) q(N_f - 1)^{K_f - 1} + \ell' \right\}_{\ell'=1}^{\mathcal{L}_{\mathrm{f-Block2}}/K_f}. \tag{5.84}$$

Since the ℓ'-th element of the previous set corresponds to the last symbol extension of the ℓ'-th alignment block of femto user f_{k',φ_f}, the evaluation of (5.83) at the ℓ'-th element in (5.84) allows to determine the only set of rows of f-Block 2 that should have an identity matrix $\mathbf{I}_{(N_f + N_m)}$ in the ℓ' block column of the beamforming matrix of femto

user f_{k',φ_f}. The remaining rows in each block column of the beamforming matrix should be filled with an $(N_m + N_f) \times (N_m + N_f)$ zero matrix, $\mathbf{0}_{(N_m+N_f)}$.

According to the resulting structure of the beamformng matrix, during each symbol extension in (5.84), the FAP φ_f only transmits signals to femto user f_{k',φ_f}. To ensure the decodability of these signals, which are the same as the data stream $\mathbf{u}_{\ell'}^{[f_{k',\varphi_f}]}$ repeatedly transmitted over the symbol extensions associated with ℓ' group of femto user f_{k',φ_f}, the receiver of this femto user has to set N_f-th channel mode. On the contrary, to satisfy the interference alignment requirement given in the definition of alignment block, the remaining femto users f_{j',φ_f}, with $j' \neq k'$, have to set the same channel mode as the one used by its antenna during the ℓ'-th *group* of femto user f_{k',φ_f}. Since the femto user f_{j',φ_f} has the same channel mode along the symbol extensions of the ℓ'-th *group* of femto user f_{k',φ_f}, the channel state of femto user f_{j',φ_f} during the ℓ'-th symbol extension in (5.84) equals

$$g_{f_{j',\varphi_f}}(p_f(\ell',k')q(N_f-1)^{k'-1} + \varsigma_f(\ell',k')) \tag{5.85}$$

with $g_{f_{k',\varphi_f}}(\cdot)$, $p_f(\ell',k')$ and $\varsigma_f(\ell',k')$ defined in (5.77), (5.81) and (5.82), respectively. In this way, the antenna switching pattern of all femto users during f-Block 2 is fully determined.

5.5.2.3 Design of S-Block 2 and cognitive cancellation of the interference

Once the antenna switching pattern and the beamforming matrices are designed for S-Block 1, the S-Block 2 can be easily constructed. Notice that each element within S-Block 2 provides an additional symbol extension to complete each alignment block of a specific macro user. Since there are $\mathcal{L}_{\text{f-SS}}(N_m-1)^{K_m-1}$ alignment blocks for each one of the K_m macro users with $\mathcal{L}_{\text{f-SS}}$ defined in (5.66), the S-Block 2 comprises

$$\mathcal{L}_{\text{S-Block2}} = K_m\, \mathcal{L}_{\text{f-SS}}\, (N_m-1)^{Km-1} \tag{5.86}$$

symbol extensions, which are divided in K_m blocks, each associated with one specific macro user. For macro user m_k, the corresponding sub-block is formed by the following

set of symbol extensions

$$\left\{\mathcal{L}_{\text{f-SS}} + (k-1)\mathcal{L}_{\text{f-SS}}(N_m-1)^{K_m-1} + \ell\right\}_{\ell=1}^{\mathcal{L}_{\text{S-Block2}}/K_m}. \tag{5.87}$$

The ℓ-th element of the previous set corresponds to the last symbol extension of the ℓ-th alignment block of macro user m_k. As a result, the evaluation of (5.83) at the ℓ-th element in (5.87) yields the only set of rows of S-Block 2 that should have an identity matrix $\mathbf{I}_{(N_f+N_m)}$ in the ℓ block column of the beamforming matrix of macro user m_k.

Due to the resulting structure of the beamforming matrix of macro user m_k, the macro BS only transmits signals to macro user m_k during each symbol extension specified in (5.87). To ensure the decodability of the signals transmitted over the ℓ-th symbol extension in (5.87), which corresponds to the data stream $\mathbf{u}_\ell^{[m_k]}$ repeatedly transmitted along the ℓ-th *group* of macro user m_k, the antenna of user m_k sets the N_m-th mode. On the contrary, during the ℓ-th symbol symbol extension in (5.73) any other macro user $m_j \neq m_k$ has to set the same channel mode as the one used by its antenna during the ℓ-th *group* of macro user m_k. Since the macro user m_j has the same channel mode along the symbol extensions of the ℓ-th *group* of macro user m_k, from (5.73) notice that the channel state of macro user m_j during the ℓ-th symbol extension in (5.87) equals

$$g_{m_j}(p_m(\ell,k)(N_m-1)^k + \varsigma_m(\ell,k)) \tag{5.88}$$

with $g_{m_j}(\cdot)$, $p_m(\ell,k)$ and $\varsigma_m(\ell,k)$ defined in (5.72), (5.74) and (5.75), respectively. In this way, the repeated transmissions of $\mathbf{u}_\ell^{[m_k]}$ along the ℓ-th alignment block of macro user m_k are aligned into one dimension in the signal space of macro user m_k. Furthermore, macro user m_j can measure and subtract the macro intracell interference created by the transmission of $\mathbf{u}_\ell^{[m_k]}$ during the ℓ-th *group* of macro user m_k. Recall that due to the fact that femtocell transmission does not cause interference to the macro users, the signals transmitted by the FAPs do not hamper the macro users when decoding their desired data and cancelling the intracell interference.

As we have shown, the beamforming matrix and the antenna switching pattern of the femto users satisfy the decodability and alignment conditions during S-Block 1. Thus, we can easily check that each femto user can remove all the femto intracell interference and decode all its desired data, i.e. $\left\{\mathbf{u}_{\ell'}^{[f_{k'},\varphi_f]}\right\}_{\ell'=1}^{\mathcal{L}_{\text{f-Block2}}/K_f}$. However, due to the transmission

of the macro BS to the macro users during S-Block 1, this is only possible if the macro-femto interference is fully cancelled. Toward this goal, the femto users will employ the symbol extensions of S-Block 2 in a cognitive fashion. First, to measure the signal $\mathbf{u}_{\ell}^{[m_k]}$ transmitted from the macro BS during the ℓ-th symbol extension in (5.87), the FAP φ_f does not transmit any signal to its femto users along S-Block 2. As a result, considering that the signal transmitted to each of the femto users is the result of multiplying its beamforming matrix with the data vector provided in (5.78), during S-Block 2 the beamforming matrix of the femto users is an all zero matrix $\mathbf{0}_{a_f,b_f}$ with $a_f = (N_m + N_f)\mathcal{L}_{\mathrm{S-Block2}}/K_m$ and $b_f = (N_m+N_f)\mathcal{L}_{\mathrm{f-Block2}/K_f}$. Later, to ensure that the measured signal is aligned with the $N_m - 1$ transmissions of $\mathbf{u}_{\ell}^{[m_k]}$ along the ℓ-th *group* of macro user m_k, the antenna of each femto user f_{k',φ_f} sets the same channel mode as the one employed along ℓ-th group of macro user m_k. In particular, during the ℓ-th symbol extension in (5.87), from (5.73) we can check that the channel mode of femto user $f_{k',f}$ is

$$g_{f_{k',\varphi_f}}\left(p_m(\ell,k)(N_m-1)^k + \varsigma_m(\ell,k)\right) \tag{5.89}$$

for $k' \in \{1,2,\ldots,K_f\}$ and all $f \in \{1,2,\ldots,F\}$ and with $g_{f_{k',\varphi_f}}(\cdot)$, $p_m(\ell,k)$ and $\varsigma_m(\ell,k)$ defined in (5.77), (5.74) and (5.75), respectively. With this procedure, note that each femto user f_{k',φ_f} can apply zero-forcing based on the signal received during the ℓ-th symbol extension of (5.87) in order to remove the macro-femto interference caused by the repeated transmission of $\mathbf{u}_{\ell}^{[m_k]}$ along the ℓ-th *group* of macro user m_k.

5.5.3 Achievable Degrees of Freedom

In the proposed scheme the macro BS employs BIA transmission independently of the femto tier transmission. As we have shown in Chapter 2 each user attains N_m DoF in each of the $(N_m-1)^{K_m-1}$ alignment blocks, which are repeated $\mathcal{L}_{\mathrm{f-SS}}$ times. Therefore, the normalized sum-DoF per symbol extension for the macro users is given by

$$\mathrm{DoF}_{\mathrm{macro}} = \frac{\mathcal{L}_{\mathrm{f-SS}}\left(K_m N_m (N_m-1)^{K_m-1}\right)}{\mathcal{L}_{\mathrm{S-Block1}} + \mathcal{L}_{\mathrm{S-Block2}}} = \frac{N_m K_m}{N_m + K_m - 1}. \tag{5.90}$$

As was expected, the achievable DoF are not affected by the femto tier deployment, and therefore, do not depend on any of its parameters.

In the proposed scheme, each femto user employs $q\,(N_f-1)^{K_f-1}$ alignment blocks with q defined in (5.65). Each of these alignment blocks is formed by N_f symbol extensions over which the femto user receives N_f desired data beams transmitted from the FAP. Since the femto intracell and macro-femto intercell interference can be fully removed by applying the antenna switching pattern and beamforming matrices of Ssection 5.5.2, each femto user can attain N_f DoF in each alignment block. Since $\mathcal{L}_{\mathrm{S-Block1}}$ symbol extensions are employed for femto transmission and $\mathcal{L}_{\mathrm{S-Block2}}$ are required to measure the macro-femto interference in a cognitive fashion, the normalized sum-DoF per symbol extension for the femto users is

$$\mathrm{DoF}_{\mathrm{femto}} = \frac{N_f K_f (N_m-1)}{(N_m+K_m-1)(N_f+K_f-1)}. \tag{5.91}$$

5.5.4 Achievable Rates

Until now this work has been focused on the achievable DoF. To complete the characterization of the proposed cogBIA scheme, this section analyzes its performance in the finite SNR regime. Assuming equal power allocation to each stream, we derive the closed-form expressions of the achievable rates for cogBIA. For comparison purposes, we will use the achievable rates of nBIA and sBIA that have been derived in Chapters 2 and 4, respectively.

Macro users are not affected by interference caused by the transmission of the FAPs. In consequence, their achievable rates are given by the sBIA expression in absence of intercell interference (see Chapter 2, Section 2.4). Thus, the normalized rate per symbol extension of the macro user m_k is

$$R^{[m_k]} = B_m \mathbb{E}\left[\log\det\left(\mathbf{I}+\bar{P}_m \mathbf{H}^{[m_k]}{\mathbf{H}^{[m_k]}}^H \mathbf{R}_{\tilde{\mathbf{z}}}^{[m_k]\,-1}\right)\right], \tag{5.92}$$

where the channel matrix $\mathbf{H}^{[m_k]}$ is defined in (5.3) and $B_m = \frac{1}{N_m+K_m-1}$ is the ratio of alignment blocks per macro user over the total number of symbol extensions. Since equal power allocation to each stream is assumed, $\bar{P}_m = \frac{N_m+K_m-1}{N_m^2 K_m} P_m$ is the power allocated to each symbol, and

$$\mathbf{R}_{\tilde{\mathbf{z}}}^{[m_k]} = \begin{bmatrix} K_m \mathbf{I}_{N_m-1} & \mathbf{0} \\ \mathbf{0} & 1 \end{bmatrix} \tag{5.93}$$

is the covariance matrix of the noise after zero-forcing cancelation at the receiver.

For the femto user f_{k',φ_f} subject to interference from the macro BS, the signal $\tilde{\mathbf{y}}^{[f_{k',\varphi_f}]} = \left[\tilde{y}^{[f_{k',\varphi_f}]}(1), \ldots, \tilde{y}^{[f_{k',\varphi_f}]}(N_f)\right]^T$ received during a generic alignment block after zero-forcing interference cancelation can be written as

$$\begin{bmatrix} \tilde{y}^{[f_{k',\varphi_f}]}[1] \\ \vdots \\ \tilde{y}^{[f_{k',\varphi_f}]}[N_f] \end{bmatrix} = \begin{bmatrix} \mathbf{h}^{[f_{k',\varphi_f}]}(1)^T \\ \vdots \\ \mathbf{h}^{[f_{k',\varphi_f}]}(N_f)^T \end{bmatrix} \mathbf{u}_\ell^{[f_{k',\varphi_f}]} + \tilde{\mathbf{z}}^{[f_{k',\varphi_f}]}, \tag{5.94}$$

where

$$\tilde{\mathbf{z}}^{[f_{k',\varphi_f}]} = \begin{bmatrix} z^{[f_{k',\varphi_f}]}[1] - \sum_{\tau=1}^{K_m+K_f-1} z[\tau] \\ \vdots \\ z^{[f_{k',\varphi_f}]}[N_f-1] - \sum_{\tau=1}^{K_m+K_f-1} z[\tau] \\ z^{[f_{k',\varphi_f}]}[N_f] - \sum_{\tau=1}^{K_m} z[\tau] \end{bmatrix}. \tag{5.95}$$

Since equal power allocation is assumed and the FAPs do not transmit during m-Block 2, the power allocated to each symbol transmitted by the FAP is $\bar{P}_f = \frac{N_f+K_f-1}{N_f^2 K_f} P_f$. Moreover, $(N_f-1)^{K_f-1}$ alignment blocks repeated $(N_m-1)^{K_m}$ times are employed for transmitting to each femto user over the entire supersymbol. Hence, the ratio of alignment blocks per femto user over the total supersymbol length is

$$B_f = \frac{N_m - 1}{(N_m + K_m - 1)(N_f + K_f - 1)}. \tag{5.96}$$

Therefore, the normalized rate of each femto user f_{k',φ_f} is

$$R^{[f_{k',\varphi_f}]} = B_f \mathbb{E}\left[\log\det\left(\mathbf{I} + \bar{P}_f \mathbf{H}^{[f_{k',\varphi_f}]} \mathbf{H}^{[f_{k',\varphi_f}]H} \mathbf{R}_{\tilde{\mathbf{z}}}^{[f_{k',\varphi_f}]^{-1}}\right)\right], \tag{5.97}$$

where the channel matrix of user f_{k',φ_f} is given by

$$\mathbf{H}^{[f_{k',\varphi_f}]} = \left[\mathbf{h}^{[f_{k',\varphi_f}]}(1)^T \quad \ldots \quad \mathbf{h}^{[f_{k',\varphi_f}]}(N_f)^T\right]^T, \tag{5.98}$$

and

$$\mathbf{R}_{\tilde{\mathbf{z}}}^{[f_{k',\varphi_f}]} = \begin{bmatrix} (K_m + K_f)\,\mathbf{I}_{N_f-1} & \mathbf{0} \\ \mathbf{0} & K_m \end{bmatrix} \tag{5.99}$$

is the covariance matrix of the noise for each femtocell user after zero-forcing cancelation.

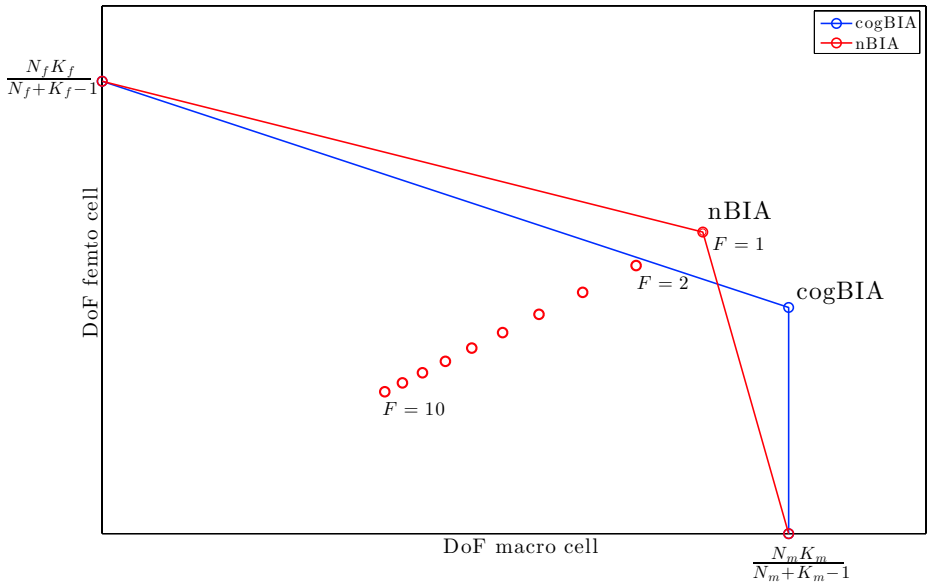

FIGURE 5.12: DoF region of macro users and each femtocell for cellular and cognitive BIA. The achievable sum-DoF is depicted for $F = (1, 10)$.

5.6 Simulation Results

The region of the sum-DoF achievable in each femtocell regarding the one achieved in the macro tier is depicted in Figure 5.12. For $F = 1$ it can be seen that nBIA achieves greater sum-DoF of both tiers comparing with cogBIA. Although this is true in general, it is possible to find examples where even at $F = 1$ this assertion does not hold. However, notice that nBIA does not attain the optimal DoF in any tier. In contrast, by using cogBIA, the optimal DoF in the macrocell is always achieved while femto users reach the DoF given by (5.91). As the number of FAPs deployed within the macro coverage increases, the same DoF as using nBIA are achievable in each femtocell by the proposed cogBIA scheme with only $F = 3$. In other words, the same DoF as employing a cooperative scheme such as nBIA are achievable in each femtocell by using cogBIA while the macrocell users still achieve the optimal DoF is absence of CSIT. For $F = 10$ it can be seen that the performance of nBIA is considerably affected.

Figure 5.13 shows the achievable sum-DoF in the entire network, i.e. over the $K_m + FK_f$ users deployed in the proposed scenario. Consider F femtocells where each FAP is equipped with $N_f = 2$ antennas serving $K_f = 2$ users. It can be seen in Figure 5.13 that cogBIA overcomes the sum-DoF achieved by nBIA when more that $F = 3$ femtocells

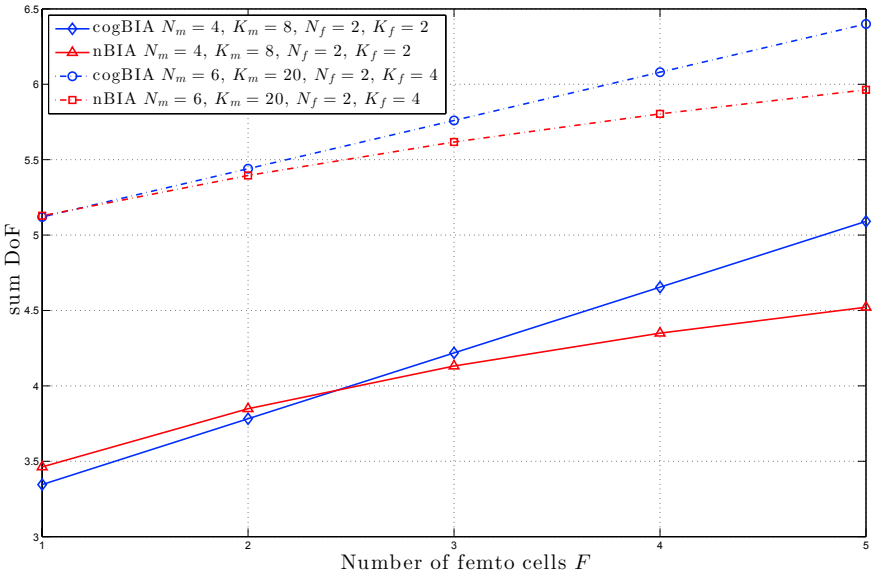

FIGURE 5.13: Sum-DoF of macrocell and femto tier for nBIA and cogBIA.

are in the coverage area of the macro BS. Similarly, only $F = 2$ femtocells are enough to obtain more sum-DoF by cogBIA that using a cooperative scheme such as nBIA. It is interesting to remark that the achievable sum-DoF of the entire network grows linearly regarding the amount of femtocells deployed for the proposed cogBIA scheme. However, this growth is inversely proportional to the amount of the femtocells deployed for nBIA as can be checked in (5.59)-(5.60).

A comparison of the sum-rates attained with cogBIA, nBIA, sBIA and FR where the bandwidth is split between macro and femto tier is shown in Figure 5.14. In similar fashion to [95], we consider a one-dimensional configuration where the FAP of interest is located at a distance d from the macro BS. Moreover, the path loss model of [37] is assumed, which is given by

$$g(d) = \frac{G_0 \delta^\kappa}{\delta^\kappa + d^\kappa}, \tag{5.100}$$

where κ is the propagation exponent, δ is the 3 dB breakpoint distance, and G_0 fixes the transmitted power at the BS. For the Macro BS, $\kappa = 3.8$, $\delta = 0.05$ km and $G_0 = 80$ dB, whereas for the FAP, $\kappa = 5$, $\delta = 5$ m and $G_0 = 20$ dB.

As can be seen in Figure 5.14, the sum-rate achieved by the femto users in the femtocell of interest by using cogBIA overcomes the performance of sBIA, i.e. when macro BS and FAP do not manage the inter-tier interference, in a wide range of distances between

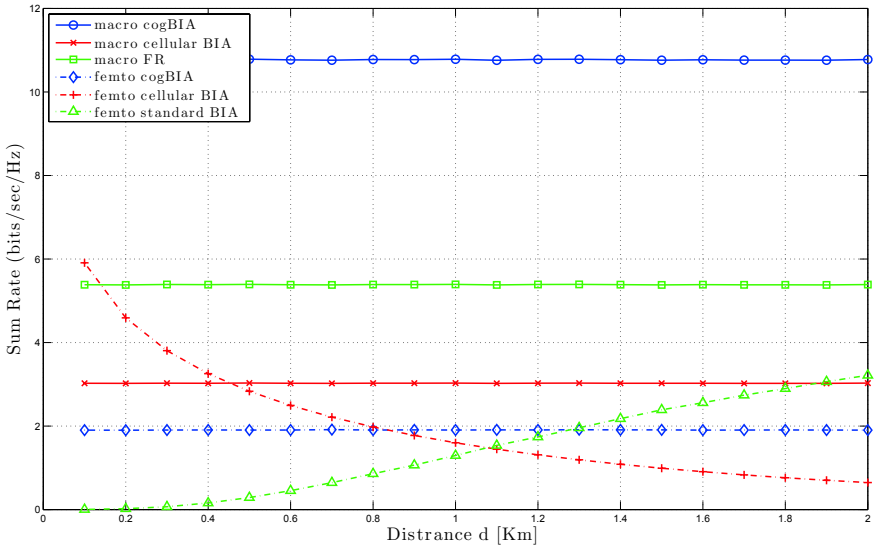

FIGURE 5.14: Comparison of the sum achievable rates of macro and femto users for nBIA, cogBIA, standard BIA used by the FAPs over the entire supersymbol, and standard BIA together to FR for macro users. $N_m = 6$, $K_m = 10$, $F = 12$, $N_f = 2$, $K_f = 2$.

macro BS and FAP. Specifically, the interference due to macro BS transmission can be treated optimally as noise for a distance between macro BS and FAP beyond 1.3 Km, from where sBIA achieves greater sum-rate than cogBIA. Besides, notice that since cogBIA does not involve any penalty for the rate of macro users, the same performance is achieved in the macro tier by using both schemes, cogBIA or sBIA. On the other hand, the sum-rate achieved by nBIA for femtocell users is greater in comparison with cogBIA until a distance of 0.8 Km. However, taken into consideration the network resources needed to its implementation, this improvement results futile. Moreover, and even more important, the macro users suffer a considerable penalty regarding the performance achieved by cogBIA or sBIA. Note that by employing an orthogonal approach such as FR where the available bandwidth is halved between macro and femto tiers, the achievable rates of the macro users are also divided by 2. Furthermore, consider the sum-rate achieved by the femto users for sBIA at a distance of 3 Km as the achievable sum-rate in absence of inter-tier interference because of the path loss. Thus, the proposed FR scheme would achieve this sum rate divided by 2. We can easily check that it is lower than the sum-rate achieved by cogBIA in the whole range of distance between macro BS and FAP.

5.7 Conclusions

In this chapter, we analyze the use of BIA schemes in heterogenous cellular networks. We derive an extension of the network BIA scheme presented in Chapter 4. Basically, macro users are treated as private users that only receive signal from their corresponding macro BS, whereas femto users can be considered as shared users that receive a useful signal strength from their corresponding FAP and also from the macro BS. It is demonstrated that this approach does not result optimal in DoF because of the particular topology of the multi-tier heterogenous cellular network. Indeed, the achievable sum-DoF does not scale with the number of femtocells deployed within the coverage of a macro BS.

Encouraged by the non-optimality of network BIA in heterogenous networks, we derive the DoF region of the two-tier cellular network. We demonstrate that the upper tier, i.e. the macro users in our case, can achieve the optimal DoF in absence of CSIT while the lower tier, i.e. the femtocells within the macro BS coverage, achieve non-zero DoF. After that, we derive a BIA scheme based on cognitive femtocells that achieves the outer-bound of the DoF region for two-tier networks. It is shown that macro BS transmits independently of the femtocell deployment within its coverage. Since cooperation between both tiers is avoided, macro users achieve the optimal sum-DoF without CSIT as in a MISO BC. On the other hand, femto users leverage the structure of the BIA supersymbol and the transmission beamforming of the macro BS to remove the inter-tier interference in a cognitive fashion. Femto users attain a significant amount of DoF without affecting the rates of the macro user. It is shown that the proposed scheme can yield the optimal sum-DoF at femto users subject to optimal sum-DoF for the macro users. Furthermore, the proposed strategy does not require any CSIT or data exchange between the macro BS and the femtocells. Only synchronization is needed to implement the proposed cognitive BIA. Comparing with the previously proposed schemes, cognitive BIA overcomes the sum-rate achieved by the femto users in a wide range of interference received from the macro BS.

Chapter 6

Blind Interference Alignment for practical channels

This chapter consider the use of BIA in practical channels where the users operate at finite SNR regime and the physical channel only remains constant over a determined coherence time. The use of orthogonal resource allocation combined with BIA transmission allows to handle both limitations. The solution to the optimization problem that achieves the most favorable trade-off between multiplexing gain, noise increase and coherence time is obtained avoiding the need for CSIT. It is shown through computer simulations that this approach improves considerably the use of BIA in practical channels.

6.1 Introduction

The performance of BIA schemes has been widely analyzed in this work. Until now the research efforts have focused on deriving the DoF for homogeneous and heterogeneous cellular networks in absence of CSIT and how to achieve these DoF. However, it is necessary to recall that the DoF metric assumes SNR $\rightarrow \infty$. Although the achievable DoF is an excellent metric to describe the potential of a transmission scheme, it is unavoidable to analyze the performance of BIA at finite SNR regime. Furthermore, it has been also assumed that the physical channel between the transmitter and users remains constant over the entire supersymbol. That is, the channel of each user only depends on

the preset mode selected at any time. This is not exactly true in real implementations, then physical channel varies and can only be considered constant during a period of time denoted as coherence time.

For practical implementations the SNR of each receiver is finite and the channel only remains constant during a period of coherence time. As we have shown in previous chapters, the BIA schemes cancel the interference by subtracting these interfering terms using the signals received in other symbol extensions of the considered supersymbol. Hence, a noise increase appears just due to this subtraction. In consequence, the sum-rate performance at finite SNR is highly handicapped because of the noise increase inherent in any BIA scheme. At this point, it is interesting to remark that the noise increase is proportional to the number of users served. For instance, checking the results obtained in previous works such as [95, 96] we can conclude that a SNR above 14 dB is required when the number of users equals 6 to outperform the rate assuming a Single User (SU) MISO channel without CSIT. On the other hand, to the best of our knowledge, all the previous works assume a constant channel over the entire supersymbol. This issue is presented as a drawback in [145], where an alternative supersymbol design based on grouping users is proposed to reduce its length at expense of losing DoF with respect to the optimal value.

Interestingly, when the fbwBIA scheme was presented in Chapter 4 we called attention to the benefits of using an orthogonal approach such as bandwidth division joint to BIA schemes; few users are served in each band, and therefore, less terms of interference must be subtracted bringing down considerably the noise increase, and a reduction of the supersymbol length is achieved. Following this idea, in this chapter we devise a practical BIA (pBIA) scheme based on the implementation of standard BIA schemes transmitting data to different sets of users grouped in an orthogonal fashion (over different frequency bands or time slots). By employing the proposed pBIA scheme the achieved sum-DoF decreases because of the use of orthogonal resource division. Nevertheless, at expenses of this loss in DoF, fewer terms of interference must be subtracted in each division, which reduces the noise power and also the supersymbol length. The optimization problem that solves this trade-off can be expressed easily as a function of the resource division given by pBIA.

The contributions of this chapter can be summarized as follows

- We analyze the performance of BIA in practical scenarios where the users operate at finite SNR regime over varying channels.
- We propose the use of orthogonal resource allocation joint to BIA schemes with the aim of managing the multiplexing gain, noise increase, and channel coherence time.
- The optimization problem that achieves the optimal resource division is formulated in this chapter. We derive a closed-form expression of the optimal value as a function of the system parameters such as the number of transmit antennas, N_t, the amount of active users K, and the SNR of the set of users. Notice that CSIT is not required to obtain this solution.
- We show through computer simulations that the proposed pBIA scheme improves the achievable sum-rate considerably regarding pure BIA approaches while it relaxes the coherence time requirements.
- We present an experimental evaluation of the BIA scheme in a hardware testbed. It is shown that BIA can outperform other transmission schemes based on CSIT such as LZFB, which achieves higher sum-rates theoretically, because of the implementation impairments related to providing accurate CSIT.

6.2 System model

For simplicity we consider a MISO BC as proposed in Chapter 2. The transmitter is equipped with N_t antennas that send data to K active users, each equipped with one reconfigurable antenna. The antenna of each user can switch its radiation pattern among a set of N_t preset modes. The signal transmitted at time t is given by $\mathbf{x}(t)$, where $\mathbf{x}(t) = \begin{bmatrix} x_1, & \ldots, & x_{N_t} \end{bmatrix} \in \mathbb{C}^{N_t \times 1}$. However, the assumption of constant channel over the transmission of the entire supersymbol does not hold. Let us denote $\mathbf{h}\left(l^{[k]}(t)|t\right) \in \mathbb{C}^{N_t \times 1}$ as the channel between user k and the transmitter at time t when the preset mode $l^{[k]}(t)$ is selected. Thus, the signal received by the user k at time t can be written as

$$y^{[k]}(t) = \mathbf{h}\left(l^{[k]}(t)|t\right)^T \mathbf{x}(t) + z^{[k]}(t), \tag{6.1}$$

where $z^{[k]} \sim \mathcal{CN}(0,1)$ is AWGN.

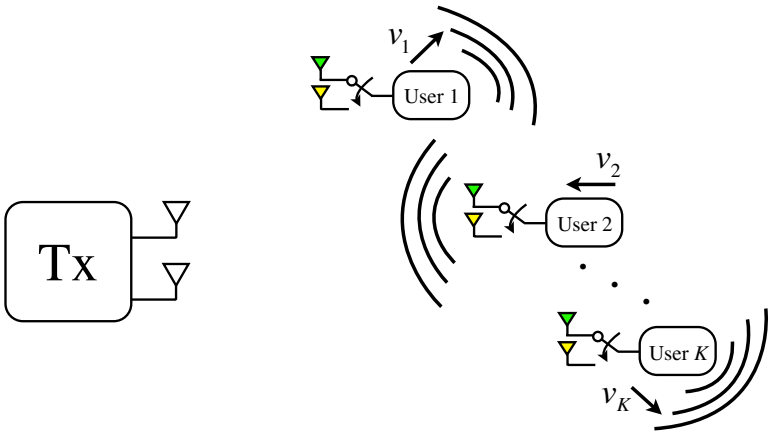

FIGURE 6.1: MISO BC scenario with $N_t = 2$ transmit antennas and K users equipped with reconfigurable antennas. Each receiver moves at velocity v_k generating a time-selective fading channel.

It is assumed that the transmitted signal is subject to an average power constraint $E\left\{\|\mathbf{x}(t)\|^2\right\} \leq P$. The channel coefficients between the transmitter and users are i.i.d. complex Gaussian random variables of zero mean. Furthermore, the physical channel is not strictly constant in time. It is assumed that each user is moving with a velocity v_k generating a time-selective fading channel because of the Doppler spread [146]. In this setting, the channel between transmitter and each user varies due to the Doppler effect, which is characterized by a frequency deviation $f_D = \frac{v_k}{\lambda}$ with λ denoting the wavelength of the wireless signal. Indeed, by applying the Clarke model [147], the coherence time of each user is given by

$$Tc \approx \frac{0.423}{f_D}. \tag{6.2}$$

In the considered setting, we also assume that the transmitter does not know any channel state information other than the coherence time and the received SNR of each user. For simplicity, we focus on the temporal dimension without loss of generality. Therefore, each symbol extension corresponds to a time slot t.

6.3 Blind Interference Alignment for varying channels

Until now, it has been assumed that the channel stays constant during the transmission of the BIA supersymbol. This section analyzes the performance achieved by BIA in

	1	2	3
User 1	$\mathbf{h}^{[1]}(1\|1)$	$\mathbf{h}^{[1]}(2\|2)$	$\mathbf{h}^{[1]}(1\|3)$
User 2	$\mathbf{h}^{[2]}(1\|1)$	$\mathbf{h}^{[2]}(1\|2)$	$\mathbf{h}^{[2]}(2\|3)$

FIGURE 6.2: The supersymbol structure for the $K = 2$, $N_t = 2$ MISO BC during a varying channel.

previous toy examples when the physical channel is not constant over the entire supersymbol. After that, the closed-form expression of the achievable rates for the MISO BC under channel variations are derived.

6.3.1 Toy example $K = 2$ user $N_t = 2$ MISO Broadcast Channel

For illustrative purposes, consider the $N_t = 2$ transmit antennas and $K = 2$ active users case. Following the BIA scheme and considering a non-constant channel, the supersymbol for this case is as shown in Figure 6.2. Notice that in contrast to the supersymbol described in Figure 2.3 for the same scenario, a physical channel that varies in each slot is taken into consideration. Focused on user 1, the received signal during the transmission of the supersymbol is given by

$$\begin{bmatrix} y^{[1]}[1] \\ y^{[1]}[2] \\ y^{[1]}[3] \end{bmatrix} = \begin{bmatrix} \mathbf{h}^{[1]}(1|1)^T \\ \mathbf{h}^{[1]}(2|2)^T \\ \mathbf{0} \end{bmatrix} \mathbf{u}_1^{[1]} + \begin{bmatrix} \mathbf{h}^{[1]}(1|1)^T \\ \mathbf{0} \\ \mathbf{h}^{[1]}(1|3)^T \end{bmatrix} \mathbf{u}_1^{[2]} + \begin{bmatrix} z^{[1]}[1] \\ z^{[1]}[2] \\ z^{[1]}[3] \end{bmatrix}, \tag{6.3}$$

where following the same lines as in previous chapters, $\mathbf{u}_\ell^{[k]} \in \mathbb{C}^{N_t \times 1}$ is the symbol containing N_t DoF transmitted to user k during its ℓ-th alignment block.

It can be seen that, as occurs in Chapter 2, simultaneous transmission is employed in the first symbol extensions while the symbols $\mathbf{u}_1^{[1]}$ and $\mathbf{u}_1^{[2]}$ are transmitted in orthogonal fashion during the second and third symbol extensions, respectively. Hence, assuming that the physical channel remains constant during the 3 symbol extensions that comprise the proposed supersymbol, it is clear that the interference is aligned as is show in (2.4). In consequence, user 1 can remove the interference because of the transmission of $\mathbf{u}_1^{[2]}$ by measuring it at symbol extension $\{3\}$ and subtracting it from the symbol extension $\{1\}$ afterwards. Let us consider again the toy example where $N_t = 2$ and $K = 2$. If the

channel varies in each symbol extension, the received signal at user 1 after zero-forcing, which is shown in (2.4) for constant channel, can be written now as

$$\begin{bmatrix} y^{[1]}(1) - y^{[1]}(3) \\ y^{[1]}(2) \end{bmatrix} = \begin{bmatrix} \mathbf{h}^{[1]}(1|1)^T \\ \mathbf{h}^{[1]}(2|2)^T \end{bmatrix} \mathbf{u}_1^{[1]} + \underbrace{\begin{bmatrix} \left(\mathbf{h}^{[1]}(1|1)^T - \mathbf{h}^{[1]}(1|3)^T\right) \\ \mathbf{0} \end{bmatrix}}_{\Delta\mathbf{H}^{[1]}} \mathbf{u}_1^{[2]} + \begin{bmatrix} z^{[1]}(1) - z^{[1]}(3) \\ z^{[1]}(2) \end{bmatrix}. \tag{6.4}$$

Notice that a new element given by the differences of the channel at symbol extensions 1 and 3 for the preset mode 1 appears in (6.4). In consequence, the interference because of $\mathbf{u}_1^{[2]}$ transmission cannot be fully cancelled at user 1. On the other hand, this term could be treated as noise when it is small enough.

6.3.2 Toy example $K = 3$ users $N_t = 3$ MISO Broadcast Channel

1	2	3	...	8	9	10	11	12	13	14	15	16	17	18	19	20
$\mathbf{h}^{[1]}(1\|1)$	$\mathbf{h}^{[1]}(2\|2)$	$\mathbf{h}^{[1]}(1\|3)$	...	$\mathbf{h}^{[1]}(2\|8)$	$\mathbf{h}^{[1]}(3\|9)$	$\mathbf{h}^{[1]}(3\|10)$	$\mathbf{h}^{[1]}(3\|11)$	$\mathbf{h}^{[1]}(3\|12)$	$\mathbf{h}^{[1]}(1\|13)$	$\mathbf{h}^{[1]}(2\|14)$	$\mathbf{h}^{[1]}(1\|15)$	$\mathbf{h}^{[1]}(2\|16)$	$\mathbf{h}^{[1]}(1\|17)$	$\mathbf{h}^{[1]}(2\|18)$	$\mathbf{h}^{[1]}(1\|19)$	$\mathbf{h}^{[1]}(2\|20)$
$\mathbf{h}^{[2]}(1\|1)$	$\mathbf{h}^{[2]}(1\|2)$	$\mathbf{h}^{[2]}(2\|3)$	...	$\mathbf{h}^{[2]}(2\|8)$	$\mathbf{h}^{[2]}(1\|9)$	$\mathbf{h}^{[2]}(2\|10)$	$\mathbf{h}^{[2]}(1\|11)$	$\mathbf{h}^{[2]}(2\|12)$	$\mathbf{h}^{[2]}(3\|13)$	$\mathbf{h}^{[2]}(3\|14)$	$\mathbf{h}^{[2]}(3\|15)$	$\mathbf{h}^{[2]}(3\|16)$	$\mathbf{h}^{[2]}(1\|17)$	$\mathbf{h}^{[2]}(1\|18)$	$\mathbf{h}^{[2]}(2\|19)$	$\mathbf{h}^{[2]}(2\|20)$
$\mathbf{h}^{[3]}(1\|1)$	$\mathbf{h}^{[3]}(1\|2)$	$\mathbf{h}^{[3]}(1\|3)$	...	$\mathbf{h}^{[3]}(2\|8)$	$\mathbf{h}^{[3]}(1\|9)$	$\mathbf{h}^{[3]}(1\|10)$	$\mathbf{h}^{[3]}(2\|11)$	$\mathbf{h}^{[3]}(2\|12)$	$\mathbf{h}^{[3]}(1\|13)$	$\mathbf{h}^{[3]}(1\|14)$	$\mathbf{h}^{[3]}(2\|15)$	$\mathbf{h}^{[3]}(2\|16)$	$\mathbf{h}^{[3]}(3\|17)$	$\mathbf{h}^{[3]}(3\|18)$	$\mathbf{h}^{[3]}(3\|19)$	$\mathbf{h}^{[3]}(3\|20)$

FIGURE 6.3: The supersymbol structure for the $K = 3$, $N_t = 3$ MISO BC during a varying channel.

Consider now a more complex toy example where the transmitter is equipped with $N_t = 3$ antennas serving $K = 3$ users. The corresponding supersymbol is shown in Figure 6.3. Thus, the signal received at user 1 during its first alignment block comprising the symbol extension $\{1, 2, 9\}$ can be written as

$$\begin{bmatrix} y^{[1]}[1] \\ y^{[1]}[2] \\ y^{[1]}[9] \end{bmatrix} = \underbrace{\begin{bmatrix} \mathbf{h}^{[1]}(1|1)^T \\ \mathbf{h}^{[1]}(2|2)^T \\ \mathbf{h}^{[1]}(3|9)^T \end{bmatrix}}_{\mathbf{H}^{[1]}} \mathbf{u}_1^{[1]} + \begin{bmatrix} \mathbf{h}^{[1]}(1|1)^T \left(\mathbf{u}_1^{[2]} + \mathbf{u}_1^{[3]}\right) \\ \mathbf{h}^{[1]}(2|2)^T \left(\mathbf{u}_2^{[2]} + \mathbf{u}_2^{[3]}\right) \\ \mathbf{0} \end{bmatrix} + \begin{bmatrix} z^{[1]}[1] \\ z^{[1]}[2] \\ z^{[1]}[9] \end{bmatrix}. \tag{6.5}$$

Notice that the first two symbol extensions are polluted by the interference because of the transmission to the remaining users. Following the BIA scheme for the MISO BC described in Chapter 2, the interference at the first element of (6.5), which corresponds to the transmission of $\mathbf{u}_1^{[2]}$ and $\mathbf{u}_1^{[3]}$ can be measured at the channel mode 1, i.e. $\mathbf{h}^{[1]}(1|t)$,

during the symbol extensions {13} and {17} of user 1, respectively. Similarly, user 1 can measure the interference because of the transmission of $\mathbf{u}_2^{[2]}$ and $\mathbf{u}_2^{[3]}$ at channel mode $\mathbf{h}^{[1]}(2|t)$ in the symbol extensions {14} and {18}, respectively. Thus, the signal after zero-forcing interference subtraction during the first alignment block of user 1 is given by

$$\begin{aligned}\tilde{\mathbf{y}}^{[k]} = \begin{bmatrix} y^{[1]}[1] - y^{[1]}[13] - y^{[1]}[17] \\ y^{[1]}[2] - y^{[1]}[14] - y^{[1]}[18] \\ y^{[1]}[9] \end{bmatrix} &= \underbrace{\begin{bmatrix} \mathbf{h}^{[1]}(1|1)^T \\ \mathbf{h}^{[1]}(2|2)^T \\ \mathbf{h}^{[1]}(3|9)^T \end{bmatrix}}_{\mathbf{H}^{[1]}} \mathbf{u}_1^{[1]} \\ &+ \underbrace{\begin{bmatrix} \left(\mathbf{h}^{[1]}(1|1) - \mathbf{h}^{[1]}(1|13)\right)^T \mathbf{u}_1^{[2]} + \left(\mathbf{h}^{[1]}(1|1) - \mathbf{h}^{[1]}(1|17)\right)^T \mathbf{u}_1^{[3]} \\ \left(\mathbf{h}^{[1]}(2|2) - \mathbf{h}^{[1]}(2|14)\right)^T \mathbf{u}_2^{[2]} + \left(\mathbf{h}^{[1]}(2|2) - \mathbf{h}^{[1]}(2|18)\right)^T \mathbf{u}_1^{[3]} \\ \mathbf{0} \end{bmatrix}}_{\text{channel variations}} \\ &+ \underbrace{\begin{bmatrix} z^{[1]}[1] - z^{[1]}[13] - z^{[1]}[17] \\ z^{[1]}[2] - z^{[1]}[14] - z^{[1]}[18] \\ z^{[1]}[9] \end{bmatrix}}_{\text{noise increase}}.\end{aligned} \tag{6.6}$$

It can be seen in (6.6) that the subtraction of the terms of interference because of transmission to all other users leaves a trace when the channel varies during the considered supersymbol. Therefore, we can conclude that pure BIA transmission schemes[1] are not resilient to channel variations. However, the interference because of channel variations could be treated optimally as noise when it is small enough. Furthermore, the received noise increases proportionally to the amount of users served by the transmitter because of the interference subtraction process inherent in any BIA scheme. As a conclusion after analyzing this toy example, we can assert that channel variations and noise increase are the two limiting factors when using BIA in practical implementations. The following subsection is devoted to derive the general closed-form expressions of the achievable rates of BIA for varying and SNR limited channels.

[1]Note that all other BIA schemes follow a similar decoding methodology. This analysis can be easily extend to any BIA scheme.

6.3.3 Achievable rates for the varying channel

For the general case, the interference subtraction involves to use measurements altered by channel variations. We define $\mathbf{t}_{m,\ell}^{[k]} \in \mathbb{C}^{K\times 1}$ as the vector that contains the temporal indexes of the symbol extensions involved in the interference subtraction process of the alignment block ℓ of user k at preset mode l. The first entry of $\mathbf{t}_{\ell,m}^{[k]}(1)$ corresponds to the symbol extension from Block 1 over which user k sets the l-th channel mode of the ℓ-th alignment block. The remaining entries $j = 2, \ldots, K$ of the vector $\mathbf{t}_{\ell,m}^{[k]}(j)$ contain the temporal indexes associated with the symbol extensions from Block 2 used to remove the interference terms received by user k during the l-th element of its ℓ-th alignment block, i.e. $\mathbf{t}_{\ell,m}^{[k]}(1)$. For instance, $\mathbf{t}_{1,1}^{[1]} = \{1, 3\}$ is the vector that contains the symbol extensions for the first element of (6.4). Similarly, this vector corresponds to $\mathbf{t}_{1,1}^{[1]} = \{1, 13, 17\}$ for the symbol extensions involved in the first element of the alignment block of user 1 in (6.6).

$$
\begin{bmatrix} y^{[k]}\left[t_{\ell,1}^{[k]}(1)\right] \\ \vdots \\ y^{[k]}\left[t_{\ell,N_t-1}^{[k]}(1)\right] \\ y^{[k]}\left[t_{\ell,N_t}^{[k]}(1)\right] \end{bmatrix} = \begin{bmatrix} \mathbf{h}^{[k]}\left(1|t_{\ell,1}^{[k]}(1)\right) \\ \vdots \\ \mathbf{h}^{[k]}\left(N_t-1|t_{\ell,N_t-1}^{[k]}(1)\right) \\ \mathbf{h}^{[k]}\left(N_t|t_{\ell,N_t}^{[k]}(1)\right) \end{bmatrix} \mathbf{u}_{\ell}^{[k]}
$$

$$
+ \underbrace{\begin{bmatrix} \sum_{j=2}^{K}\left(\mathbf{h}^{[k]}\left(1|t_{\ell,1}^{[k]}(1)\right) - \mathbf{h}^{[k]}\left(1|t_{\ell,1}^{[k]}(j)\right)\right)\mathbf{u}_{\ell'}^{[j]} \\ \vdots \\ \sum_{j=2}^{K}\left(\mathbf{h}^{[k]}\left(N_t-1|t_{\ell,N_t-1}^{[k]}(1)\right) - \mathbf{h}^{[k]}\left(N_t-1|t_{\ell,N_t-1}^{[k]}(j)\right)\right)\mathbf{u}_{\ell'}^{[j]} \\ \mathbf{0} \end{bmatrix}}_{\Delta\mathbf{H}^{[k]}(\ell)}
$$

$$
+ \underbrace{\begin{bmatrix} z^{[k]}\left[t_{\ell,1}^{[k]}(1)\right] - \sum_{j=2}^{K}\left[t_{\ell,1}^{[k]}(j)\right] \\ \vdots \\ z^{[k]}\left[t_{\ell,N_t-1}^{[k]}(1)\right] - \sum_{j=2}^{K}\left[t_{\ell,N_t-1}^{[k]}(j)\right] \\ z^{[k]}\left[t_{\ell,N_t}^{[k]}(1)\right] \end{bmatrix}}_{\tilde{\mathbf{z}}^{[k]}}. \tag{6.7}
$$

It is interesting to compare with the same equation when the physical channel remains constant given by (2.24). Note that a new term appears because of the subtraction of non-equal channel values over the considered supersymbol. In consequence, the signal

in each alignment block depends on its position in the supersymbol. Assuming that the term given by the channel variations is treated as noise, the N_t DoF comprised in the symbol $\mathbf{u}_{\ell}^{[k]}$ during the ℓ-th alignment block of user k are decodable by solving the equation system given by

$$\tilde{\mathbf{y}}^{[k]}(\ell) = \mathbf{H}(\ell)^{[k]}\mathbf{u}_{\ell}^{[k]} + \Delta\mathbf{H}^{[k]}(\ell)\bar{\mathbf{u}}_{\ell'}^{[j]} + \tilde{\mathbf{z}}^{[k]}(\ell). \tag{6.8}$$

In contrast to (2.25) the decoding process depends on the position of the alignment block ℓ in the predefined supersymbol. Thus, the channel matrix of user k during the ℓ-th alignment block is

$$\mathbf{H}^{[k]}(\ell) = \begin{bmatrix} \mathbf{h}^{[k]}\left(1|t_{\ell,1}^{[k]}(1)\right) \\ \vdots \\ \mathbf{h}^{[k]}\left(N_t-1|t_{\ell,N_t-1}^{[k]}(1)\right) \\ \mathbf{h}^{[k]}\left(N_t|t_{\ell,N_t}^{[k]}(1)\right) \end{bmatrix} \in \mathbb{C}^{N_t\times N_t}, \tag{6.9}$$

the matrix that contains the residual elements because of the interference subtraction over a non-constant supersymbol is given by

$$\Delta\mathbf{H}^{[k]}(\ell) = \begin{bmatrix} \sum_{j=2}^{K}\mathbf{h}^{[k]}\left(1|t_{\ell,1}^{[k]}(1)\right) - \mathbf{h}^{[k]}\left(1|t_{\ell,1}^{[k]}(j)\right) \\ \vdots \\ \sum_{j=2}^{K}\mathbf{h}^{[k]}\left(N_t-1|t_{\ell,N_t-1}^{[k]}(1)\right) - \mathbf{h}^{[k]}\left(N_t-1|t_{\ell,N_t-1}^{[k]}(j)\right) \\ \mathbf{0} \end{bmatrix} \in \mathbb{C}^{N_t\times N_t}, \tag{6.10}$$

and $\tilde{\mathbf{z}}^{[k]}(\ell) \sim \mathcal{CN}\left(0, \mathbf{R}_{\tilde{z}}\right)$ is the noise after zero-forcing interference cancellation where the covariance matrix is given by (2.27), (2.32) or (2.32) depending on the power allocation strategy. For simplicity, constant power allocation is assumed in this chapter so that it is given by

$$\mathbf{R}_{\tilde{z}} = \begin{bmatrix} (2K-1)\,\mathbf{I}_{N_t-1} & \mathbf{0} \\ \mathbf{0} & 1 \end{bmatrix}. \tag{6.11}$$

Therefore, assuming varying channels, the normalized rate per symbol extension of the user k can be written as

$$R_{varC}^{[k]} = \frac{1}{N_t+K-1}\mathbb{E}\left[\log\det\left(\mathbf{I} + P_{str}\mathbf{H}^{[k]}(\ell)\mathbf{H}^{[k]}(\ell)^{H}{\mathbf{R}_{\tilde{z},varC}}^{-1}\right)\right] \tag{6.12}$$

where the covariance matrix of the noise plus interference due to the channel variations is

$$\mathbf{R}_{\tilde{z},varC} = \mathbf{R}_{\tilde{z}} + P_{str}\mathbb{E}\left[\Delta\mathbf{H}^{[k]}(\ell)\Delta\mathbf{H}^{[k]}(\ell)^{H}\right], \tag{6.13}$$

and P_{str} is the average power assigned to each stream according to the power allocation strategy (2.27), (2.32), or (2.35). Since constant power allocation has been assumed in this chapter, $P_{str} = \frac{P}{N_t}$.

6.4 Practical Blind Interference Alignment transmission

Until now we have shown that BIA achieves the optimal DoF in absence of CSIT in many scenarios. However, as it has been shown in the previous section, there exist two main hurdles to achieve a reliable BIA transmission in practical scenarios

- Limited power transmission involves to amplify the noise because of the interference subtraction process of BIA. In other words, at finite SNR regime, the multiplexing gain achieved with BIA results futile when many terms of interference must be subtracted.
- Practical channels are not constant in time/frequency. Therefore, the supersymbol length, which increases exponentially regarding the amount of users, is a limitation for the implementation of BIA schemes in practical scenarios where the physical channel only stays constant during a coherence time period.

In order to deal with both limitations, we suggest to employ simple orthogonal resource allocation joint to the BIA schemes developed in previous chapters. This approach will be denoted as practical BIA (pBIA) from now on. For simplicity we focus on BIA for the MISO BC described in Chapter 2. The extension of pBIA to other BIA schemes is straightforward.

The proposed pBIA scheme divides the transmission resource, either bandwidth or time, in α slices transmitting only to a portion of the total users in each one. Notice that orthogonal resource allocation is in fact a simple form of interference alignment without the need for CSIT [68]. Therefore, the BIA transmission over a MISO BC with N_t transmit antennas and K users is divided in α MISO BCs where BIA for N_t transmit

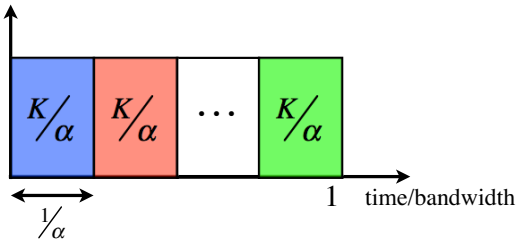

FIGURE 6.4: Resource division for the pBIA scheme. The whole resource is divided in α slices.

antennas and $\frac{K}{\alpha}$ users is carried out in each one[2]. Figure 6.4 shows a generic example of the proposed orthogonal resource allocation joint to BIA.

For illustrative purposes consider the toy example shown in Figure 6.5 where the transmitter is equipped with 2 antennas serving 4 users. Hence, the supersymbol comprises 5 symbol extensions and each user must subtract 3 terms of interference. According to (2.23), the achievable DoF for this case is $\frac{8}{5}$. Assuming this setting, the proposed pBIA scheme splits the time/bandwidth in 2 equal slices. Therefore, BIA transmission for $N_t = 2$ and only $K = 2$ users is employed in each portion of the available bandwidth. In consequence, $\frac{4}{3}$ DoF are achievable in each slice, and therefore, $\frac{1}{2}\left(\frac{4}{3} + \frac{4}{3}\right) = \frac{4}{3}$ DoF are achievable in the whole setting. That is $\frac{4}{15}$ less than BIA for $N_t = 2$ and $K = 4$. At expenses of this loss in DoF, the required coherence time has been reduced to the duration of 3 symbol extensions and only 1 term of interference must be subtracted by each user.

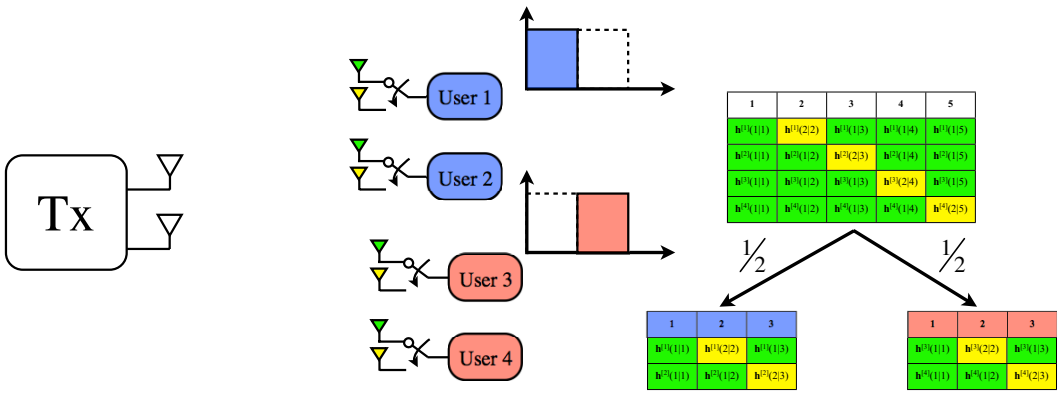

FIGURE 6.5: Resource division for the pBIA scheme in the $N_t = 2$, 4-users MISO BC.

[2]If $\frac{K}{\alpha}$ is not an integer, the resource is divided in $\lceil \frac{K}{\alpha} \rceil$ bands where every band is allocated to $\lfloor \frac{K}{\alpha} \rfloor$ users but the last band where $\mod(K, \alpha)$ users are assigned.

As we have shown, two benefits are obtained with the proposed pBIA scheme. First, only a portion of the total users is involved in the subtraction of the interference. Hence, the noise increase inherent in BIA schemes can be handled by dividing the transmission resource while grouping the users in each piece of resource time or bandwidth. Secondly, shorter supersymbols are required in each slice, and therefore, a relaxation of the required coherence time is obtained. On the other hand, pBIA involves a penalty in DoF regarding the optimal, because of the use of orthogonal resource allocation. Therefore, a trade-off between multiplexing gain, noise increment, and coherence time is expected when using pBIA in a realistic scenario.

6.4.1 Achievable Degrees of Freedom

With the pBIA scheme the available resource, either bandwidth or time, is divided in α slices grouping the total K users in sets of $\frac{K}{\alpha}$ users in each slice as is shown in Figure 6.4. The interference between the groups of $\frac{K}{\alpha}$ users is aligned because of the previous orthogonal resource allocation. Besides, a BIA scheme for N_t transmit antennas and $\frac{K}{\alpha}$ users is employed to align the interference between the users served in each slice. In consequence, the supersymbol length in each slice is reduced to

$$\mathcal{L}_{\text{pBIA}} = (N_t - 1)^{\frac{K}{\alpha}} + \frac{K}{\alpha}(N_t - 1)^{\frac{K}{\alpha}-1}. \tag{6.14}$$

On the other hand, the use of pBIA involves to divide a MISO BC for K receivers in α MISO BCs serving $\frac{K}{\alpha}$ receivers each, both for N_t transmit antennas. Since the achievable sum-DoF in each MISO BC is given by (2.23), the achievable sum-DoF by using pBIA is given by

$$\text{DoF}_{\text{pBIA}} = \sum_{i=1}^{\alpha} \frac{1}{\alpha} \cdot \frac{N_t \frac{K}{\alpha}}{N_t + \frac{K}{\alpha} - 1} = \frac{1}{\alpha} \cdot \frac{N_t K}{N_t + \frac{K}{\alpha} - 1}. \tag{6.15}$$

It is interesting to analyze the limits of the achievable DoF of pBIA. For $\alpha = 1$ pBIA coincides with the pure BIA transmission scheme and the achievable sum-DoF is given by (2.23). In contrast, pBIA corresponds to a fully orthogonal scheme when $\alpha = K$, and therefore, the sum-DoF is fixed to 1 DoF divided between the K users.

6.4.2 Achievable Rates

Assuming that the physical channel does not vary during the transmission of the entire supersymbol, the achievable rate by the k-th for the pBIA scheme can be easily derived from (2.34). Taking into consideration that a BIA scheme for N_t transmit antennas and only $\frac{K}{\alpha}$ users is carried out over portion $\frac{1}{\alpha}$ of the transmission resource is employed in each slice, the normalized rate per symbol extension achieved by user k for the pBIA scheme is

$$R_{\text{pBIA}}^{[k]} = \frac{1}{\alpha} \cdot \frac{1}{N_t + \frac{K}{\alpha} - 1} \mathbb{E}\left[\log\det\left(\mathbf{I} + P_{str}\mathbf{H}^{[k]}\mathbf{H}^{[k]^H}\mathbf{R}_{\tilde{z}}^{-1}(\alpha)\right)\right], \tag{6.16}$$

where $\mathbf{H}^{[k]}$ is given by (2.25). Since constant power allocation over the entire supersymbol has been assumed in this chapter, the average power assigned to each stream is $P_{str} = \frac{P}{N_t}$. Moreover, only the $\frac{K}{\alpha} - 1$ terms of interference because of the transmission to users in the same slice must be subtracted by each user. Hence, the covariance matrix for pBIA is given by

$$\mathbf{R}_{\tilde{z}} = \begin{bmatrix} (2\frac{K}{\alpha} - 1) & \mathbf{0} \\ \mathbf{0} & 1 \end{bmatrix}. \tag{6.17}$$

It is interesting to remark that because of the orthogonal resource allocation a penalty $\frac{1}{\alpha}$ appears in the achievable rate of user k. At expense of this penalty, from (6.17) we can notice that the increase of the noise due to the interference subtraction has been lessened in comparison with the standard BIA scheme described in Chapter 2. Besides, the supersymbol length has been reduced considerably according to (6.14).

Similarly, when the decoding process of each symbol is affected by the channel variations over a considered supersymbol, the achievable rate of the k-th user can be derived following the lines of (6.16). Considering a BIA scheme for $\frac{K}{\alpha}$ users and N_t transmit antennas over a portion $\frac{1}{\alpha}$ of the total transmission resource the normalized rate per symbol extension achieved by user k is

$$R_{\text{pBIA},varC}^{[k]} = \frac{1}{\alpha} \cdot \frac{1}{N_t + \frac{K}{\alpha} - 1} \mathbb{E}\left[\log\det\left(\mathbf{I} + P_{str}\mathbf{H}^{[k]}(\ell)\mathbf{H}^{[k]}(\ell)^H\mathbf{R}_{\tilde{z},varC}{}^{-1}\right)\right] \tag{6.18}$$

where $\mathbf{R}_{\tilde{z},varC}$ is given by (6.13). Assuming constant power allocation, the covariance matrix of the noise after zero forcing $\mathbf{R}_{\tilde{z}}$ is given by (6.17) and $P_{str} = \frac{P}{N_t}$. As it occurs

when the channel remains constant over the entire supersymbol, notice that a penalty $\frac{1}{\alpha}$ appears because of the orthogonal approach of pBIA.

6.4.3 Optimal orthogonal resource allocation for practical Blind Interference Alignment

The question that naturally arises after analyzing the performance of the proposed pBIA scheme is *how to find the optimal resource division to achieve the most favorable trade-off between coherence time, multiplexing gain, and noise increase?* To determine the value of α that achieves this trade-off, which is denoted as α_{opt}, we focus on maximizing the achievable sum-rate. Note that in contrast to most of the optimization problem solutions, the amount of information available is quite limited for pBIA transmission. Therefore, the solution α_{opt} cannot depend on CSIT knowledge. It could be referred to as a *blind resource allocation* optimization problem. In this sense, it is assumed that the transmitter only knows the coherence time and the SNR of the users.

The first step to solve the described trade-off consists in selecting a resource division large enough to consider the physical channel constant over the entire supersymbol. That is, a value of resource division α able to ensure that the transmission period of the pBIA supersymbol is shorter than the coherence time T_c of the system. Hence, the rate equation given by (6.16) can be used from now on. In particular, assuming constant power allocation and bands of the same size, the normalized sum-rate per symbol extension achieved by pBIA when $\frac{K}{\alpha}$ users are served in each one of the α slices can be written as

$$R_{\Sigma\text{pBIA}} = \sum_{i=1}^{\alpha} \sum_{k=1}^{\frac{K}{\alpha}} \frac{1}{\alpha} \cdot \frac{1}{N_t + \frac{K}{\alpha} - 1} \mathbb{E}\left[\log\det\left(\mathbf{I} + P_{str}\mathbf{H}^{[k]}\mathbf{H}^{[k]^H}\mathbf{R}_{\tilde{z}}^{-1}(\alpha)\right)\right]. \tag{6.19}$$

Considering that the users are statistically equivalent, the optimal resource division α_{opt} can be obtained by solving the following optimization problem

$$\begin{aligned} \underset{\alpha}{\text{maximize}} \quad & \frac{\frac{K}{\alpha}}{N_t + \frac{K}{\alpha} - 1} \mathbb{E}\left[\log\det\left(\mathbf{I} + \frac{P}{N_t}\mathbf{H}^{[k]}\mathbf{H}^{[k]^H}\mathbf{R}_z^{-1}(\alpha)\right)\right] \\ \text{subject to} \quad & \alpha \in [1, K] \\ & \mathcal{L}_{\text{pBIA}} \in [0, T_c] \end{aligned} \tag{6.20}$$

The optimization problem (6.20) is non-convex and difficult to solve by applying standard optimization tools. To obtain a more tractable problem it is assumed that the systems operates at medium SNR regime and the approximation $\log(1+SNR) \approx \log(SNR)$ is reasonable. Note that at low SNR, BIA or even other IA schemes do not perform well and fully orthogonal schemes achieve better performance.

Given the previous approximation, the optimization problem can be written as

$$\begin{aligned} \underset{x}{\text{maximize}} \quad & f(x) \\ \text{subject to} \quad & x \in [1, K]\,, \end{aligned}$$

where $x \equiv \frac{K}{\alpha}, x \in [1, K]$ and

$$\begin{aligned} f(x) = & \frac{x}{N_t + x - 1} \mathbb{E}\left[\log\det\left(\frac{P}{N_t}\mathbf{H}^{[k]}{\mathbf{H}^{[k]}}^H \mathbf{R}_{\tilde{z}}^{-1}(\alpha)\right)\right] = \\ & \frac{x}{N_t + x - 1} \cdot \left(\log\left(\frac{P}{N_t}\right)^{N_t} - \log\det(R_{\tilde{z}}) + \mathbb{E}\left[\log\det \mathbf{H}^{[k]}{\mathbf{H}^{[k]}}^H\right]\right) \\ & \frac{x}{N_t + x - 1} \cdot \left(N_t \log\left(\frac{P}{N_t}\right) - (1 - N_t)\log\left(2x - 1\right) + \mathbb{E}\left[\log\det \mathbf{H}^{[k]}{\mathbf{H}^{[k]}}^H\right]\right) \end{aligned} \tag{6.21}$$

where the determinant of the diagonal matrix $\mathbf{R}_{\tilde{z}}$ is given by

$$\log\left(\det\begin{bmatrix} (2\frac{K}{\alpha} - 1) & \mathbf{0} \\ \mathbf{0} & 1 \end{bmatrix}\right) = \log\left(2\frac{K}{\alpha} - 1\right)^{N_t - 1} = (N_t - 1)\log(2x - 1). \tag{6.22}$$

Furthermore, since $\mathbf{H}^{[k]} \sim \mathcal{CN}(0, \mathbf{I}_{N_t})$, $\mathbf{H}^{[k]}{\mathbf{H}^{[k]}}^H$ is a Wishart matrix $\boldsymbol{W} \sim W_{N_t}(N_t, \mathbf{I})$, applying [134, Theorem 2.11], it is verified that

$$\mathbb{E}\left[\log\det\left(\mathbf{H}^{[k]}{\mathbf{H}^{[k]}}^H\right)\right] = \sum_{l=0}^{N_t - 1} \psi\left(N_t - l\right), \tag{6.23}$$

where $\psi(\cdot)$ is the Euler digamma function. Hence, we can rewrite $f(x)$ as

$$f(x) = \frac{x}{N_t + x - 1}\left(Z - (1 - N_t)\log\left(2x - 1\right)\right), \tag{6.24}$$

where the terms that do not depend on $x \equiv \frac{K}{\alpha}$ are grouped in

$$Z = N_t \log\left(\frac{P}{N_t}\right) + \sum_{l=0}^{N_t - 1} \psi\left(N_t - l\right). \tag{6.25}$$

Notice that the optimal resource division α_{opt} is obtained by solving $\frac{\partial f(x)}{\partial x}|_{x^*} = 0$. However, it is not possible to obtain a closed-form solution of this equation. To obtain an analytical expression of the resource division, the following approximation is proposed

$$\log(2x-1) \approx \frac{x-1}{\mu x+1}, \tag{6.26}$$

where μ is the value in the middle of the x range, i.e. $\frac{K}{2}$. Therefore,

$$\mu = \left(\frac{\frac{K}{2}-1}{\log(K-1)} - 1\right)\frac{2}{K}. \tag{6.27}$$

After employing the previous approximation, the derivative of $f(x)$ with respect to x is given by

$$\begin{aligned}\frac{\partial f(x)}{\partial x} = \frac{1}{N_t+x-1}\Bigg(\left(1-\frac{x}{N_t+x-1}\right)\left(\frac{(1-N_t)(x-1)}{\mu x+1}+Z\right)\\ +\frac{(1-N_t)x}{\mu x+1}\left(1-\frac{\mu(x-1)}{\mu(x+1)}\right)\Bigg),\end{aligned} \tag{6.28}$$

and the resulting optimal resource division, denoted as α^*, is obtained by solving $\frac{\partial f(x)}{\partial x}|_{x^*} = 0$, which can be written as the solution to a second order equation

$$ax^2 + bx + c = 0, \tag{6.29}$$

where

$$\begin{aligned} a &= \mu Z - N_t - 1,\\ b &= Z(1+\mu) + 2(1-N_t),\\ c &= N_t - 1 + Z. \end{aligned}$$

If x^* denotes the positive solution of (6.29), we have that

$$\alpha^* = \begin{cases} 1 & \text{if } \frac{K}{x^*} < 1 \\ \text{round}\left(\frac{K}{x^*}\right) & \text{if } 1 \leq \frac{K}{x^*} \leq K \\ K & \text{if } \frac{K}{x^*} > K \end{cases} \tag{6.30}$$

Notice that this solution only depends on the system parameters N_t, K, and the received power P, i.e. the user SNR.

6.5 Simulation Results

The performance of the proposed pBIA for different values of α is shown in Figure6.6. For these results, coherence time is assumed large enough to consider the channel constant over the entire supersymbol. It can be seen that the sum-rate is a concave function at medium SNR regime where there exists an optimal value α_{opt} that maximizes the system sum-rate. Recall that the optimal sum-rate at high and low SNR is achieved at $\alpha_{\text{opt}} = 1$ (BIA applied over the whole resource) and $\alpha_{\text{opt}} = K$ (fully orthogonal transmission), respectively. As the SNR decreases, notice that α_{opt} corresponds to a larger resource division. The solution of the optimization problem described in 6.30 is $\alpha^* = \{1, 4, 7\}$ at the aforementioned values of SNR, respectively. As expected, due to the approximations employed to derive α^*, this solution is not absolutely accurate regarding the theoretic optimal resource division. However, the penalty is typically small. We can check that at SNR = 22 dB the approximation $\log(1 + SNR) \approx \log(SNR)$ is not very accurate and the value of α^* is not exactly the optimal. Nevertheless, as the SNR decreases, the sum-rate around the optimal point becomes flatter, and therefore, a small deviation with respect to α_{opt} does not involve a great penalty.

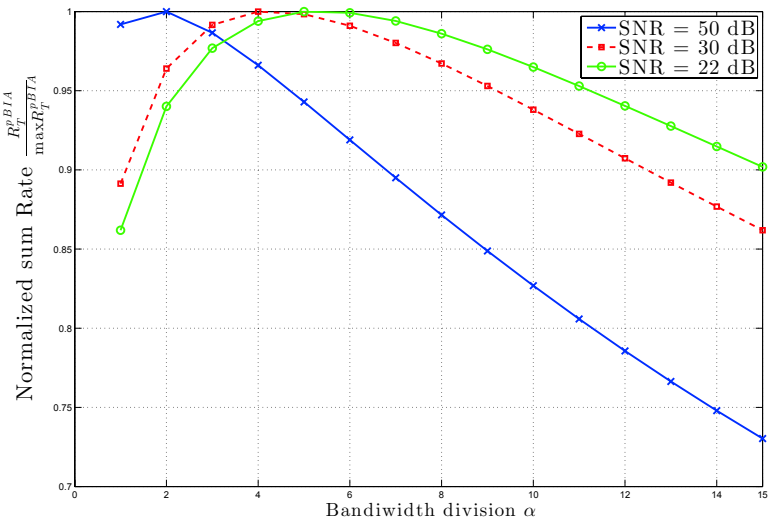

FIGURE 6.6: Normalized sum-rate versus bandwidth division. $N_t = 4$, $K = 60$.

With the aim of analyzing the achievable DoF of pBIA, Figure 6.7 shows the sum-DoF for the optimal resource division α_{opt} plotted in Fig. 6.6. As expected, at high

SNR values, the value of α that maximizes the sum-rate of the system, i.e. α_{opt}, also maximizes the sum-DoF. Therefore, pBIA transmission is optimal in relation to both the sum-DoF and the sum-rate. However, when pBIA is applied in a setting with finite values of SNR, there is a loss in DoF comparing with the optimal DoF achieved by the use of BIA in only one slice. This loss in the DoF is caused by the application of orthogonal transmission. At the expense of the DoF loss, the orthogonal transmission is aimed at reducing the increase of the noise power caused by the interference subtraction step of BIA, which severely affects the achievable sum-rate. As an example, for the proposed MISO BC, there is a loss in the achievable DoF if pBIA is applied when $\alpha = 6$. Nonetheless, by employing the previous resource division, it is possible to achieve better sum-rate than the BIA transmission over the whole resource, either time or frequency.

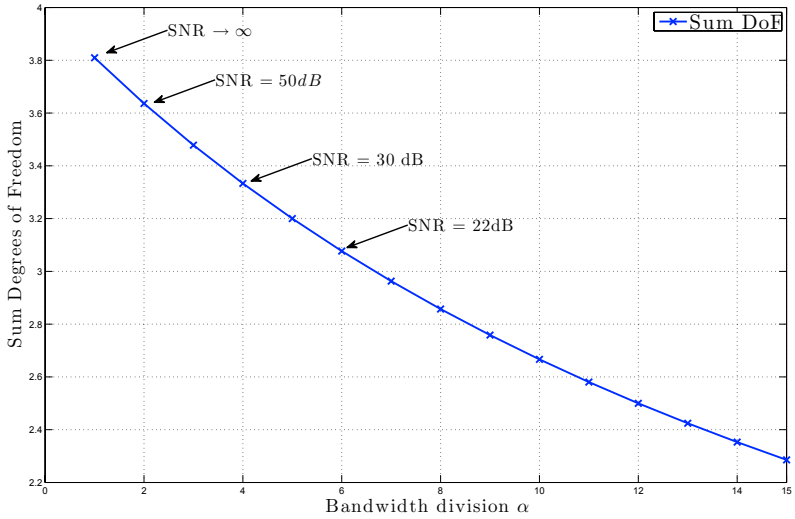

FIGURE 6.7: Achievable sum-DoF regarding the bandwidth division. $N_t = 4$, $K = 60$.

LTE parameters for the 10 MHz configuration with a carrier frequency of 2 GHz are considered in the following simulations. Moreover, a Doppler spread with $f_D = 55.5$ Hz of frequency deviation is assumed. Hence, the coherence time given by (6.2) is 7.6 msec.

The cumulative distribution functions (CDF) of the sum-rate in a scenario with $N_t = 2$ and $K = 100$ users for different resource division values are depicted in Figure 6.9. Notice that the supersymbol for this case comprises 101 symbol extensions, which corresponds to a transmission period much lower than the coherence time. Therefore, we can assume that the achievable sum-rate is not limited by channel variations for this case. However,

since each user has to subtract 99 interference terms, the sum-rate is severely degraded by the noise increase due the inherent interference subtraction of BIA. It can be seen that the achievable sum-rate increases by applying pBIA with an orthogonal division given by α^*. In particular, the application of pBIA in the considered setting allows most of the users to achieve a sum-rate improvement of at least 1 bit/sec/Hz.

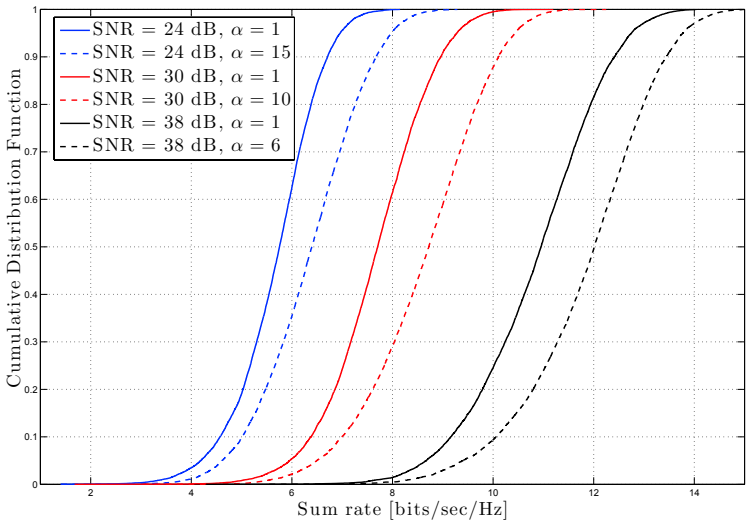

FIGURE 6.8: Cumulative function of the sum-rate for the standard BIA and pBIA at different SNR values. $N_t = 2$, $K = 90$. No Doppler.

Figure 6.9 shows the CDF of the sum-rate for pBIA and BIA ($\alpha = 1$) schemes when $N_t = 3$ and $K = 14$ considering both varying and constant channel. Notice that for this setting the supersymbol comprises more than 10^5 symbol extensions. Therefore, the performance of BIA is limited by the coherence time while the degradation of the SNR due to zero-forcing does not play a major role since only 13 interference terms must be subtracted. Checking the values when $\alpha = 1$ and Doppler spread is considered, it can be seen that the channel variations penalize considerably the sum-rate. However, note that the CDF curves when $\alpha = 2$, whether channel variations are considered or not, overlap with the $\alpha = 1$ case assuming constant channel over the entire supersymbol. That is, pBIA mitigates the effect of a non-constant channel without penalizing the achievable sum-rates. In other words, pBIA allows to manage the coherence time requirement while obtaining an optimal trade-off between multiplexing gain and noise increase.

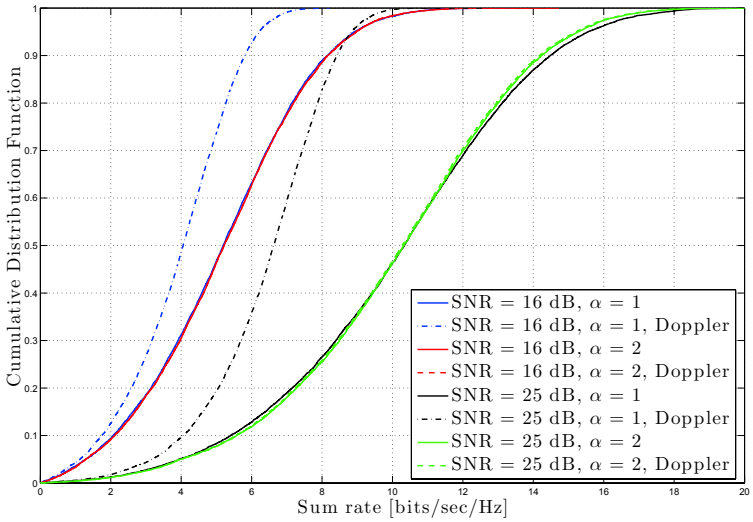

FIGURE 6.9: Cumulative function of the sum-rate for standard BIA and pBIA at different SNR values. $N_t = 3$, $K = 14$. Doppler $f_D = 55.5$ Hz.

6.6 Experimental Evaluation of Blind Interference Alignment

To understand the impact of BIA schemes in realistic implementations we carried out an experimental evaluation of BIA in the MIMO testbed of University of Cantabria [148]. In contrast to other hardware implementations such as [149] where IA for the 3-user IC is evaluated offline, in [150] the authors present a IA study based on the same testbed as used in this section for BIA. This work identifies the main practical issues that degrade the IA performance in real implementations, concluding that imperfect CSIT is the key limiting factor. Encouraged by this fact, we compare the evaluation of BIA with a scheme such as LZFB that requires CSIT knowledge. The proposed experiments are based on a typical configuration of a LTE system for a bandwidth of 5 MHz where a turbocode with a coding rate of $\frac{2}{3}$ is employed for channel coding.

6.6.1 Measurement Set-up and Methodology

Following the lines of this chapter, a MISO BC is considered in the proposed testbed. The transmitter is equipped with 2 antennas that serve 2 users equipped with a reconfigurable antenna each. The transmitter and the receivers are located in a lecture room at the

TABLE 6.1: System parameters of the BIA testbed

Parameter	**Value**
Signal bandwidth	5 MHz
RF carrier	5600 MHz
Number of subcarriers	512
Subcarrier spacing	15 KHz
Data subcarriers	316
Null/Guard subcarriers	32
Cyclic prefix	1/8 of the OFDM symbol length
Sampling frequency	40 Msamples/sec
Sampling rate	8 samples/symbol
DAC&ADC	resolution 14 bits
Root-raised cosine roll off	40%

University of Cantabria. The receivers are separated around approximately 4 meters away from the transmitter with direct line of sight. Since the measurements are done in an isolated room, the coherence time is large enough to consider that the channel remains constant during each iteration. With the aim to simulate the behaviour of reconfigurable antennas, two independent antennas from each node are taken into account. Therefore, two streams, which correspond to the preset modes 1 and 2, respectively, are received by each user.

The transmit and receive sides can be modeled as a combination of hardware and software parts. In [148, 151] these elements are described in detail. The system parameters correspond to a LTE configuration for a 5 MHz bandwidth and 512 subcarriers. In order to obtain a sampling frequency of 7.68 MHz typical of this LTE configuration, a resampling factor is applied. The parameters of the testbed are shown in Table 1. In the presented implementation, the source bits can be mapped to a BPSK, QPSK, 16 QAM or 32 QAM constellation with one symbol per subcarrier. It is assumed that all the subcarriers of the OFDM symbol employ the same constellation in each iteration. Notice that this parameter fixes the sum-throughput of the proposed BIA implementation. The pilot symbols are always mapped to QPSK. Besides, LTE channel coding is assumed, a $\frac{2}{3}$ turbo-encoder is employed in this work. Regarding the noise, the testbed is characterized by an average SNR of 16 dB.

The measurement methodology for LZFB transmission is shown in Figure 6.10(a). However, the same scheme can be employed for other techniques based on CSIT such as IA

or BD. The frame structure is composed by a training stage, where orthogonal transmission is mandatory. It contains a PN sequence for synchronization and a pilot sequence (PLT) for channel estimation. This sequence corresponds to entire OFDM symbol where each subcarrier contains a known QPSK symbol. Once the channel has been estimated, it is sent to the transmitters in order to calculate the corresponding precoding matrices and generate the data signals. This process involves about 5 seconds to be done. After that, 10 OFDM symbols are sent simultaneously to each user. Besides, since relative phases and time offsets have to be constant over the channel transmission, phase synchronization is required to implement full CSIT techniques.

On the other hand, as other techniques that do not require CSIT knowledge, the implementation of BIA does not require any training stage, backhaul links or phase synchronization. As can be seen in Figure 6.10(b) and (6.3), the OFDM symbols are transmitted simultaneously during the first stage, which corresponds to first time slot (Block 1) of the supersymbol of Figure 6.2. After that, symbols to users 1 and 2 are transmitted in an orthogonal fashion according to the Block 2 of the supersymbol. Additionally, since sequential transmission is used during Block 2, a pilot sequence is also transmitted to get the CSIR required to solve the equation system of (6.4)[3]. Note that, although synchronization requirements are more relaxed for the BIA scheme, PN sequences are transmitted in order to detect the beginning of each frame.

6.6.2 Evaluation results

The theoretical achievable sum-rates of LZFB and BIA are shown in Figure 6.11. At first sight LZFB exceeds the performance of BIA. This result should not surprise us, since LZFB achieves 2 sum-DoF while the performance of BIA is only $\frac{4}{3}$ sum-DoF for the considered setting. Focused on the average SNR = 16 dB of our testbed, BIA achieves 4 bits/sec/Hz. Due to the LTE channel coding, the spectral efficiency, i.e. the bits of the constellation employed in each, can be considered close to the capacity. Therefore, each user would obtain a bit error rate (BER) close to zero for a spectral efficiency of 2 bits/sec/Hz, i.e. by employing a QPSK constellation to transmit each stream. On the other hand, LZFB attains 5.5 bits/sec/Hz for the same SNR. In consequence, from a theoretical point of view, it is expected that LZFB overcomes the performance of BIA.

[3]It is assumed that the coherence time is large enough to consider the channel variations as a source of interference.

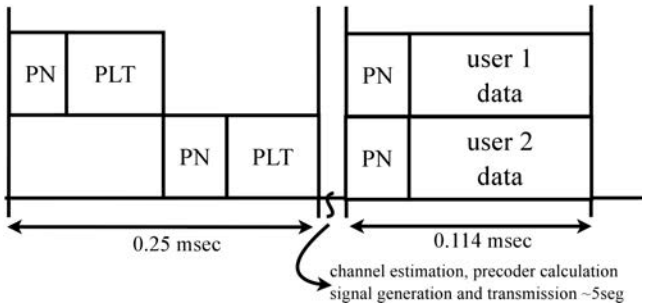

(a) Frame structure for LZFB (full CSIT)

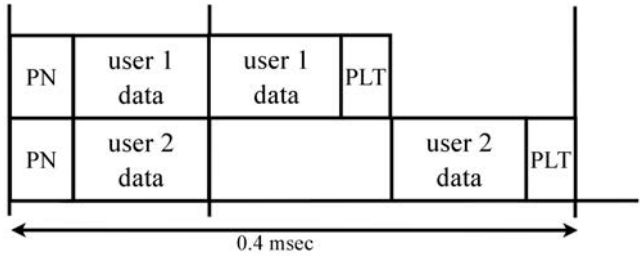

(b) Frame structure for BIA

FIGURE 6.10: Frame structure for LZFB and BIA transmission schemes

The BER for LZFB and BIA schemes is depicted in Figure 6.12. Note that the horizontal axis represents the sum-throughput taking into account the costs of CSIT and the structure of the frames shown in Figure 6.10. Each point corresponds to the constellation employed to map the transmitted symbols (BPSK, QPSK, 16-QAM, and 32-QAM), which determines the sum-throughput. It can be seen that LZFB achieves a lower BER for a sum-throughput below 12 Mbps. However, BIA obtains a better performance when more dense constellations are applied (e.g. when the symbols are mapped in a QPSK constellation, BIA achieves a BER of $3 \cdot 10^{-4}$ for 13.3 Mbps while LZFB obtains a BER close to $1 \cdot 10^{-1}$ for 15 Mbps).

Checking the results shown in Figure 6.12, the performance of BIA and LZFB can be confusing. According to the theoretical sum-rate shown in Figure 6.11, it was expected that LZFB overcomes the performance of BIA, however this only happens when a low density constellation such a BPSK is employed. This effect can be easily explained because of schemes based on CSIT such as LZFB are heavily handicapped by channel estimation errors, synchronization drifts, and variations of the estimated channel, which do not depend directly on the SNR of the system. On the other hand, BIA is mainly limited by SNR. Therefore, it is expected that BIA achieves even better performance than LZFB at higher SNR values in many practical environments.

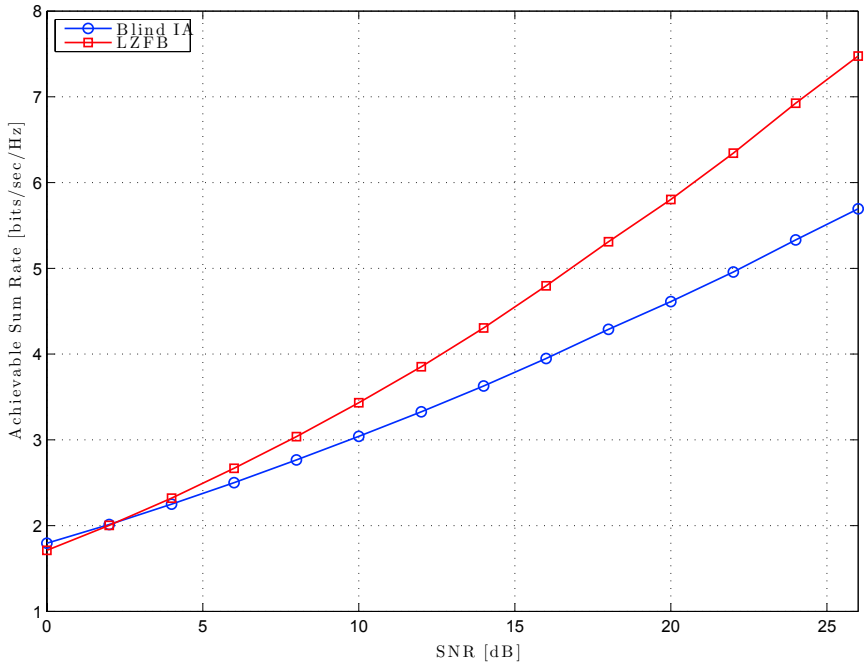

FIGURE 6.11: Theoretical sum-rate of LZFB and BIA transmission schemes at medium SNR regime

6.7 Conclusions

In this chapter, the use of BIA schemes in practical time-varying channels and where the users operate at finite SNR is evaluated. It is shown that both limitations, coherence time and SNR are the two main hurdles to overcome for the implementation of BIA. Specifically, it is demonstrated that the interference subtraction methodology inherent in the BIA schemes leads to a trace of interference when the physical channel varies along the supersymbol. Moreover, the subtraction of received signals involves a noise increase proportional to the amount of users, and therefore, the multiplexing gain achieved by BIA, which also increases with the amount of users, results futile when many terms of interference must be subtracted.

We propose a combination of the standard BIA scheme for the MISO BC and orthogonal resource allocation to handle the supersymbol length and the amount of interference terms that must be subtracted, i.e. coherence time and limited SNR. By applying BIA to send data to users over orthogonal transmission resources, bandwidth or time, the proposed scheme aims at maximizing the sum-rate, which does not necessarily correspond

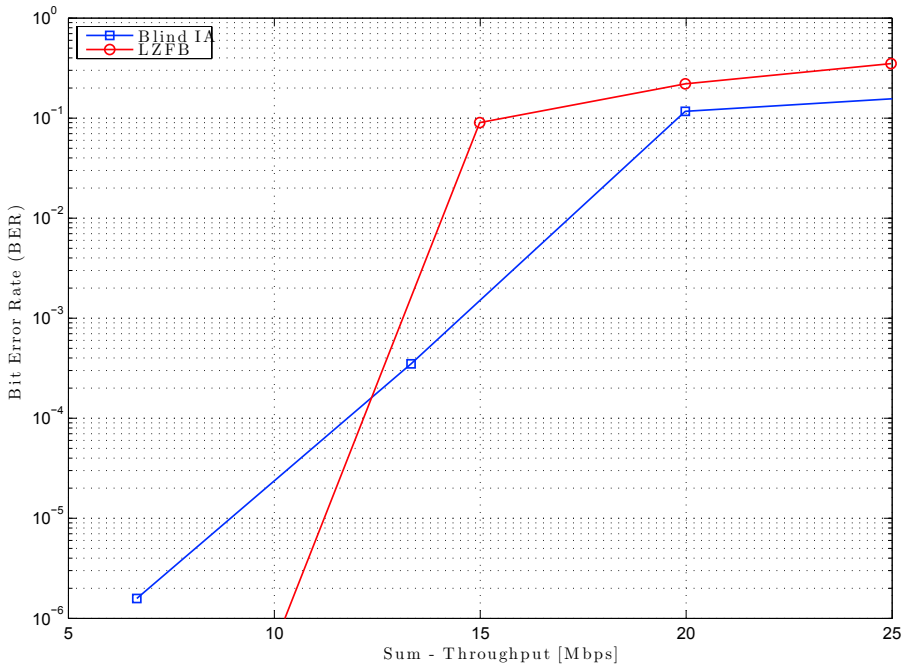

FIGURE 6.12: BER vs sum-throughput for LZFB and BIA transmission schemes

to the optimal sum-DoF at finite SNR. Furthermore, the length of the supersymbol, which increases exponentially as the amount of users served, can be reduced significantly, relaxing the coherence time requirement. The optimization problem to obtain the optimal resource division is formulated in this chapter and a blind solution, i.e. without the need for CSIT, is derived. Simulation results show that this approach allows to manage the trade-off among multiplexing gain, coherence time and noise increase. Finally, the results obtained through a hardware testbed lead us to confirm that the use of BIA outperforms the throughput achieved by schemes based on CSIT because of the impairments of providing CSIT.

Chapter 7

Conclusions and Future Directions

7.1 Summary

In this dissertation, we have analyzed the use of BIA transmission schemes in cellular networks. At first sight, the BIA scheme originally devised for the MISO BC results attractive for cellular networks, its implementation is nonetheless not straightforward. An extension of the original BIA scheme where the set of BSs forms a cooperative network MIMO is proposed in this work. It is shown that a fully cooperative approach results inefficient because of the lack of full connectivity in cellular networks. Moreover, fully cooperative BIA involves to use an unacceptable supersymbol length and the terms of interference given by transmission to the rest of users in the whole network must be subtracted, and therefore, increasing considerably the noise after interference cancellation.

First, we consider the use of BIA in homogeneous cellular networks in absence of CSIT based on the topology of the network as an information resource to design the transmission strategy. An outer bound of the DoF is derived for general partially connected networks with single-antenna receivers when CSIT knowledge is not available. After that, differentiating between *shared* users that receive a strong signal from the set of BSs and *private* users located in the inner cell that can treat the signal from neighbor BSs optimally as noise, we present several BIA schemes with the aim of reaching the

optimal sum-DoF in cellular networks. It is shown that data sharing among the BSs when transmitting to shared users allows to design a BIA scheme that cancels both intracell and intercell interference. Although this approach improves significantly the rates of the cell-edge users at low SNRs, there is a loss in DoF because identical data are sent by all BSs that transmit to shared users. Moreover, it involves the use of backhaul links for providing data sharing, which is one of the issues that blind transmission schemes try to avoid. Then, the use of flexible bandwidth allocation is proposed to avoid the interference between both groups of users, private and shared, by transmitting to them in different frequency bands within the available bandwidth. In consequence, a cooperative BIA scheme can be devised for transmitting to shared users while standard BIA transmission is employed for private users reusing the BIA code due to the partial connectivity. Although this scheme achieves more DoF in comparison with the use of data sharing in most of the cases, it is still suboptimal in DoF because of the use of an orthogonal scheme to avoid the interference between both groups of users. By appropriately combining the BIA schemes corresponding to the private and the shared users in a way that leverages the partial connectivity a BIA scheme that achieves the optimal DoF in symmetric cellular networks is presented. For asymmetric cellular networks, an extension of this scheme is also devised to minimize the loss of optimality in DoF because of asymmetric impairments. Interestingly, in absence of CSIT, schemes based on the network topology overcome the DoF achieved by fully cooperative BIA schemes, even when full connectivity among the whole set of BSs and all users is assumed. As a main conclusion, we can assert that partial connectivity in cellular networks should be treated as a resource instead of a limitation. Furthermore, a considerable reduction of the supersymbol length is attained in comparison with the fully cooperative scheme, rendering the scheme more robust to temporal and frequency variations of the channels.

Secondly, following the previous approach based on the network topology, we consider the use of BIA in heterogenous cellular networks. Specifically, for macro-femto networks, it is demonstrated that the cooperative BIA schemes lead to a loss in DoF because of the particular topology of this kind of networks. In consequence, the DoF achieved by macro users are heavily penalized due to transmission of their corresponding macro BS to femto users while the femtocells are inefficiently treated as a macro BS, i.e. as in homogenous cellular networks. Moreover, it is shown that the sum-DoF does not scale with the amount of femtocells deployed, which considering a dense femtocell scenario

penalizes the network performance significantly. Encouraged by this fact, we derive the linear DoF of the two-tier cellular network subject to optimality in sum-DoF for the upper tier. Then, a cognitive-based BIA scheme is derived to reach that optimal DoF performance. For macro-femto cellular networks, it is demonstrated that the macro BS transmits independently of the femtocell deployment within its coverage, and therefore, achieving the optimal DoF as in a MISO BC. Meanwhile, femto users achieve non-zero DoF exploiting the supersymbol structure to measure the interference subspace because of macro BS transmission in a cognitive fashion. It is shown that the proposed cognitive BIA scheme for macro-femto networks outperforms other transmission schemes. To do so, the proposed approach does not require any CSIT or data exchange between macro BS and the FAPs. Instead, a simple coordination between the macro BS and the femtocells is required in order to transmit to macro and femto users in a synchronized fashion, respectively.

We finally analyze the implementation of BIA schemes in practical scenarios. Coherence time and finite SNR are pointed out as the main limitations of BIA in practical channels. First, they require a coherence time large enough to consider that the physical channel remains constant over the entire supersymbol. If this assumption was violated, the BIA schemes would suffer a loss in both the sum-DoF and the achievable sum-rate. The second limitation is related to the non-negligible increase of the noise power caused by the subtraction of the interfering signals. This increase of the noise power does not involve any loss of optimality in DoF. However, for finite SNRs, maximizing the sum-DoF does not ensure the maximization of the sum-rate. As a result, the increase of the noise power can reduce the sum-rate achieved by BIA schemes. This dissertation shows that, since sum-DoF, noise power, and supersymbol length grow as the amount of user increases, there exists a trade-off between multiplexing gain, sum-rate at finite SNR, and coherence time when BIA is applied in practical channels. Orthogonal resource allocation joint to the BIA schemes presented in this work is proposed to handle both limitations. It is demonstrated that, at expenses of a loss in DoF, this practical BIA approach optimizes the sum-rate of the network. Moreover, it is interesting to remark that any resource allocation strategy applied to blind schemes should not depend on CSI. We devise a practical BIA scheme that allows to obtain the optimal resource division depending only on the system parameters, coherence time, and users SNRs. To complete the study of BIA schemes in practical scenarios, we present an experimental evaluation

of BIA in a hardware testbed. It is shown that BIA outperforms a transmission scheme based on CSIT such as LZFB because of the hardware impairments and the costs of providing CSIT.

7.2 Future Directions

Blind Interference Alignment for practical channels. The practical BIA scheme developed in this dissertation is subject to very rigid constraints such as same SNR for the whole set of users or same size of the resource partitions. To improve the resource allocation in BIA schemes, which plays a major role to optimize the sum-rate, future works would consider more flexible resource allocation schemes. Moreover, channel variations and how to deal with this limitation will focus our future research.

Multi-tier networks. Theoretical limits in absence of CSIT. Future cellular will be extremely heterogeneous, two-tier networks can be extended to multi-tier scenarios where macro, micro, pico, femto cells and relays coexist generating environments limited by inter-tier interference. Since providing CSIT or cooperation among the different tiers results unaffordable, the use of BIA will be proposed as in the cognitive scheme devised in this work. In this sense, future work focuses on analyzing the performance of BIA using stochastical geometry theory for modeling muti-tier environments.

Massive MIMO in heterogenous networks. Massive MIMO transmission has been presented as a key element for future cellular networks. However, the interaction of the massive MIMO tier and small cells, which also are considered an element for future networks, is still an open issue. Cognitive approaches based on BIA schemes for small cells can be developed for mitigating the inter-tier interference without requiring CSIT or cooperation among the different tiers, e.g. between massive antenna BS and small cells.

Practical applications. The main theme of this dissertation was the use of BIA schemes in cellular networks. Future works will investigate the use of BIA in other applications. More specifically, we will focus on MIMO Free Space Optical Systems, where CSIT is unfeasible to obtain and the two main hurdles for the implementation of BIA, namely coherence time and finite SNR, do no represent a major limitation. On the other hand, we analyze the wireless energy harvesting as a source of interference, where

as it occurs in optical systems, CSIT is not a quantifiable measurement. BIA schemes can deal with both sources of interference, caused by data and energy transmission.

Publications

Journal Papers

1. M. Morales-Céspedes, J. Plata-Chaves, D. Toumpakaris, S.A. Jafar, and A. García Armada, "Blind Interference Alignment for Cellular Networks," *IEEE Transactions on Signal Processing*, vol.63, no.1, pp.41,56, Jan.1, 2015

2. M. Morales-Céspedes, J. Plata-Chaves, D. Toumpakaris, S.A. Jafar, and A. García Armada, "Cognitive Blind Interference Alignment for Macro-Femto Cellular Networks" *IEEE Transactions on Signal Processing*, in review process

Conference Papers

1. M. Morales-Céspedes, A. García Armada, "Zero-Forcing Coordinated Base Station Transmission for Femtocell Systems", 2011 IEEE 73rd in Vehicular Technology Conference (VTC Spring), pp.1-5, 15-18 May 2011.

2. M. Morales-Céspedes, A. Santos Rodríguez, "Achievable throughput with Block Diagonalization on OFDM indoor demonstrator", 2012 16th IEEE Mediterranean in Electrotechnical Conference (MELECON), pp.920-925, 25-28 March 2012.

3. M. Morales-Céspedes, J. Gutierrez Terán, A. García Armada, "Achievable throughput with Block Diagonalization on OFDM indoor demonstrator", 2013 Proceedings of the 21st European in Signal Processing Conference (EUSIPCO), pp.1-5, 9-13 Sept. 2013.

4. M. Morales-Cespedes, J. Plata-Chaves, D. Toumpakaris, and A. Garcia Armada, "On the choice of blind interference alignment strategy for cellular systems with data sharing" *2014 IEEE International Conference on Communications (ICC)*, pp.5735-5740, 10-14 June 2014.

5. M. Morales-Céspedes, M. Sanchez Fernandez, A. García Armada, "Experimental Evaluation of Blind Interference Alignment", in 2015 IEEE 81s Vehicular Technology Conference (VTC Spring), pp.1-5, 11-14 May 2015

6. M. Morales-Céspedes, J. Plata-Chaves, D. Toumpakaris, and A. Garcia Armada, "Cognitive blind interference alignment for macro-femto cellular networks" *in 2014 IEEE Global Communications Conference (GLOBECOM),* , pp.5735-5740, 10-14 June 2014.

Bibliography

[1] D. Goodman. Trends in cellular and cordless communications. *Communications Magazine, IEEE*, 29(6):31–40, June 1991. ISSN 0163-6804. doi: 10.1109/35.79400.

[2] A. Furuskar, S. Mazur, F. Muller, and H. Olofsson. EDGE: enhanced data rates for GSM and TDMA/136 evolution. *IEEE Personal Communications*, 6(3):56–66, Jun 1999. ISSN 1070-9916. doi: 10.1109/98.772978.

[3] R. Kalavakunta and A. Kripalani. Evolution of mobile broadband access technologies and services -considerations and solutions for smooth migration from 2G to 3G networks. In *IEEE International Conference on Personal Wireless Communications 2005. ICPWC 2005.*, pages 144–149, Jan 2005. doi: 10.1109/ICPWC.2005.1431320.

[4] D. Calin, P. Gardell, A. Mackay, T.B. Morawski, L. Pinzon, R. Sackett, and H. Zhang. A new approach to capacity growth planning for CDMA networks. In *12th International Telecommunications Network Strategy and Planning Symposium, 2006. NETWORKS 2006.*, pages 1–6, Nov 2006. doi: 10.1109/NETWKS.2006.300417.

[5] H. Sampath, S. Talwar, J. Tellado, V. Erceg, and A. Paulraj. A fourth-generation MIMO-OFDM broadband wireless system: design, performance, and field trial results. *IEEE Communications Magazine*, 40(9):143–149, Sep 2002. ISSN 0163-6804. doi: 10.1109/MCOM.2002.1031841.

[6] H. Bolcskei. MIMO-OFDM wireless systems: basics, perspectives, and challenges. *IEEE Wireless Communications*, 13(4):31–37, Aug 2006. ISSN 1536-1284. doi: 10.1109/MWC.2006.1678163.

[7] T.S. Rappaport, Shu Sun, R. Mayzus, Hang Zhao, Y. Azar, K. Wang, G.N. Wong, J.K. Schulz, M. Samimi, and F. Gutierrez. Millimeter wave mobile communications for 5G cellular: It will work! *IEEE Access*, 1:335–349, 2013. ISSN 2169-3536. doi: 10.1109/ACCESS.2013.2260813.

[8] P. Demestichas, A. Georgakopoulos, D. Karvounas, K. Tsagkaris, V. Stavroulaki, Jianmin Lu, Chunshan Xiong, and Jing Yao. 5G on the horizon: Key challenges for the radio-access network. *IEEE Vehicular Technology Magazine*, 8(3):47–53, Sept 2013. ISSN 1556-6072. doi: 10.1109/MVT.2013.2269187.

[9] F Boccardi, R.W. Heath, A. Lozano, T.L. Marzetta, and P. Popovski. Five disruptive technology directions for 5G. *IEEE Communications Magazine*, 52(2):74–80, February 2014. ISSN 0163-6804. doi: 10.1109/MCOM.2014.6736746.

[10] J.G. Andrews, S. Buzzi, Wan Choi, S.V. Hanly, A. Lozano, A.C.K. Soong, and J.C. Zhang. What will 5G be? *IEEE Journal on Selected Areas in Communications*, 32(6):1065–1082, June 2014. ISSN 0733-8716. doi: 10.1109/JSAC.2014.2328098.

[11] Zhu Ji and K.J.R. Liu. Cognitive radios for dynamic spectrum access - dynamic spectrum sharing: A game theoretical overview. *IEEE Communications Magazine*, 45(5):88–94, May 2007. ISSN 0163-6804. doi: 10.1109/MCOM.2007.358854.

[12] Jianfeng Wang, M. Ghosh, and K. Challapali. Emerging cognitive radio applications: A survey. *IEEE Communications Magazine*, 49(3):74–81, March 2011. ISSN 0163-6804. doi: 10.1109/MCOM.2011.5723803.

[13] H. Elsawy, E. Hossain, and M. Haenggi. Stochastic geometry for modeling, analysis, and design of multi-tier and cognitive cellular wireless networks: A survey. *IEEE Communications Surveys Tutorials*, 15(3):996–1019, Third 2013. ISSN 1553-877X. doi: 10.1109/SURV.2013.052213.00000.

[14] Z. Hasan, H. Boostanimehr, and V.K. Bhargava. Green cellular networks: A survey, some research issues and challenges. *IEEE Communications Surveys Tutorials*, 13(4):524–540, Fourth 2011. ISSN 1553-877X. doi: 10.1109/SURV.2011.092311.00031.

[15] R.C. Daniels and R.W. Heath. 60 GHz wireless communications: emerging requirements and design recommendations. *IEEE Vehicular Technology Magazine*, 2(3):41–50, Sept 2007. ISSN 1556-6072. doi: 10.1109/MVT.2008.915320.

[16] Shu Sun, T.S. Rappaport, R.W. Heath, A. Nix, and S. Rangan. Mimo for millimeter-wave wireless communications: beamforming, spatial multiplexing, or both? *IEEE Communications Magazine*, 52(12):110–121, December 2014. ISSN 0163-6804. doi: 10.1109/MCOM.2014.6979962.

[17] Zhouyue Pi, Junil Choi, and Robert W. Heath Jr. Millimeter-wave gbps broadband evolution towards 5G: Fixed access and backhaul. *CoRR*, abs/1507.03969, 2015. URL `http://arxiv.org/abs/1507.03969`.

[18] G.H. Dohler, L.E. Garcia-Munoz, S. Preu, S. Malzer, S. Bauerschmidt, J. Montero-de Paz, E. Ugarte-Munoz, A. Rivera-Lavado, V. Gonzalez-Posadas, and D. Segovia-Vargas. From arrays of THz antennas to large-area emitters. *IEEE Transactions on Terahertz Science and Technology*, 3(5):532–544, Sept 2013. ISSN 2156-342X. doi: 10.1109/TTHZ.2013.2266541.

[19] A. Jimenez, R.C. Guzman, L.E. Garcia-Munoz, D. Segovia, and G. Carpintero. Continuous wave millimeter and terahertz generation using a photonic integrated circuit. In *38th International Conference on Infrared, Millimeter, and Terahertz Waves (IRMMW-THz), 2013*, pages 1–1, Sept 2013. doi: 10.1109/IRMMW-THz.2013.6665695.

[20] M.A. Khalighi and M. Uysal. Survey on free space optical communication: A communication theory perspective. *IEEE Communications Surveys Tutorials*, 16 (4):2231–2258, Fourthquarter 2014. ISSN 1553-877X. doi: 10.1109/COMST.2014.2329501.

[21] A. Goldsmith, S.A. Jafar, N. Jindal, and S. Vishwanath. Capacity limits of MIMO channels. *IEEE Journal on Selected Areas in Communications*, 21(5):684–702, June 2003. ISSN 0733-8716. doi: 10.1109/JSAC.2003.810294.

[22] D. Gesbert, S. Hanly, H. Huang, S. Shamai Shitz, O. Simeone, and Wei Yu. Multi-Cell MIMO cooperative networks: A new look at interference. *IEEE Journal on Selected Areas in Communications*, 28(9):1380–1408, December 2010. ISSN 0733-8716. doi: 10.1109/JSAC.2010.101202.

[23] J. Hoydis, S. ten Brink, and M. Debbah. Massive MIMO in the UL/DL of cellular networks: How many antennas do we need? *IEEE Journal on Selected Areas in Communications*, 31(2):160–171, February 2013. ISSN 0733-8716. doi: 10.1109/JSAC.2013.130205.

[24] E. Larsson, O. Edfors, F. Tufvesson, and T. Marzetta. Massive MIMO for next generation wireless systems. *IEEE Communications Magazine*, 52(2):186–195, February 2014. ISSN 0163-6804. doi: 10.1109/MCOM.2014.6736761.

[25] H.S. Dhillon, R.K. Ganti, F. Baccelli, and J.G. Andrews. Modeling and analysis of K-tier downlink heterogeneous cellular networks. *IEEE Journal on Selected Areas in Communications*, 30(3):550–560, April 2012. ISSN 0733-8716. doi: 10.1109/JSAC.2012.120405.

[26] D. Lopez-Perez, I. Guvenc, G. de la Roche, M. Kountouris, T.Q.S. Quek, and Jie Zhang. Enhanced intercell interference coordination challenges in heterogeneous

networks. *IEEE Wireless Communications*, 18(3):22–30, June 2011. ISSN 1536-1284. doi: 10.1109/MWC.2011.5876497.

[27] J.G. Andrews, H. Claussen, M. Dohler, S. Rangan, and M.C. Reed. Femtocells: Past, present, and future. *IEEE Journal on Selected Areas in Communications*, 30(3):497–508, April 2012. ISSN 0733-8716. doi: 10.1109/JSAC.2012.120401.

[28] Q.H. Spencer, A.L. Swindlehurst, and M. Haardt. Zero-forcing methods for downlink spatial multiplexing in multiuser MIMO channels. *IEEE Transactions on Signal Processing*, 52(2):461–471, Feb 2004. ISSN 1053-587X. doi: 10.1109/TSP.2003.821107.

[29] Taesang Yoo and A. Goldsmith. On the optimality of multiantenna broadcast scheduling using zero-forcing beamforming. *IEEE Journal on Selected Areas in Communications*, 24(3):528–541, March 2006. ISSN 0733-8716. doi: 10.1109/JSAC.2005.862421.

[30] S. Shim, Jin Sam Kwak, R.W. Heath, and J.G. Andrews. Block diagonalization for multi-user MIMO with other-cell interference. *IEEE Transactions on Wireless Communications*, 7(7):2671–2681, July 2008. ISSN 1536-1276. doi: 10.1109/TWC.2008.070093.

[31] N. Ravindran and N. Jindal. Limited feedback-based block diagonalization for the MIMO broadcast channel. *IEEE Journal on Selected Areas in Communications*, 26(8):1473–1482, October 2008. ISSN 0733-8716. doi: 10.1109/JSAC.2008.081013.

[32] Changho Suh and D. Tse. Interference alignment for cellular networks. In *46th Annual Allerton Conference on Communication, Control, and Computing, 2008*, pages 1037–1044, Sept 2008. doi: 10.1109/ALLERTON.2008.4797673.

[33] Changho Suh, M. Ho, and D.N.C. Tse. Downlink interference alignment. *IEEE Transactions on Communications*, 59(9):2616–2626, September 2011. ISSN 0090-6778. doi: 10.1109/TCOMM.2011.070511.100313.

[34] Wonjae Shin, Namyoon Lee, Jong-Bu Lim, Changyong Shin, and Kyunghun Jang. On the design of interference alignment scheme for two-cell MIMO interfering broadcast channels. *IEEE Transactions on Wireless Communications*, 10(2):437–442, February 2011. ISSN 1536-1276. doi: 10.1109/TWC.2011.120810.101097.

[35] D. Aziz, M. Mazhar, and A. Weber. Multi user inter cell interference alignment in heterogeneous cellular networks. In *Vehicular Technology Conference (VTC Spring), 2014 IEEE 79th*, pages 1–5, May 2014. doi: 10.1109/VTCSpring.2014.7022994.

[36] V. Ntranos, M.A. Maddah-Ali, and G. Caire. Cellular interference alignment. *IEEE Transactions on Information Theory*, 61(3):1194–1217, March 2015. ISSN 0018-9448. doi: 10.1109/TIT.2015.2389244.

[37] Sean A. Ramprashad, G. Caire, and H.C. Papadopoulos. Cellular and network MIMO architectures: MU-MIMO spectral efficiency and costs of channel state information. In *2009 Conference Record of the Forty-Third Asilomar Conference on Signals, Systems and Computers*, pages 1811–1818, Nov 2009. doi: 10.1109/ACSSC.2009.5470211.

[38] I. Katzela and M. Naghshineh. Channel assignment schemes for cellular mobile telecommunication systems: A comprehensive survey. *IEEE Communications Surveys Tutorials*, 3(2):10–31, Second 2000. ISSN 1553-877X. doi: 10.1109/COMST.2000.5340800.

[39] M.-S. Alouini and A. Goldsmith. Area spectral efficiency of cellular mobile radio systems. In *IEEE 47th Vehicular Technology Conference, 1997,*, volume 2, pages 652–656 vol.2, May 1997. doi: 10.1109/VETEC.1997.600409.

[40] V. Chandrasekhar, J.G. Andrews, and Alan Gatherer. Femtocell networks: a survey. *IEEE Communications Magazine*, 46(9):59–67, September 2008. ISSN 0163-6804. doi: 10.1109/MCOM.2008.4623708.

[41] Wei Yu and J.M. Cioffi. Sum capacity of gaussian vector broadcast channels. *IEEE Transactions on Information Theory*, 50(9):1875–1892, Sept 2004. ISSN 0018-9448. doi: 10.1109/TIT.2004.833336.

[42] P. Viswanath and D.N.C. Tse. Sum capacity of the vector gaussian broadcast channel and uplink-downlink duality. *IEEE Transactions on Information Theory*, 49(8):1912–1921, Aug 2003. ISSN 0018-9448. doi: 10.1109/TIT.2003.814483.

[43] S. Vishwanath, N. Jindal, and A. Goldsmith. Duality, achievable rates, and sum-rate capacity of gaussian MIMO broadcast channels. *IEEE Transactions on Information Theory*, 49(10):2658–2668, Oct 2003. ISSN 0018-9448. doi: 10.1109/TIT.2003.817421.

[44] D.N.C. Tse, P. Viswanath, and Lizhong Zheng. Diversity-multiplexing tradeoff in multiple-access channels. *IEEE Transactions on Information Theory*, 50(9): 1859–1874, Sept 2004. ISSN 0018-9448. doi: 10.1109/TIT.2004.833347.

[45] S.A. Jafar and M.J. Fakhereddin. Degrees of freedom for the MIMO interference channel. *IEEE Transactions on Information Theory*, 53(7):2637–2642, July 2007. ISSN 0018-9448. doi: 10.1109/TIT.2007.899557.

[46] S.A. Jafar and S. Shamai. Degrees of freedom region of the MIMO X channel. *IEEE Transactions on Information Theory*, 54(1):151–170, Jan 2008. ISSN 0018-9448. doi: 10.1109/TIT.2007.911262.

[47] V.R. Cadambe and S.A. Jafar. Interference alignment and degrees of freedom of the K-user interference channel. *IEEE Transactions on Information Theory*, 54 (8):3425–3441, Aug 2008. ISSN 0018-9448. doi: 10.1109/TIT.2008.926344.

[48] Chiachi Huang, Syed Ali Jafar, Shlomo Shamai, and Sriram Vishwanath. On degrees of freedom region of MIMO networks without CSIT. *CoRR*, abs/0909.4017, 2009. URL `http://arxiv.org/abs/0909.4017`.

[49] C.S. Vaze and M.K. Varanasi. The degree-of-freedom regions of MIMO broadcast, interference, and cognitive radio channels with no CSIT. *IEEE Transactions on Information Theory*, 58(8):5354–5374, Aug 2012. ISSN 0018-9448. doi: 10.1109/TIT.2012.2201349.

[50] D.J. Love, R.W. Heath, and T. Strohmer. Grassmannian beamforming for multiple-input multiple-output wireless systems. *IEEE Transactions on Information Theory*, 49(10):2735–2747, Oct 2003. ISSN 0018-9448. doi: 10.1109/TIT.2003.817466.

[51] M.A. Maddah-Ali and D. Tse. Completely stale transmitter channel state information is still very useful. *IEEE Transactions on Information Theory*, 58(7): 4418–4431, July 2012. ISSN 0018-9448. doi: 10.1109/TIT.2012.2193116.

[52] A. Ghasemi, A.S. Motahari, and A.K. Khandani. On the degrees of freedom of X channel with delayed CSIT. In *2011 IEEE International Symposium on Information Theory Proceedings (ISIT)*, pages 767–770, July 2011. doi: 10.1109/ISIT.2011.6034238.

[53] Tiangao Gou and S.A. Jafar. Optimal use of current and outdated channel state information: Degrees of freedom of the MISO BC with mixed CSIT. *IEEE Communications Letters*, 16(7):1084–1087, July 2012. ISSN 1089-7798. doi: 10.1109/LCOMM.2012.050412.120702.

[54] C.S. Vaze and M.K. Varanasi. The degrees of freedom region and interference alignment for the MIMO interference channel with delayed CSIT. *IEEE Transactions on Information Theory*, 58(7):4396–4417, July 2012. ISSN 0018-9448. doi: 10.1109/TIT.2012.2194270.

[55] Sheng Yang, M. Kobayashi, D. Gesbert, and Xinping Yi. Degrees of freedom of time correlated MISO broadcast channel with delayed CSIT. *IEEE Transactions*

on Information Theory, 59(1):315–328, Jan 2013. ISSN 0018-9448. doi: 10.1109/TIT.2012.2215953.

[56] R. Tandon, S.A. Jafar, S. Shamai Shitz, and H.V. Poor. On the synergistic benefits of alternating CSIT for the MISO broadcast channel. *IEEE Transactions on Information Theory*, 59(7):4106–4128, July 2013. ISSN 0018-9448. doi: 10.1109/TIT.2013.2249573.

[57] S. Lashgari, A.S. Avestimehr, and C. Suh. Linear degrees of freedom of the X -channel with delayed CSIT. *IEEE Transactions onInformation Theory*, 60(4): 2180–2189, April 2014. ISSN 0018-9448. doi: 10.1109/TIT.2014.2307053.

[58] Namyoon Lee and R.W. Heath. Not too delayed CSIT achieves the optimal degrees of freedom. In *2012 50th Annual Allerton Conference on Communication, Control, and Computing (Allerton)*, pages 1262–1269, Oct 2012. doi: 10.1109/Allerton.2012.6483363.

[59] T. Cover. Broadcast channels. *IEEE Transactions on Information Theory*, 18(1): 2–14, Jan 1972. ISSN 0018-9448. doi: 10.1109/TIT.1972.1054727.

[60] Mari Kobayashi, Yingbin Liang, Shlomo Shamai, and Mérouane Debbah. On the compound MIMO broadcast channels with confidential messages. *CoRR*, abs/0906.3200, 2009. URL `http://arxiv.org/abs/0906.3200`.

[61] H. Weingarten, S. Shamai, and G. Kramer. On the compound mimo broadcast channel. *presented at the Information Theory Workshop*, Jan 2007.

[62] Tiangao Gou, S.A. Jafar, and Chenwei Wang. On the degrees of freedom of finite state compound wireless networks. *IEEE Transactions on Information Theory*, 57 (6):3286–3308, June 2011. ISSN 0018-9448. doi: 10.1109/TIT.2011.2137130.

[63] Hua Sun, Chunhua Geng, and S.A. Jafar. Topological interference management with alternating connectivity. In *2013 IEEE International Symposium on Information Theory Proceedings (ISIT)*, pages 399–403, July 2013. doi: 10.1109/ISIT.2013.6620256.

[64] Chunhua Geng, Hua Sun, and S.A. Jafar. Multilevel topological interference management. In *2013 IEEE Information Theory Workshop (ITW)*, pages 1–5, Sept 2013. doi: 10.1109/ITW.2013.6691291.

[65] Jinyuan Chen, P. Elia, and S.A. Jafar. On the vector broadcast channel with alternating CSIT: A topological perspective. In *2014 IEEE International Symposium on Information Theory (ISIT)*, pages 2579–2583, June 2014. doi: 10.1109/ISIT.2014.6875300.

[66] Chunhua Geng, N. Naderializadeh, A.S. Avestimehr, and S.A. Jafar. On the optimality of treating interference as noise. *IEEE Transactions on Information Theory*, 61(4):1753–1767, April 2015. ISSN 0018-9448. doi: 10.1109/TIT.2015.2408342.

[67] Yingyuan Gao, Gang Wang, and S.A. Jafar. Topological interference management for hexagonal cellular networks. *IEEE Transactions on Wireless Communications*, 14(5):2368–2376, May 2015. ISSN 1536-1276. doi: 10.1109/TWC.2014.2385851.

[68] Syed Ali Jafar. Elements of cellular blind. *CoRR*, abs/1203.2384, 2012. URL `http://arxiv.org/abs/1203.2384`.

[69] S.A. Jafar. Topological interference management through index coding. *IEEE Transactions on Information Theory*, 60(1):529–568, Jan 2014. ISSN 0018-9448. doi: 10.1109/TIT.2013.2285151.

[70] G. Caire and S. Shamai. On the achievable throughput of a multiantenna gaussian broadcast channel. *IEEE Transactions on Information Theory*, 49(7):1691–1706, July 2003. ISSN 0018-9448. doi: 10.1109/TIT.2003.813523.

[71] Jun Zhang, Runhua Chen, J.G. Andrews, and R.W. Heath. Coordinated multi-cell MIMO systems with cellular block diagonalization. In *Conference Record of the Forty-First Asilomar Conference on Signals, Systems and Computers, 2007. ACSSC 2007.*, pages 1669–1673, Nov 2007. doi: 10.1109/ACSSC.2007.4487516.

[72] Zukang Shen, Runhua Chen, J.G. Andrews, R.W. Heath, and B.L. Evans. Sum capacity of multiuser MIMO broadcast channels with block diagonalization. *IEEE Transactions on Wireless Communications*, 6(6):2040–2045, June 2007. ISSN 1536-1276. doi: 10.1109/TWC.2007.05831.

[73] Rui Zhang. Cooperative multi-cell block diagonalization with per-base-station power constraints. *IEEE Journal on Selected Areas in Communications*, 28(9): 1435–1445, December 2010. ISSN 0733-8716. doi: 10.1109/JSAC.2010.101205.

[74] C.M. Yetis, Tiangao Gou, S.A. Jafar, and A.H. Kayran. On feasibility of interference alignment in MIMO interference networks. *IEEE Transactions on Signal Processing*, 58(9):4771–4782, Sept 2010. ISSN 1053-587X. doi: 10.1109/TSP.2010.2050480.

[75] O. Gonzalez, C. Beltran, and I. Santamaria. A feasibility test for linear interference alignment in MIMO channels with constant coefficients. *IEEE Transactions on Information Theory*, 60(3):1840–1856, March 2014. ISSN 0018-9448. doi: 10.1109/TIT.2014.2301440.

[76] M.A. Maddah-Ali, A.S. Motahari, and A.K. Khandani. Communication over MIMO X channels: Interference alignment, decomposition, and performance analysis. *IEEE Transactions on Information Theory*, 54(8):3457–3470, Aug 2008. ISSN 0018-9448. doi: 10.1109/TIT.2008.926460.

[77] K. Gomadam, V.R. Cadambe, and S.A. Jafar. Approaching the capacity of wireless networks through distributed interference alignment. In *IEEE Global Telecommunications Conference, 2008. IEEE GLOBECOM 2008*, pages 1–6, Nov 2008. doi: 10.1109/GLOCOM.2008.ECP.817.

[78] Tiangao Gou and S.A. Jafar. Degrees of freedom of the K user $m \times n$ mimo interference channel. *IEEE Transactions on Information Theory*, 56(12):6040–6057, Dec 2010. ISSN 0018-9448. doi: 10.1109/TIT.2010.2080830.

[79] H. Maleki, S.A. Jafar, and S. Shamai. Retrospective interference alignment over interference networks. *IEEE Journal of Selected Topics in Signal Processing*, 6(3): 228–240, June 2012. ISSN 1932-4553. doi: 10.1109/JSTSP.2011.2181155.

[80] S.A. Jafar. Exploiting channel correlations - simple interference alignment schemes with no csit. In *Global Telecommunications Conference (GLOBECOM 2010), 2010 IEEE*, pages 1–5, Dec 2010. doi: 10.1109/GLOCOM.2010.5683592.

[81] S.A. Jafar. Blind interference alignment. *IEEE Journal of Selected Topics in Signal Processing*, 6(3):216–227, June 2012. ISSN 1932-4553. doi: 10.1109/JSTSP.2012.2187877.

[82] B.A. Cetiner, Hamid Jafarkhani, Jiang-Yuan Qian, Hui Jae Yoo, A. Grau, and F. De Flaviis. Multifunctional reconfigurable MEMS integrated antennas for adaptive MIMO systems. *IEEE Communications Magazine*, 42(12):62–70, Dec 2004. ISSN 0163-6804. doi: 10.1109/MCOM.2004.1367557.

[83] N. Haridas, A.T. Erdogan, T. Arslan, Anthony J. Walton, S. Smith, Tom Stevenson, C. Dunare, A. Gundlach, J. Terry, Petros Argyrakis, K. Tierney, A. Ross, and T. O'Hara. Reconfigurable MEMS antennas. In *Conference on Adaptive Hardware and Systems, 2008. AHS '08. NASA/ESA*, pages 147–154, June 2008. doi: 10.1109/AHS.2008.28.

[84] A. Grau, Hamid Jafarkhani, and F. De Flaviis. A reconfigurable multiple-input multiple-output communication system. *IEEE Transactions on Wireless Communications*, 7(5):1719–1733, May 2008. ISSN 1536-1276. doi: 10.1109/TWC.2008.060905.

[85] Yu Zhou, R.S. Adve, and S.V. Hum. Design and evaluation of pattern reconfigurable antennas for MIMO applications. *IEEE Transactions on Antennas and Propagation*, 62(3):1084–1092, March 2014. ISSN 0018-926X. doi: 10.1109/TAP.2013.2284874.

[86] Dau-Chyrh Chang. Reconfigurable antennas for digital data communication systems. In *2014 IEEE International Workshop on Electromagnetics (iWEM)*, pages 1–1, Aug 2014. doi: 10.1109/iWEM.2014.6963605.

[87] J. Costantine, Y. Tawk, S.E. Barbin, and C.G. Christodoulou. Reconfigurable antennas: Design and applications. *Proceedings of the IEEE*, 103(3):424–437, March 2015. ISSN 0018-9219. doi: 10.1109/JPROC.2015.2396000.

[88] Tiangao Gou, Chenwei Wang, and S.A. Jafar. Aiming perfectly in the dark - blind interference alignment through staggered antenna switching. In *Global Telecommunications Conference (GLOBECOM 2010), 2010 IEEE*, pages 1–5, Dec 2010. doi: 10.1109/GLOCOM.2010.5684149.

[89] Tiangao Gou, Chenwei Wang, and S.A. Jafar. Aiming perfectly in the dark-blind interference alignment through staggered antenna switching. *IEEE Transactions on Signal Processing*, 59(6):2734–2744, June 2011. ISSN 1053-587X. doi: 10.1109/TSP.2011.2129517.

[90] Chenwei Wang, Tiangao Gou, and S.A. Jafar. Interference alignment through staggered antenna switching for MIMO BC with no CSIT. In *2010 Conference Record of the Forty Fourth Asilomar Conference on Signals, Systems and Computers (ASILOMAR),*, pages 2081–2085, Nov 2010. doi: 10.1109/ACSSC.2010.5757915.

[91] Minho Yang, Sang-Woon Jeon, and Dong Ku Kim. Linear degrees of freedom of MIMO broadcast channels with reconfigurable antennas in the absence of CSIT. *CoRR*, abs/1409.5532, 2014. URL `http://arxiv.org/abs/1409.5532`.

[92] Chenwei Wang. Degrees of freedom characterization: The 3-user SISO interference channel with blind interference alignment. *IEEE Communications Letters*, 18(5):757–760, May 2014. ISSN 1089-7798. doi: 10.1109/LCOMM.2014.030714.140177.

[93] Yi Lu, Wei Zhang, and K.B. Letaief. Blind interference alignment with diversity in two-user interference channel. In *2013 IEEE/CIC International Conference on Communications in China (ICCC)*, pages 275–280, Aug 2013. doi: 10.1109/ICCChina.2013.6671128.

[94] Yi Lu, Wei Zhang, and K.B. Letaief. Blind interference alignment with diversity in K-user interference channels. *IEEE Transactions on Communications*, 62(8):2850–2859, Aug 2014. ISSN 0090-6778. doi: 10.1109/TCOMM.2014.2333516.

[95] Chenwei Wang, H.C. Papadopoulos, S.A. Ramprashad, and G. Caire. Design and operation of blind interference alignment in cellular and cluster-based systems. In *Information Theory and Applications Workshop (ITA), 2011*, pages 1–10, Feb 2011. doi: 10.1109/ITA.2011.5743601.

[96] Chenwei Wang, H.C. Papadopoulos, S.A. Ramprashad, and G. Caire. Improved blind interference alignment in a cellular environment using power allocation and cell-based clusters. In *2011 IEEE International Conference on Communications (ICC)*, pages 1–6, June 2011. doi: 10.1109/icc.2011.5962838.

[97] S. Akoum, Chung Shue Chen, M. Debbah, and R.W. Heath. Data sharing coordination and blind interference alignment for cellular networks. In *Global Communications Conference (GLOBECOM), 2012 IEEE*, pages 4273–4277, Dec 2012. doi: 10.1109/GLOCOM.2012.6503789.

[98] Yi Lu and Wei Zhang. Downlink blind interference alignment for cellular networks. In *Global Communications Conference (GLOBECOM), 2014 IEEE*, pages 3337–3342, Dec 2014. doi: 10.1109/GLOCOM.2014.7037322.

[99] A. Ghosh, N. Mangalvedhe, R. Ratasuk, B. Mondal, M. Cudak, E. Visotsky, T.A. Thomas, J.G. Andrews, P. Xia, H.S. Jo, H.S. Dhillon, and T.D. Novlan. Heterogeneous cellular networks: From theory to practice. *IEEE Communications Magazine*, 50(6):54–64, June 2012. ISSN 0163-6804. doi: 10.1109/MCOM.2012.6211486.

[100] Ping Xia, Han-Shin Jo, and J.G. Andrews. Fundamentals of inter-cell overhead signaling in heterogeneous cellular networks. *IEEE Journal of Selected Topics in Signal Processing*, 6(3):257–269, June 2012. ISSN 1932-4553. doi: 10.1109/JSTSP.2011.2181939.

[101] M. Morales Cespedes and A. Garcia Armada. Zero-forcing coordinated base station transmission for femtocell systems. In *2011 IEEE 73rd Vehicular Technology Conference (VTC Spring)*, pages 1–5, May 2011. doi: 10.1109/VETECS.2011.5956271.

[102] F. Pantisano, M. Bennis, W. Saad, and M. Debbah. Cooperative interference alignment in femtocell networks. In *Global Telecommunications Conference (GLOBECOM 2011), 2011 IEEE*, pages 1–6, Dec 2011. doi: 10.1109/GLOCOM.2011.6133906.

[103] Hyun-Ho Lee and Young-Chai Ko. Linear transceiver design based on interference alignment for MIMO heterogeneous networks. In *2012 IEEE 23rd International Symposium on Personal Indoor and Mobile Radio Communications (PIMRC)*, pages 1645–1650, Sept 2012. doi: 10.1109/PIMRC.2012.6362612.

[104] M. Morales Cespedes and A. Santos Rodriguez. Statistical characterization of zero-forcing coordinated base station transmission for femtocell environments. In *2012 16th IEEE Mediterranean Electrotechnical Conference (MELECON)*, pages 920–925, March 2012. doi: 10.1109/MELCON.2012.6196578.

[105] F. Pantisano, M. Bennis, W. Saad, M. Debbah, and M. Latva-aho. Interference alignment for cooperative femtocell networks: A game-theoretic approach. *IEEE Transactions on Mobile Computing*, 12(11):2233–2246, Nov 2013. ISSN 1536-1233. doi: 10.1109/TMC.2012.196.

[106] F. Pantisano, M. Bennis, W. Saad, M. Debbah, and M. Latva-aho. On the impact of heterogeneous backhauls on coordinated multipoint transmission in femtocell networks. In *2012 IEEE International Conference on Communications (ICC),*, pages 5064–5069, June 2012. doi: 10.1109/ICC.2012.6364418.

[107] G. Gur, S. Bayhan, and F. Alagoz. Cognitive femtocell networks: an overlay architecture for localized dynamic spectrum access [dynamic spectrum management]. *IEEE Wireless Communications*, 17(4):62–70, August 2010. ISSN 1536-1284. doi: 10.1109/MWC.2010.5547923.

[108] A. Adhikary, V. Ntranos, and G. Caire. Cognitive femtocells: Breaking the spatial reuse barrier of cellular systems. In *Information Theory and Applications Workshop (ITA), 2011*, pages 1–10, Feb 2011. doi: 10.1109/ITA.2011.5743563.

[109] Shin-Ming Cheng, Shou-Yu Lien, Feng-Seng Chu, and Kwang-Cheng Chen. On exploiting cognitive radio to mitigate interference in macro/femto heterogeneous networks. *IEEE Wireless Communications*, 18(3):40–47, June 2011. ISSN 1536-1284. doi: 10.1109/MWC.2011.5876499.

[110] S. Al-Rubaye, A. Al-Dulaimi, and J. Cosmas. Cognitive femtocell. *IEEE Vehicular Technology Magazine*, 6(1):44–51, March 2011. ISSN 1556-6072. doi: 10.1109/MVT.2010.939902.

[111] M. Bennis and S.M. Perlaza. Decentralized cross-tier interference mitigation in cognitive femtocell networks. In *2011 IEEE International Conference on Communications (ICC)*, pages 1–5, June 2011. doi: 10.1109/icc.2011.5962649.

[112] S. Kaimaletu, R. Krishnan, S. Kalyani, N. Akhtar, and B. Ramamurthi. Cognitive interference management in heterogeneous femto-macro cell networks. In *2011 IEEE International Conference on Communications (ICC)*, pages 1–6, June 2011. doi: 10.1109/icc.2011.5962617.

[113] T. Zahir, K. Arshad, A. Nakata, and K. Moessner. Interference management in femtocells. *IEEE Communications Surveys Tutorials*, 15(1):293–311, First 2013. ISSN 1553-877X. doi: 10.1109/SURV.2012.020212.00101.

[114] Yong Sheng Soh, T.Q.S. Quek, M. Kountouris, and G. Caire. Cognitive hybrid division duplex for two-tier femtocell networks. *IEEE Transactions on Wireless Communications*, 12(10):4852–4865, October 2013. ISSN 1536-1276. doi: 10.1109/TWC.2013.090313.121264.

[115] F. C. Kavasoglu, Y. Huang, and B. D. Rao. Semi-blind interference alignment techniques for small cell networks. *IEEE Transactions on Signal Processing*, 62 (23):6335–6348, 2014. ISSN 1053-587X. doi: 10.1109/TSP.2014.2364012.

[116] V. Kalokidou, O. Johnson, and R. Piechocki. Blind interference alignment in general heterogeneous networks. In *IEEE 25th Annual International Symposium on Personal, Indoor, and Mobile Radio Communication, 2014. PIMRC 2014*, pages 816–820, 2014.

[117] M. Morales Cespedes, A. Garcia Armada, and J. Gutierrez Teran. Achievable throughput with block diagonalization on OFDM indoor demonstrator. In *2013 Proceedings of the 21st European Signal Processing Conference (EUSIPCO)*, pages 1–5, Sept 2013.

[118] S.A. Jafar and S. Shamai. Degrees of freedom region of the MIMO X channel. *IEEE Transactions on Information Theory*, 54(1):151–170, Jan 2008. ISSN 0018-9448. doi: 10.1109/TIT.2007.911262.

[119] Hoon Huh, A. Tulino, and G. Caire. Network-MIMO cellular systems: Large-system analysis and low-overhead downlink scheduling. In *2011 IEEE Statistical Signal Processing Workshop (SSP),*, pages 693–696, June 2011. doi: 10.1109/SSP.2011.5967796.

[120] A. Lapidoth, S. Shamai, and M. Wigger. On the capacity of fading MIMO broadcast channels with imperfect transmitter side information. *presented at the 43rd Annu. Allerton Conf. Communications and Control and Computing*, Sep 2005.

[121] V.R. Cadambe, S.A. Jafar, and Chenwei Wang. Interference alignment with asymmetric complex signaling-settling the host-madsen-nosratinia conjecture. *IEEE Transactions on Information Theory*, 56(9):4552–4565, Sept 2010. ISSN 0018-9448. doi: 10.1109/TIT.2010.2053895.

[122] Tiangao Gou and S.A. Jafar. Degrees of freedom of the K user $m \times n$ mimo interference channel. *IEEE Transactions on Information Theory*, 56(12):6040–6057, Dec 2010. ISSN 0018-9448. doi: 10.1109/TIT.2010.2080830.

[123] J.T. Bernhard, R. Wang, R. Clark, and P. Mayes. Stacked reconfigurable antenna elements for space-based radar applications. In *Antennas and Propagation Society International Symposium, 2001. IEEE*, volume 1, pages 158–161 vol.1, July 2001. doi: 10.1109/APS.2001.958816.

[124] Chunhua Geng, Hua Sun, and S.A. Jafar. On the optimality of treating interference as noise: General message sets. *IEEE Transactions on Information Theory*, 61(7): 3722–3736, July 2015. ISSN 0018-9448. doi: 10.1109/TIT.2015.2432751.

[125] A. Nosratinia, T.E. Hunter, and A. Hedayat. Cooperative communication in wireless networks. *IEEE Communications Magazine*, 42(10):74–80, Oct 2004. ISSN 0163-6804. doi: 10.1109/MCOM.2004.1341264.

[126] S. Venkatesan, A. Lozano, and R. Valenzuela. Network MIMO: Overcoming intercell interference in indoor wireless systems. In *Conference Record of the Forty-First Asilomar Conference on Signals, Systems and Computers, 2007. ACSSC 2007.*, pages 83–87, Nov 2007. doi: 10.1109/ACSSC.2007.4487170.

[127] G. Caire, Sean A. Ramprashad, and H.C. Papadopoulos. Rethinking network MIMO: Cost of CSIT, performance analysis, and architecture comparisons. In *Information Theory and Applications Workshop (ITA), 2010*, pages 1–10, Jan 2010. doi: 10.1109/ITA.2010.5454094.

[128] M. Morales Cespedes, J. Plata-Chaves, D. Toumpakaris, and A. Garcia Armada. On the choice of blind interference alignment strategy for cellular systems with data sharing. In *2014 IEEE International Conference on Communications (ICC)*, pages 5735–5740, June 2014. doi: 10.1109/ICC.2014.6884236.

[129] M. Morales-Cespedes, J. Plata-Chaves, D. Toumpakaris, S.A. Jafar, and A. Garcia Armada. Blind interference alignment for cellular networks. *IEEE Transactions on Signal Processing*, 63(1):41–56, Jan 2015. ISSN 1053-587X. doi: 10.1109/TSP.2014.2362104.

[130] T. Gou and S. A. Jafar. Optimal use of current and outdated channel state information: Degrees of freedom of the MISO BC with mixed CSIT. *IEEE Communications Letters*, 16(7):1084–1087, 2012.

[131] A. Ghosh, R. Ratasuk, B. Mondal, N. Mangalvedhe, and T. Thomas. LTE-advanced: Next generation wireless broadband technology [invited paper]. *IEEE Wireless Communications*, 17(3):10–22, June 2010. ISSN 1536-1284. doi: 10.1109/MWC.2010.5490974.

[132] P. Bhat, S. Nagata, L. Campoy, I. Berberana, T. Derham, Guangyi Liu, Xiaodong Shen, Pingping Zong, and Jin Yang. LTE-advanced: an operator perspective.

IEEE Communications Magazine, 50(2):104–114, February 2012. ISSN 0163-6804. doi: 10.1109/MCOM.2012.6146489.

[133] S. A. Jafar. *Interference Alignment: A New Look at Signal Dimensions in a Communication Network*. Foundations and Trends in Communications and Information Theory.

[134] A. M. Tulino and S. Verdú. *Random Matrix Theory and Wireless Communications*. Foundations and Trends in Communications and Information Theory.

[135] Peng Lin, Jin Zhang, Yanjiao Chen, and Qian Zhang. Macro-femto heterogeneous network deployment and management: from business models to technical solutions. *IEEE Wireless Communications*, 18(3):64–70, June 2011. ISSN 1536-1284. doi: 10.1109/MWC.2011.5876502.

[136] N. Saquib, E. Hossain, Long Bao Le, and Dong In Kim. Interference management in OFDMA femtocell networks: issues and approaches. *IEEE Wireless Communications*, 19(3):86–95, June 2012. ISSN 1536-1284. doi: 10.1109/MWC.2012.6231163.

[137] A. Abdelnasser, E. Hossain, and Dong In Kim. Clustering and resource allocation for dense femtocells in a two-tier cellular OFDMA network. *IEEE Transactions on Wireless Communications*, 13(3):1628–1641, March 2014. ISSN 1536-1276. doi: 10.1109/TW.2014.011614.131163.

[138] A. Golaup, M. Mustapha, and L.B. Patanapongpibul. Femtocell access control strategy in UMTS and LTE. *IEEE Communications Magazine*, 47(9):117–123, September 2009. ISSN 0163-6804. doi: 10.1109/MCOM.2009.5277464.

[139] Jin-Seok Kim and Tae-Jin Lee. Handover in UMTS networks with hybrid access femtocells. In *12th International Conference on Advanced Communication Technology 2010 (ICACT)*, volume 1, pages 904–908, Feb 2010.

[140] D. Xenakis, N. Passas, L. Merakos, and C. Verikoukis. Mobility management for femtocells in LTE-advanced: Key aspects and survey of handover decision algorithms. *IEEE Communications Surveys Tutorials*, 16(1):64–91, First 2014. ISSN 1553-877X. doi: 10.1109/SURV.2013.060313.00152.

[141] V. Chandrasekhar, J. G. Andrews, T. Muharemovic, Z. Shen, and A. Gatherer. Power control in two-tier femtocell networks. *IEEE Transactions on Wireless Communications*, 8(8):4316–4328, 2009.

[142] V. Chandrasekhar and J. G. Andrews. Spectrum allocation in tiered cellular networks. *IEEE Transactions on Communications*, 57(10):3059–3068, 2009.

[143] T. D. Novlan, R. K. Ganti, A. Ghosh, and J. G. Andrews. Analytical evaluation of fractional frequency reuse for heterogeneous cellular networks. *IEEE Transactions on Communications*, 60(7):2029–2039, 2012.

[144] L. Huang, G. Zhu, and X. Du. Cognitive femtocell networks: an opportunistic spectrum access for future indoor wireless coverage. *IEEE Wireless Communications*, 20(2):44–51, 2013. ISSN 1536-1284. doi: 10.1109/MWC.2013.6507393.

[145] Heecheol Yang, Wonjae Shin, and Jungwoo Lee. Grouping based blind interference alignment for K-user MISO interference channels. In *2015 IEEE International Symposium on Information Theory (ISIT)*, pages 2827–2831, June 2015. doi: 10.1109/ISIT.2015.7282972.

[146] A.J. Paulraj and B. Papadias Constantinos. Space-time processing for wireless communications. In *1997 IEEE International Conference on Acoustics, Speech, and Signal Processing, 1997. ICASSP-97*, volume 1, pages 1–4 vol.1, Apr 1997. doi: 10.1109/ICASSP.1997.598843.

[147] R.H. Clarke. A statistical theory of mobile-radio reception. In *Bell Systems Technology Journal*, volume 1, pages 957–1000, July 1968.

[148] L. Vielva, J. Via, J. Gutiérrez, O. González, J. Ibánez, and I. Santamaría. Building a web platform for learning advanced digital communications using a MIMO testbed. In *Acoustics Speech and Signal Processing (ICASSP), 2010 IEEE International Conference on*, pages 2942–2945, March. 2010. doi: 10.1109/ICASSP.2010.5496148.

[149] O. El Ayach, S.W. Peters, and R.W. Heath. The feasibility of interference alignment over measured MIMO-OFDM channels. *IEEE Transactions on Vehicular Technology*, 59(9):4309–4321, Nov. 2010. ISSN 0018-9545. doi: 10.1109/TVT.2010.2082005.

[150] O. González, D. Ramírez, I. Santamaría, J.A. García-Naya, and L. Castedo. Experimental validation of interference alignment techniques using a multiuser MIMO testbed. In *2011 International ITG Workshop on Smart Antennas (WSA)*, Feb. 2011. doi: 10.1109/WSA.2011.5741921.

[151] M. Morales Céspedes, J. Gutiérrez Terán, and A. García Armada. Achievable throughput with block diagonalization on ofdm indoor demonstrator. In *2013 European Signal Processing Conference (EUSIPCO 2013)*, September. 2013.